THE
PHYSICAL REVIEW

A journal of experimental and theoretical physics established by E. L. Nichols in 1893

SECOND SERIES, VOL. 78, NO. 1 APRIL 1, 1950

The Range-Energy Curves for Alpha-Particles and Protons

WILLIAM P. JESSE AND JOHN SADAUSKIS
Argonne National Laboratory, Chicago, Illinois
(Received October 27, 1949)

Previous experiments have shown that in argon there exists a very good proportionality between the energy of an alpha-particle and the total ionization produced by it. In air this proportionality is not found, the ionization decreasing more rapidly than energy at low alpha-energies. Range-energy curves determined in the region 0–5 Mev, where the ionization in air is used as a measure of the alpha-energy, hence give too low energy values. Such curves, when corrected to equivalent ionization values in argon, show much better agreement with range and energy data derived from nuclear reactions. The range-energy curve for protons, derived from the alpha-curve, also shows improved agreement with nuclear data when the corrected alpha-range-energy curve is substituted for the old.

INTRODUCTION

IN a recent paper,[1] evidence has been presented for believing that in argon the ionization produced by a single alpha-particle is to a very good approximation proportional to the energy of the alpha-particle. From the work of Stetter[2] for alpha-particles in air, it was also shown that such a direct proportionality does not exist in air but that the relative ionization decreases markedly as the energy of the alpha-particle approaches zero.

As has already been pointed out in brief,[3] these findings have a very important bearing on the accuracy of the range-energy curves in current use for alpha-particles. Since, in the region from 0–5 Mev, there are no natural emitters of alpha-particles for which the absolute energies have been determined accurately, the range-energy curves in this region were of necessity constructed by estimating the energy of a slowed down alpha-particle by means of the ionization produced in some gas—almost universally air. Such curves are thus in reality range-ionization in air curves, and if the alpha-ionization in air is not proportional to the alpha-energy, they are subject to error, especially in the low energy regions. In the work of Holloway and Livingston,[4] the authors explicitly state that their curve is valid only if this direct proportionality in air exists. In the following paper, we have found means of converting the Holloway Livingston (henceforth denoted by H and L) ionization in air values to equivalent ionization in argon values, where, we believe, the above proportionality is almost exact. This results in a much more consistent agreement for the energy values from the range-energy curve with data from alpha-energies derived from nuclear transformations.

For clarity, the successive steps in the presentation below are indicated as follows:

I. Establishment of curve showing relative ionization in argon and in air for alpha-particles of different energies.
A. Experimental results from Sm-Po comparison in argon and in air.
B. Results of Gray-Gurney.
C. Further experimental measurements following method of Gurney.
II. Establishment of corrected range-energy curve for alpha-particles.
A. Correction of Holloway-Livingston curve from argon-air ionization ratios.
B. Attempt to establish absolute curve.
C. Comparison of original and corrected curves.
III. Comparison of energies derived from range-energy curves from known alpha-ranges with independently determined energies.
IV. Derived proton range-energy curve from alpha-particle curve.
V. Range-energy tables for protons and alpha-particles.

[1] Jesse, Forstat, and Sadauskis, Phys. Rev. **77**, 782 (1950).
[2] G. Stetter, Zeits. f. Physik **120**, 639 (1943).
[3] W. P. Jesse and J. Sadauskis, Phys. Rev. **75**, 1110 (1949); Phys. Rev. **76**, 163 (1949).
[4] M. G. Holloway and M. S. Livingston, Phys. Rev. **54**, 18 (1938).

TABLE I. Experimental values for different gases, relative to hydrogen, of W for alpha-particles of various ranges compared with that for a 20-mm range α-particle.

Residual range (mm of air)	2.5	5.0	7.5	10.0	15.0	20.0
Initial energy of α-particle (Mev)	0.33	0.9	1.4	1.9	2.7	3.4
Helium	1.00_1	1.00_2	0.98_8	1.00_6	0.99_7	(1.000)
Air, also N_2 and O_2	1.08_2	1.06_4	1.04_8	1.03_1	1.00_6	(1.000)
Neon	0.99_2	0.99_2	0.99_8	0.99_5	0.99_4	(1.000)
Argon	1.01_0	1.00_4	1.00_3	0.99_6	0.99_0	(1.000)

I. ESTABLISHMENT OF CURVE SHOWING RELATIVE IONIZATION IN ARGON AND IN AIR FOR ALPHA-PARTICLES OF DIFFERENT ENERGIES

A. Experimental Results from Sm-Po Comparison in Argon and in Air

A series of measurements has been made, both in argon and in air, to determine the ratio of the total ionization produced by an alpha-particle from samarium to that produced by a polonium alpha. As in our previous work, the ionization charge from a single

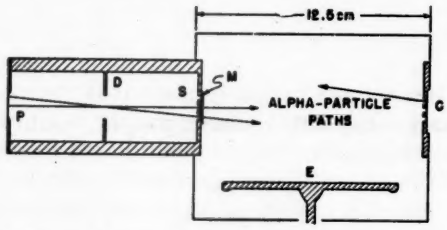

FIG. 1. Schematic diagram of collimating absorption cell and ionization chamber.

alpha-particle was collected in an ion chamber and amplified by means of the vibrating-reed electrometer. The sudden jump recorded by the pen of the Brown recorder, into which the vibrating-reed feeds, is taken as a measure of the charge collected.

The ion chamber used for this comparison was cylindrical in shape with an internal diameter of 16 cm and height of 6 cm. The central electrode was a circular plate of stainless steel 14.5 cm in diameter. At its center and flush with the surface was a button of polished nickel on which the polonium sample was deposited. On both the faces of the electrode and on both stainless steel disks inserted in the ends of the chamber, samarium nitrate was sprayed in a thin layer from solution. The liquid spray was made up by diluting with water the solution obtained by treating a very pure sample of samarium oxide with nitric acid. Because of the large area covered, it was possible to get a counting rate in the chamber of three or four counts/min. and yet have the sample layer so thin as to give no serious self-absorption. The latter was judged by the calculated thickness of the layer from the amount of samarium nitrate sprayed on, and more accurately from the appearance of the plotted samarium alpha-peaks. These showed only a very small deviation from symmetry on the low energy side.

The ratio of alpha-ionization $(Sm/Po)_{argon}$ was determined from the mean of four runs to be 0.411, while $(Sm/Po)_{air}$ gave 0.390 as a mean for three runs. The ratio of these two values is 1.05_3. The "energies" for the Sm α, computed on the assumption of a direct proportionality between ionization and alpha-energy, are then 2.17_8 Mev and 2.06_9 Mev for argon and air, respectively, for an assumed energy for the polonium alpha of 5.298_4 Mev. The five percent discrepancy between these two values is much more than the error of experiment, estimated at not more than one percent. Thus, we have again the same evidence of departure in air from a linear relation between alpha-ionization and alpha-energy that was noted in our previous paper.

B. Results of Gray-Gurney

Such a dissimilarity between air and a group of gases comprising hydrogen and the noble gases has already been pointed out by L. H. Gray[5] on the basis of experimental measurements by Gurney.[6] These measurements were made on a collimated beam of alpha-particles partially stopped by passage through an air absorption cell in which the pressure of the air could be varied. For each approximately monoenergetic band of alpha-particles thus obtained, the ionization relative to that in hydrogen was measured for each gas. The anomalous behavior of air is shown in Table I, taken from the paper of Gray. Here in air the relative energy W to

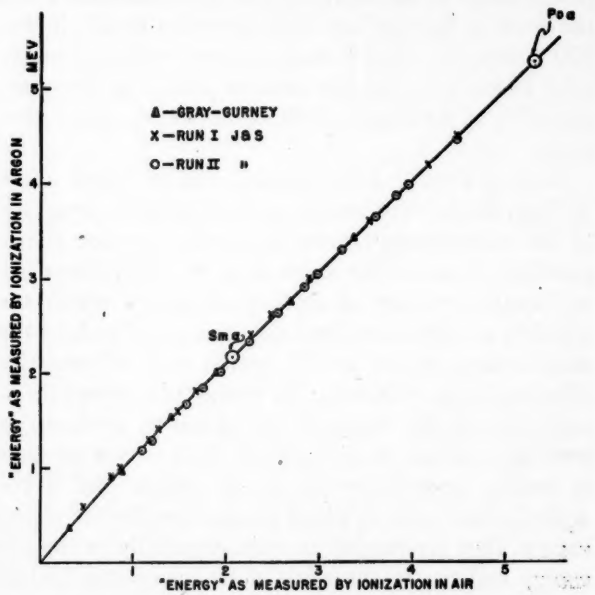

FIG. 2. "Energy" as measured by ionization in argon against "energy" as measured by ionization in air.

[5] L. H. Gray, Proc. Camb. Phil. Soc. **40**, 95 (1944).
[6] R. W. Gurney, Proc. Roy. Soc. A **107**, 332 (1925).

TABLE II. Ionization measurements relative to polonium in argon and in air.

"Energies" measured in air, Mev	5.30	4.00	3.5	3.0	2.5	2.0	1.5	1.00	0.50	0.30
"Energies" measured in argon	5.30	4.035	3.553	3.069	2.583	2.100	1.611	1.110	0.567	0.344
Ratio	1.00	1.009	1.015	1.023	1.033	1.050	1.074	1.110	1.134	1.147
Corresponding range from H and L curve	3.842	2.516	2.096	1.719	1.373	1.066	0.790	0.549	0.328	0.232
Energies from absolute argon measurements Mev	5.30	4.009	3.518	3.030	2.544	2.062	1.573			

make an ion pair increases with decreasing alpha-energy, in marked contrast to the behavior in the other gases.

C. Further Experimental Measurements Following Method of Gurney

We have made a series of measurements for the comparison of the relative ionization in argon and in air by essentially the same method as that used by Gurney, but covering a much larger range of alpha-energies. A collimating absorption cell (Fig. 1) allowed alpha-particles to pass through a perforated circular disk S into an ion chamber where they moved almost parallel to the surface of the collecting plate E. The ionization from each single alpha-particle was measured, both in argon and in air, by the method already described. The collimating chamber was an aluminum cylinder of 2.0-cm internal diameter and length 5.3 cm. The platinum plate P carrying the active polonium deposit was inserted at the base of the cylinder and was masked down by a plate with a circular aperture of 0.6 cm diameter. At the other end of the collimating cylinder the alpha particles passed into the ion chamber through the disk S pierced with a large number of small holes. These holes were 0.04 cm in diameter and covered a circular region 0.6 cm in diameter. This latter disk was covered with a gas-tight mica window M of about 0.6 mg/cm² equivalent thickness. A collimating aperture D half-way down the tube reduced the possibility of alpha-particles scattered from the walls emerging into the ion chamber.

The ionization for each group of alphas was measured, always relative to a standard polonium alpha-particle from a shallow collimating system C symmetrically placed with regard to the absorption cell, but diametrically opposite in the ion chamber. A small correction was always made here for the ions lost in the collimating holes.

The air admitted to the absorption cell was freed from moisture and carbon dioxide by passage through phosphorus pentoxide and potassium hydroxide tubes. From careful measurements of the temperature and pressure of the air in the cell, one could compute the relative air density, and hence the effective range absorbed by the air in the cell.

In Fig. 2, a curve is plotted from the above data. The ordinate for each point on the curve represents the ionization of a given alpha-particle relative to polonium in argon, and the abscissa represents the corresponding ionization value in air. For convenience, these values are expressed in "energies" calculated from a value for the polonium alpha of 5.298_4 Mev. The plot includes the samarium-polonium point, two runs with the

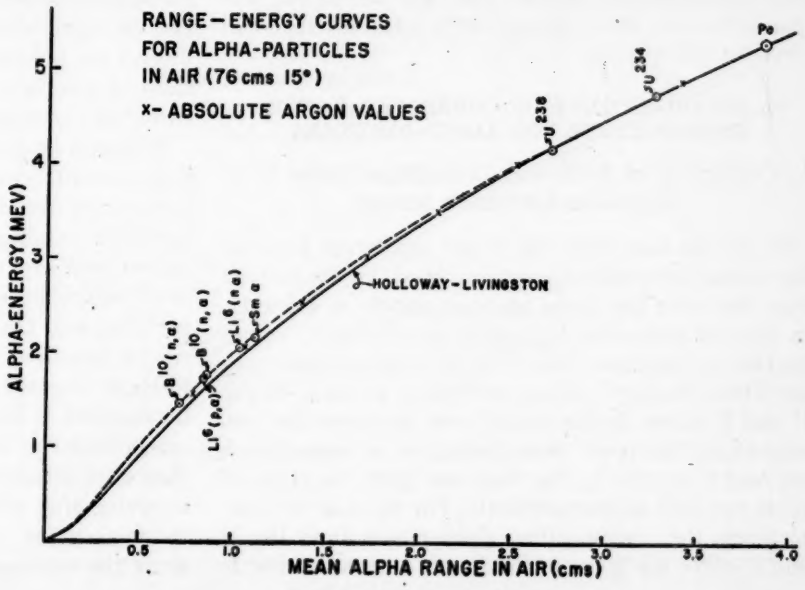

FIG. 3. A comparison of the H and L and H and L corrected range-energy curves.

TABLE III. Comparison of alpha-energies from range curves with independently determined energies.

Reaction	Range data Source	Range cm	α-energies derived from ranges H and L Mev	Corrected H and L Mev	Energies derived independently of ranges α-energy Mev	Q-value	Source
$B^{10}(n,\alpha)$	Bower, Bretcher, and Gilbert[a] (corr.)	0.73_5					
	O'Ceallagh and Davis[b]	0.71_5					
	Bøggild[c]	0.70_9					
	Mean	0.72_0	1.35_5	1.46_8	1.47_4	2.31_6	Chao, Lauritsen, and Tollestrup[h]
$B^{10}(n,\alpha)$(ground)	Bøggild[c]	0.846					
	O'Ceallagh and Davis[b]	0.89_0					
	Mean	0.86_8	1.64_9	1.76_0	1.77_9	2.79_4	Chao, Lauritsen, and Tollestrup[h]
$Li^6(n,\alpha)$	Bøggild and Minnhagen[d]	1.04	1.95_4	2.06_1	2.06_0	4.78_8	Tollestrup, Fowler, and Lauritsen[i]
$Li^6(p,\alpha)$	Neuert[e]	0.85	1.61_3	1.72_4	1.72_6	4.01_7	Tollestrup, Fowler, and Lauritsen[i]
Sm α	Cuer and Lattes[f]	1.12	2.10	2.19	2.18		J and S
U^{238} α	Wytzes and Van der Maas[g]	2.70_2	4.19_6	4.20_0	4.18_0		Clark, Spencer-Palmer, and Woodward[j]
U^{234} α	Wytzes and Van der Maas[g]	3.25_8	4.76_0	4.76_0	4.76_3		Clark, Spencer-Palmer, and Woodward[j]

[a] Bower, Bretscher, and Gilbert, Proc. Camb. Phil. Soc. 34, 290 (1938).
[b] C. O'Ceallagh and W. T. Davies, Proc. Roy. Soc. A 167, 81 (1938).
[c] J. K. Bøggild, Kgl. Danske, Vid. Sels. Math-Fys. Medd. 23, No. 4 (1945).
[d] J. K. Bøggild and L. Minnhagen, Phys. Rev. 75, 782 (1949).
[e] H. Neuert, Physik Zeits. 36, 629 (1935).
[f] P. Cuer and C. M. G. Lattes, Nature 158, 197 (1946).
[g] S. A. Wytzes and G. J. Van der Maas, Physica 13, 49 (1947).
[h] Chao, Lauritsen, and Tollestrup, Phys. Rev. 76, 586 (1949).
[i] Tollestrup, Fowler, and Lauritsen, Phys. Rev. 76, 428 (1949).
[j] Clark, Spencer-Palmer, and Woodward, British Atomic Energy Projects Reports BR-521, 522 (1944).

absorption cell with two windows each of about 0.63 mg/cm², and points from the Gray-Gurney determinations. Since Gurney's data do not include alphas with residual range greater than 2.0 cm in air (air "energy"=3.38 Mev) his highest point is fitted to the curve for this "energy."

II. ESTABLISHMENT OF CORRECTED RANGE-ENERGY CURVE FOR ALPHA-PARTICLES

A. Correction of Holloway-Livingston Curve from Argon-Air Ionization Ratios

As can be seen from Fig. 2 ,the agreement between the various determinations is very good. Values derived from the curve are shown more accurately in Table II. In the first horizontal row are shown "energy" values relative to polonium from ionization measurements in air. These "energy" values correspond to those on the H and L curve. In the second row are given the corresponding "energies" from ionization in argon which are read from Fig. 2. The third row gives the ratios of these two sets of measurements. For the sake of completeness the corresponding alpha-ranges from the H and L curve are given in the fourth horizontal row. It is at once apparent that the energy values determined in argon are in places more than 100 kev higher than the original ones determined in air. This discrepancy is particularly marked in the region of low alpha-energies, just the region where the H and L curve has been known to give too low energy values for various nuclear reactions. A complete plot of the H and L curve and the corrected curve are shown in Fig. 3.

It should be pointed out that so far no evidence has been presented to prove or disprove the essential correctness of the H and L curve in representing the ionization in air as a function of alpha-particle range. In our own experiments the absorption cell was used as a somewhat imperfect monochromator for alpha-particles, and the *ratio* of ionization for argon and air can be measured without any precise knowledge of the residual ranges. In fact, the only thing which needs to be assumed is the constancy of conditions within the monochromator during the period of the comparison. Hence the absolute accuracy of the derived argon curve in giving true energies can be no better than the absolute accuracy with which the H and L curve represents the corresponding relation for conditions in air.

B. Attempt to Establish Absolute Curve

An attempt has been made to determine an absolute range-ionization in argon curve for comparison with the above derived curve. This involves an accurate estimate of the residual range for each alpha-particle used and hence of the portion of the range absorbed in each case by the air cell and the mica window. Since the stopping power of mica is a function of the energy of the alpha-particle, any exact determination of the window correction becomes difficult.

An estimate of this variable correction was made experimentally by an auxiliary run supplementing our second run. An additional window, cut from the same small piece of mica, was put just before the original window, and a series of measurements in argon was again made with varying air pressures in the absorption cell. From the single and double window plots of ionization in argon, relative to polonium, against effective range absorbed by the air in the absorption cell, it was possible to determine extrapolated ionization values for a windowless cell.

One further small correction was made because of the fact that in the absorption cell with a slightly divergent beam of alpha-particles, the average path was greater than the geometrical length of the cell, 5.344 cm. This resulted in increasing this effective length by 0.35 percent. The range absorbed in the air of the cell was then calculated, subtracted from the mean range of the polonium alpha, 3.842 cm, to obtain the residual range in argon. From a plot of the extrapolated ionization in argon against such ranges the "energy" values shown in the last horizontal row of Table II were obtained, corresponding to the range values in row 4. These values are also shown as small crosses in Fig. 3.

The agreement between such values and those derived from the H and L curve in row 2 is only fair, the directly measured energy values being some 30 to 40 kev lower for the alpha-particles of lower energy. Such an energy difference would correspond to an underestimate of the absorbed range values for the direct measurement by about 0.015 cm. Considering the uncertainty of the window corrections, such an underestimate seems quite possible. Perhaps the principal value of the direct measurements is to exemplify the difficulties in determining range-energy curves by what seems at first glance the ideal method; i.e., direct range determinations in air from particles artificially accelerated in a high voltage apparatus.

C. Comparison of Original and Corrected Curves

In Fig. 3 is shown the original H and L curve as a full line and as a dashed line the corrected curve obtained from the H and L curve and the values given in Fig. 2 and Table II. For each H and L energy value, derived from ionization in air, is substituted the corresponding "energy" as measured from ionization in argon taken from Fig. 2. The absolute measurements in argon from Table II are shown as small crosses but no use was made of these values in drawing the corrected curve. It is believed, largely because of the uncertainties connected with the window correction, that these data are inherently less accurate than those derived from the apparently carefully constructed H and L curve and our argon-air ionization ratios.

It should be noted that Holloway and Livingston in the construction of their original curve used their ionization in air values only up to a range of 2.8 cm (4.3 Mev) and joined the lower curve to a curve extra-

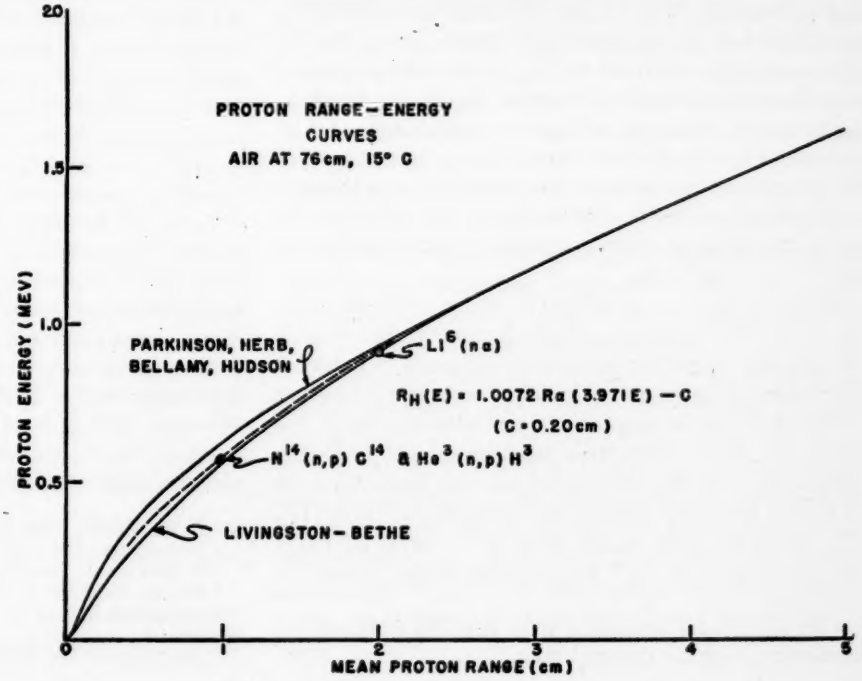

FIG. 4. A comparison of range-energy curves for protons.

TABLE IV. Comparison of proton energies from range curves with independently determined energies.

Reaction	Range Cm	Source	Derived energy from curves—Mev: Parkinson, Herb, Bellamy and Hudson	Livingston and Bethe	Corrected Livingston and Bethe	Independently determined energies Mev
$N^{14}(n,p)C^{14}$	0.991	Hughes and Eggler[a]	0.623	0.557	0.575	0.581
$N^{14}(n,p)C^{14}$	1.00	Cornog, Franzen, and Stephens[b]	0.627	0.561	0.579	0.581
$He^{3}(n,p)H^{3}$	0.980	Hughes and Eggler[a]	0.620	0.552	0.572	0.569
$Li^{6}(n,\alpha)H^{3}$	2.00	Bøggild and Minnhagen[c]	0.933	0.910	0.919	0.911[d]

[a] D. J. Hughes and C. Eggler, Phys. Rev. 73, 809 (1948).
[b] Cornog, Franzen, and Stephens, Phys. Rev. 74, 1 (1948).
[c] See footnote d of Table III.
[d] See footnote i of Table III.

polated from the accurately known range and energy values for alpha-particles of 5.3 Mev and above. Hence in the region from 4 to 5 Mev their curve is no longer a pure range-ionization in air curve, and it is a matter of judgment as to how large a correction should be here applied. Somewhat arbitrarily, therefore, no further corrections were applied above about 2.8-cm range and the corrected curve was made to merge into the original H and L curve smoothly at about this point. Had the full corrections been applied, this would have resulted in a raising of energy values in the region by about 20 kev. The drawing of the curve in this way is, in part, justified by the slightly better agreement obtained with the directly determined range and energy values for the alpha-particle from U^{234}, as shown below.

III. COMPARISON OF ENERGIES DERIVED FROM RANGE-ENERGY CURVES FROM KNOWN ALPHA-RANGES WITH INDEPENDENTLY DETERMINED ENERGIES

In Table III is shown a compilation of energy values derived from the H and L and H and L corrected curves from the use of alpha-particle ranges given in the literature. These derived energy values are compared with directly determined energies found elsewhere in the literature. It should perhaps be emphasized that the agreement here is, in most cases, an absolute one, since the corrected curve was not constructed to pass through any calibration points, but solely by the use of the H and L curve with our own corrections relating argon and air.

Where ranges are measured in some other gas than air, as is often the case in cloud-chamber work, a rather complicated correction must often be made in reducing the measured ranges to equivalent ranges in air, because of the variation in stopping power with energy of the gases used. Such a correction has been calculated for the alpha-range for the $B^{10}(n,\alpha)Li^{7*}$ reaction from the work of Bower, Bretcher, and Gilbert (reference a, Table III). The value has been raised from an uncorrected range of 0.70 cm to 0.735 cm.* This is not as large a correction as Gilbert[7] himself has recently suggested. For the other two values for $B^{10}(n,\alpha)$ and in the work of Bøggild and Minnhagen such corrections have apparently been made by the authors. In the older determination of Neuert for the range of the alpha-particle from the reactions $Li^{6}(n,\alpha)H^{3}$, carried out in a cloud chamber filled with hydrogen, apparently no correction of this sort was made. Hence this range value must be regarded as more uncertain. Account was, however, taken of the variation in stopping power with energy in a photographic emulsion by Cuer and Lattes[8] in the determination of the range in air of the alpha-particle from samarium. Their value is also in agreement with the older direct determination in air of 1.13 cm by Hosemann.[9]

It will be seen in vertical column 4, Table III, that the H and L curve gives, in general, much lower energy values than those derived from direct measurements (vertical column 6) made largely by the magnetic deflection of alpha-particles by the group† at the California Institute of Technology. On the other hand, the energy values derived from the ranges from the corrected H and L curve show an agreement with the absolute values far better than one has a right to expect. From the limited accuracy of the data, particularly the range measurements, an agreement within one percent would be very satisfactory. The almost exact agreement in several places is undoubtedly due purely to chance.

It should be noted that in the absence of absolute energy measurements for the alpha-particles from Sm, U^{238}, and U^{234}, energy values derived from relative ionization measurements in argon have been used. The direct comparison in argon for Sm with Po by Jesse and Sadauskis, already mentioned, has been used to obtain the energy value 2.18 Mev. Likewise, the values for U^{234} and U^{238} are taken from argon ionization comparisons. Clark, Spencer-Palmer, and Woodward[10] have found values of 4.763 and 4.180 Mev for these two

* We are indebted to Professor H. A. Bethe for a private communication giving this corrected value.

[7] C. W. Gilbert, Proc. Camb. Phil. Soc. 44, 447 (1948).
[8] See reference f of Table III.
[9] R. Hosemann, Zeits. f. Physik 99, 405 (1936).
† We are indebted to Professor W. A. Fowler for a private communication giving us these values before their formal publication.
[10] See reference j of Table III.

alpha-particles. It should be pointed out that the correctness of these energy values depends upon the assumption as to a direct proportionality between ionization in argon and energy, which is just the same assumption upon which rests the correctness of the energy values given by the corrected range-energy curve. Hence any agreement between the values in columns 5 and 6 does not, for the last three values, indicate in itself that these are necessarily the true energy values corresponding to the given ranges. The agreement does indicate, however, the consistency of the various argon ionization measurements.

IV. DERIVED PROTON RANGE-ENERGY CURVE

In the region above 0.3 Mev, Livingston and Bethe[11] have derived a range energy relation for the proton from that of the alpha-particle by the use of the equation $R_H(E)=1.0072R\alpha(3.971E)-C$. This equation is simply an expression of the fact that two particles of unequal masses lose energy at the same rate for equal velocities, and that the rate of loss of energy is proportional to the square of the particle charge. $R\alpha$ and R_H denote, respectively, the corresponding alpha- and proton ranges and $C=0.20$ cm is an empirical constant introduced from the cloud-chamber measurements of Blackett to account for the difference in behavior of protons and alpha-particles at low energies. Here, because of the capture and loss of electrons, the charge ratio between the alpha-particle and proton does not remain precisely two to one.

Since the proton range-energy curve was based on the corresponding alpha-curve, any change in the latter obviously necessitates a change in the former. Accordingly, the proton curve has been recalculated with the values for the corrected H and L curve substituted for the older values. As shown in Fig. 4, the corrected curve in the region of 0.5 Mev is about 20 kev higher than the former Livingston and Bethe curve, but is still lower than the experimental curve of Parkinson, Herb, Bellamy, and Hudson.[12]

The relation between these curves is best shown in Table IV where the derived energies from known range values are compared with directly determined energies. In the first three horizontal rows, proton ranges from cloud-chamber determinations for the (n,p) reactions for N^{14} and He^3 are used to determine the energies from each of the three range-energy curves. These derived energies are to be compared with the corresponding energies calculated from the $(n-H^1)$ mass difference. In these calculations $(n-H^1)$ was somewhat arbitrarily chosen[13,14] as 0.778 Mev and the C^{14} and H^3 β-end points were taken to be 155 and 19 kev, respectively.

TABLE V. Alpha-energy values for tabulated mean ranges in air 15° and 760 mm.

Mean ranges cm	Alpha-energies Mev	Interpolation differences	Mean ranges cm	Alpha-energies Mev	Interpolation differences
0.20	0.271		2.2	3.668	
		0.111			0.117
0.25	0.382		2.3	3.785	
		0.126			0.111
0.30	0.508		2.4	3.896	
		0.127			0.107
0.35	0.635		2.5	4.003	
		0.126			0.100
0.40	0.761		2.6	4.103	
		0.121			0.097
0.45	0.882		2.7	4.200	
		0.112			0.100
0.50	0.994		2.8	4.300	
		0.111			0.100
0.55	1.105		2.9	4.400	
		0.109			0.102
0.60	1.214		3.0	4.502	
		0.106			0.100
0.65	1.320		3.1	4.602	
		0.102			0.100
0.70	1.422		3.2	4.702	
		0.103			0.096
0.75	1.525		3.3	4.798	
		0.099			0.093
0.80	1.624		3.4	4.891	
		0.099			0.096
0.85	1.723		3.5	4.987	
		0.093			0.092
0.90	1.816		3.6	5.079	
		0.092			0.090
0.95	1.908		3.7	5.169	
		0.087			0.091
1.00	1.995		3.8	5.260	
		0.167			0.090
1.10	2.162		3.9	5.350	
		0.159			0.090
1.20	2.321		4.0	5.440	
		0.149			0.087
1.30	2.470		4.1	5.527	
		0.153			0.087
1.40	2.620		4.2	5.614	
		0.147			0.084
1.50	2.767		4.3	5.698	
		0.140			0.085
1.60	2.907		4.4	5.783	
		0.137			0.086
1.70	3.044		4.5	5.870	
		0.130			0.083
1.80	3.174		4.6	5.953	
		0.132			0.082
1.90	3.306		4.7	6.035	
		0.129			0.085
2.00	3.425		4.8	6.120	
		0.124			0.082
2.10	3.549		4.9	6.202	
		0.119			0.081
			5.0	6.281	

The energy values computed on the basis of the value of $(n-H^1)$ chosen agree very well with the values derived from ranges for the corrected Livingston and Bethe curve, but the energy values from their original curve are almost 20 kev too low. The Parkinson, Herb, Bellamy, and Hudson curve give definitely higher values.

In the last row of the table is given the comparison from the cloud-chamber determination of Bøggild and Minnhagen for the range 6.00 cm of the tritium particle in the reaction $Li^6(n,\alpha)H^3$. The equivalent range for a corresponding proton is 2.00 cm. The corresponding energy as calculated from the work of Tollestrup, Fowler, and Lauritsen (see footnote i of Table III) for a Q-value of 4.788 Mev is 0.911 Mev. Since the corrected and uncorrected Livingston and Bethe curves converge at about this point, the curves give very nearly the same energy value, both showing good agreement with the absolute determination.

The relation used to derive the proton curve is obviously inexact at low energies, since for energies near zero it would give a negative proton range. The equation, therefore, has not been used for proton energies less than 0.3 Mev. A plausible curve can, of course, be extrapolated to the origin, falling slightly higher than the original Livingston-Bethe curve, but such a procedure can hardly give very exact values. Hence no values have been computed for energies lower than 0.3 Mev.

[11] M. S. Livingston and H. A. Bethe, Rev. Mod. Phys. **9**, 245 (1937).
[12] Parkinson, Herb, Bellamy, and Hudson, Phys. Rev. **52**, 75 (1937).
[13] Shoupp, Jennings, and Sun, Phys. Rev. **75**, 1 (1949).
[14] Taschek, Jarvis, Argo, and Hemmendinger, Phys. Rev. **75**, 1268 (1949).

TABLE VI. Proton energies as a function of mean proton range in air at 15° and 760 mm.

Mean proton ranges cm	Proton energies Mev	Interpolation differences	Mean proton ranges cm	Proton energies Mev	Interpolation differences
0.4	0.302		2.7	1.103	
		0.055			0.025
0.5	0.357	0.049	2.8	1.128	0.026
0.6	0.406	0.047	2.9	1.154	0.025
0.7	0.453	0.046	3.0	1.179	0.023
0.8	0.499	0.042	3.1	1.202	0.024
0.9	0.541	0.040	3.2	1.226	0.024
1.0	0.581	0.038	3.3	1.250	0.024
1.1	0.619	0.037	3.4	1.274	0.022
1.2	0.656	0.036	3.5	1.296	0.022
1.3	0.692	0.036	3.6	1.318	0.022
1.4	0.728	0.036	3.7	1.340	0.022
1.5	0.764	0.032	3.8	1.362	0.022
1.6	0.796	0.031	3.9	1.384	0.022
1.7	0.827	0.032	4.0	1.406	0.022
1.8	0.859	0.030	4.1	1.428	0.022
1.9	0.889	0.030	4.2	1.450	0.021
2.0	0.919	0.029	4.3	1.471	0.021
2.1	0.948	0.029	4.4	1.492	0.021
2.2	0.977	0.025	4.5	1.513	0.021
2.3	1.002	0.025	4.6	1.534	0.020
2.4	1.027	0.024	4.7	1.554	0.020
2.5	1.051	0.026	4.8	1.574	0.020
2.6	1.077	0.026	4.9	1.594	0.020
			5.0	1.614	

V. RANGE-ENERGY TABLES FOR PROTONS AND ALPHA-PARTICLES

For useful reference the results for these alpha- and proton range-energy relations are shown in Tables V and VI. Here the corresponding energies are given for mean ranges increasing in equal steps. All range values are given for air at 15°C and 760-mm pressure. For convenience, interpolation values are tabulated showing the energy change for the range interval indicated, that is, the average slope of the range-energy curve at this point. Parenthetically, it may be noted that the use of such slopes on the range-energy curve provides probably the most accurate method of determining energies from range data, provided one has a standard particle of known energy for comparison. Thus, if one measures experimentally the small difference between the ranges of an unknown and known alpha-particle, then the energy difference between the two alphas may be computed from the slope of the range-energy curve in this region and the final result may be fairly accurate, even though the range-energy curve may give incorrect absolute energy values.

It is believed that the energy values for alpha-particles in Table V are accurate to within about 30 kev below 1 Mev and to 20 kev thereafter. The estimation of error in the proton values is more difficult, since the only calibration points in the low energy region depend on the value of $(n-H^1)$ for which there is still some degree of uncertainty. The comparatively large empirical constant $C=0.2$ cm in the transformation equation also offers an additional uncertainty. Unless, however, the true value of $(n-H^1)$ should prove eventually to be quite different from the value 778 kev assumed, it is believed that the energy values given are accurate to within 20 kev. Similar range-energy curves have recently been constructed by H. A. Bethe and are to be found in a publication of the Brookhaven National Laboratory. These are in good agreement with the present work. This is rather to be expected since the data used and the methods of construction are almost the same.

ACKNOWLEDGMENTS

It is a pleasure to express our thanks to Professor H. A. Bethe and Dr. Francis R. Shonka for many stimulating discussions of this subject. Our thanks are also due to Mr. L. C. Ellsworth for his skillful construction of the ionization chambers used.

Disintegration of Te^{121} and Te^{123} Isomers*

ROBERT KATZ,** R. D. HILL, AND M. GOLDHABER
Department of Physics, University of Illinois, Urbana, Illinois
(Received December 29, 1949)

Line intensities in the conversion electron spectra of Te^{121} and Te^{123} were evaluated in a variable field, 180° focusing beta-ray spectrograph. Electron-electron coincidences were obtained between the transition pairs 82–213 kev in Te^{121} and 88.5–159 kev in Te^{123}. Decay schemes for the two isomers are shown.

INTRODUCTION

THE disintegration of Te^{121} and Te^{123} isomers has been studied (a) through the activity of the tellurium fraction chemically separated from deuteron bombarded antimony and, (b) through the activity induced by pile bombardment of a Te sample enriched in Te^{122}. Sources of type (a) had been shown to exhibit: a 120–143 day activity;[1,2] a 16–17 day activity[2] interpreted as K-capture from the ground state of Te^{121} to the 610 kev excited state[3] of Sb^{121}; a "two-step" isomeric transition;[3,4] conversion electrons corresponding to 82, 88.5, 159, and 213 kev transitions.[5] Conversion electrons corresponding to 88.5 and 159 kev transitions were found in a type (b) source.[6]

We have sought to establish that both isomers, Te^{121} and Te^{123}, decay to the ground state in two steps by showing that there are coincidences between transitions. In order to aid in the construction of a decay scheme we also endeavored to determine the conversion coefficients.

COINCIDENCE MEASUREMENTS

By means of coincidence measurements in a "double slit" beta-ray spectrograph, electrons from the 82 and 213 kev transitions were shown to be in coincidence with each other. Similarly conversion electrons from the 88.5 and 159 kev transitions were also shown to be in coincidence. Coincidence rates obtained were 1.4 ± 0.05 c/m for the former pair and 3.3 ± 0.13 c/m for the latter pair with chance rates of 0.03 and 0.04 c/m, respectively. As different slit openings were used in these two determinations, the rates are only illustrative of magnitude of coincidences which can be achieved in a "double-slit" beta-ray spectrograph. The spectrograph insert used for these experiments is shown in Fig. 1. A different type of "double-slit" spectrograph has been previously described by Feather, Kyles and Pringle.[7]

Electron-gamma coincidences were also measured with a similar arrangement to Fig. 1, except that the gamma-ray counter was mounted directly behind the source. These experiments showed the existence of 159

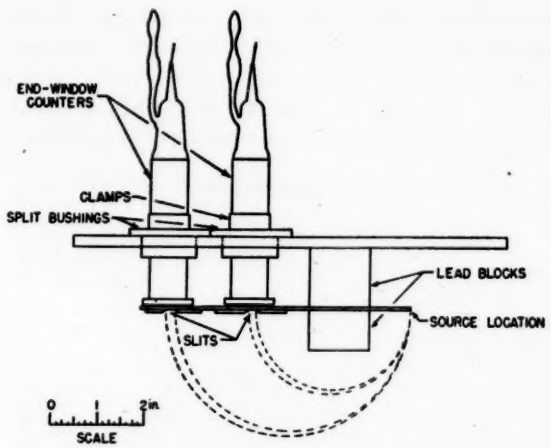

FIG. 1. Electron-electron coincidence insert.

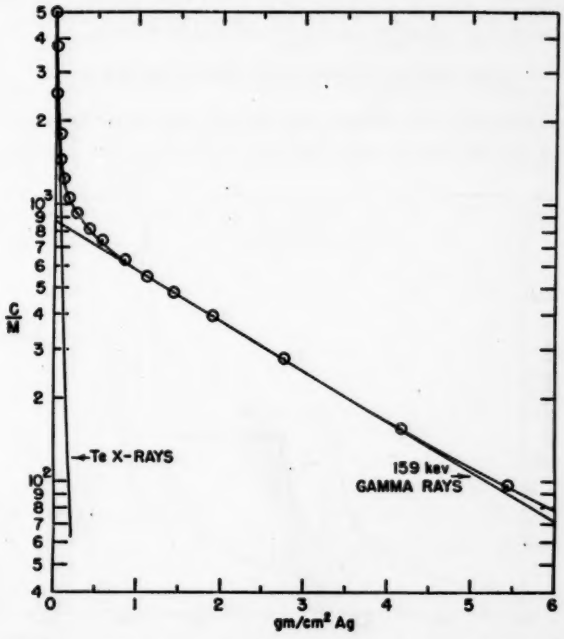

FIG. 2. Silver absorption of Te^{123} x-rays and gamma-rays.

* Assisted by the Joint Program of ONR and AEC.
** AEC Predoctoral Fellow; present address: Kansas State College, Manhattan, Kansas.
[1] Seaborg, Livingood, and Kennedy, Phys. Rev. **57**, 363 (1940).
[2] J. E. Edwards and M. L. Pool, Phys. Rev. **69**, 140 (1946).
[3] Burson, Bittencourt, Duffield, and Goldhaber, Phys. Rev. **70**, 566 (1946).
[4] Bittencourt and M. Goldhaber, Phys. Rev. **70**, 780 (1946).
[5] R. D. Hill and J. W. Mihelich, Phys. Rev. **74**, 1847 (1948).
[6] R. D. Hill, Phys. Rev. **76**, 333 (1949).
[7] Feather, Kyles, and Pringle, Proc. Phys. Soc. London **61**, 466 (1948).

TABLE I. Relative intensities of conversion lines of Te^{121} and Te^{123}.

Isomer	Conversion line	Area under line (arbitrary units)	Peak height (arbitrary units)	Relative* intensity
Te^{121}	82-K	3420±850	306±26	75
Te^{121}	82-L	3930±980	473±26	100
Te^{121}	82-M	560±140	107±32	18
Te^{121}	213-K	371±37	108±7	16
Te^{121}	213-L	53±5	14±5	2.2
Te^{123}	88.5-K	2430±600	253±23	57
Te^{123}	88.5-L	3510±880	374±25	84
Te^{123}	88.5-M	560±140	115±21	19
Te^{123}	159-K	600±60	153±8	24
Te^{123}	159-L	61±6	19±8	2.8

* *Note:* The relative intensities of the lines of Te^{121} compared to those of Te^{123} are significant only for a particular source and change with time due to the different decay periods of the two isomers.

and 213 kev gamma-radiation in coincidence with electrons from the 88.5 and 82 kev transitions, respectively. The existence of the unconverted 159 kev gamma-radiation, which had previously not been reported, was demonstrated by absorption of the gamma radiation from the source (b). Figure 2 shows the absorption of the 159 kev gamma-ray in silver. There is no indication of the 88.5 kev gamma-rays, and one can conclude that this transition is nearly completely internally converted.

Since Hill and Mihelich[5] had observed conversion lines which might be interpreted as L and M lines of a 36.5 kev transition, we also looked for unconverted 36.5 kev gamma-rays in both Te^{121} and Te^{123}. Using a xenon-filled counter to emphasize radiation of this energy and by means of matched barium and iodine absorbers we could show that, if present, this gamma-radiation was of intensity less than two percent of the total x- and gamma-radiation of either source.

ELECTRON INTENSITY MEASUREMENTS

The conversion electron spectrum of a type (a) source was studied in a variable field, 180° focusing beta-ray spectrometer with a thin end window counter (0.9 mg/cm² mica) as detector. The spectrum obtained is shown in Fig. 3. Window correction data were obtained by placing a sheet of mica (1.9 mg/cm²) over the counter and re-determining the peak intensities of the conversion lines. The correction data were in good agreement with the published curve of Feather, Kyles, and Pringle.[7] Line intensities were obtained by averaging the relative intensities obtained by two methods of evaluation. It has been shown by Lawson and coworkers[8,9] that both the peaks of the experimental lines, and the areas under the normalized lines (that is, the experimental data divided by the focusing magnetic field) should yield identical results. A complication, however, is introduced by scattering. Source scattering removes electrons from the peaks, and scattering from the source backing adds electrons to the low energy tails. Thus relative intensities determined on peak analysis may be expected to be too low, while values based on area analysis may be too high. The average values of the relative line intensities obtained by the two methods of analysis may be expected to be closer to the true values and these are shown in Table I. These values were used to compute conversion coefficients and N_K/N_L ratios. Computation of the conversion coefficients was based on the assumption of complete conversion of the parent 82 and 88.5 kev transitions. A separate investigation of the spectrum (not shown in Fig. 3) was made to determine the intensity of conversion electrons of the 610 kev transition in Sb^{121}.

The comparison of experimental and theoretical results is given in Table II. In general, they confirm the earlier observations based on photographic intensity measurement.[5,6] However, the conclusions with regard to the 213 kev transition are notably clearer. For the 159 and 213 kev transitions the K-shell conversion coefficients are consistent with purely 2^1 magnetic radi-

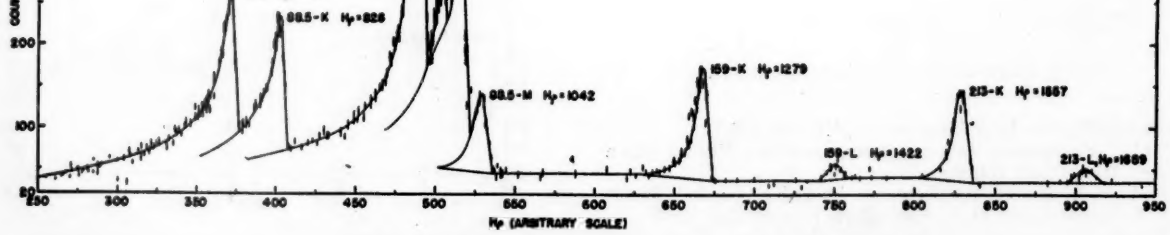

FIG. 3. Conversion electron spectra of Te^{121} and Te^{123}.

[8] J. L. Lawson and A. W. Tyler, Rev. Sci. Inst. 11, 17 (1940).
[9] J. L. Lawson and J. M. Cork, Phys. Rev. 57, 982 (1940).

TABLE II. Comparison of experimental and theoretical results.

Isomer	Transition energy (kev)	Lifetime (sec.) Experimental $\times(1+Ne/N\gamma)$	Lifetime (sec.) Theoretical†	N_K/N_L Experimental	N_K/N_L Theoretical	N_K/N_γ Experimental	N_K/N_γ Theoretical
Te^{121}	82	1.0×10^{10}	5.6×10^{11} ($l=5$)	0.75±0.10	2.85, 2^4 mag.* 0.06, 2^5 el.*		375, 2^4 mag.* 470, 2^5 el.*
	213		1.1×10^{-9} ($l=2$)	7.3±0.3	11.8, 2^1 mag.** 7.11, 2^2 el.*	0.085±0.035	0.084, 2^1 mag.*** 0.097, 2^2 el.***
Te^{123}	88.5	0.6×10^{10}	2.4×10^{11} ($l=5$)	0.68±0.10	3.3, 2^4 mag.* 0.1, 2^5 el.*		300, 2^4 mag.* 375, 2^5 el.*
	159		5.1×10^{-9} ($l=2$)	8.9±0.8	11.9, 2^1 mag.** 6.1, 2^2 el.*	0.18±0.08	0.175, 2^1 mag.*** 0.27, 2^2 el.***
Sb^{121}	610		7.0×10^{-12} ($l=2$)			0.004±0.002	0.004, 2^2 el.***

† Theoretical lifetimes have been calculated from the formula used by Axel and Dancoff, Phys. Rev. 75, 1297 (1949).
* Theoretical values of N_K/N_L have been obtained from the analyses of Hebb and Nelson (see reference 11) and Drell (see reference 12).
** Theoretical values of N_K/N_L have been obtained from curves of Lowen and Tralli (see reference 13).
*** Theoretical values of N_K/N_γ have been obtained from the tables computed by Rose and others (see reference 10).

ations. Theoretical values here used are the accurate numerical values obtained by Rose and others.[10] For the N_K/N_L ratios of the same transitions, however, the experimental values lie between those for 2^1 magnetic and 2^2 electric. S. Frankel, of this Department, has been unable to confirm the existence of the previously[4] reported delayed transition in a source of type (a). He used scintillation counters, which should be more reliable in this lifetime region than Geiger-Müller counters, and finds an upper limit of 2×10^{-8} sec. for the half-lives of the 213 and 159 kev excited states.*

Theoretical values used for analysis here were obtained from the approximate analytical expressions derived by Hebb and Nelson[11] and by Drell,[12] and also from the curves of Lowen and Tralli.[13] No assignments of the proportions of magnetic to electric radiations will be made from these values as it appears probable that both theory and experiment are not sufficiently accurate at this stage. The decay schemes proposed for the Te^{121} and Te^{123} isomers are shown in Fig. 4.

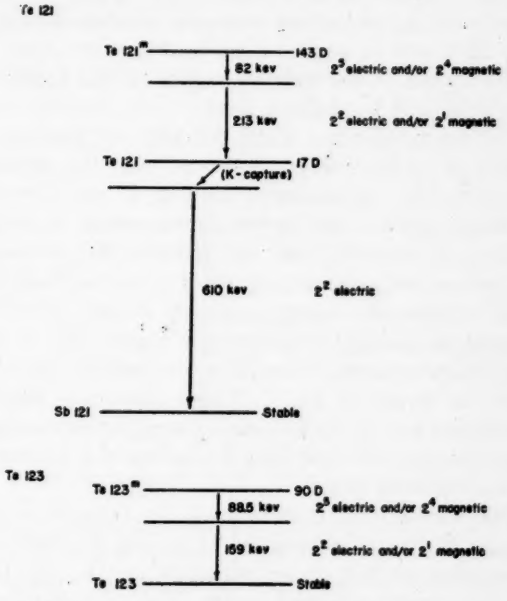

FIG. 4. Proposed decay schemes of Te^{121} and Te^{123} isomers.

[10] M. E. Rose *et al.*, "Tables of *K*-shell conversion coefficients" (privately distributed).

* *Note added in proof:* See also M. Deutsch and W. E. Wright, Phys. Rev. 77, 139 (1950).

[11] M. H. Hebb and E. Nelson, Phys. Rev. 58, 486 (1940).

[12] S. D. Drell, Phys. Rev. 75, 132 (1949); S. D. Drell, Ph.D. thesis, University of Illinois (1949).

[13] I. S. Lowen and N. Tralli, Phys. Rev. 75, 529 (1949).

Relative Yield Functions for π^--Mesons from Carbon*

STANLEY B. JONES AND R. STEPHEN WHITE
Radiation Laboratory, Department of Physics, University of California, Berkeley, California
(Received December 28, 1949)

This paper describes determinations of the relative yield curves for π^--mesons generated by alpha-particle and proton beams striking carbon targets. The mesons counted had energies of 2–10 Mev and angles to the beam direction up to about 45°.

THE artificial production of mesons has made possible the determination of meson yield as a function of the energy of the bombarding particle. This paper reports such determinations for π^--mesons generated by the Berkeley 184-inch cyclotron with both proton and alpha-particle beams incident upon a carbon target with the restriction that only mesons of energies 2–10 Mev and of angle to the beam up to about 45° were counted. A preliminary report of this study has been published in abstract form.[1]

The beam energies were selected by placing the targets at predetermined distances from the center of the cyclotron. As indicated in Fig. 1, the π-mesons produced at the target move approximately in circular orbits in the magnetic field. In particular, the π^--mesons circulate in the counterclockwise direction as illustrated. Some of the low energy ones are slowed down and stopped in stacked photographic plates placed from four inches to seven inches from the leading edge of the target as shown in Fig. 2. These plates are then examined for meson tracks over an area corresponding to meson energies of 2–10 Mev by means of a microscope with a traveling stage.

The bombardments were made by using the carbon targets illustrated schematically in Fig. 2. The target dimensions in the plane perpendicular to the beam direction are 1 inch by 3 inches. The thickness for the alpha-particle beam was $\frac{1}{16}$ inch with an exposure time of 20 minutes and for the proton beam, $\frac{1}{32}$ inch with an exposure time of 30 seconds. Most of the mesons originate from the small target area, measuring 1 inch along the leading edge by $\frac{1}{8}$ inch perpendicular to the edge, which first intercepts the beam, since this region is most intensely bombarded by the cyclotron beam. This was found by monitoring the target with thin polystyrene.

The integral of the beam-current was obtained by observing the relative amounts of C^{11} formed in the $C^{12}(\alpha,\alpha n)C^{11}$ and $C^{12}(p,pn)C^{11}$ reactions for the alpha-particle and proton bombardments, respectively, through measurement of the positron activity of C^{11} which has a half-life of 20.5 minutes. A correction was made for the decay of the C^{11} activity in the target during the bombardment by alpha-particles. A correction for the variation of the cross section for $C^{12}(\alpha,\alpha n)C^{11}$ [2] and $C^{12}(p,pn)C^{11}$ [3] with energy was also included.

For this work, Ilford 50 micron C-2 and Eastman 100 micron NTB nuclear emulsions on standard 1-inch by 3-inch glass plates were used for the alpha-particle and proton exposures, respectively. At each beam energy, a single plate from the center of a stack of at least five plates was selected for study. Each plate was scanned to a depth of 2 mm from the leading edge for a measured distance along the edge. Nearly identical areas were scanned on the plates for the various beam energies and meson density over the scanned and adjacent areas did not change rapidly. The number of mesons counted in each case was corrected for the corresponding integrated beam current, plate thickness, and area scanned.

The apparatus was selective for π^--mesons. However, positive mesons might possibly have entered the plates

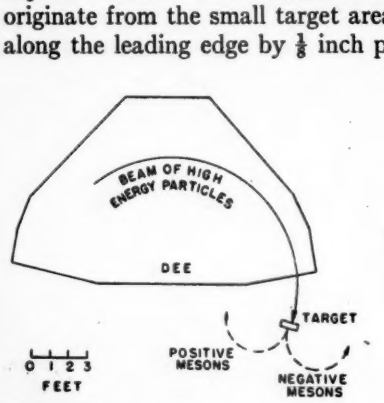

FIG. 1. Plan view of cyclotron (meson trajectories enlarged).

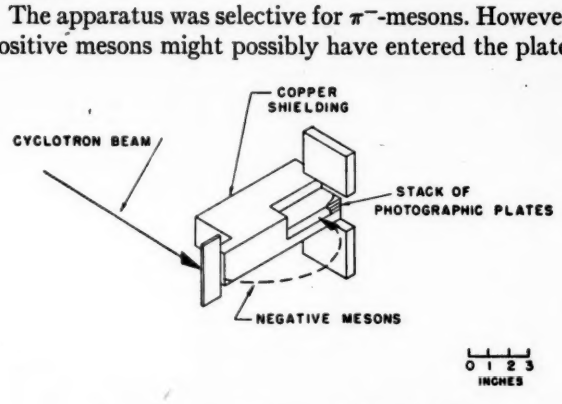

FIG. 2. Schematic diagram of plate holder.

* This paper is based on work performed under the auspices of the AEC.

[1] S. B. Jones and R. S. White, Phys. Rev. **75**, 1468 (1949); Phys. Rev. **76**, 588 (1949).

[2] R. L. Thornton and R. W. Senseman, Phys. Rev. **72**, 872 (1947).

[3] Aamodt, Peterson, and Phillips (to be published).

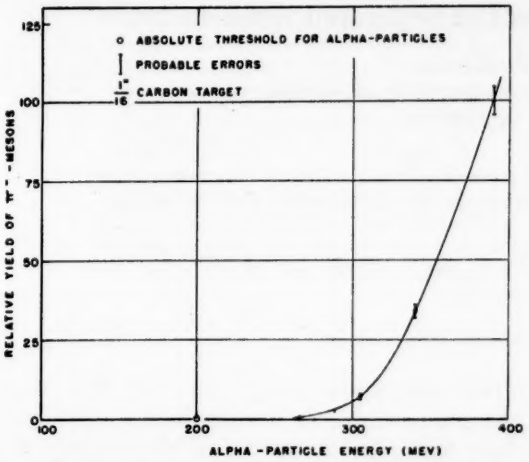

FIG. 3. Meson excitation curve for alpha-particles normalized to 100 at 390 Mev with a meson energy interval of 2–10 Mev.

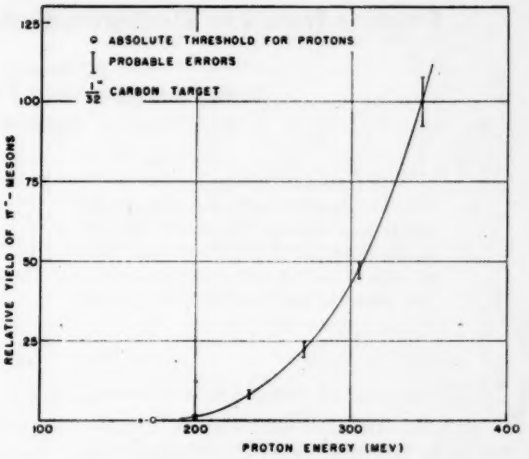

FIG. 4. Meson excitation curve for protons, normalized to 100 at 345 Mev with a meson energy interval of 2–10 Mev.

and it is certain that some μ-mesons entered the plates. In order to include only π^--mesons, we counted only σ-mesons (star forming mesons). Since few, if any, μ^--mesons form stars,[4,5] the total number of π^--mesons in the energy interval examined will then be proportional to the number of σ-mesons since a fixed fraction of π^--mesons form stars.[6]

The data are given in Table I.

Plots of the data in the tables are given in Figs. 3 and 4. W. H. Barkas, by the method of energy and momentum balance, has calculated the absolute minimum threshold for meson production using the most favorable reactions.[7] These are indicated in the figures.

It should be emphasized that this study does not give the relative total cross section for π^--meson production but only the relative yields in a particular meson energy interval. V. Peterson[8] measured an absolute differential cross section for π^--mesons produced by 390-Mev alpha-particles on a $\frac{1}{4}$-inch carbon target. For π^--mesons of energy 2–5 Mev and of angles with the beam direction up to about 45° he found a value of $3.0\pm0.8\times10^{-32}$ cm^2 Mev^{-1} steradian^{-1} per carbon nucleus. Richman and Wilcox[9] measured a value of $2.1\pm0.6\times10^{-28}$ cm^2 steradian^{-1} per carbon nucleus at 90 degrees to the beam direction for the combined cross section for both π^--mesons and π^+-mesons produced by 345-Mev protons on carbon.

TABLE I. Data on mesons from carbon.

Beam energy	No. σ-mesons observed	Relative volume scanned	Relative integrated beam current	Corrected relative yield
		I. Alpha-particle beam		
390	241	1.00	1.00	100 percent
340	109	0.740	1.80	34
305	24	0.797	1.87	7
265	4	0.806	3.85	0.5
		II. Proton beam		
345	75	1.00	1.00	100 percent
305	126	1.08	3.30	47
270	46	0.794	3.57	22
235	19	0.944	3.46	8
200	3	1.12	3.76	1
165	0	1.23	1.97	0

The authors are indebted to Professor Ernest O. Lawrence for his continued interest in this work. We also wish to thank Professor R. L. Thornton and Drs. Eugene Gardner, C. M. G. Lattes, and Hugh Bradner for much helpful discussion. We are very grateful to James Vale and the cyclotron crew for making the bombardments.

[4] W. Y. Chang, Rev. Mod. Phys. **21**, 166 (1949).
[5] Goldschmidt, Clermont, King, Muirhead, and Ritson, Proc. Phys. Soc. London **61**, 183 (1948).
[6] F. L. Adelman and S. B. Jones, Phys. Rev. **75**, 1468 (1949).
[7] W. H. Barkas, Phys. Rev. **75**, 1109 (1949).
[8] V. Peterson, private communication.
[9] C. Richman and H. Wilcox, Phys. Rev. **78**, 85 (1950).

Protons from the Deuteron Bombardment of Separated Neon Isotopes*

A. ZUCKER AND W. W. WATSON
*Sloane Physics Laboratory, Yale University,** New Haven, Connecticut*
(Received December 16, 1949)

With neon gas enriched either to 93 percent Ne^{22} or to 99 percent Ne^{20} we confirm the observations with less well-concentrated isotopes by Elder, Motz, and Davison on the $Ne^{20}(d,p)Ne^{21}$ and $Ne^{22}(d,p)Ne^{23}$ reactions. Aided by the enrichment factor of 3 for Ne^{21} in the "heavy" neon, we find a long-range proton group from $Ne^{21}(d,p)Ne^{22}$ with a Q of 6.79±0.10 Mev for the reaction. Consideration of these and other reactions involving neon isotopes show that the mass of Ne^{21} is 21.00062±0.00010 and that this new proton group indicates an excited state at 1.37 Mev in the Ne^{22} nucleus.

WITH targets of neon gas containing either 93 percent Ne^{22} or 99 percent Ne^{20} we have repeated the deuteron bombardment experiments most recently carried out in this laboratory by Elder, Motz, and Davison.[1] Our measurements with these better-separated isotopes completely confirm their observations on the $Ne^{20}(d,p)Ne^{21}$ and $Ne^{22}(d,p)Ne^{23}$ reactions. In addition, even though the Ne^{21} content in this "heavy" gas had been enriched to only about 0.75 percent, or a factor of three, we have succeeded in locating a long-range proton group from the reaction $Ne^{21}(d,p)Ne^{22}$ with the Ne^{22} nucleus in an excited state 1.37 Mev above ground.

These isotope enrichments were produced in a multistage thermal diffusion apparatus.[2] The gas pressure in the target box was about 16 cm of Hg for the investigation of the proton groups from the bombardment of Ne^{20} and Ne^{22}, and about 70 cm of Hg in the search for the elusive protons from $Ne^{21}(d,p)Ne^{22}$. In the bombardment region the deuterons had an energy of 2.9 Mev for the first reactions, but an energy of 3.12 Mev for the study of the $Ne^{21}(d,p)Ne^{22}$ reaction since the entrance foil was then thinner. Hot calcium shavings were used to remove any air contamination in the neon. Our failure to detect any trace of the ubiquitous long-range group of protons from $N^{14}(d,p)N^{15}$ indicated that this purification was fairly complete. The emitted protons were counted in all cases only at 90° with the incident beam, by means of a single proportional counter.

TABLE I. Reaction energies and energy levels of the neon isotopes.

	Proton range (cm)	Q(Mev)	Energy level (Mev)
$Ne^{20}(d,p)Ne^{21}$	24.04	1.68±0.07	2.82
	35.26	2.73±0.06	1.77
	53.62	4.19±0.07	0.31
	57.96	4.50±0.09	ground
$Ne^{21}(d,p)Ne^{22}$	103.0	6.79±0.10	1.37
$Ne^{22}(d,p)Ne^{23}$	19.31	1.13±0.10	1.75
	26.73	1.90±0.07	0.98
	37.42	2.88±0.06	ground

The yields of protons of various energies for the Ne^{20} and Ne^{22} bombardments are shown in Fig. 1. Comparison of the two curves shows clearly which proton groups are to be assigned to each isotope. In particular, it is quite evident that both members of the partly resolved double group of longest range belong to $Ne^{20}(d,p)Ne^{21}$, thus fixing with fair precision the ground-state Q-value for this reaction. The extrapolated ranges and calculated Q-values for each of these proton groups are assembled in Table I. Although we find no indication of a still-longer-range proton group from the Ne^{21} bombardment, we conclude from the argument given below that the single low-intensity group with an extrapolated mean range of 103±2 cm does not involve the ground state of the resulting Ne^{22} nucleus.

It is of interest to see whether these and the other reactions depicted in Fig. 2 lead to a consistent set of masses for the neon isotopes. The most accurately known neon mass is that of Ne^{20}. Mattauch and Flammersfeld in their recently published survey[3] give the value 19.99890±0.000047 for this mass. The Q for the reaction $Na^{23}(p,\alpha)Ne^{20}$ is +2.14±0.07 Mev, or 0.00230 atomic mass units.[4] This Q plus the Ne^{20} mass just quoted give 22.99697 for the mass of Na^{23}. The $Na^{23}(d,\alpha)Ne^{21}$ reaction[5] has a Q equivalent to +0.00725 mass units. With 22.99697 for the mass of Na^{23}, this leads to a value 21.00056 for the mass of Ne^{21}. Based on the 19.99890 Ne^{20} mass, our Q of 4.50±0.09 Mev for the $Ne^{20}(d,p)Ne^{21}$ reaction gives 21.00067 for the mass of Ne^{21}. These two values for the mass of Ne^{21} agree well within their probable errors, and they exactly straddle the value 21.00062±0.00009 calculated by Mattauch and Flammersfeld from all available data.

With this Na^{23} mass and the maximum β-ray energy of 4.3±0.3 Mev (corrected)[6] reported by Pollard and

* Part of a dissertation to be submitted by A. Zucker in partial fulfillment of the requirements for the degree of Doctor of Philosophy at Yale University.
** Assisted by the AEC.
[1] Elder, Motz, and Davison, Phys. Rev. **71**, 917 (1947).
[2] Watson, Onsager, and Zucker, Rev. Sci. Inst. **20**, 924 (1949).
[3] J. Mattauch and A. Flammersfeld, Zeits. f. Naturforschung (special issue) (1949).
[4] J. M. Freeman and A. S. Baxter, Nature **162**, 696 (1948).
[5] E. B. M. Murrell and C. L. Smith, Proc. Roy. Soc. **173**, 410 (1939).
[6] E. Bleuler and W. Zünti, Helv. Phys. Acta, **19**, 375 (1946).

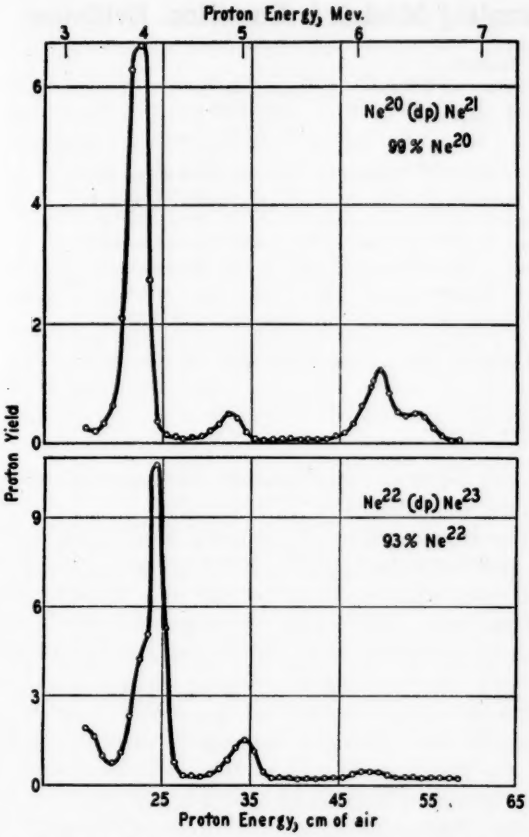

FIG. 1. Yield of protons from the deuteron bombardment of separated neon isotopes with observation at 90° with the incident beam.

Watson[7] for $Ne^{23} \rightarrow Na^{23}$, one calculates 23.00160 $\pm$0.00040 for the mass of Ne^{23}. Mattauch and Flammersfeld estimate from all reported evidence that the mass of Ne^{23} is 23.00203$\pm$0.00017. Using this higher value, we calculate from our Q of 2.88$\pm$0.06 Mev for $Ne^{22}(d,p)Ne^{23}$ that Ne^{22} has a mass of 21.99852, in excellent agreement with Mattauch and Flammersfeld's weighted estimate of 21.99850$\pm$0.00015. A better

[7] E. C. Pollard and W. W. Watson, Phys. Rev. 58, 15 (1940).

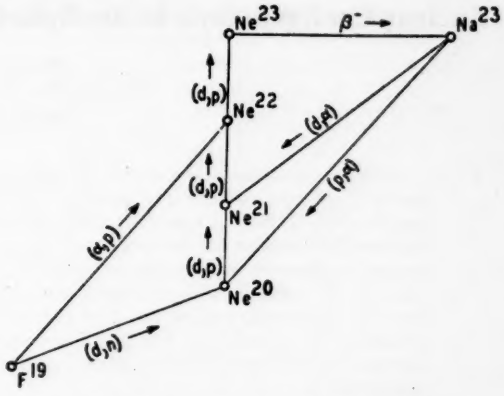

FIG. 2. Nuclear reactions involving neon isotopes.

determination of the mass of Ne^{23} could be made by a more accurate determination of the maximum energy of the electrons emitted by this nucleus.

If the Q of 6.79$\pm$0.10 Mev calculated for our observed $Ne^{21}(d,p)Ne^{22}$ reaction applied to the ground state of Ne^{22}, the 21.99850 value for Ne^{22} would give 20.99919 for the mass of Ne^{21}. The difference between this and the correct mass 21.00062 amounts to 1.37 Mev, indicating that our proton group involves an excited state of this energy in the Ne^{22} nucleus. This is to be compared with the observation by May and Vaidyanathan[8] in their study of the reaction $F^{19}(\alpha,p)Ne^{22}$ that the first excited level of the Ne^{22} nucleus lies at 1.5 Mev above its ground state. Our failure to observe the more energetic protons involving the ground state of Ne^{22} is understandable since (1) our enrichment factor of 3 made detection of these excited state protons barely possible, and (2) from comparison with the proton distributions from Ne^{20} and Ne^{22} bombardment, we might expect the missing longest-range protons to be considerably less numerous than the shorter-range protons from the same reaction.

We wish to thank Dr. H. T. Motz and Professor E. C. Pollard for helpful discussions.

[8] A. N. May and R. Vaidyanathan, Proc. Roy. Soc. 155, 519 (1936).

Nuclear Configurations in the Spin-Orbit Coupling Model. I. Empirical Evidence

MARIA GOEPPERT MAYER
Argonne National Laboratory, Chicago, Illinois
(Received December 7, 1949)

An extreme one particle model of the nucleus is proposed. The model is based on the succession of energy levels of a single particle in a potential between that of a three-dimensional harmonic oscillator and a square well. (1) Strong spin orbit coupling leading to inverted doublets is assumed. (2) An even number of identical nucleons are assumed to couple to zero angular momentum, and, (3) an odd number to the angular momentum of the single odd particle. (4) A (negative) pairing energy, increasing with the j value of the orbit is assumed. With these four assumptions all but 2 of the 64 known spins of odd nuclei are satisfactorily explained, and all but 1 of the 46 known magnetic moments. The two spin discrepancies are probably due to failure of rule (3). The magnetic moments of the five known odd-odd nuclei are also in agreement with the model. The existence, and region in the periodic table, of nuclear isomerism is correctly predicted.

NUCLEI containing 2, 8, 20, 28, 50, 82 or 126 neutrons or protons are particularly stable.[1] These closed shells have been explained in different ways.[2,3] It has also been pointed out that the "magic numbers" can be explained on the basis of a single particle picture with the assumption of strong spin-orbit coupling.[4] The detailed evidence supporting this point of view will be discussed in this paper.

I. THE SHELLS

The single particle orbits for the neutrons and protons in a nucleus are determined by a potential energy which has a shape somewhat between that of a square well and a three-dimensional isotropic oscillator. The level order for these two potentials is closely related. In Table I the order of the levels is given. The first line contains the oscillator quantum number. The levels which would be degenerate for the oscillator are grouped together. The eigenfunctions of any such group have the same parity. The order of levels in each group is that calculated for the square well. The major quantum number in the second line counts the number of spherical nodes. The third line contains the number of neutrons or protons which completely fill all states up to each oscillator level. For the square-well potential, the grouping of energy levels indicated above exists only for the low lying eigenfunctions and explains the stability of the numbers 2, 8, and 20. Beyond $n=2$, the grouping is no longer pronounced; $3s$ and $1h$, and also $3p$ and $1i$, have approximately the same energy in a square well calculation.

TABLE I. Order of energy levels for a potential somewhat between that of a square well and of a three-dimensional isotropic oscillator.

$n=$	0	1	2	3		4		5			6			
	$1s$	$1p$	$1d$	$2s$	$1f$	$2p$	$1g$	$2d$	$3s$	$1h$	$2f$	$3p$	$1i$	$2g$	$3d$	$4s$
N or $Z=$	2	8		20		40			70			112				

The grouping of oscillator levels does not explain the occurrence of the higher magic numbers; it is apparent that their stability must be due to a different cause. Assume that there exists a strong spin-orbit coupling such that the orbits with higher total angular momenta, $j=l+\frac{1}{2}$, have a higher binding energy. Since this coupling should depend on the orbital angular momentum, l, and be higher for large l values, it is greatest for the first level in each of the oscillator groups. For this level, the state with $j=l+\frac{1}{2}$ will be lowered in energy towards the group with lower n, the state with $j=l-\frac{1}{2}$ raised, so that a gap occurs at this point. Table II contains the order of levels obtained from those of the square well by spin-orbit coupling. It is seen that the shells so obtained correspond exactly to the magic numbers.

In the middle of the shell, spin-orbit coupling may give rise to crossing of some levels.

II. ASSUMPTIONS

As will be shown in the detailed discussion, the following assumptions are adequate to explain the observed facts in all but a very few exceptional cases:

(1) The succession of energies of single particle orbits is that of a square well with strong spin orbit coupling giving rise to inverted doublets.

(1a) For given l, the level $j=l+\frac{1}{2}$ has invariably lower energy and will be filled before that for $j=l-\frac{1}{2}$.

(1b) Pairs of spin levels within one shell, which arise from adjacent orbital levels in the square well in such a way that spin-orbit coupling tends to bring their energy closer together can, and very often will, cross. Examples are $d_{3/2}$ and $s_{1/2}$; $f_{5/2}$, $p_{3/2}$; $p_{1/2}$, $g_{9/2}$; $g_{7/2}$, $d_{5/2}$; $s_{1/2}$, $h_{11/2}$; $p_{1/2}$, $i_{13/2}$. These level pairs may cross to have their energy order reversed from that of Table II.

(2) An even number of identical nucleons in any orbit with total angular momentum quantum number j will always couple to give a spin zero and no contribution to the magnetic moment.

[1] W. Elsasser, J. de phys. et rad. 5, 625 (1934); M. G. Mayer, Phys. Rev. 74, 235 (1948).
[2] E. Feenberg and K. C. Hammack, Phys. Rev. 75, 1877 (1949).
[3] L. W. Nordheim, Phys. Rev. 75, 1894 (1949).
[4] Haxel, Jensen, and Suess, Phys. Rev. 75, 1766 (1949); M. G. Mayer, Phys. Rev. 75, 1969 (1949).

(3) An odd number of identical nucleons in a state j will couple to give a total spin j and a magnetic moment equal to that of a single particle in that state.

(4) For a given nucleus the "pairing energy" of the nucleons in the same orbit is greater for orbits with larger j.

The last assumption leads to the prediction that the higher j value appears less often as the spin of odd nuclei than the energy order of Table II predicts. For instance, if the $3s_{1/2}$ level has slightly lower energy than $h_{11/2}$, but if the pairing energy of $h_{11/2}$ exceeds that of $s_{1/2}$ by more than this difference, the spin 11/2 would not occur in odd nuclei, but 1/2 would be observed instead.

There is some theoretical justification for assumptions 2, 3, and 4, and this will be discussed in the next paper.

Assumption 2 has the consequence that all even-even nuclei have spin zero. The main testing ground for the level assignment consists then in the spins and magnetic moments of the nuclei of odd A. According to the assumptions we will adopt for these nuclei the extreme one-particle picture, ascribing both spin and magnetic moments to the last odd proton or neutron.

III. MAGNETIC MOMENTS OF ODD A NUCLEI

If assumption 3 were exactly correct, the magnetic moments of all odd nuclei could be computed by the vector model from the known gyromagnetic ratios of proton and neutron. The two possible cases, $l=j-\frac{1}{2}$ and $l=j+\frac{1}{2}$ for given j value lead to two computed lines in a plot of magnetic moment μ against j for nuclei with odd neutron number and two (different) lines for nuclei with odd proton number. These theoretical lines will be referred to as "Schmidt lines."[5] The experimental values lie in between the Schmidt lines, but do not coincide with them. For each j value the magnetic moments seem to fall into two groups, one reasonably close to the line corresponding to $l=j+\frac{1}{2}$, the other scattered from near the line corresponding to $l=j-\frac{1}{2}$ to about halfway. It turns out that the assignment of levels made attributes to the first group an odd nucleon in a state $l=j+\frac{1}{2}$, to the second one $l=j-\frac{1}{2}$. In the later discussion l-values as derived from magnetic moments will be quoted only if the magnetic moment of the nucleus is rather close to one of the two Schmidt lines.

The deviation of the magnetic moments from the Schmidt lines may be taken as an indication of the crudity of the single particle model. However, there is no indication that the magnetic moments for nuclei with one particle more or less than a closed shell fit the Schmidt lines any better than others, which might have been expected, since one would be inclined to expect greater validity of the single particle model in these cases.

For a given value of j, the different possible l-values correspond to eigenfunctions of opposite parity. Determination of l consequently means determination of parity. Since the transition probabilities of β-decays depend on change of parity, these probabilities furnish a check on the somewhat shaky measurements of l-values by the magnetic moments (Section VII).

[5] T. Schmidt, Zeits. f. Physik **106**, 358 (1937); H. H. Goldsmith and D. R. Inglis, Brookhaven Publications.

TABLE II. Order of energy levels obtained from those of a square well potential by spin-orbit coupling.

Osc. no.	Square well	Spin term	No. of states	Shells	Total no.
0	$1s$	$1s_{1/2}$	2	2	2
1	$1p$	$1p_{3/2}$	4	6	8
		$1p_{1/2}$	2		
2	$1d$	$1d_{5/2}$	6	12	20
		$1d_{3/2}$	4		
	$2s$	$2s_{1/2}$	2		
3	$1f$	$1f_{7/2}$	8	8	28
		$1f_{5/2}$	6	22	50
	$2p$	$2p_{3/2}$	4		
		$2p_{1/2}$	2		
		$1g_{9/2}$	10		
4	$1g$	$1g_{7/2}$	8	32	82
		$2d_{5/2}$	6		
	$2d$	$2d_{3/2}$	4		
	$3s$	$3s_{1/2}$	2		
		$1h_{11/2}$	12		
5	$1h$	$1h_{9/2}$	10	44	126
		$2f_{7/2}$	8		
	2	$2f_{5/2}$	6		
		$3p_{3/2}$	4		
	$3p$	$3p_{1/2}$	2		
		$1i_{13/2}$	14		
6	$1i$	$1i_{11/2}$			
	$2g$				
	$3d$				
	$4s$				

IV. DETAILED DISCUSSION OF SPINS AND MAGNETIC MOMENTS FOR ODD NUCLEI

Spins and l-values, insofar as the latter are unambiguous, are contained in Table III. It will be seen that there are only two serious discrepancies between expected and observed spins, and one between magnetic moments.

TABLE III. Spins of Even-Odd Nuclei. When two isotopes occur, individual spin values are given only when they are different. Orbital values are listed only when the magnetic moments are unambiguous.

No. of neutrons or protons	Odd protons			Odd neutron			O=Neutron, X=Proton Spin					No. odd p or n	Levels
	Element	Mass no.	Orbit	Mass no.	Orbit	Element	Mass no.	Orbit	p 1 1/2	3/2	d 2 5/2	f 3 7/2	g 4 9/2		
1	H	1	s	3	s	He	3	s	⊗					1	$1s$
3	Li	7	p							X				3	$p_{3/2}$
5	B	11	p			Be	9	p		⊗				5	
7	N	15	p			C	13	p	⊗					7	$p_{1/2}$
9	F	19	s						X					9	
11	Na	23								X				11	$d_{5/2}$
13	Al	27	d			Mg	25	d			⊗			13	
15	P	31				Si	29		⊗					15	$s_{1/2}$
17	Cl	35	d	37	d	S	33			⊗				17	$d_{3/2}$
19	K	39	d	41	d	S	35			⊗				19	
21	Sc	45	f									X		21	$f_{7/2}$
23	V	51										X		23	
25	Mn	55									X			25	
27	Co	59	g									X		27	
29	Cu	63		65						X				29	$p_{3/2}$
31	Ga	69								X				31	
33	As	75								X				33	
35	Br	79		81						X				35	$f_{5/2}$
37	Rb	85	$f(5/2)$	87	$p(3/2)$	Zn	67	f		X	⊗			37	
39	Y	89							X					39	$p_{1/2}$
41	Cb	93	g			Ge	73						⊗	41	$g_{9/2}$
43	Tc					Se	77		O					43	
45	Rh													45	
47	Ag	107	p	109	p	Kr	83	g	X				O	47	
49	In	113	g	115	g	Sr	87	g					⊗	49	
51	Sb	121	$d(5/2)$	123	$g(7/2)$	Zr	91				⊗	X		51	$g_{7/2}$
53	I	127		129	(7/2)	Mo	95		O		X	X		53	$d_{5/2}$
55	Cs	133	g	137	g							X		55	
57	La	139	g									X		57	
59	Pr	141									X			59	
61	Pm													61	
63	Eu	151		153	f	Cd	111	s	O		X			63	
65	Tb	159				Cd	s, Sn	s	O	X				65	$h_{11/2}$
67	Ho	165				Sn	117	s	O			X		67	
69	Tm					Sn	119	s	(X)					69	
71	Lu	175	g			Te	123		O			X		71	
73	Ta	181	g			Te	125		O			X		73	
75	Re	185		187		Xe	129	s	O		X			75	
77	Ir	191	(1/2)	193	(3/2)	Xe	131	d	X	⊗				77	$d_{3/2}$
79	Au	197	d			Ba	135	d		⊗				79	
81	Tl	203		205		Ba	137	d	X	O				81	$s_{1/2}$
83	Bi	209	h										X	83	$h_{9/2}$

(A) Nuclei with Less Than 20 Neutrons or Protons

For nuclei up to $_8O_8^{16}$ no discrepancies occur, and the level order $s_{1/2}$, $p_{3/2}$, $p_{1/2}$ is strictly adhered to. The nucleus with 9 protons $_9F_{10}^{19}$, has definitely an $s_{1/2}$ orbit. This seems to suggest that for a nucleus as small as this the potential well is steeper than an oscillator. Nevertheless, one would expect the 9th and 10th proton to pair in $d_{5/2}$ states (assumption 4), and $_{11}Na_{12}^{23}$ to have a proton configuration of $(d_{5/2})^3$ with a spin 5/2 or possible $(d_{5/2})^2 s_{1/2}$ and a spin 1/2. However, here the first serious discrepancy occurs. The spin of $_{11}Na_{12}^{23}$ is 3/2. The magnetic moment of this nucleus would indicate a $p_{3/2}$ rather than a $d_{3/2}$ orbit (Section VIII).

From then on, the filling of the shell is regular and indicates the level order $d_{5/2}$, $s_{1/2}$, $d_{3/2}$. Both $_{13}Al_{14}^{27}$ and $_{12}Mg_{13}^{25}$ have $d_{5/2}$ orbits. At 14 the $d_{5/2}$ levels should be filled. Fourteen, in fact, should be a magic number, if the spin-orbit coupling in light nuclei were sufficiently strong to overcome the spacing of the oscillator levels (see Section IX).

(B) Odd Nuclei with $20 < N$ or $Z \leq 50$

During the first 8 steps, the eight $f_{7/2}$ orbits should be filled up. Consequently, the spin of 7/2 should occur for all odd neutron or proton numbers between 20 and 28. Only odd proton spins are measured in this region, and with one exception they are all 7/2. This exception, the second serious discrepancy encountered, is $_{25}Mn_{30}^{55}$, which is expected to have a proton configuration $(f_{7/2})^5$, and consequently, a spin of 7/2; but has actually a spin of 5/2 and a magnetic moment corresponding to a d

level. The magnetic moment of $_{27}Co_{32}^{59}$ seems to indicate $g_{7/2}$ rather than $f_{7/2}$. The limits of error on this measurement are, however, so great that this assignment is uncertain. At N or $Z=28$ the $f_{7/2}$ levels are filled, and no spin of 7/2 should or does occur between 29 and 49. Beyond 28, the experimental indications are that the level order is

$$p_{3/2} \quad f_{5/2} \quad p_{1/2} \quad g_{9/2},$$

namely $p_{3/2}$ and $f_{5/2}$ have crossed but seem to have approximately the same energy. Both levels will be completely filled at N or $Z=38$, and in between 29 and 37 inclusive spins of 3/2 are measured for every odd number, with the exception of $_{37}Rb_{48}^{85}$ and $_{30}Zn_{37}^{67}$, with 37 protons and neutrons, respectively, which show $f_{5/2}$ orbits. The $f_{5/2}$ orbits fill in preferentially in pairs, in accordance with rule 4.

Between 38 and 50, only the levels $p_{1/2}$ and $g_{9/2}$ remain to be filled, and only spins of 1/2 and 9/2 are encountered. The magnetic moments, in the cases where they are measured, are consistent with $p_{1/2}$ and $g_{9/2}$. $_{50}Y_{39}^{89}$, with 39 neutrons, has spin 1/2; $_{32}Ge_{41}^{73}$ and $_{41}Cb_{52}^{93}$, with 41 neutrons or protons respectively, have $g_{9/2}$ orbits. That later on, at 43 neutrons and 47 protons spins of 1/2 occur again, indicates that $p_{1/2}$ and $g_{9/2}$ have closely the same energy, and the greater pairing energy (rule 4) is causing the $g_{9/2}$ orbital to fill in pairs. The isomerism in this region (see Section VI) bears out this contention.

All eigenfunction in this shell, with the exception of $g_{9/2}$, have odd parity.

Up to this point, spins and l-values for odd neutron or odd proton numbers are identical, except for the two isotopes of silver, $Z=47$, and $_{36}Kr_{47}^{83}$, which have $p_{1/2}$ and $g_{9/2}$ levels respectively.

(C) Odd Nuclei with Odd Nucleon Number between 50 and 82

The over-all predictions for this shell are: (1) No spins of 9/2 should occur. In practice none are encountered. (2) All eigenfunctions of the shell, except those for $h_{11/2}$, should be even. An exception is found in $_{63}Eu_{90}^{153}$, which has a magnetic moment indicating $f_{5/2}$, instead of the expected $d_{5/2}$, and is the one serious discrepancy encountered in the magnetic moments.

The $h_{11/2}$ orbits are filled in this region, and one would expect to encounter spins of 11/2. None are found in the ground states of the atoms. Isomeric states of spin 11/2 are, however, encountered frequently (see Section VI). It must be postulated that the $h_{11/2}$ orbits are filled preferentially by pairs, according to rule 4.

In detail, the situation for protons is this: The level order, leaving out for the moment the $h_{11/2}$ levels, is

$$g_{7/2} \quad d_{5/2} \quad d_{3/2} \quad s_{1/2}.$$

The beginning of the shell is completely regular. $d_{5/2}$ and $g_{7/2}$ have approximately the same energy; $_{51}Sb$ has two stable isotopes, one with a $d_{5/2}$, the other with a $g_{7/2}$ level. The stable isotope of $_{53}I_{74}^{127}$ has a $d_{5/2}$ level, the radioactive $_{53}I_{76}^{129}$ has $g_{7/2}$. 55 and 57 protons have spins and magnetic moments corresponding to $g_{7/2}$. At 58, $g_{7/2}$ should be filled and actually only spins 5/2 occur after 58. At 64 protons both $d_{5/2}$ and $g_{7/2}$ should be completely filled, and the spin of 3/2 for $_{65}Tb_{94}^{159}$ bears this out.

TABLE IV. Spins and magnetic moments for five odd-odd nuclei.

	Neutron state	Proton state	Spin	Exp.	Calc.
$_{3}Li_{3}^{6}$	$p_{3/2}$	$p_{3/2}$	1	0.82	0.63
$_{5}B_{5}^{10}$	$p_{3/2}$	$p_{3/2}$	3	1.80	1.88
$_{7}N_{7}^{14}$	$p_{1/2}$	$p_{1/2}$	1/2	0.40	0.37
$_{11}Na_{11}^{22}$	$d_{5/2}$	$d_{5/2}$	3	1.75	1.73
$_{19}K_{21}^{40}$	$f_{7/2}$	$d_{3/2}$	4	−1.29	−1.70

From now on irregularities occur which must be attributed to the filling of the $h_{11/2}$ level. It seems that between 66 and 74 protons the $h_{11/2}$ levels suddenly fill in, to the extent of redissolving the previously formed $g_{7/2}$ and $d_{5/2}$ shells. The reason for this may be Feenberg's "wine bottle" effect.[2] The end of the shell is again regular. Spins of 3/2 appear twice, and the thallium isotopes at 81 protons have spins 1/2.

The situation for neutrons is somewhat different. At 51 neutrons, $_{40}Zr_{51}^{91}$, a spin of 5/2 is found. The spin of $_{42}Mo_{53}^{95}$, with 53 neutrons, is given as 1/2, but the measurement is too doubtful to be believed.* The outstanding feature is the occurrence of spin 1/2 for all odd neutron nuclei from 63 to 75. Actually, if $h_{11/2}$ and $s_{1/2}$ have approximately the same energy and the $h_{11/2}$ fill in regularly, one would expect a string of 7 spins of 1/2 to occur due to the very strong pairing effect of 11/2 compared to 1/2.

Towards the end of the shell the $s_{1/2}$ level seems to be filled, and $d_{3/2}$ orbits occur. The level order for odd neutrons seems to be

$$d_{5/2} \quad g_{7/2} \quad s_{1/2} \quad d_{3/2} \quad h_{11/2}.$$

The pairing energy for $h_{11/2}$ orbits tends to depress the energy of pairs of $h_{11/2}$ in this scheme to below that of the $s_{1/2}$ pairs.

In this whole region, the last odd proton, in contrast with the odd neutron, is usually found in an orbit of high angular momentum. The Coulomb repulsion, which tends to concentrate the charge on the outside, is probably responsible for this difference between odd proton and odd neutron numbers.

(D) Odd Nuclei with Neutrons or Protons between 82 and 126

Very few spins are known in this part of the isotope table. The shell begins and ends correctly with $h_{9/2}$ at

* *Note added in proof:* According to a private communication from J. E. Mack, the spins of $_{42}Mo_{53}^{95}$ and $_{42}Mo_{55}^{97}$ are either 5/2 or 7/2.

$_{83}Bi_{126}^{209}$, and ends with $p_{1/2}$ at $_{82}Pb_{125}^{207}$ with 125 neutrons. The $i_{13/2}$ orbits should be filled, but one might expect them to "hide," as the $h_{11/2}$ orbits do. All other orbits should have odd parity.

V. ODD-ODD NUCLEI

Spins and magnetic moments are known for the five odd-odd nuclei, and are listed in Table IV. The states of the odd neutron and proton are also given. To predict the spins of the nuclei one would have to understand the coupling between the angular momenta of the two odd nucleons, which is evidently not such as to make the total spin zero. The only empirical indication given by the first four of the nuclei in Table IV, which have the neutron and proton in the same state, is that the eigenfunction is symmetric in the proton and neutron.

Feenberg[6] has pointed out that the magnetic moments of these nuclei, calculated on the basis of the orbit assignments above, are in excellent agreement with the experimental values.

VI. EXCITED STATES OF ODD NUCLEI

(A) Electric Dipole Transitions

The states within one shell consist of all but the highest j value obtainable from an oscillator level with quantum number n, plus the highest j value obtained from level $n+1$; this latter has a j value larger by at least 2 than any other level in the shell. Oscillator levels of the same n value have identical parity.

Low-lying excited states in odd nuclei should be those in which the odd nucleon is raised to another level in the same shell. Since γ-ray transitions corresponding to electric dipole require change in parity, and spin change by not more than one, one can make the prediction: *γ-rays between low lying states are never electric dipole transitions.*

(B) Isomeric States for Odd Nuclei

Isomerism in odd nuclei should occur when the two lowest levels available for the odd nucleon have very different spin. It is seen that this level assignment first predicts this situation between 39 and 49, where $g_{9/2}$ and $p_{1/2}$ compete. The existence of "islands of isomerism" has been pointed out by Feenberg and Hammack[2] and by Nordheim.[3]

The compilation by Segrè and Helmholtz[7] actually lists isomeric states for $_{20}Ca_{29}^{49}$, $_{22}Ti_{29}^{51}$, and $_{33}As_{38}^{71}$ in which the odd nucleon is the 29th or 33rd. The first two cases have been reinvestigated by M. Goldhaber[8] and found not to show isomerism. $_{33}As_{38}^{71}$ is then the only nucleus in which an isomeric state exists which does not fit the level scheme.

In agreement with the level assignment, isomerism occurs very frequently for Z or N between 39 and 49. 26 odd nuclei with the odd value of N or Z between 39 and 49 are known to have isomeric states. Beyond Z or $N=50$ the competition is between $1g_{7/2}$ and $2d_{5/2}$ and should not lead to isomeric states. The first isomerism occurs at 63 neutrons, Cd^{111}. From then on, to the end of the shell at 82, isomerism is again frequent.

The assignment of levels given ascribes all cases of isomerism in odd nuclei with the odd Z or N between 39 and 49 to the small difference in energy between $p_{1/2}$ and $g_{9/2}$. The isomeric transition should consequently be magnetic 2^4th pole in all cases. The Λ-value for all transitions should be 5. This is not in agreement with experiment. The isomeric states of the two indium isotopes $_{49}In_{64}^{113}$ and $_{49}In_{66}^{115}$ agree perfectly with the assignment, but, for instance, the two silver isotopes, $_{47}Ag_{60}^{107}$ and $_{47}Ag_{62}^{109}$ have isomeric states which decay much faster and are characterized by $\Lambda=4$.

Between 50 and 82, $h_{11/2}$ has the opposite parity from the other levels. All isomerism between 63 and 81 which has odd Λ-values has to be ascribed to the occurrence of this state. A clear-cut example of this is $_{56}Ba_{31}^{137}$, with 81 neutrons. The ground state is measured to be $d_{3/2}$. The isomeric transition has a lifetime corresponding to $\Lambda=5$, which requires spin change of at least 4 and change of parity, and agrees with the assignment $h_{11/2}$ for the isomeric level.

Other examples are the isomeric states of the 6 odd tellurium isotopes from $A=121$ to $A=131$ with neutron numbers from 67 to 77.[9] All 6 isotopes have isomeric transitions corresponding to magnetic 2^4 poles, or spin change of 4 and change in parity. In the lighter three of the isotopes this transition is followed by a γ-ray, which at least for Te^{123} and Te^{125} is consistent with magnetic dipole, or no change in parity, spin change of 1. For Te^{123} and Te^{125} the spins of the ground state are measured to be 1/2. If it is accepted that this is to be interpreted as $s_{1/2}$, one finds that the levels in ascending order are

$$s_{1/2} \quad d_{3/2} \quad h_{11/2},$$

just as given in Section IV, (c). For the three heavier tellurium isotopes the following γ-ray is absent, which may be understood by assuming that the $s_{1/2}$ level is now filled, and the ground state is $d_{3/2}$.

VII. β-DECAY FOR ODD NUCLEI

The transition probabilities for β-decay depend on change of spin and parity. The shell model gives a method of assigning spin and parity to an odd nucleus in the cases in which no measurements exist. The extent to which a β-transition between the ground states of parent and daughter nucleus is permitted can then be calculated. It is also possible to predict the properties of some of the low excited levels. The over-all agreement between theory and experiment is very satisfactory. To

[6] E. Feenberg, Phys. Rev. **76**, 1275 (1949).
[7] Emilio Segrè and A. C. Helmholz, Rev. Mod. Phys. **21**, 271 (1949).
[8] M. Goldhaber, private communication.
[9] R. D. Hill, Phys. Rev. **76**, 186 (1949); J. C. Bowe and Gertrude Scharff-Goldhaber, Phys. Rev. **76**, 437 (1949).

demonstrate this would require an extensive table. Such tables have been published by Nordheim[3] and Feenberg and Hammack.[2] Although the shell assignments in those two papers are entirely different, the resulting predictions are surprisingly similar. A detailed compilation of the level assignment for β-decay on the basis of the jj shell model is being prepared by S. Moszkowski.

The most unambiguous part of the predictions is that of parity. The β-transitions thereby contribute materially to the confirmation of the assignment of orbital angular momenta, which determine the parity.

The few startling contradictions, notably C^{14} and P^{32} occur mostly in even A nuclei.

VIII. THE TWO SPIN DISCREPANCIES

In Section IV, two major disagreements were encountered, $_{11}Na_{12}^{23}$, which should have a proton configuration $(d_{5/2})^3$, is found to have a spin of 3/2. The other case is $_{25}Mn_{30}^{55}$ with protons in a state $(f_{7/2})^5$ which has a spin of 5/2. In both cases the magnetic moments are not such as to indicate a violation of rule 1, the order of spin-orbit coupled levels; Na behaves more like a $p_{3/2}$ than a $d_{3/2}$ state, and Mn more like $d_{5/2}$ than $f_{5/2}$. It is tempting to ascribe the violation to a breakdown of rule 3. Three protons in a state $d_{5/2}$ can couple to give a spin 3/2, although as a rule the energy for the state with spin 5/2 is lower. The state with spin 3/2 is a definite configuration and permits a calculation of the magnetic moment; this value lies closer to the measured magnetic moment of $_{11}Na_{12}^{23}$ than either of the Schmidt lines. The same situation holds for $_{25}Mn_{30}^{55}$. The values are given in Table V. In the second column is the experimentally measured magnetic moment. The third column has the values calculated for $(d_{5/2})^3$ $J=3/2$ and $(f_{7/2})^5$, $J=5/2$, respectively. The last two columns give the two Schmidt line values.

IX. THE MAGNITUDE OF THE SPIN-ORBIT COUPLING

A calculation on the basis of meson theory by Gaus[10] indicates that the splitting between the levels with $j=l-\frac{1}{2}$ and $j=l+\frac{1}{2}$ is proportional to $(2l+1)A^{-2/3}$. The splitting responsible for the occurrence of the magic numbers should consequently not be very different for the different shells. A formula of this type would also explain the fact that the shell structure seems to be more pronounced for neutrons than for protons, since the neutron shells fill at smaller A values.

The empirical evidence indicates that the spin orbit coupling induces a splitting of the two j values, $l+\frac{1}{2}$ and $l-\frac{1}{2}$ by 2 Mev in the region of higher l-values. The value of at least 2 Mev was estimated from α-decay energies[11] for the extra stability of 126 neutrons, due to the $i_{13/2}$ and $i_{11/2}$ splitting. A similar value was previously estimated for the extra stability of 82 neutrons.[1]

TABLE V. Experimental and calculated values of magnetic moments.

	μ exp.	μ calc.	μ $l=j-\frac{1}{2}$	μ $l=j+\frac{1}{2}$
$_{11}Na_{12}^{23}$	2.21	2.8	3.78	0.12
$_{25}Mn_{30}^{55}$	3	4	4.8	0.87

The shell at 28 is not too strongly marked. It has been suggested,[12] however, that $_{26}Fe_{30}^{56}$ may owe its extreme abundance to the original creation of $_{28}Ni_{28}^{56}$ with subsequent decay to $_{26}Fe_{30}^{56}$. Nothing seems to be known about the lifetime of $_{28}Ni_{28}^{56}$.

Recently, some evidence was obtained indicating extra stability for 14 neutrons or protons. The energy released by the β-decay[13] of $_{13}Al_{16}^{29}$ is greater than would be estimated from the decay energy of neighboring nuclei with the same isotopic spin. In this process, a $d_{3/2}$ neutron is transformed into a $d_{5/2}$ proton. The excess energy is about 1.7 Mev.

The splitting of the $1p_{3/2}$ and $1p_{1/2}$ levels in Li^7 is 0.48 Mev, if one interprets the excited state to be $p_{1/2}$. Inglis[14] has pointed out that this assignment encounters some experimental difficulties. The extrapolation of the formula of Gauss would lead to about 2 Mev for the splitting rather than 1/2 Mev. A perturbation calculation on the symmetric eigenfunction for Russel-Saunders coupling shows, however, that the splitting in Li^7 is only one-third of that obtained for a single nucleon in the P-shell. A splitting of 1.5 Mev for a single nucleon is about the extrapolated value.

There is no adequate theoretical reason for the large observed value of the spin orbit coupling. The Thomas splitting has the right sign, but is utterly inadequate in magnitude to account for the observed values. A proper type of meson potential can be made to predict splitting qualitatively similar to the Thomas splitting, and therefore qualitatively similar to the observed, but greater in magnitude than the Thomas splitting, although usually somewhat less than the observed value.

[10] H. Gaus, private communication by C. F. von Weizsäcker.

[11] Perlman, Ghiorso, and Seaborg, Phys. Rev. 74, 1730 (1948).
[12] O. Haxel, private communication from C. F. von Weizsäcker.
[13] Seidlitz, Bleuler, and Tendam, Phys. Rev. 76, 861 (1949).
[14] D. R. Inglis, Phys. Rev. 74, 1876 (1948).

Nuclear Configurations in the Spin-Orbit Coupling Model. II. Theoretical Considerations

MARIA GOEPPERT MAYER
Argonne National Laboratory, Chicago, Illinois
(Received December 7, 1949)

The assumption of short-range attractive forces between identical nucleons in the jj coupling model of nuclear structure is in agreement with the empirically observed spins.

I

IT has been pointed out previously that the magic numbers in nuclei can be understood if one assumes the existence of a strong spin-orbit coupling.[1] The sign of this is such as to lower the energy of the higher total angular momentum. Observed and theoretical spin values of odd nuclei are in good agreement.[2] Detailed investigation of the empirical material indicates that the following three rules are obeyed:

1. An even number of identical nucleons in the same orbit with total angular momentum j couple such that the resultant total spin is $J=0$.
2. An odd number of identical particles in an orbit with angular momentum, j, couple to a resultant total spin $J=j$.
3. Of two orbits in the same nucleus, that of higher angular momentum has the greater magnitude of the (negative) pairing energy.

No attempt is made to explain the strong spin-orbit coupling.

The object of this paper is to investigate if there are any theoretical reasons for these empirical rules.

For this purpose, it was assumed that an attractive potential acts between identical nucleons. For reasons of definite and easy evaluation this was assumed to have the shape of a δ-function. Only the interaction of several identical nucleons in the different degenerate eigenfunctions belonging to the same total angular momentum quantum-number j was investigated.

The assumption of a δ-function attraction between identical nucleons is perhaps in contradiction with the square-well and single-particle orbit picture. Nevertheless, it might be of interest to note that this assumption can explain qualitatively the empirical rules.

The calculation was made in a straightforward but inelegant manner, for eigenfunctions up to $j=7/2$. The results have a much more simple form than the method would lead one to expect. However, no general proof, for all j values, of the simple result (11) and (12) is given here.

II. METHOD

It was assumed that the single-particle eigenfunctions of a nucleon are determined by coupling of the spin to orbits in a spherically symmetric potential. If the total (half-integer) angular momentum quantum number is j, its projection on the z axis m_j, the eigenfunctions will be written ψ_{mj}. The ψ's are the well-known linear combinations of products of spin functions with purely orbital functions, χ, in a spherically symmetric potential

$$\chi_m{}^{nl}=(2\pi)^{-\frac{1}{2}}e^{im\varphi}\Theta_m{}^l(\vartheta)R_{nl}(r). \quad (1)$$

Here ϑ and φ denote the Euler angles and $\Theta_m{}^l(\vartheta)$ are the normalized Legendre functions with integer l. The ψ-functions for given j contain only either $l=j+\frac{1}{2}$ or $l=j-\frac{1}{2}$.

The radial part of the wave function $R(r)$ depends on the precise shape of the well, and nothing will be assumed about it except that it is normalized.

It is now assumed that there exist attractive forces between identical particles 1 and 2 in the single-particle quantum state of the same j value. For the purpose of definite and easy calculation the attractive potential (1, 2) was assumed to be a δ-function, i.e., zero if the position of the two particles does not coincide, so that:

$$V(1,2)=-g\delta(\varphi_1-\varphi_2)\delta(\cos\vartheta_1-\cos\vartheta_2)r_2{}^{-2}\delta(r_1-r_2), \quad (2)$$

$$\int V(1,2)r_2{}^2dr_2\sin\vartheta_2d\vartheta_2d\varphi_2=-g. \quad (3)$$

The strength of the interaction, g, is positive for attractive forces. For a δ-function potential, ordinary and Majorana forces are identical.

III. CALCULATION

The calculation was done in a straightforward way up to $l=3$, $j=7/2$. The interaction energy between a pair of identical nucleons 1 and 2 in single-particle eigenfunctions $\psi_{mj}{}^j$ and $\psi_{mj'}{}^j$ belonging to the same j is

$$E_{m_jm_j'}{}^j=A_{m_jm_j'}{}^j-B_{m_jm_j'}{}^j, \quad (4)$$

where

$$A_{m_jm_j'}{}^j=\int\int|\psi_{mj}(1)|^2V(1,2)|\psi_{mj'}(2)|^2d(1)d(2) \quad (5)$$

is the direct integral, and

$$B_{m_jm_j'}{}^j=\int\int\psi_{mj}(1)\psi_{mj'}{}^*(1)V(1,2)\times\psi_{mj}{}^*(2)\psi_{mj'}(2)d(1)d(2) \quad (6)$$

the exchange integral.

[1] Haxel, Jensen, and Suess, Phys. Rev. 75, 1969 (1949); M. G. Mayer, Phys. Rev. 75, 1766 (1949).
[2] M. G. Mayer, preceding paper.

For evaluation, the ψ_{m_j} are expressed in terms of spin functions and the orbital functions (1). It is seen that then the integration over spin, and over the two angles ϑ and φ can be performed directly. The radial function $R(r)$, however, is unknown, and consequently all terms (3) and (4) will be proportional to the same integral over the radial part of the wave function

$$I^{nl}=(g/4\pi)\int_0^\rho R_{nl}{}^4(r)r^2dr. \tag{7}$$

In this expression, ρ is the nuclear radius. Since attraction was stipulated, g as well as I are positive. Since the radial wave function is assumed to be normalized over the volume of the nucleus it is seen that I_{nl} is inversely proportional to the volume of the nucleus, or to the total number, A, of particles, in the nucleus,

$$I_{nl}=C/A. \tag{8}$$

I_{nl} is then roughly independent of n and l, but varies with the size of the nucleus. This will be indicated by leaving off the subscripts l and n in I.

A straightforward but tedious calculation of the interaction was undertaken. The integration over ϑ contains expressions of the type

$$i_{mm'}{}^l=\int[\Theta_m{}^l(\vartheta)]^2[\Theta_{m'}{}^l(\vartheta)]^2\sin\vartheta d\vartheta; \tag{9}$$

and occasionally such hybrids as

$$i_{123}{}^3=\int\Theta_1{}^3(\vartheta)[\Theta_2{}^3(\vartheta)]^2\Theta_3{}^3(\vartheta)\sin\vartheta d\vartheta. \tag{10}$$

Such integrals were evaluated up to $l=3$ (f-functions) and appropriately inserted into (4). The interaction between any pair of identical particles is thereby known. For more than two identical particles with angular momentum j the interaction energy is simply the sum of that for all possible pairs.

For several identical nucleons in orbits of the same j a number of total spins J are possible. However, for antisymmetric eigenfunctions up to $j=7/2$, each possible J value occurs only once. It is consequently possible to calculate the binding energy associated with each of the J values from the diagonal elements (4) of the interaction by the method of traces.[3] The energy for the antisymmetric linear combination of product ψ_{m_j}'s associated with a total spin J is the following expression: The difference between the sum of the energies of all product eigenfunctions for which $\Sigma m_j=J$, and the same quantity for all products with $\Sigma m_j=J+1$. In this manner, the energies associated with all total spins J were computed.

IV. RESULTS

The results have the following simple form:

The state of lowest energy for n identical nucleons in orbits with total angular momentum j is the one with

(1) For n even, $J=0$. It has the energy

$$E_0=-(n/2)[(2j+1)/2]I. \tag{11}$$

(2) For n odd, $J=j$. It has the energy

$$E_j=[(n-1)/2][(2j+1)/2]I. \tag{12}$$

The calculation predicts then that the lowest state is the one which appears empirically in the spins (rules 1 and 2, Section I).

The interaction energy is proportional to the number of pairs in a shell; an odd nucleon is not bound by the shell at all. Since I (Eqs. (7) and (8)) is roughly independent of n and l, the binding energy of a pair at given nuclear volume, or mass number A, is proportional to $2j+1$. This is in conformity with the empirical rule 3 of Section I.

In addition, this calculation also contains the variation of binding energies for even and odd nucleons. Equations (11) and (12), upon inserting the value (8) for I, show that the extra binding energy for an even nucleon compared to that of an odd one is

$$E_{\text{even}}-E_{\text{odd}}=-[(2j+1)/2A]\cdot C, \tag{13}$$

where C depends on the strength of the interaction. The empirical expression for this quantity is[4]

$$E_{\text{even}}-E_{\text{odd}}=-(36/A^{11/4})\text{ millimass units.} \tag{14}$$

Since the average j value increases with A, the dependence on the nuclear size of expressions (13) and (14) is not very different. If one wanted to attribute the odd-even variation in binding energies numerically to (13), C would be about 25 Mev.

[3] See, for instance, Condon and Shortley, *Theory of Atomic Spectra* (The Macmillan Company, New York, 1936).

[4] N. Bohr and Y. A. Wheeler, Phys. Rev. 56, 426 (1939).

Simultaneity in the Compton Effect† ††

ROBERT HOFSTADTER AND JOHN A. MCINTYRE†††
Palmer Physical Laboratory, Princeton University, Princeton, New Jersey
(Received December 5, 1949)

The Bothe-Geiger experiment has been repeated under improved conditions of time resolution, obtained by using stilbene scintillation counters. The recoil electron and scattered photon are emitted together within a time interval of less than 1.5×10^{-8} second. The electron and photon are also projected without a delay larger than 1.5×10^{-8} second after arrival of a quantum. The familiar concepts used in discussions of the Compton effect are shown to be valid.

I. INTRODUCTION

A CELEBRATED experiment by Bothe and Geiger[1] (1925) demonstrated that in a single Compton encounter the recoil electron and scattered photon appear simultaneously. Simultaneous, in this experiment, meant "occurring together within a time interval of 10^{-3} second." This experiment was important at its time since it differentiated sharply between the theory of the Compton process as we now know it[2] and an alternative theory[3] in which the recoil electron and photon are not simultaneous and in which the conservation laws of energy and momentum hold only in a statistical manner.

Later events[4] have confirmed the original picture of Compton. Although in 1936 some doubt was expressed concerning simultaneity in the Compton process[5] the work of many investigators showed that the original experiment of Bothe and Geiger was correctly interpreted. The later investigators[6–11] however, did not reduce the measured interval of simultaneity to less than 10^{-4} second. The results of the quoted experiments rest on statistical interpretations of the data in which half (or more) of the coincidence observations were assigned to chance or background effects. Thus, the number of coincidences constituted a small fraction of the total number of observed coincidences. There is little doubt that the interpretations were correct. However, it has generally been stated by the authors of the papers, that a clear-cut and unequivocal proof of the individual Compton process was still lacking.

The purpose of this paper is to show that such a direct proof can be given and that the Compton process is indeed simultaneous within a period of 1.5×10^{-8} second or less. These results are made possible by the advances in fast counting techniques in the last two years.

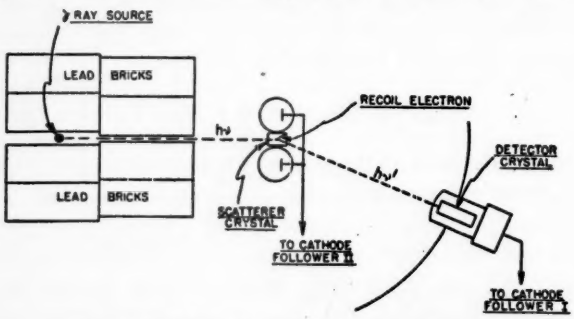

FIG. 1. Sketch of Compton scattering apparatus.

II. EXPERIMENTAL

A. Apparatus

Figure 1 shows a schematic view of the experimental arrangement.[12] The source of radiation is a cobalt rod of dimensions, $\frac{1}{8}$ in. diam.$\times\frac{3}{8}$ in. long, which emits the radiation Co^{60} (1.17, 1.33 Mev). The source strength is approximately 20 millicuries. A fine pencil of gamma-rays is formed by collimation of the radiation by a channel ($\frac{1}{8}$ in.$\times\frac{1}{8}$ in.) in two adjoining lead blocks of total path length 27.5 cm.

The pencil of gamma-rays passes through a "scatterer" crystal cube of stilbene ($\frac{1}{2}$ in. on a side). Figure 2 shows the trace left by this gamma-ray beam in a photographic plate (Eastman 103–0) placed at the position of the crystal. The outline of the stilbene scatterer is also shown in its relative position as used in the experiment. It may be seen that the beam is small, well collimated and passes through the middle of the crystal cube. Two matched (1P21) photo-multiplier tubes view the scatterer crystal. The electrical outputs of these photo-multiplier tubes are connected in parallel. The scatterer crystal, as implied by its name, is used as a scatterer but actually has a double function since it also provides the recoil electron light pulse or scintillation which the photo-multiplier tubes detect.

The scattered photon, in general leaves the scatterer

† A preliminary account of early results was given at the Washington Meeting of the American Physical Society, April 28–30, 1949; Phys. Rev. 76, 172 (1949).
†† Assisted by the ONR and the AEC.
††† N.R.C. predoctoral fellow.
[1] W. Bothe and H. Geiger, Zeits. f. Physik 32, 639 (1925).
[2] A. H. Compton, Phys. Rev. 21, 483 (1923); P. Debye, Physik. Zeits. 24, 161 (1923).
[3] Bohr, Kramers, and Slater, Phil. Mag. 47, 785 (1924).
[4] A. H. Compton and A. W. Simon, Phys. Rev. 26, 289 (1925).
[5] R. S. Shankland, Phys. Rev. 49, 8 (1936).
[6] W. Bothe and H. Maier Leibnitz, Gott. Nach. Phys. No. 2, 127 (1936); Phys. Rev. 50, 187 (1936).
[7] J. C. Jacobsen, Nature 138, 25 (1936).
[8] W. E. Burcham and W. B. Lewis, Proc. Camb. Phil. Soc. 32, 637 (1936).
[9] Crane, Gaerttner, and Turin, Phys. Rev. 50, 302 (1936).
[10] E. J. Williams and E. Pickup, Nature 138, 461 (1936).
[11] R. S. Shankland, Phys. Rev. 52, 414 (1937).
[12] R. Hofstadter and J. A. McIntyre, Phys. Rev. 76, 1269 (1949).

and moves out into the surrounding air. A second longer stilbene crystal, which we have called the "detector," is placed in a position on a circle around the scatterer, as shown in Fig. 1. Some of the scattered photons will have Compton encounters with the electrons of this crystal thus again producing electron recoil pulses. The detector crystal is a rectangular parallelopiped of dimensions $\frac{1}{2}$ in$\times\frac{1}{2}$ in.$\times$1 in., and is viewed by a pair of matched photomultipliers connected in parallel. Thus if the Compton process is simultaneous, some coincidences in time should be observed between the pulses in the scatterer and detector. In most of the experiments the center of the detector was placed at a distance of 7.3 cm from the center of the scatterer. The detector crystal therefore subtends a plane angle of approximately 10° at the center of the scatterer.

The detector is placed on a "spectrometer" arm and may be placed at various distances, up to 30 cm from the center of the scatterer crystal. Thin metal housings for both sets of photo-multipliers are used to shield the tubes from undesired light signals.

The coincidences have been detected by photographing the scatterer and detector pulses on an oscilloscope screen. Figure 3 illustrates the method used. In the figure each pair of photo-multipliers is connected with a cathode follower through a pulse shaping circuit. The cathode followers are connected to fast amplifiers with half-power point, on the high frequency side, at 19 megacycles/second. The amplifier and pulse shaping circuit designs are due to W. C. Elmore.[13] The connections to the amplifiers are made through coaxial lines which are used for delay purposes.

The pulse from the detector cathode follower is taken also to the sweep circuit of a cathode-ray oscillograph[14] through a Model 501* amplifier. The delay line I in the detector circuit is long enough (200 feet) to allow the rise of the detector pulse to be seen. The delay thus allowed for is the time necessary for the trigger circuit to start a sweep. The amplifier pulse in the detector circuit is applied to the upper plate of the pair of vertical plates of the oscillograph, as shown in Fig. 3. Typical stilbene detector traces are shown in Fig. 4 labeled "a."

The scatterer circuit resembles the detector circuit

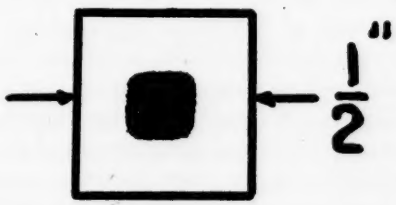

FIG. 2. Photograph of gamma-ray beam at position of scatterer crystal. The outline is that of the stilbene scatterer.

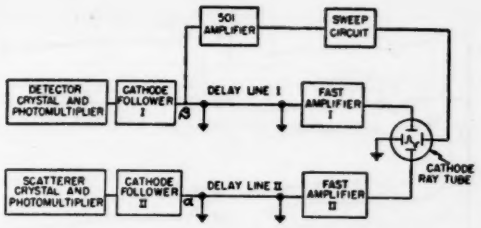

FIG. 3. Block diagram of scheme for detecting small time differences.

except that a longer delay line II is used (290 feet) and the 501 amplifier is dispensed with since the useful trigger is already supplied by the detector circuit. The amplifier output of the scatterer circuit is brought to the lower vertical plate of the CRO. Whereas the detector crystal provides an "up" pulse as seen in Fig. 4 marked "a," the scatterer supplies a down pulse, delayed with respect to the detector pulse, as shown in "b" of Fig. 4. If the detector and scatterer pulses are truly simultaneous then the corresponding time interval between the two pulses should be the same as the time interval when known simultaneous pulses are applied to the detector and scatterer circuits. If simultaneous, the delay between the two pulses in the typical Compton traces should be due merely to the difference in length of the delay lines I and II.**

Not all traces initiated by the detector correspond to Compton encounters originating from the collimated Co^{60} beam. Room contamination, natural background gammas and cosmic rays may actuate the detector crystal without a corresponding down pulse such as is observed in the Compton encounters. The traces marked "a" in Fig. 4 represent such background pulses. Those marked "b" are the true Compton double pulses. In this experiment, the discriminator bias of the triggered sweep circuit was set at such a value that only those traces appeared whose detector pulses were larger than about four or five times the average height of noise pulses. If noise pulses were permitted to trigger the sweep many more traces would have been observed but photography of the pulses would have been made difficult by the superposition of a large number of pulses. In the experiment at 90°, Fig. 7, the bias was lowered somewhat to permit smaller detector pulses to be observed.

Recoil electrons which are produced by Compton encounters in the scatterer may be projected or scattered in directions to enter the detector and cause spurious simultaneous pulses. In this experiment, such "electron coincidences" have been avoided by placing a $\frac{1}{16}$-in. absorber sample of aluminum in front of the detector.

[13] W. C. Elmore, to be published.
[14] V. Fitch and E. W. Titterton, Rev. Sci. Inst. 18, 821 (1947).
* Rise time 1.0×10^{-7} second, gain $3\times10^{+5}$.

** The transit time of electrons in the photomultiplier tubes ($\sim2\times10^{-8}$ second) cancels out when the difference in time between two pulses is measured. The spread in transit times is too small to measure with this apparatus (R. D. Sard, J. App. Phys. 17, 768 (1946)).

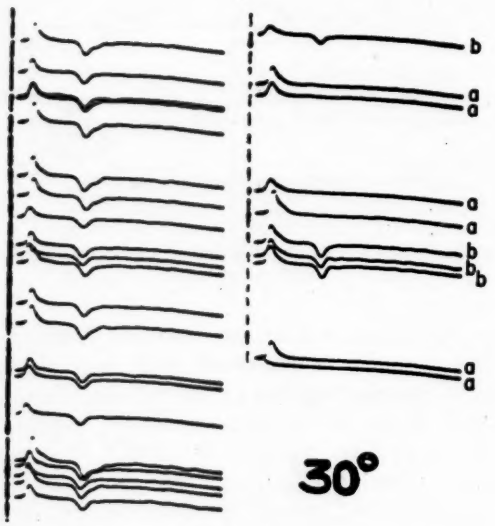

FIG. 4. Synthetic and Compton pulses at 30°. Time interval between peaks is 0.16 microsecond.

B. Calibration

Figures 4–7 show samplings of results obtained at photon scattering angles of 30°, 50°, 70°, and 90°. At 30° and 50° whole sections of the film are reproduced as originally taken. At 70° and 90° the Compton pulses occur at a low rate so that individual "b" type traces were taken from the film and collected together for the composite pictures used in the figures. Each of the "b" type traces is clear evidence for the individual Compton process.

At the left in Figs. 4 and 5 synthetic simultaneous pulses are shown. These pulses were obtained by opening the scatterer circuit at point α in Fig. 3 and supplying delay line II and scatterer amplifier with the detector pulse from β. The detector circuit was undisturbed otherwise. The detector pulse therefore appears in both the up and down positions, the up pulse corresponding to amplifier I and the down pulse to amplifier II. This method of obtaining simultaneous pulses will be called "method A."

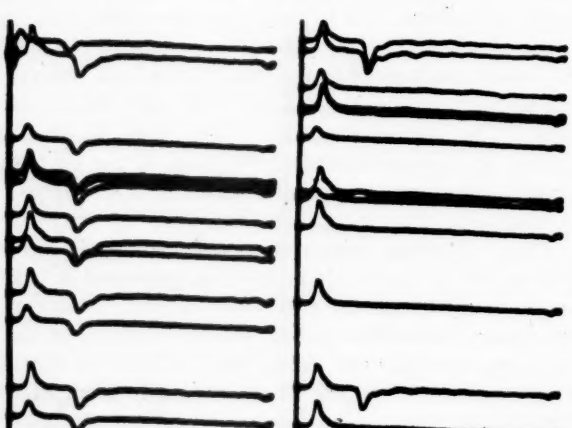

FIG. 5. Pulses at 50°.

Figure 8 shows synthetic simultaneous pulses produced by method A and a calibration signal from a 10-megacycle standard oscillator. It can be seen that the time interval between the pulse peaks is approximately 0.16 microsecond. It may also be observed that the sweep is not exactly uniform and thus the time scale not exactly linear with distance.

Method A does not really provide "true simultaneous" pulses in our comparison for the reason that the scatterer photo-multipliers and the cathode follower of the scattering circuit have not been used in exactly the same manner as in investigating Compton traces. To test this point we have placed one each of the detector and the scatterer photo-multipliers (the former without detector crystal present) adjacent to the scatterer crystal. Thus both photo-multipliers view the same pulses in the same crystal—the scatterer. Both pulses are now amplified and treated in the same manner as in studying Compton pulses. This method of obtaining precise simultaneous pulses gave results exactly equivalent to those of method A within the experimental error. We have preferred method A for most of our work since only small changes in the electrical connections are required in going from Compton traces to such simultaneous traces. More elaborate changes in the equipment are required in going from Compton traces to the traces of method B.

When the initiating detector pulse is small (bottom of Fig. 4) the sweep is observed to start at a position on the screen somewhat displaced to the left of the starting place for a large detector pulse. This, of course, is due to the time taken for the signal to reach the bias level of the sweep trigger circuit. In a large pulse the rise is steep and the time small. For a small pulse the time is roughly half the pulse base when converted to time units and therefore relatively long. As a consequence, traces appear in slightly different parts of the screen and are subject to the effects of non-linearity of the sweep. This fact has resulted in small variations in the distance between peaks in the pulses of methods A and B and in Compton coincidences. We have observed a maximum variation in the time-equivalence of the peak-to-peak measurements of about 1.5×10^{-8} second. This is considered to be the largest source of experimental error in the measurements here reported.

In Fig. 9 the upper trace shows a sample of an accidental occurrence of a scatterer pulse in the sweep interval of about 0.52 microsecond. The rate of occurrence of such accidentals can be estimated from the separate counting rates of scatterer and detector and is of the order of two per thousand traces. Our experimental data indicate two accidentals in 1137 traces.

III. RESULTS AND OBSERVATIONS

Figures 4–7 show at a glance that the Compton pulses are simultaneous to within 2×10^{-8} second. This value may be narrowed a little by more careful measurements, described below.

The pulses of Figs. 4, 5, 6, and 7 have been measured, along with many others, and compared with the traces of method A, such as those shown at the left in Figs. 4 and 5. Table I summarizes the results so obtained. In each of the 89 traces measured, the recoil electron and

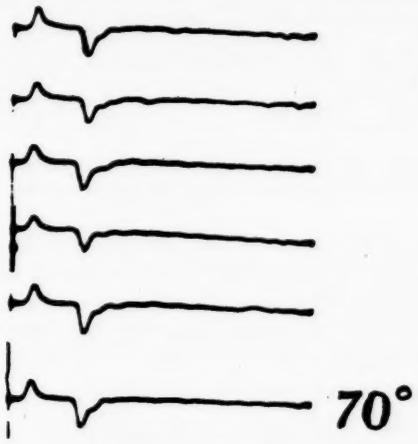

FIG. 6. Compton coincidences at 70°.

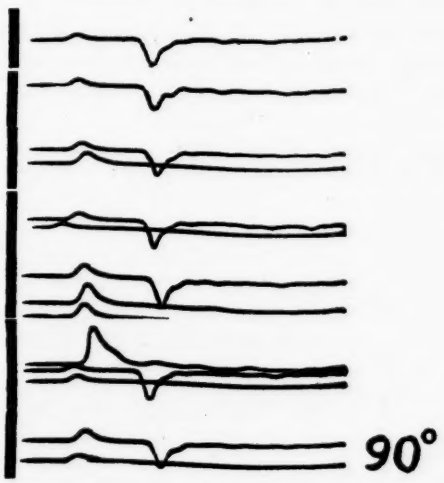

FIG. 7. Compton coincidences at 90°.

scattered photon pulses lie within $\pm1.5\times10^{-8}$ second of the standard 0.16 microsecond delay interval. We have excluded obvious accidental "near coincidences" of the type of Fig. 9 which occur in 0.2 percent of all traces. We consider this a proof that the Compton process is a simultaneous one wherein simultaneous means "occurring within an interval of 1.5×10^{-8} second." It would seem that there can be no doubt about simultaneity because of poor statistics of the data. Further since there is no difference outside the

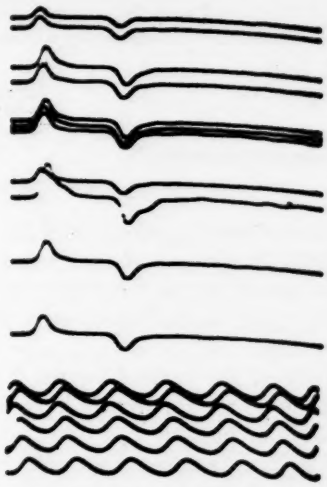

FIG. 8. Synthetic simultaneous pulses and calibrating 10 megacycle signal.

experimental error between the Compton pulses and the synthetic pulses obtained with delay lines, we may say that there is no constant or variable delay between arrival of the incident photon and the emission of recoil electron and scattered photon. This observation agrees with the experiment of Piccard and Stahel (1936).[15]

It may be observed that the scattered photon pulses are, on the average, larger than the recoil electron pulses at the angular position of 30°. In this position the photon has the average energy of 0.96 Mev while the recoil electron has the average energy of 0.29 Mev. At 90° the photon energy is 0.38 Mev and the recoil electron 0.87 Mev. At 55° scattering angle the energies are equal. It can be seen from Figs. 4–7 how these facts are reflected in the pulse heights. An exact correlation cannot be expected because of the varying energy given up by the scattered photon to the detector crystal and the relatively poorer optics of that system. The scatterer system has better optics since all light pulses originate in or near the center of the stilbene cubes (see Fig. 2). In fact, the observations made with method B show that the light flashes detected by two photo-

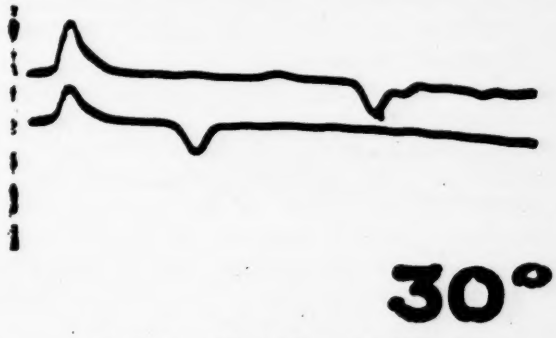

FIG. 9. An accidental "near coincidence."

[15] A. Piccard and S. Stahel, J. de phys. et rad. 8, 326 (1936). See also Hoffman, Shenstone, and Turner, Phys. Rev. 50, 1092 (1936).

TABLE I.

Total number of intervals measured	89
Standard deviation of set	5.5×10^{-9} second
Outside limits	$\pm10\times10^{-9}$ second
Difference between averages of Compton and true simultaneous intervals.	-5.0×10^{-9} second

multipliers, facing two opposing sides of the stilbene cube, are within 20 percent of each other. The recoil electron light pulses in the scatterer are also quite uniform at any given angle. Examples of this behavior can be seen in Figs. 4–7.

From a study of the various figures it can be seen that the stilbene pulses apparently have a decay time which lies within or possibly just outside the rise time of our amplifier. These pulses are therefore well matched to this problem. It can be seen in Fig. 10 that the decays are longer in materials such as naphthalene, anthracene, and naphthalene-anthracene. In these cases the scatterer has been made of the materials quoted. In all cases the detector has been a stilbene crystal. The results also show that the stilbene pulses have a rise time less than 1.5×10^{-8} second.

A final incidental observation may be made to the effect that the method outlined may be used to provide a source of gamma-rays varying from the value of the homogeneous incident pencil of gamma-rays down to a value of about 200 kilovolts at 180°.

IV. CONCLUSIONS

A finding of non-simultaneity would be of great physical significance[16–19] if the interval of time were larger than the expected quantum-theoretical interval. The quantum-theoretical expectation values of observing the recoil electron and the scattered quantum are high when the time interval is of the order λ/c where λ is the Compton wave-length and c the velocity of light. This time is of the order of 10^{-20} second and so lies much beyond the limit of present technical skills. Nevertheless, the experiment here reported represents the closest approach to the theoretical time limit which has so far been demonstrated. The experiment shows clearly the validity of the concepts used in the familiar derivations of the Compton formulas.

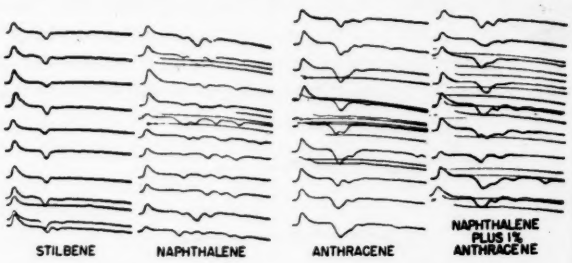

FIG. 10. Compton coincidences using stilbene, naphthalene anthracene and naphthalene+1 percent anthracene as scatterers.

V. ACKNOWLEDGMENT

We wish to acknowledge with thanks the continued interest of Drs. R. Ladenburg and M. G. White. We also wish to thank Mr. F. B. Harrison for preparing the stilbene crystals. This work has been assisted by the Joint Program of the ONR and the AEC.

[16] P. A. M. Dirac, Nature 137, 298 (1936).
[17] E. J. Williams, Nature 137, 614 (1936).
[18] R. Peierls, Nature 137, 904 (1936).
[19] N. Bohr, Nature 138, 25 (1936).

On the Dirac Theory of Spin 1/2 Particles and Its Non-Relativistic Limit*

LESLIE L. FOLDY
Case Institute of Technology, Cleveland, Ohio

AND

SIEGFRIED A. WOUTHUYSEN†
University of Rochester, Rochester, New York

(Received November 25, 1949)

By a canonical transformation on the Dirac Hamiltonian for a free particle, a representation of the Dirac theory is obtained in which positive and negative energy states are separately represented by two-component wave functions. Playing an important role in the new representation are new operators for position and spin of the particle which are physically distinct from these operators in the conventional representation. The components of the time derivative of the new position operator all commute and have for eigenvalues all values between $-c$ and c. The new spin operator is a constant of the motion unlike the spin operator in the conventional representation. By a comparison of the new Hamiltonian with the non-relativistic Pauli-Hamiltonian for particles of spin $\frac{1}{2}$, one finds that it is these new operators rather than the conventional ones which pass over into the position and spin operators in the Pauli theory in the non-relativistic limit.

The transformation of the new representation is also made in the case of interaction of the particle with an external electromagnetic field. In this way the proper non-relativistic Hamiltonian (essentially the Pauli-Hamiltonian) is obtained in the non-relativistic limit. The same methods may be applied to a Dirac particle interacting with any type of external field (various meson fields, for example) and this allows one to find the proper non-relativistic Hamiltonian in each such case. Some light is cast on the question of why a Dirac electron shows some properties characteristic of a particle of finite extension by an examination of the relationship between the new and the conventional position operators.

INTRODUCTION

A FREE Dirac particle of mass m is described by a four-component wave function Ψ satisfying the Dirac equation,

$$H\Psi=(\beta m+\boldsymbol{\alpha}\cdot\mathbf{p})\Psi=i(\partial\Psi/\partial t), \tag{1}$$

where $\mathbf{p}$ is the momentum operator for the particle, $\boldsymbol{\alpha}$ and β are the well known Dirac matrices (assumed here to be in their usual representation with β diagonal), and units have been used in which $\hbar$ and c are unity. The eigenfunctions of the Hamiltonian operator satisfy the equation:

$$(\beta m+\boldsymbol{\alpha}\cdot\mathbf{p})\psi=E\psi. \tag{2}$$

The eigenfunctions are of the form $u(\mathbf{p})e^{-\mathbf{p}\cdot\mathbf{x}}$. For each value of the momentum $\mathbf{p}$ there are four linearly independent spinors[1] $u(\mathbf{p})$ corresponding to the two eigenvalues $\pm(m^2+p^2)^{\frac{1}{2}}$ of the energy and the two eigenvalues ±1 of the z component of an operator $\boldsymbol{\Sigma}$ (defined later in Eq. (26)) related to the spin operator for the particle.

Except in certain trivial cases, for a given sign of the energy at least three of the components of $u(\mathbf{p})$ are different from zero. However, two of the four components go to zero as the momentum goes to zero, while at least one of the other two components remains finite. In the above representation, for positive-energy eigenfunctions, the last two (or *lower*) components vanish with vanishing momentum, while for negative-energy eigenfunctions, the first two (or *upper*) components vanish with vanishing momentum.

Of course any spinor Ψ may be split into the sum of two spinors Φ and X, having only upper and lower components respectively, in the following manner:

$$\Psi=\Phi+X, \quad \Phi=(1+\beta/2)\Psi, \quad X=(1-\beta/2)\Psi,$$

but the spinors Φ and X do not represent states of definite energy in the above representation.

In the non-relativistic limit, where the momentum of the particle is small compared to m, it is well known that a Dirac particle (that is, one with spin $\frac{1}{2}$) can be described by a two-component wave function in the Pauli theory. The usual method of demonstrating that the Dirac theory goes into the Pauli theory in this limit makes use of the fact noted above that two of the four Dirac-function components become small when the momentum is small. One then writes out the equations satisfied by the four components and solves, approximately, two of the equations for the small components. By substituting these solutions in the remaining two equations, one obtains a pair of equations for the large components which are essentially the Pauli spin equations.[2]

The above method of demonstrating the equivalence of the Dirac and Pauli theories encounters difficulties, however, when one wishes to go beyond the lowest order approximation. One then finds that the "Hamiltonian" associated with the large components is no longer Hermitian in the presence of external fields because of the appearance of an "imaginary electric moment" for the particle. Furthermore, all four components must again be used in calculating expectation values of operators to

* Supported by the AEC and the ONR.

† Now at the Zeeman Laboratory, University of Amsterdam, Amsterdam, Holland.

[1] See, for example, W. Heitler, *The Quantum Theory of Radiation* (Oxford University Press, New York, 1944), Chapter 3. We shall use the term spinor for any four-component column (or row) matrix occurring in the Dirac theory.

[2] See, for example, W. Pauli, *Handbuch der Physik*, 2. Aufl., Bd. 24, Teil 1.

order v^2/c^2. Apart from these difficulties, however, there are some serious questions concerning the properties of corresponding operators in the Dirac theory and the Pauli theory even in lowest order. Thus, in the Dirac theory the operator representing the velocity of the particle is the operator $\boldsymbol{\alpha}$ whose components have only the eigenvalues ± 1. On the other hand, in the Pauli theory the operator representing the velocity of the particle is taken to be $\mathbf{p}/m$ whose components have eigenvalues embracing all real numbers. Furthermore, different components of the velocity operator in the Dirac theory do not commute and therefore are not simultaneously measurable with arbitrary precision, while different components of the velocity operator in the Pauli theory do commute and can therefore be measured simultaneously with arbitrary precision. One can well ask how the operators which purportedly represent the same physical variable in the two theories can have such completely different properties.

One can conclude from the above discussion that the relation between the Dirac theory and the Pauli theory is by no means clear from the usual method of descending from four- to two-component wave functions, and that further clarification of the connection between the theories would be desirable. In what follows we present an alternative method for passing from four- to two-component wave functions in the Dirac theory which alternative method clarifies many of the questions left open by the usual treatment. The method consists of a transformation to a new representation for the Dirac theory, putting the theory in a form closely analogous to the Pauli theory and permitting a direct comparison of the two. Specifically, we shall show that:

(1) For a free Dirac particle there exists a representation of the Dirac theory in which, for both relativistic and non-relativistic energies, positive-energy states and negative-energy states are separately described by two-component wave functions.

(2) There exists in the Dirac theory another position operator than the usual one; this operator has the property that its time derivative is the operator $\mathbf{p}/(m^2+p^2)^{\frac{1}{2}}$ for positive-energy states and $-\mathbf{p}/(m^2+p^2)^{\frac{1}{2}}$ for negative-energy states corresponding to the conventional concept of the velocity of the particle. It is this new position operator (which we call the *mean-position operator*) that in the non-relativistic limit is interpreted as the position operator of the Pauli theory.

(3) While the z component of the spin operator, $\boldsymbol{\sigma}=(1/2i)[\boldsymbol{\alpha}\times\boldsymbol{\alpha}]$, in the Dirac theory is not a constant of the motion, there exists in the Dirac theory another spin operator $\boldsymbol{\Sigma}$ (which we call the *mean-spin operator*) whose z component is a constant of the motion. In the non-relativistic limit, the operator $\boldsymbol{\Sigma}$ is the one which is interpreted as the spin operator in the Pauli theory.

(4) From a study of the transformation to the new representation further insight can be obtained into the question of why the Dirac particle has a magnetic moment and why it appears to show a behavior characteristic of a particle with finite extension of the order of its Compton wave-length.

(5) In the presence of interaction, such as with an external electromagnetic field, one can still make a transformation which leads to a representation involving two-component wave functions. The transformation, which previously could be made exactly, must now be made by an infinite sequence of transformations which process leads to a Hamiltonian which is an infinite series in powers of $(1/m)$, where m is the mass of the particle. This series is presumably semi-convergent in the sense that for given external fields, a finite number of terms of the series is a better-and-better approximation to the exact Hamiltonian, the larger the value of m. For strong interactions which strongly couple free-particle states of positive and negative energy, this representation is of little value; however, for sufficiently weak interactions, a finite number of terms of the series may be employed to obtain relativistic corrections to any order in $(1/m)$. In this way one can obtain the proper non-relativistic limit for the Hamiltonian representing a Dirac particle interacting with any type of external field.

THE FREE DIRAC PARTICLE

The essential reason why four components are in general necessary to describe a state of positive or negative energy in the representation of the Dirac theory corresponding to Eq. (1) is that the Hamiltonian in this equation contains odd operators,[3] specifically the components of the operator $\boldsymbol{\alpha}$. If it is possible to perform a canonical transformation on Eq. (1) which brings it into a form which is free of odd operators, then it will be possible to represent positive- and negative-energy states by wave functions having only two components in each case, the other pair of components being identically zero. We shall now show that there exists a canonical transformation which accomplishes just this end.

If S is an Hermitian operator, then the transformation,

$$\Psi' = e^{iS}\Psi, \tag{3}$$

$$H' = e^{iS}He^{-iS} - ie^{iS}(\partial e^{-iS}/\partial t), \tag{4}$$

[3] An odd operator in the Dirac theory is a Dirac matrix which has only matrix elements connecting upper and lower components of the wave function, while an even operator is one having no such matrix elements. Of the sixteen linearly independent matrices in the Dirac theory, the matrices 1, β, $\boldsymbol{\sigma}=1/2i[\boldsymbol{\alpha}\times\boldsymbol{\alpha}]$ and $\beta\boldsymbol{\sigma}$ are even, while the matrices $\boldsymbol{\alpha}$, $\beta\boldsymbol{\alpha}$, $\gamma^5=-i\alpha^1\alpha^2\alpha^3$ and $\beta\gamma^5$ are odd. The product of two even matrices or of two odd matrices is an even matrix, while the product of an odd matrix and an even matrix is an odd matrix. The matrix β commutes with all even matrices and anticommutes with all odd matrices in the Dirac theory. This last fact allows one to write any matrix as the sum of an odd and an even matrix in a simple way, namely:

$$m=\tfrac{1}{2}\{m+\beta m\beta\}+\tfrac{1}{2}\{m-\beta m\beta\},$$

where the first term on the right is the even part of the matrix and the second term is the odd part of the matrix m.

leaves Eq. (1) in the Hamiltonian form:

$$H'\Psi'=i(\partial\Psi'/\partial t). \tag{5}$$

(It must be remembered that in a canonical transformation of this type a physical variable whose operator-representative in the old representation is T has for its operator-representative in the new representation the operator:

$$T'=e^{iS}Te^{-iS}.) \tag{6}$$

Let us make a transformation of this type on Eq. (1) with S the non-explicitly time-dependent operator:

$$S=-(i/2m)\beta\alpha\cdot\mathbf{p}w(p/m), \tag{7}$$

where w is a function of the operator[4] (p/m) whose form is to be determined such that H' is free of odd operators. With this choice of S one may readily show that

$$\begin{aligned}H'&=e^{iS}He^{-iS}=e^{2iS}H\\&=[\cos(pw/m)+(\beta\alpha\cdot\mathbf{p}/p)\sin(pw/m)]H\\&=\beta[m\cos(pw/m)+p\sin(pw/m)]\\&\quad+\alpha\cdot\mathbf{p}/p[p\cos(pw/m)-m\sin(pw/m)].\end{aligned} \tag{8}$$

We see from this that H' will be free of odd operators if we choose

$$w(p/m)=(m/p)\tan^{-1}(p/m), \tag{9}$$

and with this choice, we obtain

$$H'=\beta(m^2+p^2)^{\frac{1}{2}}=\beta E_p, \tag{10}$$

where E_p represents the *operator* $(m^2+p^2)^{\frac{1}{2}}$.

Equation (5), with H' given by (10), now has solutions such that the upper components represent positive energies and the lower components negative energies, for splitting Ψ' into its upper and lower components:

$$\Psi'=\Phi'+X',$$
$$\Phi'=\tfrac{1}{2}(1+\beta)\Psi',\quad X'=\tfrac{1}{2}(1-\beta)\Psi',$$

reduces Eq. (5) to the two uncoupled equations:

$$E_p\Phi'=i(\partial\Phi'/\partial t), \tag{11}$$

$$-E_pX'=i(\partial X'/\partial t). \tag{12}$$

In order for one to understand completely the nature of the transformation which we have performed, however, it is necessary to investigate in greater detail the manner in which the wave function and certain operators transform. A general wave function can be expressed in the form:

$$\Psi(\mathbf{x})=\int u(\mathbf{p}')\exp(i\mathbf{p}'\mathbf{x})d\mathbf{p}'=\Psi_+(\mathbf{x})+\Psi_-(\mathbf{x}), \tag{13}$$

$$\Psi_+(\mathbf{x})=\int\frac{1}{2}\left[1+\frac{\beta m+\alpha\cdot\mathbf{p}'}{E_{p'}}\right]u(\mathbf{p}')\exp(i\mathbf{p}'\cdot\mathbf{x})d\mathbf{p}', \tag{14}$$

$$\Psi_-(\mathbf{x})=\int\frac{1}{2}\left[1-\frac{\beta m+\alpha\cdot\mathbf{p}'}{E_{p'}}\right]u(\mathbf{p}')\exp(i\mathbf{p}'\cdot\mathbf{x})d\mathbf{p}', \tag{15}$$

where Ψ_+ represents the positive energy part and Ψ_- the negative energy part of Ψ. Now

$$\begin{aligned}e^{iS}&=\exp\left(\frac{1}{2m}\frac{\beta\alpha\cdot\mathbf{p}}{p}\tan^{-1}\frac{p}{m}\right)\\&=\cos[\tfrac{1}{2}\tan^{-1}(p/m)]+(\beta\alpha\cdot\mathbf{p}/p)\sin[\tfrac{1}{2}\tan^{-1}(p/m)]\\&=\left[\frac{E_p+m}{2E_p}\right]^{\frac{1}{2}}+\frac{\beta\alpha\cdot\mathbf{p}}{p}\left[\frac{E_p-m}{2E_p}\right]^{\frac{1}{2}}\\&=\frac{\beta\{\beta m+\alpha\cdot\mathbf{p}+\beta E_p\}}{[2E_p(E_p+m)]^{\frac{1}{2}}},\end{aligned} \tag{16}$$

and hence

$$\Psi_+'=e^{iS}\Psi_+=\left(\frac{1+\beta}{2}\right)\int\left[\frac{2E_{p'}}{E_{p'}+m}\right]^{\frac{1}{2}}\times\frac{1}{2}$$
$$\times\left[1+\frac{\beta m+\alpha\cdot\mathbf{p}'}{E_{p'}}\right]u(\mathbf{p}')\exp(i\mathbf{p}'\cdot\mathbf{x}')d\mathbf{p}'=\Phi', \tag{17}$$

$$\Psi_-'=e^{iS}\Psi_-=\left(\frac{1-\beta}{2}\right)\int\left[\frac{2E_{p'}}{E_{p'}+m}\right]^{\frac{1}{2}}\times\frac{1}{2}$$
$$\times\left[1-\frac{\beta m+\alpha\cdot\mathbf{p}'}{E_{p'}}\right]u(\mathbf{p}')\exp(i\mathbf{p}'\cdot\mathbf{x}')d\mathbf{p}'=X', \tag{18}$$

$$\Psi'=e^{iS}\Psi=\Psi_+'+\Psi_-'. \tag{19}$$

We may legitimately identify Ψ_+' with Φ' and Ψ_-' with X' since the presence of the factors $(1+\beta)/2$ and $(1-\beta)/2$ shows that these functions have only upper and lower components, respectively. Thus we see that indeed the transformation is such as to lead to a representation in which upper components correspond to positive energies and lower components to negative energies.

Furthermore, since

$$u(\mathbf{p}')=\frac{1}{(2\pi)^3}\int\Psi(\mathbf{x}')\exp(-i\mathbf{p}'\cdot\mathbf{x}')d\mathbf{x}',$$

we have

$$\Psi'(\mathbf{x})=\int K(\mathbf{x},\mathbf{x}')\Psi(\mathbf{x}')d\mathbf{x}', \tag{20}$$

where

$$K(\mathbf{x},\mathbf{x}')=\frac{1}{(2\pi)^3}\int\left[\frac{2E_{p'}}{E_{p'}+m}\right]^{\frac{1}{2}}$$
$$\times\left[1+\frac{\beta(\beta m+\alpha\cdot\mathbf{p}')}{E_{p'}}\right]\exp(i\mathbf{p}'\cdot(\mathbf{x}-\mathbf{x}'))d\mathbf{p}'. \tag{21}$$

[4] A function $T(\mathbf{p})$ of the operator $\mathbf{p}$ is to be interpreted (in the coordinate representation) as defined by its Taylor expansion in powers of $(\mathbf{p}-\mathbf{p}_0)$, where $\mathbf{p}_0$ is any constant vector (c number), wherever the expansion converges, and by the analytic continuation of this series elsewhere; or, alternatively, by its integral-operator representation:

$$T(\mathbf{p})\Psi(\mathbf{x})=\frac{1}{(2\pi)^3}\int\int T(\mathbf{p}')\exp[i\mathbf{p}'\cdot(\mathbf{x}-\mathbf{x}')]\Psi(\mathbf{x}')d\mathbf{p}'d\mathbf{x}'.$$

Since $K(\mathbf{x}, \mathbf{x}')$ is not a Dirac delta-function in its space dependence, the transformation of Ψ is an integral rather than a point transformation. In general, Ψ' at a given point is constituted from contributions depending on Ψ over a neighborhood of dimensions of the order of a Compton wave-length of the particle about the point. Thus a wave function which in the old representation corresponded to a state in which the particle was definitely located at one point, passes over in the new representation into a wave function which apparently corresponds to the particle being spread out over a finite region.

The key to understanding this rather unusual statement lies in the fact that in the new representation, the operator-representative for the position of the particle is no longer the operator $\mathbf{x}$, but the rather complicated operator:

$$\mathbf{x}'=e^{iS}\mathbf{x}e^{-iS}=\mathbf{x}-\frac{i\beta\boldsymbol{\alpha}}{2E_p}+\frac{i\beta(\boldsymbol{\alpha}\cdot\mathbf{p})\mathbf{p}-[\boldsymbol{\sigma}\times\mathbf{p}]p}{2E_p(E_p+m)p}. \quad (22)$$

But if this is the case, then what is the operator-representative $\mathbf{X}$ in the old representation of the physical variable whose operator-representative in the new representation is $\mathbf{X}'=\mathbf{x}$? We find

$$\mathbf{X}=e^{-iS}\mathbf{x}e^{iS}=\mathbf{x}+\frac{i\beta\boldsymbol{\alpha}}{2E_p}-\frac{i\beta(\boldsymbol{\alpha}\cdot\mathbf{p})\mathbf{p}+[\boldsymbol{\sigma}\times\mathbf{p}]p}{2E_p(E_p+m)p}. \quad (23)$$

In order to interpret this new "position" operator, we calculate its time derivative:

$$\frac{d\mathbf{X}}{dt}=i[H,\mathbf{X}]=\frac{\mathbf{p}}{E_p}\cdot\frac{\{\beta m+\boldsymbol{\alpha}\cdot\mathbf{p}\}}{E_p}. \quad (24)$$

But since $\Lambda_p=(\beta m+\boldsymbol{\alpha}\cdot\mathbf{p})/E_p$ has the value $+1$ when applied to a positive energy wave function and the value -1 when applied to a negative energy wave function,[5] we see that the time derivative of $\mathbf{X}$ is just the "conventional" velocity operator $+\mathbf{p}/E_p$ for positive energy states and $-\mathbf{p}/E_p$ for negative energy states. The operator-representative of $d\mathbf{X}/dt$ in the new representation is

$$d\mathbf{X}'/dt=d\mathbf{x}/dt=i[H',\mathbf{x}]=\beta\mathbf{p}/E_p \quad (25)$$

with the same properties. We note also that since the operator $\mathbf{p}$ commutes with S, the operator-representative for the momentum in the new representation is still $\mathbf{p}$.

By comparing these results with certain well-known facts about the Dirac electron, we may understand the significance of our change in representation. In discussions of the Dirac theory one finds an analysis of the motion of a free Dirac electron which shows that the electron performs a very complicated motion, indeed.[6] Its velocity can be written as the sum of two parts: the first is essentially the conventional velocity operator

$$\frac{\mathbf{p}}{E_p}\frac{\beta m+\boldsymbol{\alpha}\cdot\mathbf{p}}{E_p},$$

but to this is added a second term representing a rapidly oscillating motion ("Zitterbewegung") which ensures that a measurement of the instantaneous value of any velocity component shall yield the velocity of light. Our results above show that a corresponding division of the position operator for the particle is also possible, the first part $\mathbf{X}$ (in the old representation) representing a sort of mean position of the particle, and the second part $\mathbf{X}-\mathbf{x}$, oscillating rapidly about zero with an amplitude of the order of the Compton wave-length of the particle. While in the old representation the position operator $\mathbf{x}$ played the dominant role, in the new representation it is the position operator $\mathbf{X}'$, which we shall call the *mean-position* operator,[7] which plays the dominant role. Also, as will become obvious later when we consider the interaction of the particle with an external field, it is the *mean-position* operator which is identified with the position operator in the non-relativistic Pauli theory.

The modification in the interpretation of operators involved in our transformation does not end here, however, but new angular momentum operators also appear. In the old representation, the orbital angular momentum of the particle whose operator-representative is $[\mathbf{x}\times\mathbf{p}]$ and the spin angular momentum of the particle whose operator-representative is $1/2\boldsymbol{\sigma}$ are not separately constants of the motion,[6] although their sum is a constant of the motion. However, as one may readily verify, the operators $[\mathbf{X}\times\mathbf{p}]$ and

$$\boldsymbol{\Sigma}=\boldsymbol{\sigma}-\frac{i\beta[\boldsymbol{\alpha}\times\mathbf{p}]}{E_p}-\frac{[\mathbf{p}\times[\boldsymbol{\sigma}\times\mathbf{p}]]}{E_p(E_p+m)}, \quad (26)$$

whose analogues in the new representation are, respectively,

$$[\mathbf{X}'\times\mathbf{p}]=e^{iS}[\mathbf{X}\times\mathbf{p}]e^{-iS}=[\mathbf{x}\times\mathbf{p}], \quad (27)$$

and

$$\boldsymbol{\Sigma}'=e^{iS}\boldsymbol{\Sigma}e^{-iS}=\boldsymbol{\sigma}, \quad (28)$$

[5] E. Schrödinger, Berl. Ber. 419 (1930); 63 (1931).

[6] See, for example, P. A. M. Dirac, *The Principles of Quantum Mechanics* (Oxford University Press, New York, 1935), Second Edition, Chapter XII. See also in this connection, reference 2, pp. 230–231.

[7] The operator, which we have designated the mean-position operator, has been discovered independently in other connections by several authors. M. H. L. Pryce (Proc. Roy. Soc. **150A**, 166 (1935)) found it useful to introduce this operator (as well as the operator which we later define as the mean spin angular momentum) in connection with the definition of coordinate and intrinsic angular momentum operators in the Born-Infeld theory, and again (Proc. Roy. Soc. **195A**, 62 (1948)) in a discussion of relativistic definitions of center of mass for systems of particles. In the latter paper, he also noted that this operator was connected with the usual position operator in the Dirac theory by a canonical transformation which is identical with the one performed above in this paper. T. D. Newton and E. P. Wigner (Rev. Mod. Phys. **21**, 400 (1949)) also found this operator in an investigation of localized states for elementary systems. The latter authors have also shown that this is the only position operator, with commuting components, in the Dirac theory which has localized eigenfunctions in the manifold of positive energy wave functions.

TABLE I. Table of operator-representatives of dynamical variables in old and new representations.

Dynamical variable	Operator-representative in old representation	Operator-representative in new representation
Position	$\mathbf{x}$	$\mathbf{x}'=\mathbf{x}-\frac{i\beta\boldsymbol{\alpha}}{2E_p}+\frac{i\beta(\boldsymbol{\alpha}\cdot\mathbf{p})\mathbf{p}-[\boldsymbol{\sigma}\times\mathbf{p}]\mathbf{p}}{2E_p(E_p+m)p}$
Momentum	$\mathbf{p}\equiv(\hbar/i)\nabla$	$\mathbf{p}'=\mathbf{p}$
Hamiltonian	$H=\beta m+\boldsymbol{\alpha}\cdot\mathbf{p}$	$H'=\beta(m^2+p^2)^{\frac{1}{2}}\equiv\beta E_p$
Velocity	$\boldsymbol{\alpha}=\dot{\mathbf{x}}$	$\boldsymbol{\alpha}'=\boldsymbol{\alpha}+\frac{\beta\mathbf{p}}{E_p}-\frac{(\boldsymbol{\alpha}\cdot\mathbf{p})\mathbf{p}}{E_p(E_p+m)}$
	β	$\beta'=(m\beta-\boldsymbol{\alpha}\cdot\mathbf{p})/E_p$
Orbital angular momentum	$[\mathbf{x}\times\mathbf{p}]$	$[\mathbf{x}'\times\mathbf{p}]$
Spin angular momentum	$\boldsymbol{\sigma}\equiv(1/2i)[\boldsymbol{\alpha}\times\boldsymbol{\alpha}]$	$\boldsymbol{\sigma}'=\boldsymbol{\sigma}+\frac{i\beta[\boldsymbol{\alpha}\times\mathbf{p}]}{E_p}-\frac{\mathbf{p}\times[\boldsymbol{\sigma}\times\mathbf{p}]}{E_p(E_p+m)}$
Mean position	$\mathbf{X}=\mathbf{x}+\frac{i\beta\boldsymbol{\alpha}}{2E_p}-\frac{i\beta(\boldsymbol{\alpha}\cdot\mathbf{p})\mathbf{p}+[\boldsymbol{\sigma}\times\mathbf{p}]\mathbf{p}}{2E_p(E_p+m)p}$	$\mathbf{X}'=\mathbf{x}$
Mean velocity	$\dot{\mathbf{X}}=\frac{\mathbf{p}}{E_p}\cdot\left\{\frac{\beta m+\boldsymbol{\alpha}\cdot\mathbf{p}}{E_p}\right\}$	$\dot{\mathbf{X}}'=\frac{\beta\mathbf{p}}{E_p}$
Mean orbital angular momentum	$[\mathbf{X}\times\mathbf{p}]$	$[\mathbf{X}'\times\mathbf{p}]=[\mathbf{x}\times\mathbf{p}]$
Mean spin angular momentum	$\boldsymbol{\Sigma}=\boldsymbol{\sigma}-\frac{i\beta[\boldsymbol{\alpha}\times\mathbf{p}]}{E_p}-\frac{[\mathbf{p}\times[\boldsymbol{\sigma}\times\mathbf{p}]]}{E_p(E_p+m)}$	$\boldsymbol{\Sigma}'=\boldsymbol{\sigma}$
Λ_p	$\Lambda_p\equiv\frac{\beta m+\boldsymbol{\alpha}\cdot\mathbf{p}}{E_p}$	$\Lambda_p'=\beta$

are separately constants of the motion. We shall denote the physical variables of which these operators are the operator-representatives as the *mean-orbital angular momentum* and *mean spin angular momentum*, respectively, of the particle. It is again these variables which are conventionally identified with the orbital angular momentum and the spin angular momentum of the particle in the non-relativistic Pauli theory. For convenience, we have listed in Table I the operator-representatives in the old representation and in the new representation of the physical variables of principal interest in the Dirac theory.

DIRAC PARTICLE IN AN EXTERNAL ELECTROMAGNETIC FIELD

We consider now the case where a Dirac particle interacts with an external field such as the electromagnetic field. Before proceeding to the general case, however, it is instructive to consider an elementary special case in order to clarify some points regarding the classification of states as either of positive or negative energy. Let us consider first a Dirac particle moving in a weak static electric field derivable from a scalar potential φ. The Hamiltonian is then

$$H=\beta m+\boldsymbol{\alpha}\cdot\mathbf{p}-e\varphi.$$

For the case of a free particle, states were classified as of positive or negative energy according as they corresponded to values of $+1$ or -1, respectively, for the operator $(\beta m+\boldsymbol{\alpha}\cdot\mathbf{p})/E_p$ which was a constant of the motion. In the present case, however, this operator does not commute with the Hamiltonian and is therefore not a constant of the motion. If we regard the electric field as a perturbation, then one can say that the electric field induces transitions of the particle between the positive- and negative-energy states of a free particle. This is one way of viewing the physical situation.

On the other hand, one knows that for sufficiently weak fields the Hamiltonian above possesses a complete set of eigenfunctions with energy eigenvalues which may be classified according to whether they are positive or negative. There exists for these weak fields a clear-cut distinction between these two sets of stationary states[8] since they are separated by a relatively large energy gap of order $2m$. Furthermore, the wave functions corresponding to positive energies show a behavior of the particle appropriate to a particle of positive mass,[9] in that the particle tends to be localized in regions of low potential energy; while the negative-energy solutions show a behavior of the particle appropriate to a particle of negative mass, in that the particle tends to be localized in regions of high potential energy.

Either of the two descriptions of the behavior of the particle in a weak field given above is of course correct, although the distinction between what are called positive- and negative-energy states is different in the two descriptions. However, the question of terminology for positive- and negative-energy states being left to our own choice, we are free to choose our definitions in such a way as to give the more graphic (and perhaps more

[8] It is assumed that the constant in the energy is chosen so that zero energy occurs approximately midway in the energy gap between the two sets of states.

[9] It is perhaps better to classify the states as states of positive or negative *mass* rather than energy, since the addition of a constant to the energy (by adding a constant to φ, for example) may upset energy classification but not the mass classification.

intuitively satisfying) description of the actual physical events which are being described. In this spirit we feel that the second description is to be preferred since it has a perfectly reasonable classical limit. It would be difficult indeed to picture classically the motion of a particle in a weak field in terms of transitions between free-particle motions with positive and negative mass.

Consider now what happens when the particle interacts with strong rather than weak fields. Under such circumstances, the division of states into those of positive and negative mass is no longer clear-cut, since the energy, separation of the two sets of states is reduced to a relatively small amount. Furthermore, the wave functions describing these states no longer appropriately describe the motion of a particle of fixed sign of mass according to our customary notions. In fact, if we try to interpret the wave function in these terms, we encounter certain well-known paradoxes—the Klein paradox, for example. While the energy of any stationary state will still have a definite sign, the statement that the particle is in a state of positive energy will no longer carry with it the validity of any intuitive conceptions as to the behavior of a classical particle with positive energy, and there will be little qualitative difference between certain states of positive energy and certain states of negative energy. Hence, in the presence of strong fields, the usefulness of a description in terms of positive and negative-energy states will be lost.

These same ideas may be carried over to the case of more general interactions. If there are any advantages to be accrued by the employment of two-component wave functions to describe states of positive and negative energy for a free particle, we may expect these advantages to be present still in the case of weak interactions, but they can scarcely survive in the case of strong interactions. To define *weak interactions* in a more quantitative fashion, we prescribe that the interaction terms have no time Fourier components comparable with or greater than m, so that no transitions between free-particle states with energy differences of this latter order of magnitude are possible; and that the interaction terms have no space Fourier components comparable with or greater than m, so that no transitions between free-particle states with momentum differences of this order of magnitude are possible. Under these conditions, if the initial state is one in which no high momentum states occur, then the momentum of the particle will remain small compared to m under the influence of the interactions. In these circumstances we have essentially a non-relativistic problem, and hence it will be in the domain of *non-relativistic problems* that a representation by means of two-component wave functions may be expected to be of value.

In the presence of interaction it no longer appears possible to make a single, simple, canonical transformation to a representation in which the Hamiltonian is free of odd operators, but instead one can always make a sequence of transformations, each of which eliminates odd operators from the Hamiltonian to one higher order in the expansion parameter[10] $1/m$. In this way one obtains in the new representation a Hamiltonian free of odd operators which is an infinite power series in powers of $1/m$. While it can hardly be expected that this series is convergent, the series is presumably an asymptotic or semi-convergent series in the sense that the sum of a finite number of terms of the series is a better-and-better approximation to the true Hamiltonian, the larger the value of m, provided the magnitude of the interaction remains fixed. The usefulness of the series is then contingent on the interactions being sufficiently weak compared to m in just the sense described above for non-relativistic problems.

Turning our attention now to the explicit calculation in the case where a Dirac particle is subject to interactions, we note first that the Hamiltonian operator can always be put in the form[3]

$$H=\beta m+\mathcal{E}+\mathcal{O}, \tag{29}$$

where $\mathcal{E}$ is an even operator and $\mathcal{O}$ is an odd operator, both of which may be explicitly time-dependent. We assume (and this is ordinarily the case) that $\mathcal{E}$ and $\mathcal{O}$ are of no lower order in $(1/m)$ than $(1/m)^0$. Consider now the canonical transformation generated by the Hermitian operator

$$S=-(i/2m)\beta\mathcal{O}. \tag{30}$$

We note that if the operator S may be regarded as small, then we can make an expansion in powers of $(1/m)$ of the Hamiltonian in the new representation:

$$\begin{aligned} H'&=e^{iS}He^{-iS}-ie^{iS}\left(\frac{\partial e^{-iS}}{\partial t}\right)\\ &=H+\frac{\partial S}{\partial t}+i\left[S,H+\frac{1}{2}\frac{\partial S}{\partial t}\right]\\ &\quad+\frac{i^2}{2!}\left[S,\left[S,H+\frac{1}{3}\frac{\partial S}{\partial t}\right]\right]+\cdots. \end{aligned} \tag{31}$$

Carrying this out explicitly for the Hamiltonian above and retaining terms only to order $(1/m)^2$, we obtain

$$\begin{aligned} H'=\beta m+\mathcal{E}+\frac{\beta}{2m}\mathcal{O}^2-\frac{1}{8m^2}\left[\mathcal{O},[\mathcal{O},\mathcal{E}]+\frac{\partial\mathcal{O}}{\partial t}\right]\\ -\frac{1}{2m}\beta\frac{\partial\mathcal{O}}{\partial t}+\frac{\beta}{2m}[\mathcal{O},\mathcal{E}]-\frac{1}{3m^2}\mathcal{O}^3+\cdots, \end{aligned} \tag{32}$$

[10] The expansion parameter may equally well be regarded as $1/c$ where c is the velocity of light. The actual dimensionless expansion parameters are the operators $(\hbar/mc)\nabla$ and $(\hbar/mc^2)(\partial/\partial t)$. From this, one sees that the successive terms of the series will decrease rapidly in magnitude if the interaction potentials do not vary appreciably in space over a Compton wave-length of the particle and in time over the period required for light to travel a Compton wave-length. This is equivalent to the restrictions imposed above on the space and time Fourier components of the interaction.

where we have made use of the fact that β commutes with all even operators and anticommutes with all odd operators in the Dirac theory. Remembering that the product of two even or two odd operators is an even operator and that the product of an odd and an even operator is an odd operator, we see that we have removed by this transformation all odd operators of order $(1/m)^0$ from the Hamiltonian although odd operators of order $(1/m)$ and higher remain and are given in the second line.

From this we see that by a sequence of further canonical transformations, the generator of the transformation at each step being chosen to be

$$S=-(i/2m)\beta \text{ (odd terms in Hamiltonian of lowest order in } 1/m), \quad (33)$$

we may successively remove odd terms from the Hamiltonian to any desired order in $(1/m)$. If we continue this process indefinitely, we obtain, as mentioned earlier, a Hamiltonian which is an infinite power series in $(1/m)$ completely free of odd operators.

Let us now apply this method to the case where the Dirac particle interacts with an external electromagnetic field. In this case the Hamiltonian is given by

$$H=\beta m-e\varphi+\boldsymbol{\alpha}\cdot(\mathbf{p}-e\mathbf{A}), \quad (34)$$

where φ and $\mathbf{A}$ are the scalar and vector potentials of the electromagnetic field evaluated at the *position* of the particle. In accordance with the procedure outlined above, we then first make the canonical transformation generated by

$$S_1=-\frac{i}{2m}\beta\boldsymbol{\alpha}\cdot(\mathbf{p}-e\mathbf{A}),$$

obtaining then for the new Hamiltonian,

$$H_1=\beta m-e\varphi+\frac{\beta}{2m}(\mathbf{p}-e\mathbf{A})^2-\frac{e}{2m}\beta\boldsymbol{\sigma}\cdot\mathbf{H}$$
$$-\frac{e}{4m^2}\boldsymbol{\sigma}\cdot\mathbf{E}\times(\mathbf{p}-e\mathbf{A})+\frac{e}{8m^2}\operatorname{div}\mathbf{E}-\frac{ie}{2m}\beta\boldsymbol{\alpha}\cdot\mathbf{E}$$
$$-\frac{1}{3m^2}[(\mathbf{p}-e\mathbf{A})^2-e\boldsymbol{\sigma}\cdot\mathbf{H}]\boldsymbol{\alpha}\cdot(\mathbf{p}-e\mathbf{H})+\cdots,$$

to terms of order $(1/m)^2$. Following with the two canonical transformations generated by

$$S_2=-\frac{i}{2m}\beta\left\{-\frac{ie}{2m}\beta\boldsymbol{\alpha}\cdot\mathbf{E}\right\},$$

and

$$S_3=-\frac{i}{2m}\beta\left\{-\frac{e}{4m^2}\beta\boldsymbol{\alpha}\cdot\frac{\partial\mathbf{E}}{\partial t}\right.$$
$$\left.-\frac{1}{3m^2}[(\mathbf{p}-e\mathbf{A})^2-e\boldsymbol{\sigma}\cdot\mathbf{H}]\boldsymbol{\alpha}\cdot(\mathbf{p}-e\mathbf{A})\right\},$$

we eliminate odd operators from the Hamiltonian of order $(1/m)$ and $(1/m)^2$ respectively and obtain the Hamiltonian

$$H_3=\beta m-e\varphi+\frac{\beta}{2m}(\mathbf{p}-e\mathbf{A})^2-\frac{e}{2m}\beta\boldsymbol{\sigma}\cdot\mathbf{H}$$
$$-\frac{e}{4m^2}\boldsymbol{\sigma}\cdot\mathbf{E}\times(\mathbf{p}-e\mathbf{A})+\frac{e}{8m^2}\operatorname{div}\mathbf{E}+\cdots, \quad (35)$$

free of odd operators to order $(1/m)^2$. In the above $\mathbf{H}=\operatorname{curl}\mathbf{A}$ and $\mathbf{E}=-\nabla\varphi-\partial\mathbf{A}/\partial t$ are the magnetic and electric field strengths evaluated at what is now essentially the *mean-position* of the particle. By further canonical transformations we could remove odd operators of still higher order, but we shall limit our discussion of the Hamiltonian in the new representation to terms of order $(1/m)^2$.

Since the Hamiltonian (36) is free of odd operators, its eigenfunctions are two-component functions corresponding again to positive and negative energies. For positive energies, the Schrödinger equation is

$$\left\{m-e\varphi+\frac{1}{2m}(\mathbf{p}-e\mathbf{A})^2-\frac{e}{2m}\boldsymbol{\sigma}\cdot\mathbf{H}-\frac{e}{4m^2}\boldsymbol{\sigma}\cdot\mathbf{E}\times(\mathbf{p}-e\mathbf{A})\right.$$
$$\left.+\frac{e}{8m^2}\operatorname{div}\mathbf{E}\right\}\Phi=i\frac{\partial\Phi}{\partial t}, \quad (36)$$

which will be recognized as essentially the Pauli equations for a non-relativistic particle of spin $\frac{1}{2}$ interacting with the electromagnetic field. The presence of the terms corresponding to the interaction of the anomalous magnetic moment of the particle with the magnetic field and the spin-orbit interaction is evident. The term proportional to $\operatorname{div}\mathbf{E}$ is a well-known correction[11] to the Pauli theory arising from the Dirac theory, and it is responsible for a relativistic shift of the S levels in the hydrogen atom (not to be confused with the Lamb-Retherford line shift).

The reason for the explicit appearance of these additional interaction terms (as well as further terms of higher order in $1/m$) in the new representation can now be understood in the light of our physical interpretation of the transformation to the new representation. In the old representation the Dirac particle interacted with the electromagnetic field only at its *position*. However, a particle which in the old representation was located at a point is in the new representation spread out over a region of dimensions of the order of a Compton wavelength in the space of its *mean-position variable*, $\mathbf{X}'=\mathbf{x}$. But in the new representation the interaction between the particle and the electromagnetic field is expressed in terms of the values of the electromagnetic-field quantities at its *mean-position*. Hence, one must expect a series of correction terms of the nature of a multipole

[11] C. G. Darwin, Proc. Roy. Soc. 118A, 654 (1928).

expansion of the field, since the particle is actually spread out over a finite region in the space of its *mean-position variable*. From this point of view the explicit appearance of the magnetic-moment interaction and the accompanying spin-orbit interaction in the Hamiltonian is to be expected. In fact, the term in div**E**, which has previously been regarded as of rather mysterious origin, can now also easily be understood since it comes from the fact that the electric charge in the new representation is also spread out over a finite region. In a static potential, the particle then moves according to a suitable average of the potential over this region. But in lowest order such an averaging process is known to lead to a term proportional to the Laplacian of the potential and this is just the character of the term in div**E**.

(In employing a finite number of terms in a Hamiltonian such as (35) it must be remembered that wave functions, transition matrix elements, and expectation values of operators computed from the Hamiltonian are only correct to terms of the order in $(1/m)$ to which terms in the Hamiltonian are retained. Thus in the case of (36) it would not be consistent to retain only terms of order $(1/m)$ in the Hamiltonian and then to employ terms of this order in second-order perturbation theory where they generate terms of order $(1/m)^2$.)

The method employed above for reducing the Hamiltonian to non-relativistic two-component form for the case of interaction with an external electromagnetic field can be employed generally for interaction of a Dirac particle with any type of external field, such as various types of meson fields. With meson fields one obtains, in different cases, various types of spin interaction with the meson field and also various types of spin-orbit coupling terms such as have been employed in discussions of spin-orbit coupling in nuclei. The discussion of the reduction to non-relativistic form in the case of the many-particle theory is left for a later communication.

ACKNOWLEDGMENTS

This investigation arose out of a conversation between the authors and Dr. A. S. Wightman to whom we are indebted for subsequent valuable discussions on this subject. One of the authors (L.L.F.) wishes to express his gratitude to the University of Rochester for the hospitality extended to him in the period in which this work was initiated. This work was supported at Case Institute of Technology by the AEC and at the University of Rochester by the joint program of the ONR and the AEC.

PHYSICAL REVIEW VOLUME 78, NUMBER 1 APRIL 1, 1950

The Nucleon Magnetic Moment in Meson Pair Theories

J. LEITE LOPES*
*Institute for Advanced Study, Princeton, New Jersey***
(Received November 30, 1949)

The contribution to the nucleon magnetic moment from an interaction of the nucleon with a spinor or scalar meson pair field is calculated. In both cases it is found to be logarithmically divergent.

THE covariant formulation of the pseudoscalar meson theory[1] together with the concepts of mass and charge renormalization[2] were applied by Case[3] to the computation of the anomalous magnetic moment of nucleons. He showed that finite results are then obtained. This is essentially due to the fact that one is now able to isolate and incorporate[2] the divergences into the mass and charge of the nucleon field thus leaving a convergent expression for the magnetic moment. This separation of the reactive terms represents an improvement over the previous treatment of this and related problems.[4] On the other hand, divergence difficulties are still encountered in the magnetic moment calculation based on the vector meson theory with tensor coupling.[5]

It is the aim of this note to report on the application of the renormalization program to the computation of nucleon magnetic moments by assuming a meson pair interaction (containing no derivatives of the fields) between the heavy particles. Two cases have been considered for the meson field, namely, the scalar (or pseudoscalar, which here amounts to the same) and the

* John Simon Guggenheim Memorial Fellow, on leave of absence from the University of Brazil, Rio de Janeiro.
** Present address: Faculdade Nacional de Filosofia, Rio de Janeiro, Brazil.

[1] S. Kanesawa and S. Tomonaga, Prog. Theor. Phys. **3**, 1 (1948); Y. Myiamoto, Prog. Theor. Phys. **3**, 124 (1948).
[2] See F. J. Dyson, Phys. Rev. **75**, 486, 1736 (1949).
[3] K. M. Case, Phys. Rev. **76**, 1 (1949); compare also J. M. Luttinger, Helv. Phys. Acta **21**, 483 (1948); M. Slotnick and W. Heitler, Phys. Rev. **75**, 1645 (1949); S. D. Drell, Phys. Rev. **76**, 427 (1949).
[4] Finite results for the nucleon magnetic moment were previously obtained by J. M. Jauch (Phys. Rev. **63**, 334 (1943)) in the conventional theory by using the lambda-limiting process; the nucleon field was treated non-relativistically.
[5] K. M. Case, Phys. Rev. **75**, 1440 (1949).

spinor one. The assumption that interactions of the type here investigated might partially contribute to the magnetic moment of nucleons is not without physical interest; indeed, the present stage of the theory of beta-decay as well as of the nuclear capture of negative mu-mesons does not seem to exclude[6] such couplings as are dealt with in this paper.

The result obtained from an interaction of the nucleon field with a spinor or a (bilinearly coupled) scalar meson field is that, even after renormalization is effected, the magnetic moment still diverges. This is not unexpected. It is a well known fact[7] that the meson pair theories give rise to nucleonic interactions strongly singular at small distances and it is reasonable to expect from these theories results more singular than those from the linear theories.

1. Let us first consider the case of a pair interaction of the nucleon field ψ with a scalar meson field ϕ_α. We shall use the four-dimensional isotopic spin formalism introduced by Case.[3] ϕ_α is a set of four real scalar fields; ϕ_1 and ϕ_2 describe each positively and negatively charged mesons; ϕ_3 describes the neutral mesons which are superposed to the charged ones in a symmetrical theory; ϕ_4 is another neutral meson field. The first three components of the isotopic spin τ_α are the conventional matrices τ_1, τ_2, τ_3, the eigenvalue $+1$ of τ_3 corresponding to a neutron, -1 to a proton; τ_4 is the unity operator in isotopic spin space.

In the interaction representation, the nucleon and scalar fields obey the uncoupled equations of motion and satisfy the following commutation rules (in units $\hbar$ and c):

$$\begin{aligned}&[\phi_\alpha(x), \phi_\beta(x')]=i\delta_{\alpha\beta}\Delta(x-x');\\ &\{\psi_\mu(x), \bar\psi_\nu(x')\}=-iS_{\mu\nu}(x-x');\\ &\{\psi_\mu(x), \psi_\nu(x')\}=\{\bar\psi_\mu(x), \bar\psi_\nu(x')\}=0.\end{aligned} \tag{1}$$

The index μ corresponds to both spin and isotopic spin components; also:*

$$S(x)=S_P(x)\tau_P+S_N(x)\tau_N, \tag{2}$$

$$\tau_P=\tfrac{1}{2}(1-\tau_3);\quad \tau_N=\tfrac{1}{2}(1+\tau_3). \tag{3}$$

The interaction hamiltonian density for the system meson-nucleon field in an external electromagnetic field A_μ is the following:

$$H=H'+H_1^{\text{ext}}+H_2^{\text{ext}}, \tag{4}$$

$$H'=\tfrac{1}{2}f_{\alpha\alpha}\bar\psi\psi\phi_\alpha{}^2+f_{i4}\bar\psi\tau_i\psi\phi_i\phi_4 \tag{5}$$

$$H_1^{\text{ext}}=-ie\bar\psi\gamma_\mu\tau_P\psi A_\mu, \tag{6}$$

$$\begin{aligned}H_2^{\text{ext}}=&-eA_\mu\{\phi_1(\partial\phi_2/\partial x_\mu)-\phi_2(\partial\phi_1/\partial x_\mu)\}\\ &+(e^2/2)\{A_\mu{}^2+(n_\lambda A_\lambda)^2\}(\phi_1{}^2+\phi_2{}^2).\end{aligned} \tag{7}$$

H' is the interaction of the nucleon with the pair field. The f's are the coupling constants; the summation over α runs from 1 to 4, over i from 1 to 3. H_1^{ext} and H_2^{ext} describe the interaction of the nucleon and meson currents, respectively, with the external electromagnetic field. The charge conjugated expressions have been omitted from (4) which is always permissible provided that one replaces the vacuum expectation value of expressions of the type $\bar\psi(x)\psi(x)$ by zero.

The Hamiltonian (5) can be expressed in the following compact form:

$$H'=\tfrac{1}{2}f_{\alpha\beta}\bar\psi\tau_\alpha\tau_\beta\psi\phi_\alpha\phi_\beta, \tag{8}$$

where the summation over α and β runs from 1 to 4; $f_{\alpha\beta}=f_{\beta\alpha}$. Gauge invariance requires further that $f_{11}=f_{22}$; $f_{14}=f_{24}$. The several possibilities regarding the charge of a meson pair are specified by the following choice of coupling constants:

Charged pair theory:

$$f_{14}=f_{24}\neq 0;\quad \text{the other } f\text{'s}=0.$$

Symmetrical pair theory:

$$\begin{aligned}&f_{14}=f_{24}\neq 0;\quad f_{11}=f_{22}\neq 0;\quad f_{33}\neq 0;\\ &\qquad\text{the other } f\text{'s}=0.\end{aligned} \tag{9}$$

Neutral pair theory:

$$f_{11}=f_{22}\neq 0;\quad f_{44}\neq 0;\quad \text{other } f\text{'s}=0.$$

The effective interaction Hamiltonian from which the nucleon magnetic moment can be evaluated in the order ef^2 is:

$$H_{\text{eff}}=H_1+H_2, \tag{10}$$

where:

$$\begin{aligned}H_1=\frac{(-i)^2}{2}\int\int dxdyP\{&-ie\bar\psi(x_0)\gamma_\mu\tau_P\psi(x_0)A_\mu(x_0),\\ &\tfrac{1}{2}f_{\alpha\beta}\bar\psi(x)\tau_\alpha\tau_\beta\psi(x)\phi_\alpha(x)\phi_\beta(x),\\ &\tfrac{1}{2}f_{\gamma\epsilon}\bar\psi(y)\tau_\gamma\tau_\epsilon\psi(y)\phi_\gamma(y)\phi_\epsilon(y)\};\end{aligned} \tag{11}$$

$$\begin{aligned}H_2=\frac{(-i)^2}{2}\int\int dxdyP&\\ \times\Big\{&-eA_\mu(x_0)\Big[\phi_1(x_0)\frac{\partial\phi_2(x_0)}{\partial x_\mu{}^0}-\phi_2(x_0)\frac{\partial\phi_1(x_0)}{\partial x_\mu{}^0}\Big]\\ &\tfrac{1}{2}f_{\alpha\beta}\bar\psi(x)\tau_\alpha\tau_\beta\psi(x)\phi_\alpha(x)\phi_\beta(x),\\ &\tfrac{1}{2}f_{\gamma\epsilon}\bar\psi(y)\tau_\gamma\tau_\epsilon\psi(y)\phi_\gamma(y)\phi_\epsilon(y)\Big\};\end{aligned} \tag{12}$$

the integrations are over the four-dimensional space and P is the chronological ordering operator introduced by Dyson.[2]

We need to evaluate the expectation value of (10) for the state defined by the meson vacuum and one nucleon present in the field. The meson vacuum expectation values of the P-brackets occurring in (11)

[6] J. Tiomno and J. A. Wheeler, Rev. Mod. Phys. 21, 144, 153 (1949).

[7] See S. Hjalmars, Arkiv. f. Fysik 1, No. 3 (1949); O. Brulin, Arkiv. f. Fysik 1, No. 4, 5 (1949), and references therein.

* The functions Δ and S_P are defined as in J. Schwinger, Phys. Rev. 74, 1439 (1948) and refer to particles with mass κ and M_P, respectively.

and (12) are:

$$\langle P\{\phi_\alpha(x)\phi_\beta(x),\,\phi_\gamma(y)\phi_\epsilon(y)\}\rangle_0$$
$$=\tfrac{1}{4}(\delta_{\alpha\gamma}\delta_{\beta\epsilon}+\delta_{\alpha\epsilon}\delta_{\beta\gamma})\Delta_F^2(x-y);$$

$$\left\langle P\left\{\phi_1(x_0)\frac{\partial\phi_2(x_0)}{\partial x_\mu^0}-\phi_2(x_0)\frac{\partial\phi_1(x_0)}{\partial x_\mu^0},\right.\right.$$
$$\left.\left.\phi_\alpha(x)\phi_\beta(x),\,\phi_\gamma(y)\phi_\epsilon(y)\right\}\right\rangle_0$$
$$=\tfrac{1}{8}\{(\delta_{1\alpha}\delta_{2\gamma}-\delta_{1\gamma}\delta_{2\alpha})\delta_{\beta\epsilon}+(\delta_{1\alpha}\delta_{2\epsilon}-\delta_{1\epsilon}\delta_{2\alpha})\delta_{\beta\gamma}$$
$$+(\delta_{1\beta}\delta_{2\gamma}-\delta_{1\gamma}\delta_{2\beta})\delta_{\alpha\epsilon}+(\delta_{1\beta}\delta_{2\epsilon}-\delta_{1\epsilon}\delta_{2\beta})\delta_{\alpha\gamma}\}$$
$$\times\left\{\Delta_F(x_0-x)\frac{\partial\Delta_F(x_0-y)}{\partial x_\mu^0}\right.$$
$$\left.-\Delta_F(x_0-y)\frac{\partial\Delta_F(x_0-x)}{\partial x_\mu^0}\right\}\Delta_F(x-y);$$

$\Delta_F(x)$ is the Feynman function.**

The one-nucleon expectation value of the P-brackets containing ψ, $\bar\psi$ can be evaluated along the lines indicated by Dyson[2] and Case.[3] The expressions thus obtained give the following expectation value for (10):

$$\langle H_{\text{eff}}\rangle=H_1{}^a+H_1{}^b+\langle H_2\rangle,$$

where:

$$H_1{}^a=-\frac{ie}{64}f_{\alpha\beta}f_{\gamma\epsilon}A_\mu\int\int dxdy\,\text{Trace}$$
$$\times\{S_F(x_0-x)\psi_\mu\tau_P S_F(x-x_0)\tau_\alpha\tau_\beta\}$$
$$\times\{\delta_{\alpha\gamma}\delta_{\beta\epsilon}+\delta_{\alpha\epsilon}\delta_{\beta\gamma}\}\Delta_F^2(x-y)\bar\psi(y)\tau_\gamma\tau_\epsilon\psi(y)\quad(13)$$

describes the vacuum polarization by meson pairs emitted by the nucleon and vanishes on account of:***

$$\text{Trace}\{S_F(x_0-x)\gamma_\mu\tau_P S_F(x-x_0)\tau_\alpha\tau_\beta\}=0.\quad(14)$$

Furthermore:

$$H_1{}^b=\frac{ie}{64}f_{\alpha\beta}{}^2A_\mu\int\int dxdy\bar\psi(x)\tau_\alpha\tau_\beta S_F(x_0-x)$$
$$\times\gamma_\mu\tau_P S_F(y-x_0)(\tau_\alpha\tau_\beta+\tau_\beta\tau_\alpha)\psi(y)\Delta_F^2(x-y)\quad(15)$$

is the analog of the Lamb-shift in the electromagnetic problem. Finally:

$$\langle H_2\rangle=\frac{ie}{8}f_{14}f_{24}A_\mu\int\int dxdy\bar\psi(x)\tau_3 S_F(y-x)\psi(y)$$
$$\times\left\{\Delta_F(x_0-x)\frac{\partial\Delta_F(x_0-y)}{\partial x_\mu^0}\right.$$
$$\left.-\Delta_F(x_0-y)\frac{\partial\Delta_F(x_0-x)}{\partial x_\mu^0}\right\}\Delta_F(x-y)\quad(16)$$

corresponds to the interaction of the meson current with the external electromagnetic field; $\langle H_2\rangle$ has opposite signs for neutron and proton and vanishes in a neutral pair theory (see relations (9) above).

Both (15) and (16) give a logarithmically divergent contribution to the magnetic moment. The divergence comes from the occurrence of the extra factor $\Delta_F(x-y)$ in the integrand as compared to the expression of the linear theory; the number of Δ_F-functions in (15) and (16) corresponds physically to the emission and reabsorption of a meson pair by the nucleon. The divergent character of $H_1{}^b$ and $\langle H_2\rangle$ can best be seen by transforming them into momentum space. $H_1{}^b$ is found to be proportional to the following integral:

$$I=A_\mu\int\int d^4k\,d^4k'\frac{\bar\psi(x_0)\tau_\alpha\tau_\beta\{i\gamma_\lambda(P_\lambda'-k_\lambda-k_\lambda')-M\}\gamma_\mu\tau_P\{i\gamma_\nu(P_\nu'-k_\nu-k_\nu')-M\}\tau_{\alpha\beta}\psi(x_0)}{\{(P_\lambda'-k_\lambda-k_\lambda')^2+M^2\}\{(P_\lambda-k_\lambda-k_\lambda')^2+M^2\}\{k_\lambda^2+\kappa^2\}\{k_\lambda'^2+\kappa^2\}};$$
$$\tau_{\alpha\beta}=\tfrac{1}{2}(\tau_\alpha\tau_\beta+\tau_\beta\tau_\alpha),$$

where $M=M_P=M_N$. I can be expressed in the following form:

$$I=2A_\mu\int\frac{d^4k'}{k_P'^2+\kappa^2}\int_0^1 dx\int_0^1 J_\mu ydy,$$

where:

$$J_\mu=\int d^4k\frac{\bar\psi(x_0)\tau_\alpha\tau_\beta\{i\gamma_\lambda(Q_\lambda'-k_\lambda)-M\}\gamma_\mu\tau_P\{i\gamma_\nu(Q_\nu-k_\nu)-M\}\tau_{\alpha\beta}\psi(x_0)}{\{(k_\lambda+C_\lambda)^2+B^2\}^3}$$
$$Q_\lambda'=P_\lambda'-k_\lambda';\quad Q_\lambda=P_\lambda-k_\lambda';\quad C_\lambda=y\{k_\lambda'-[(P_\lambda'-P_\lambda)x+P_\lambda]\};$$
$$B^2=\kappa^2(1-y)+[k_\lambda'^2-2k_\lambda'((P_\lambda'-P_\lambda)x+P_\lambda)]y-C_\lambda^2.$$

With $k_\lambda+C_\lambda=u_\lambda$, the integration over k becomes:

$$J_\mu=J_{1\mu}+J_{2\mu},$$

** See Case, reference 3, Eq. (23).

*** A more general proof of the vanishing of the vacuum polarization for certain types of coupling is given by Case, reference 3, Appendix A.

where:

$$J_{1\mu}=\int d^4u\bar{\psi}(x_0)\frac{\tau_\alpha\tau_\beta\{i\gamma_\lambda(Q_\lambda'+C_\lambda)-M\}\gamma_\mu\tau_P\{i\gamma_\nu(Q_\nu+C_\nu)-M\}\tau_{\alpha\beta}\psi(x_0)}{(u^2+B^2)^3},$$

$J_{2\mu}$ is a logarithmically divergent integral; it can be discarded since it is independent of the nucleon momentum transfer and does, therefore, give no contribution to the magnetic moment. The integration in $J_{1\mu}$ is easily carried out and it is found that $H_1{}^b$ is proportional to:

$$A_\mu\int_0^1 dx\int_0^1 ydy\int\frac{d^4k'}{k_P{}'^2+\kappa^2}\frac{\bar{\psi}(x_0)T_\mu\psi(x_0)}{B^2} \tag{17}$$

$$T_\mu=\tau_\alpha\tau_\beta\{i\gamma_\lambda(Q_\lambda'+C_\lambda)-M\}\times\gamma_\mu\tau_P\{i\gamma_\nu(Q_\nu+C_\nu)-M\}\tau_{\alpha\beta}.$$

The analysis for $\langle H_2\rangle$ can be carried out in a similar manner.

After elimination of the renormalization terms—those independent of the nucleon momentum transfer—we are left with a logarithmically divergent magnetic moment which, apart from numerical coefficients, is roughly of the form:

$$(-\sum_\alpha f_{\alpha\alpha}{}^2+f_{14}{}^2)M\int_0^\infty\frac{k'^3dk'}{(k'^2+\kappa^2)(k'^2+M^2)}$$

for the proton:

$$-f_{14}{}^2M\int_0^\infty\frac{k'^3dk'}{(k'^2+\kappa^2)(k'^2+M^2)}$$

for a neutron.

We see that the divergence of the magnetic moment is not removed by separation of the renormalization terms.

2. For an interaction of the nucleons with a spinor field φ, (5) and (7) are replaced by:

$$H'=\tfrac{1}{2}g_{\alpha\beta}\bar{\psi}\tau_\alpha\tau_\beta\psi\bar{\varphi}\tau_{\alpha\beta}'\varphi;\quad \tau_{\alpha\beta}'=\tfrac{1}{2}(\tau_\alpha'\tau_\beta'+\tau_\beta'\tau_\alpha');$$
$$H_2{}^{\text{ext}}=-ie\bar{\varphi}\gamma_\mu'\tau_e\varphi A_\mu,$$

$g_{\alpha\beta}=g_{\beta\alpha}$ are the coupling constants; the dash indicates that τ' refers to the light spinor particles. τ_e and τ_ν are analogous to τ_P and τ_N in (3).

$H_1{}^a$ also vanishes in the present case. $H_1{}^b$ and $\langle H_2\rangle$ are now as follows:

$$H_1{}^b=-\frac{ie}{64}g_{\alpha\beta}g_{\gamma\epsilon}A_\mu\int\int dxdy\bar{\psi}(x)\times\tau_\alpha\tau_\beta S_F(x_0-x)\gamma_\mu\tau_P S_F(y-x_0)\tau_\gamma\tau_\epsilon\psi(y)\times\text{Trace}\{\tau_{\gamma\epsilon}'S_F'(x-y)\tau_{\alpha\beta}'S_F'(y-x)\}; \tag{18}$$

$$\langle H_2\rangle=\frac{e}{64}g_{\alpha\beta}g_{\gamma\epsilon}A_\mu\int\int dxdy\bar{\psi}(x)\times\tau_\alpha\tau_\beta S_F(x-y)\tau_\gamma\tau_\epsilon\psi(y)\text{Trace}\{S_F'(x_0-y)\times\gamma_\mu'\tau_e S_F'(x-x_0)\tau_{\alpha\beta}'S_F'(y-x)\tau_{\gamma\epsilon}'\}, \tag{19}$$

where:

$$S_F'(x)=S_F{}^e\tau_e+S_F{}^\nu\tau_\nu.$$

Thus, for a proton:

$$H_{1P}{}^b=-\frac{ie}{64}g_{\alpha\alpha}{}^2A_\mu\int\int dxdy\bar{\psi}_P(x)S_F{}^P(x_0-x)\times\gamma_\mu S_F{}^P(y-x_0)\psi_P(y)\text{Trace}\{S_F{}^e(y-x)\times S_F{}^e(x-y)+S_F{}^\nu(y-x)S_F{}^\nu(x-y)\};$$

$$\langle H_{2P}\rangle=\frac{ie}{16}g_{14}g_{24}A_\mu\int\int dxdy\bar{\psi}_P(x)S_F{}^N(y-x)\psi_P(y)\times\text{Trace}\{S_F{}^e(x_0-y)\gamma_\mu'S_F{}^e(x-x_0)S_F{}^\nu(y-x)\}.$$

and for a neutron:

$$H_{1N}{}^b=-\frac{ie}{64}g_{14}g_{24}A_\mu\int\int dxdy\bar{\psi}_N(x)S_F{}^P(x_0-x)\times\gamma_\mu S_F{}^P(y-x_0)\psi_N(y)\text{Trace}\{S_F{}^e(y-x)S_F{}^\nu(x-y)\};$$

$$\langle H_{2N}\rangle=-\frac{ie}{16}g_{14}g_{24}A_\mu\int\int dxdy\bar{\psi}_N S_F{}^P(y-x)\psi_N(y)\times\text{Trace}\{S_F{}^e(x_0-y)\gamma_\mu'S_F{}^e(x-x_0)S_F{}^\nu(y-x)\}.$$

The same conclusion is also reached here, namely, that from both (18) and (19) a logarithmically divergent magnetic moment is derived, as in the scalar pair theory.

In conclusion, the author would like to express his appreciation to Professor Oppenheimer for the kind hospitality extended him at the Institute for Advanced Study and to him, to Dr. A. Pais and to Dr. R. Karplus for helpful discussions.

Solar Magnetic Moment and Diurnal Variation in Intensity of Cosmic Radiation*

KIRBY DWIGHT
Palmer Physical Laboratory, Princeton University, Princeton, New Jersey
(Received August 15, 1949)

The effect of the earth's magnetic field upon the orbits of primary cosmic-ray particles is computed in detail for the special case of those particles arriving vertically anywhere on the earth's surface. A procedure is evolved for taking this deflection in conjunction with the previous deflection in the magnetic field of the sun, and thereby calculating for any given cosmic-ray energy spectrum an expected diurnal variation in total cosmic-ray intensity. Examples of this procedure are given for an inverse power spectrum applied to two different magnitudes of the solar magnetic moment. The sample calculations are made for several latitudes of observation, and the expected diurnal variation is then studied as a function of the solar magnetic moment and of the energy spectrum. The phase of the variation is found to be very sensitive to the solar moment, and so it is hoped that a successful experimental determination of the diurnal variation will settle the question of the existence and magnitude of a permanent solar magnetic moment.

I. INTRODUCTION

IF, as proposed by G. E. Hale,[1] the Sun has a polar field of 50 gauss (or a magnetic moment of 10^{34} gauss-cm^3, 1000 times that of the earth), then it will have a substantial effect on the trajectories of cosmic-ray particles, producing a latitude cut-off and diurnal variations of intensity. It is important to calculate exactly what this predicted effect is, and to look for it in experiments. Then one can hope to know whether or not there exists a permanent solar magnetic moment, and if so, of what magnitude. This question is significant both for solar and for cosmic-ray physics.

As yet it has been impossible to compute from the known properties of matter theoretical values for the magnetic moments of massive rotating bodies which agree with experiment. For this reason, Blackett[2] and others have considered the possibility of the existence of a relation (not envisaged in existing theory) between rotating mass and magnetic fields. This hypothesis has given good agreement with the observed fields of several stars, but much further information is required before it can be taken seriously. One of the necessities is the resolution of the uncertainty surrounding the magnitude, or even existence, of a general solar magnetic moment.

Considerable doubt was thrown upon Hale's conclusions from measurements of the Zeeman splitting of the solar spectrum lines[1] by the fact that several of his observers failed to detect any splitting. This doubt was augmented by the failure to find a completely successful explanation of his observation of different splittings for different spectrum lines. Then, in 1935 (a year of minimum sunspot activity), Thiessen made a similar observation, and concluded that the polar field was 53 ± 10 gauss.[3] During the next few years, Babcock found variations in the total solar field. These variations inspired Thiessen to repeat his observations in 1946 (a year of maximum sunspot activity), with the astonishing result that he failed to detect any solar field as large as 5 gauss.[4] It is clear that the inconsistencies among the experimental results prevent the determination of a reliable value for the permanent solar magnetic moment, and even throw doubt on its existence.

Similar inconsistencies are also present in experimental observations of the leveling off of cosmic-ray intensity with increasing latitude of incidence. Because of the decreasing cut-off effect of the earth's magnetic field toward the poles, a continuous rise in intensity with increasing latitude is to be expected. Actually there appears to be a saturation. No natural explanation is known for such an effect except the hypothesis that low energy particles are not present in the primary radiation. This exclusion could easily be understood on the basis of a permanent solar magnetic moment, as suggested by Janossy. Thus a solar field would result in a sharp knee in the curve representing intensity as a function of latitude. However, according to some experiments the intensity continues to rise gradually, whereas in some it even decreases, and in others merely behaves irregularly.[5] Thus once more doubt arises concerning the existence of a general solar magnetic moment.

The question of what the energy spectrum really looks like is fundamental to cosmic-ray studies. It is clear that if the energy cut-off exists and cannot be accounted for on the grounds of a permanent solar magnetic moment, then we must search for an explanation in the mechanism of creation, acceleration, and energy loss of the primary cosmic-ray particles. Hence the problem of the solar moment is important for the problem of cosmic-ray origin.

* Assisted by the Joint Program of the ONR and AEC.

[1] Hale, Seares, VanMaanen, and Ellerman, Astrophys. J. 47, 206 (1918).

[2] P. M. S. Blackett, Phil. Mag. 40, 125 (1949). This article also summarizes the earlier literature.

[3] A more complete summary of observations of solar fields is given by Blackett in reference 2.

[4] G. Thiessen, Observatory 66, 230 (1946). Also H. Von Kluber, Zeits. f. Astrophys. 24 (1947) and 121 (1947).

[5] M. G. E. Cosyns, Nature 137, 616 (1936); Millikan, Neher, and Pickering, Phys. Rev. 63, 234 (1943); Biehl, Montgomery, Neher, Pickering, and Roesch, Rev. Mod. Phys. 20, 360 (1948).

It is interesting to note that both types of observations mentioned above yield for the solar moment the same order of magnitude, 10^{34} gauss-cm^3, as far as the inconsistencies permit the deduction of values. In order to investigate the solar moment further, we must assume it to exist, and then try to deduce additional consequences which can be subjected to experimental test. One such effect is a diurnal variation in intensity of cosmic radiation, deduced originally by Janossy.[6] Further analyses have been made by Epstein,[7] by Vallarta and Godart in general terms,[8] and in greater detail by Rossi.[9] Many experiments have been performed in an attempt to detect the phenomenon,[10] but they have been unsuccessful.[11] However, these observations were all made on the ground, *where there should be practically no diurnal variation.* For the particles which contribute most to the diurnal variation are those of low energy (3 Bev). At ground level there is only a minute contribution to the intensity from the particles of that energy, either directly or through secondaries. Even at airplane altitudes (30,000 ft.), the effects of 3-Bev particles are presumably too weak to be significant for observations.[12]

In this paper we give, for two different values of the solar moment, the detailed calculation of the diurnal variation for the special case of primary radiation received vertically on the earth. Mr. W. G. Stroud made experimental determinations of the diurnal variation in vertical intensity at high altitudes (95,000 ft.) in the summer of 1949. Such experiments include an appreciable solid angle about the vertical. Fortunately this spread has only a small effect.[13] Thus such experiments, together with the present calculations, should lead to further information about the magnetic moment of the sun.

II. CALCULATED EFFECT

It is easy to see why a diurnal variation in intensity is to be expected if the sun does have a permanent magnetic moment. Moving charged particles, such as cosmic rays, will be deflected in the solar field, and so will be able to approach the earth from outer space only in certain allowed directions, which form a cone,[14] called the *solar allowed cone.* Therefore at any instant, particles of a given energy can arrive at the earth's surface vertically only over a certain region. This region is fixed in space, and so a given point on the earth will pass into it and then out again as the earth rotates. Thus, a diurnal variation in intensity of primary radiation at that point is produced.

In spite of the explanation given in the previous section, physicists still felt somewhat uncomfortable that there should be no indication of any diurnal variation at ground level. The effect expected for the primary radiation was so strong that it seemed that it should have some influence upon the intensity of the secondary particles. To try to account for this disturbing situation. Alfvén[15] suggested that the orbits forbidden by the solar field might be partially filled by particles scattered by the magnetic field of the earth. Further theoretical investigations showed that, because of this scattering, particles with any given energy that can approach the earth in some direction are never completely excluded from any other direction.[16] It is estimated that for a permanent solar moment of the order of 10^{34} gauss-cm^3, the intensity in "forbidden" directions is of the order of 90 percent of the full intensity. Therefore the expected effect is much smaller, and we shall certainly have to go to high altitudes to observe it.

The solar allowed cone centers about the tangent to the earth's orbit, and opens out backward along it. All positive particles arrive at full intensity from this direction. Hence, if there were no further deflection in the magnetic field of the earth, a maximum in vertical intensity of cosmic radiation would occur at 6 P.M. Because of the terrestrial field, a positive particle arriving from the direction of the axis of the solar allowed cone will be received vertically at a given point on the earth not at 6 P.M., but somewhat earlier. Therefore, the maximum total intensity occurs before 6 P.M.

In order to find the latitude at which the phenomenon can most easily be detected, we must study the variation as a function of latitude of observation. At very low latitudes, those particles which are appreciably affected by the solar field are prevented from reaching the earth by the terrestrial field. The amount of the resulting deflection of a particle depends upon its energy. Hence at other latitudes, where entry is possible, the individual variations of intensity with time of arrival at the earth for radiation of different energies are displaced with respect to one another. Thus a distortion, or smearing out, of the total variation of intensity with time is produced which is greatest for radiation incident at low latitudes, and so here no maximum in intensity exists. At the poles there is no distortion, but then the rotation

[6] L. Janossy, Zeits. f. Physik **104**, 430 (1937).
[7] P. S. Epstein, Phys. Rev. **53**, 862 (1938).
[8] M. Vallarta and O. Godart, Rev. Mod. Phys. **11**, 180 (1939).
[9] We are indebted to B. Rossi for a chance to see his unpublished calculations (1947).
[10] S. A. Korff, Rev. Mod. Phys. **11**, 211 (1939); V. Sarabhai and P. Nicolson, Proc. Phys. Soc. **60**, 509 (1948) give further references.
[11] The diurnal effect sought here has to be distinguished from the well known, and rather small, variations in sea-level cosmic-ray intensity which are associated with changes in the temperature of the atmosphere. Such changes receive a reasonable explanation in terms of changes in the height of the meson-producing layer and in the decay of mesons on their way from that elevation to the ground.
[12] Unpublished report from M.I.T. Laboratory.
[13] Malmfors, Arkiv. f. Mat. Astr. o. Fys. **30A**, No. 12 (1944) and **32**, No. 8 (1945).
[14] L. Janossy and P. Lockett, Proc. Roy. Soc. **A178**, 52 (1941); Lemaitre and M. Vallarta, Phys. Rev. **50**, 500 (1936); M. Vallarta, Nature **139**, 839 (1937); M. Vallarta, *Applied Mathematics Series* (Toronto Press, Toronto, 1938), No. 3.
[15] H. Alfvén, Phys. Rev. **72**, 88 (1947).
[16] Kane, Shanley, and Wheeler, Rev. Mod. Phys. **21**, 51–71 (1949).

of the earth has no effect, so that again there is no diurnal variation. We conclude that intermediate latitudes will be best for observing the effect.

Sample calculated diurnal variations in vertical intensity are shown in Figs. 1–4. No allowance has been made for the difference between the magnetic axis of the earth and the geographic one, since the necessary correction is very special, having to be computed separately for incidence at different longitudes. This omission has only a slight effect upon the shape of the curve representing the diurnal variation, and leaves the phase and magnitude unaltered. The effect it does have is indicated in Fig. 5, where the corrected theory for incidence in the plane containing the two axes is compared with the approximate theory. Figure 6 shows the seasonal change. In view of the uncertainty about the existence or magnitude of the solar moment, it seemed hardly appropriate to allow for the supposed difference in orientation between the solar magnetic axis and axis of rotation.

The relative intensity is based on a scale where 100 corresponds to the case of all energies above cut-off arriving at full intensity, in order that the magnitudes of the variations can be read directly as percentages.

The smaller value of the solar magnetic moment gives rise to virtually no diurnal variation at latitudes of observation of 45° and 51°, as is shown by qualitative reasoning in the next section. It is evident from the curves that both the magnitude and phase of the variation are sensitive functions of the solar moment. Consequently, there are excellent prospects that we can obtain information about the magnitude of this moment

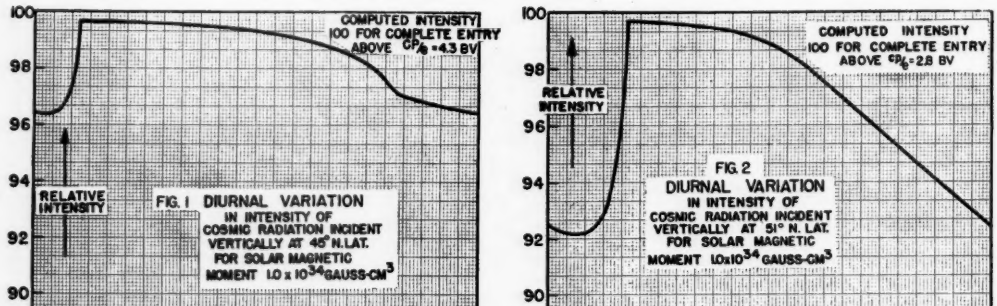
COMPUTED INTENSITY 100 FOR COMPLETE ENTRY ABOVE CP_ϕ =4.3 BV
RELATIVE INTENSITY
FIG. 1 DIURNAL VARIATION IN INTENSITY OF COSMIC RADIATION INCIDENT VERTICALLY AT 45° N.LAT. FOR SOLAR MAGNETIC MOMENT 1.0 x 10^{34} GAUSS-CM^3
LOCAL TIME
NOON
COMPUTED INTENSITY 100 FOR COMPLETE ENTRY ABOVE CP_ϕ=2.8 BV
FIG. 2 DIURNAL VARIATION IN INTENSITY OF COSMIC RADIATION INCIDENT VERTICALLY AT 51° N. LAT. FOR SOLAR MAGNETIC MOMENT 1.0x10^{34} GAUSS-CM^3
CP_ϕ =1.8 BV SOLAR MAGNETIC MOMENT 0.42 x 10^{34} GAUSS-CM^3
COMPUTED INTENSITY 100 FOR COMPLETE ENTRY ABOVE:
CP_ϕ =2.32 BV SOLAR MAGNETIC MOMENT 1.0 x 10^{34} GAUSS-CM^3
FIG. 3 DIURNAL VARIATION IN INTENSITY OF COSMIC RADIATION INCIDENT VERTICALLY AT 56° N.LAT.
COMPUTED INTENSITY 100 FOR COMPLETE ENTRY ABOVE:
CP_ϕ =2.32 BV SOLAR MAGNETIC MOMENT 1.0x10^{34} GAUSS-CM^3
CP_ϕ =0.97 BV SOLAR MAGNETIC MOMENT 0.42 x 10^{34} GAUSS-CM^3
FIG. 4 DIURNAL VARIATION IN INTENSITY OF COSMIC RADIATION INCIDENT VERTICALLY AT 66° N.LAT.
COMPUTED INTENSITY 100 FOR COMPLETE ENTRY ABOVE CP_ϕ = 2.32 BV
SIMPLE THEORY
CORRECTED THEORY
FIG. 5 CORRECTED DIURNAL VARIATION IN INTENSITY OF COSMIC RADIATION INCIDENT VERTICALLY AT 56° N.LAT. FOR SOLAR MAGNETIC MOMENT 1.0 x 10^{34} GAUSS-CM^3
COMPUTED INTENSITY 100 FOR COMPLETE ENTRY ABOVE CP_ϕ = 2.32 BV
FALL
SPRING
FIG. 6 SEASONAL CHANGE OF DIURNAL VARIATION IN INTENSITY OF COSMIC RADIATION INCIDENT VERTICALLY AT 56° N.LAT. FOR SOLAR MAGNETIC MOMENT 1.0 x 10^{34} GAUSS-CM^3

FIGS. 1–6. Sample diurnal variations in total intensity, calculated for a differential cosmic-ray spectrum. $I \sim p^{-2.75}$.

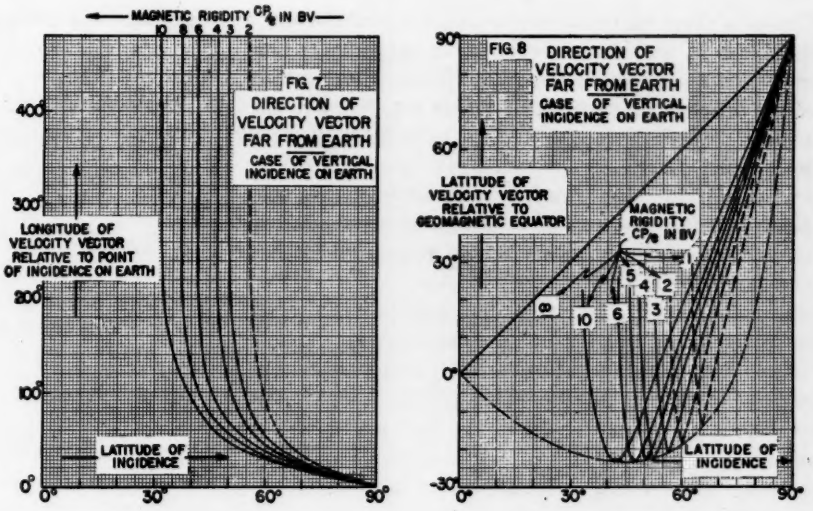

FIGS. 7–8. Fundamental deflection curves, from which the diurnal variation in total intensity can be derived.

(if any) from successful observations of the diurnal variation in vertical intensity at high altitudes and appropriate latitudes.

To obtain the examples of the diurnal variation (Figs. 1–6) as deduced from our fundamental computations, we used for convenience a differential spectrum where the full intensity of radiation of a given energy was inversely proportional to the corresponding momentum raised to the 2.75 power. Theoretical studies of the means of accelerating cosmic-ray particles predict a power law form of spectrum, and the value used here is the best experimental value at the moment.[17] It was obtained for high energies by replacing the block diagrams of experimental observations by a smooth curve. This curve deviates from the blocks for energies less than 10 Bev, but the hypothesis of energy loss via neutrinos gives an excellent quantitative adjustment of the discrepancy down to, say, 5 Bev.[17] The experiment used averaged over all directions, and allowing for the exclusion of low energy particles from some directions would improve the agreement for still lower energies. Thus the experiment does not contradict the assumption of a power law for the primary radiation. However, it is not necessary to have an analytic form for the differential spectrum in order to deduce the diurnal variation from our computations. The procedure given in this paper can be applied straightforwardly using the integral spectrum given directly by experiment.

Because of our assumption of a power law, it is to be expected that determinations of the diurnal variation by experiments on particles subject to the experimental spectrum[17] will differ in a shape from our sample calculations. But the position of the maximum and sudden rise to it should remain unaltered. The principal difference will be a drastic decrease in the magnitude of the calculated variation. Thus a successful observation of the diurnal variation will indicate through its amplitude the nature of the energy spectrum, and through its phase, the magnitude of the solar magnetic moment. More generally, *high altitude observations of the diurnal changes in intensity of primary cosmic radiation are valuable for studying both the solar magnetic moment and the cosmic-ray energy spectrum.*

[17] N. Hilberry, Phys. Rev. **60**, 7 (1941).

III. SUMMARY OF ANALYSIS

The fundamental result of our computations consists of two families of curves, plotted in Figs. 7 and 8. They give the two angles needed to describe the direction of motion at large distances from the earth for a particle which strikes the earth vertically with any energy at any latitude. From them the total diurnal variation in vertical intensity at any point on the earth's surface can be deduced to any desired degree of approximation for any type of particles, subject to any form of energy spectrum. The derivation of these fundamental curves and the process of deducing the diurnal variation from them are given in this section.

As a charged particle enters the solar system from outer space, it is deflected by the magnetic field of the sun. Then when it approaches near enough to the earth, it suffers further deflection. The problem of a charged particle acted upon simultaneously by two dipole magnetic fields is a very complex one. Fortunately we can make a simplification.

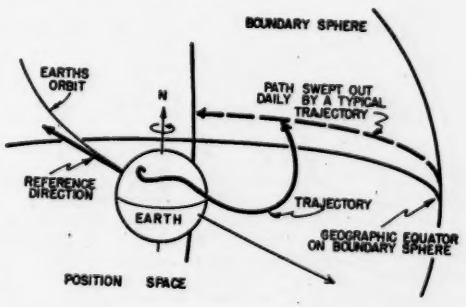

FIG. 9. The physical meaning of the integration. Diagram of position space (origin of diurnal variation).

Consider the surface about the earth where the sun's magnetic field and that of the earth are equal. This surface can be approximated by a sphere whose radius is of the order of 22 earth-radii, which we shall call the *boundary sphere*. Since the earth's field falls off very rapidly with increasing distance, we can neglect its effect outside the boundary sphere. Conversely, its field increases rapidly as we decrease r, and so inside the sphere we can neglect the sun's field compared to that of the earth.

The problem of the intensity distribution has already been solved for the region outside the boundary sphere by Kane, Shanley, and Wheeler.[16] Therefore we have only to (A) determine the behavior of the particles inside the sphere, making use of the fact that here the earth may be considered an isolated system, and then (B) apply the existing calculations as boundary conditions at the surface of the sphere. We shall treat the case of positive particles.

A. Calculation of Asymptotic Velocity Vector

To find the paths followed by positive particles, we must integrate the differential equations of motion:[18]

$$z''=\tfrac{1}{2}\frac{\partial}{\partial z}\left[1-\left(\frac{2g}{\rho}-\frac{\rho}{r^3}\right)^2\right], \tag{1}$$

$$\rho''=\tfrac{1}{2}\frac{\partial}{\partial \rho}\left[1-\left(\frac{2g}{\rho}-\frac{\rho}{r^3}\right)^2\right], \tag{2}$$

$$\rho^2\phi'=2g-\rho^2/r^3, \tag{3}$$

where primes represent differentiation with respect to arc length, r is the radial distance from the origin (center

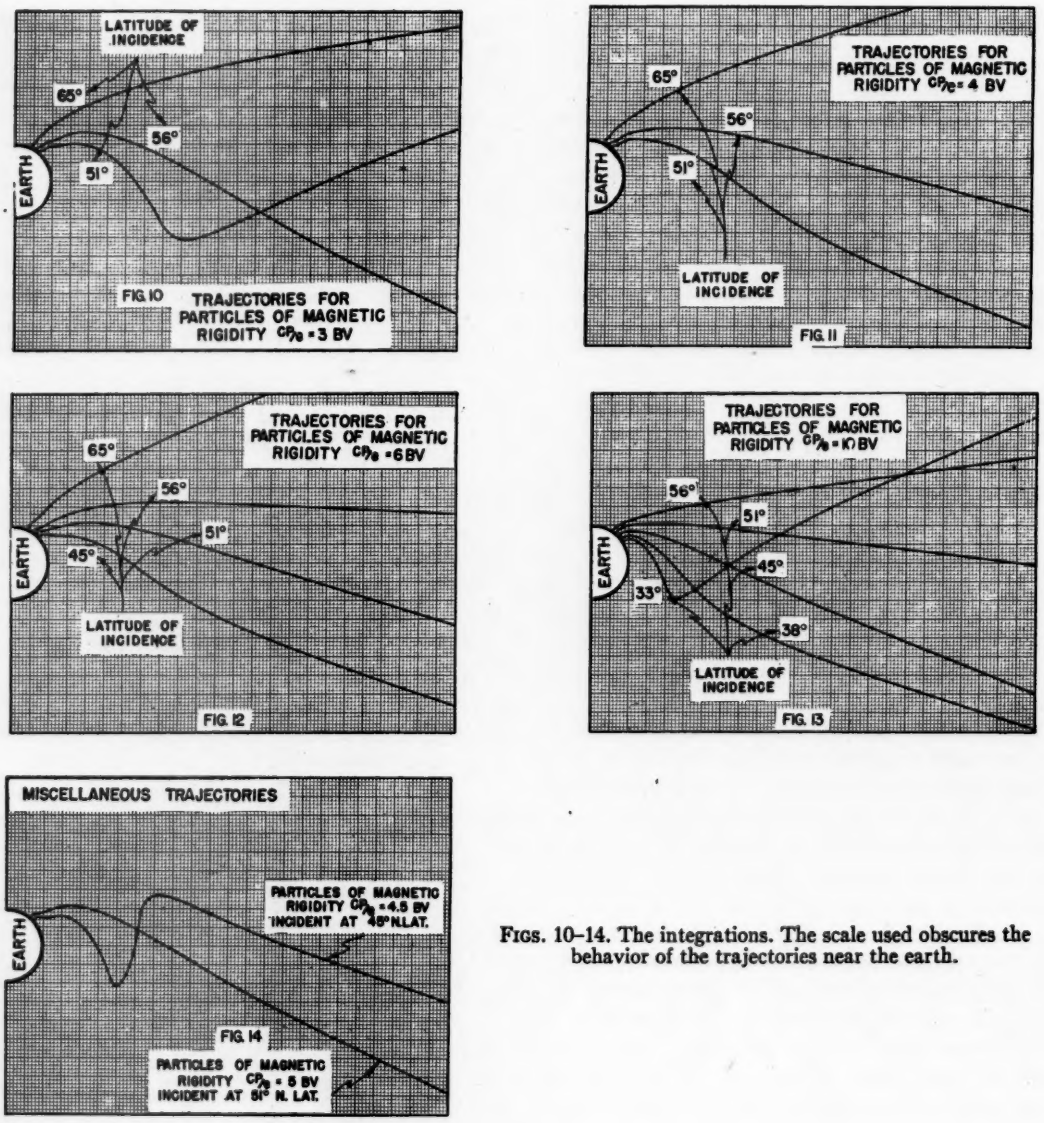
LATITUDE OF INCIDENCE
65°
56°
51°
EARTH
FIG. 10
TRAJECTORIES FOR PARTICLES OF MAGNETIC RIGIDITY cp/e = 3 BV
TRAJECTORIES FOR PARTICLES OF MAGNETIC RIGIDITY cp/e = 4 BV
FIG. 11
TRAJECTORIES FOR PARTICLES OF MAGNETIC RIGIDITY cp/e = 6 BV
45°
FIG. 12
TRAJECTORIES FOR PARTICLES OF MAGNETIC RIGIDITY cp/e = 10 BV
33°
38°
FIG. 13
MISCELLANEOUS TRAJECTORIES
PARTICLES OF MAGNETIC RIGIDITY cp/e = 4.5 BV INCIDENT AT 45° N.LAT.
FIG. 14
PARTICLES OF MAGNETIC RIGIDITY cp/e = 5 BV INCIDENT AT 51° N. LAT.

FIGS. 10–14. The integrations. The scale used obscures the behavior of the trajectories near the earth.

[18] L. Janossy, *Cosmic Rays* (Oxford University Press, London, 1946).

of the dipole), ρ and z are cylindrical coordinates defining position in the meridian plane, ϕ is the coordinate of this plane, and g is the angular momentum of the particle at infinity with respect to the dipole, expressed in dimensionless units. However, we cannot obtain a solution directly, since we know only the final conditions (the point and direction of incidence). Therefore we replace the paths of the real particles by the identical trajectories of fictitious negatively charged particles ejected vertically from the earth.

We follow the paths of the negative particles by numerical integration of the second-order differential equations of motion out to the boundary sphere, using the method of central differences.[19] This process is equivalent to integration backward along the real orbits (see Fig. 9). The trajectories far from the earth are asymptotic to straight lines. Since the velocity is virtually constant in the general region of the boundary sphere, we call its value there the *asymptotic velocity vector*.

The simultaneous integrations[20] of Eqs. (1) and (2) for several conditions of incidence are summarized graphically in Figs. 10–14. These curves in ρz space are merely the projections on the meridian plane of the trajectories. The motion of the meridian plane was calculated from the curves by using Eq. (3) and then performing a first order numerical integration.[19]

To determine the asymptotic velocity vector is the next step. The three direction cosines of a trajectory are simply z', ρ', and $\rho\phi'$, and the meridian plane has moved through an angle ϕ. All these quantities either appear directly in the integration, or can be found by means of the formula for differentiation given by Hartree.[19]

Consider the unit geomagnetic sphere in velocity space. The latitude β of the asymptotic velocity, being measured from the equator, will be given by:

$$\beta = \arcsin z'. \tag{4}$$

If we take the longitude of the initial, or terrestrial, velocity vector to be 0°, then the longitude ψ of the asymptotic velocity relative to it will be just:

$$\psi = \phi + \arctan \rho\phi'/\rho'. \tag{5}$$

Our computations yield the values given in Table I for the latitudes and longitudes of the asymptotic vector on the geomagnetic sphere.

Figures 15 and 16, derived from Table I, show the dependence of the asymptotic velocity upon the mag-

TABLE I. Longitude ψ and latitude β of the asymptotic velocity vector.

Magnetic rigidity $c\mathfrak{p}/e$	Latitude of incidence	Velocity longitude ψ	Velocity latitude β
3 Bv	51°	175.0°	16.0°
	56°	82.6°	−20.9°
	65°	37.7°	8.0°
4	51°	100.0°	−17.1°
	56°	59.5°	−13.6°
	65°	34.2°	15.5°
4.5	45°	268.0°	−13.7°
5	51°	82.6°	−22.4°
6	45°	101.5°	−16.1°
	51°	66.4°	−15.3°
	56°	47.9°	−2.9°
	65°	33.0°	22.2°
8	45°	75.6°	−19.0°
10	33°	185.0°	20.4°
	38°	115.5°	−15.7°
	45°	65.8°	−21.0°
	51°	45.0°	−6.6°
	56°	35.3°	7.3°

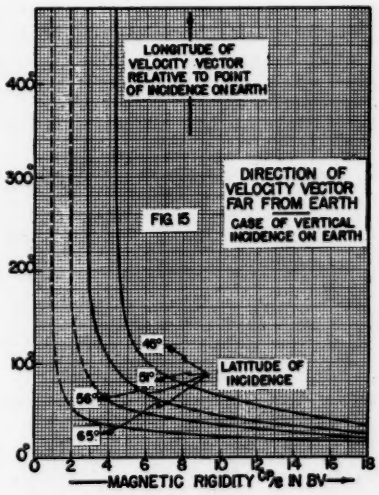

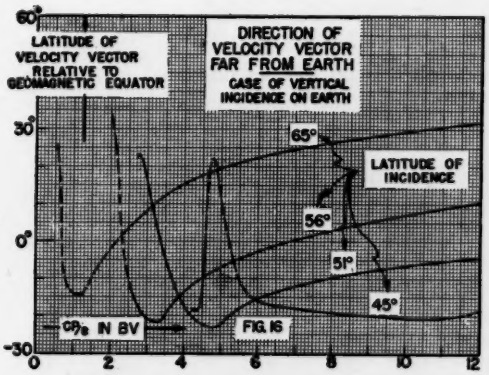

FIGS. 15–16. Deflection curves used to calculate the diurnal variation in total intensity at a given latitude of incidence.

[19] D. R. Hartree, Manchester Phil. Soc. Mem. 77, 91 (1933). To extend his method to two simultaneous equations, merely estimate both ρ_{n+1} and z_{n+1}, compute ρ_{n+1}'' and z_{n+1}'' from these estimates, and apply his process separately to ρ_n and z_n in order to complete the step in the integration. Iterate. It takes from 15 to 20 hours work on a hand computing machine to accomplish an integration.

[20] K. Dwight, senior thesis 1949, Princeton University, gives greater detail.

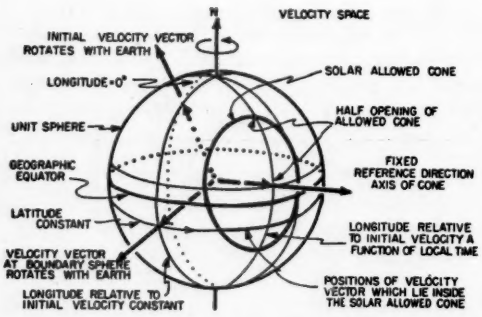
N
VELOCITY SPACE
INITIAL VELOCITY VECTOR ROTATES WITH EARTH
LONGITUDE=0°
SOLAR ALLOWED CONE
HALF OPENING OF ALLOWED CONE
UNIT SPHERE
GEOGRAPHIC EQUATOR
FIXED REFERENCE DIRECTION AXIS OF CONE
LATITUDE CONSTANT
LONGITUDE RELATIVE TO INITIAL VELOCITY A FUNCTION OF LOCAL TIME
VELOCITY VECTOR AT BOUNDARY SPHERE ROTATES WITH EARTH
LONGITUDE RELATIVE TO INITIAL VELOCITY CONSTANT
POSITIONS OF VELOCITY VECTOR WHICH LIE INSIDE THE SOLAR ALLOWED CONE

FIG. 17. The physical picture in velocity space. Diagram of velocity space (origin of diurnal variation).

netic rigidity of the particles for incidence at four different latitudes.

To find the position on the unit sphere of the asymptotic velocity for particles incident vertically at any point on the earth, it is convenient and practical to replot our values in the form of functions of latitude of incidence for various magnetic rigidities. Thus we have the fundamental families of deflection curves (see Figs. 7 and 8). By taking the intersections of these fundamental curves with lines of constant latitude, we can derive curves similar to those of Figs. 15 and 16 for any latitude of incidence.

The importance of the fundamental curves is due to their generality. First, they apply to particles of any mass. Second, to use them for the case of positive particles reaching the Southern Hemisphere, it is only necessary to reverse the signs of the latitudes—of incidence and of the asymptotic velocity vector. And finally, they apply to negative particles when the signs of all the angles are reversed. Thus we can find the asymptotic velocity vector of any type of particle received vertically anywhere on the earth.[20]

B. Derivation of Diurnal Variation from the Asymptotic Velocity

The solar allowed cone is one of directions, and not of positions, for the particle. It does not exist in position space, but only in velocity space, centering about the tangent to the earth's orbit, and opening out backward along it. We shall take this sense of the tangent for our *reference direction* (see Fig. 9). Therefore, on the unit sphere in velocity space, the allowed cone is represented by a circle drawn around that point which defines the reference direction (see Fig. 17). The opening of the cone is shown for two values of the solar moment in Fig. 18.[16]

The asymptotic velocity vector is fixed relative to the earth, and it is the rotation of the earth which produces a diurnal variation in intensity (see Fig. 9). Therefore we must consider the geographic unit sphere in velocity space, rather than the geomagnetic one, in order to compute the variation (see Fig. 17). We know the terrestrial velocity vector and the asymptotic velocity vector. These two vectors rotate together, with the earth, at the rate of 15° per hour, while the reference direction and allowed cone remain fixed in velocity space (see Fig. 17). As the velocity vectors rotate, their latitudes on the geographic sphere stay constant. Thus lines of constant latitude are the time-loci of the positions of the velocity vectors. In general, the time-locus of the asymptotic velocity will intersect the allowed cone, and so will determine the diurnal variation for particles with that given magnetic rigidity (see Fig. 17).

We can calculate just what this variation will be, breaking the process up into two parts. First we need to know the local time of day when the particles are reaching the earth from the center of their range of fully allowed directions. The time so defined will be called the *time-center* of the variation. Now the center of the intersection of the time-locus of the asymptotic velocity vector with the fully allowed cone has the same longitude as the reference direction (see Fig. 17). We consider this line of longitude to define a *reference time*, which is just 6 P.M. in local solar time.

The equation for the geographic longitude ψ^* shows that it can differ from the known geomagnetic longitude ψ by at most 0.6°,[20] which is completely negligible, and so we take $\psi^*=\psi$. This is the longitude of the asymptotic velocity relative to the terrestrial value, so that

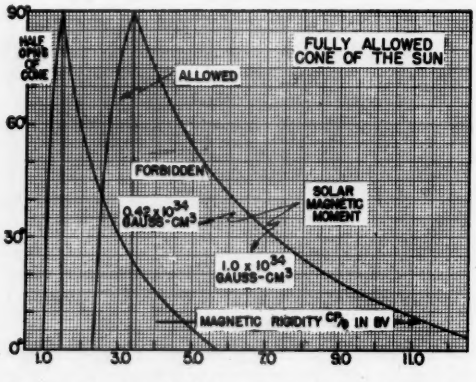

FIG. 18. The first graphical step in the derivation of the diurnal variation from the deflection curves. These curves were obtained from the table given in reference 16.

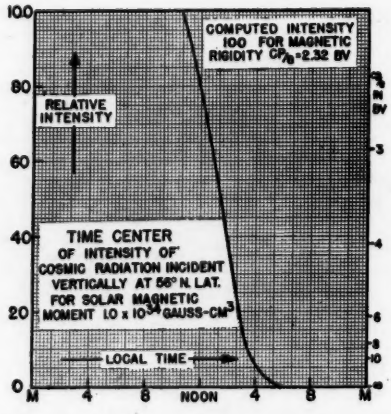

FIG. 19. The second graphical step. This graph illustrates the use of the integral spectrum.

the latter lags in time behind the former by $\psi^*/15=\psi/15$ hours. The lag is merely subtracted from the reference time in order to calculate the time-center:

$$T=6 \text{ P.M.}-\psi/15 \text{ hours.} \quad (6)$$

Since we will eventually want the total diurnal variation, it is more convenient to plot the time-center as a function of integrated intensity than as one of magnetic rigidity cp/e. The one is just as good a variable as the other, since we know from experiment the total relative intensity for all radiation with energy (momentum) greater than any given value. In Fig. 19 the time-center is plotted as a function of this integral spectrum for radiation incident at 56° N latitude. The corresponding magnetic rigidities are plotted along the right-hand edge of Fig. 19, based on the assumption of an inverse 2.75 power law for the differential spectrum relating intensity to momentum.

For the second part of the calculation of the variation, we must determine γ, the difference in geographic

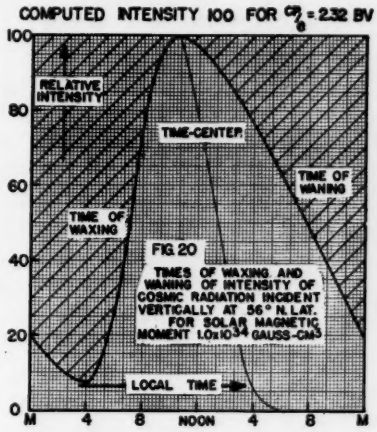
COMPUTED INTENSITY 100 FOR cp/e = 2.32 BV
RELATIVE INTENSITY
TIME-CENTER
TIME OF WANING
TIME OF WAXING
FIG. 20
TIMES OF WAXING AND WANING OF INTENSITY OF COSMIC RADIATION INCIDENT VERTICALLY AT 56° N. LAT. FOR SOLAR MAGNETIC MOMENT 1.0×10^{34} GAUSS-CM^3
LOCAL TIME
M 4 8 NOON 4 8 M

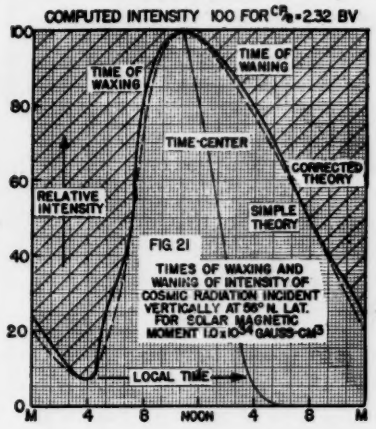
COMPUTED INTENSITY 100 FOR cp/e = 2.32 BV
TIME OF WAXING
TIME OF WANING
TIME-CENTER
CORRECTED THEORY
RELATIVE INTENSITY
SIMPLE THEORY
FIG. 21
TIMES OF WAXING AND WANING OF INTENSITY OF COSMIC RADIATION INCIDENT VERTICALLY AT 56° N. LAT. FOR SOLAR MAGNETIC MOMENT 1.0×10^{34} GAUSS-CM^3
LOCAL TIME
M 4 8 NOON 4 8 M

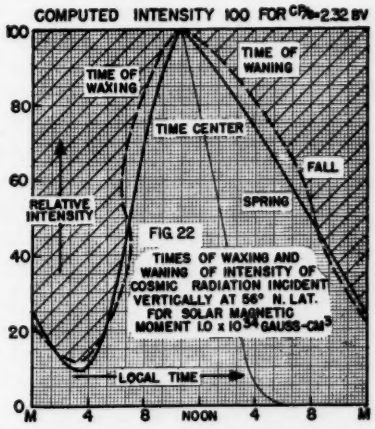
COMPUTED INTENSITY 100 FOR cp/e = 2.32 BV
TIME OF WAXING
TIME OF WANING
TIME CENTER
FALL
SPRING
RELATIVE INTENSITY
FIG. 22
TIMES OF WAXING AND WANING OF INTENSITY OF COSMIC RADIATION INCIDENT VERTICALLY AT 56° N. LAT. FOR SOLAR MAGNETIC MOMENT 1.0×10^{34} GAUSS-CM^3
LOCAL TIME
M 4 8 NOON 4 8 M

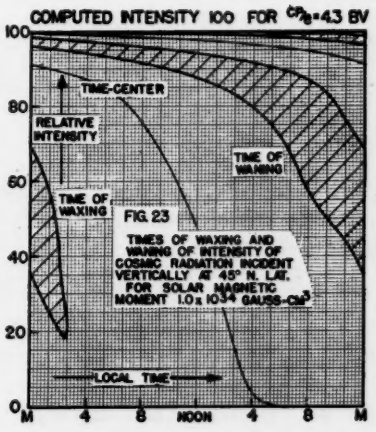
COMPUTED INTENSITY 100 FOR cp/e = 4.3 BV
TIME-CENTER
RELATIVE INTENSITY
TIME OF WANING
TIME OF WAXING
FIG. 23
TIMES OF WAXING AND WANING OF INTENSITY OF COSMIC RADIATION INCIDENT VERTICALLY AT 45° N. LAT. FOR SOLAR MAGNETIC MOMENT 1.0×10^{34} GAUSS-CM^3
LOCAL TIME
M 4 8 NOON 4 8 M

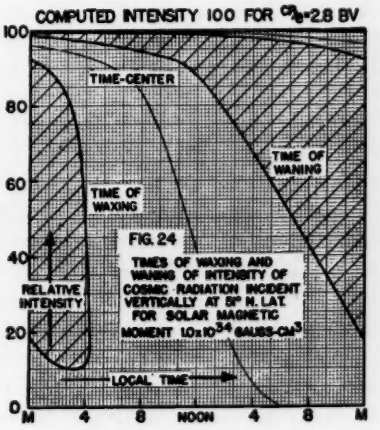
COMPUTED INTENSITY 100 FOR cp/e = 2.8 BV
TIME-CENTER
TIME OF WANING
TIME OF WAXING
RELATIVE INTENSITY
FIG. 24
TIMES OF WAXING AND WANING OF INTENSITY OF COSMIC RADIATION INCIDENT VERTICALLY AT 51° N. LAT. FOR SOLAR MAGNETIC MOMENT 1.0×10^{34} GAUSS-CM^3
LOCAL TIME
M 4 8 NOON 4 8 M

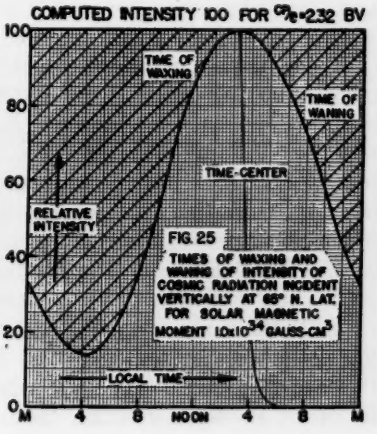
COMPUTED INTENSITY 100 FOR cp/e = 2.32 BV
TIME OF WAXING
TIME OF WANING
TIME-CENTER
RELATIVE INTENSITY
FIG. 25
TIMES OF WAXING AND WANING OF INTENSITY OF COSMIC RADIATION INCIDENT VERTICALLY AT 65° N. LAT. FOR SOLAR MAGNETIC MOMENT 1.0×10^{34} GAUSS-CM^3
LOCAL TIME
M 4 8 NOON 4 8 M

FIGS. 20–25. Samples of the third graphical step in the derivation of the diurnal variation from the deflection curves.

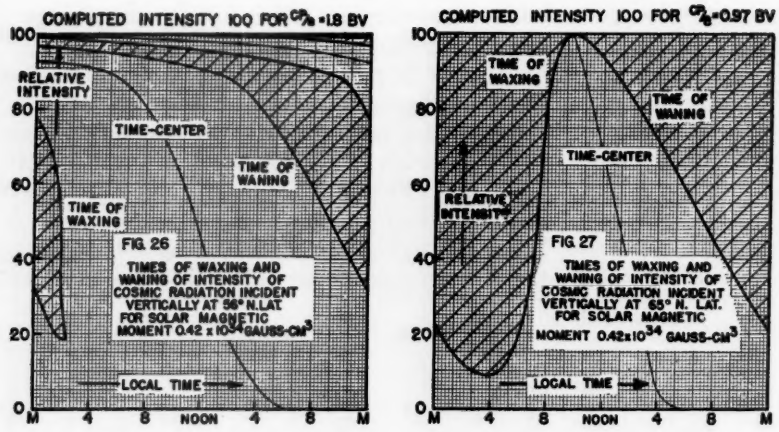
COMPUTED INTENSITY 100 FOR $C_{\frac{1}{2}}$ =1.8 BV
RELATIVE INTENSITY
TIME-CENTER
TIME OF WANING
TIME OF WAXING
FIG. 26
TIMES OF WAXING AND WANING OF INTENSITY OF COSMIC RADIATION INCIDENT VERTICALLY AT 56° N.LAT. FOR SOLAR MAGNETIC MOMENT 0.42 x 10^34 GAUSS-CM^3
LOCAL TIME
M 4 8 NOON 4 8 M
COMPUTED INTENSITY 100 FOR $C_{\frac{1}{2}}$=0.97 BV
TIME OF WAXING
TIME OF WANING
TIME-CENTER
RELATIVE INTENSITY
FIG. 27
TIMES OF WAXING AND WANING OF INTENSITY OF COSMIC RADIATION INCIDENT VERTICALLY AT 65° N. LAT. FOR SOLAR MAGNETIC MOMENT 0.42x10^34 GAUSS-CM^3
LOCAL TIME
M 4 8 NOON 4 8 M

FIGS. 26–27. Further examples of the third graphical step.

longitude between the center of the intersection of the time-locus of the asymptotic velocity with the allowed cone and the edge of this intersection (see Fig. 17). From solid geometry we obtain:[20]

$$\sin^2\gamma=\sec^2\beta^*(\sin^2\alpha-\sin^2\beta^* +2\cos\alpha\sin\beta^*\sin\zeta-\cos^2\alpha\sin^2\zeta), \quad (7)$$

where α is the half-opening of the solar allowed cone (see Fig. 18), ζ is the geographic latitude of the reference direction, and β^* is the geographic latitude of the asymptotic velocity vector. If we define η, the angle in the plane of the ecliptic between the line of its intersection with the earth's geographic equator and the reference direction, in such a manner that $\eta=0$ when the earth is nearest the sun and increases during the year, then further geometry yields:[20]

$$\sin\zeta=0.391\sin\eta. \quad (8)$$

Also, if μ is the angle between the magnetic axis of the earth and its axis of rotation, and λ is the geomagnetic longitude of incidence, then:[20]

$$\sin\beta^*=\cos\mu\sin\beta-\cos\beta\sin\mu\cos(\psi+\lambda). \quad (9)$$

Thus γ can be calculated from the fundamental deflection curves, the point of incidence, and the time of year.

Since the velocity vectors rotate at 15° per hour, the angle γ is equivalent to a time semiduration of the variation given by $\tau=\gamma/15$ hours. The *time of waxing* and *time of waning* are then computed by subtracting and adding, respectively, this semiduration of full intensity to the time-center. They represent the edges of the intersection of the time-locus with the allowed cone, are expressed in local solar time, and are functions of the energy of the radiation and the latitude of incidence.

The calculated times of waxing and waning are plotted in Fig. 20 as functions of intensity for radiation received at 56°N latitude. The shaded region in this graph indicates radiation which is "forbidden."

In Fig. 21 the times of waxing and waning obtained by the corrected theory (using β^*) for geomagnetic longitude of incidence $\lambda=0°$ [20] are compared with the results of the simple calculation (where β^* is replaced by β). All the significant properties remain unaltered (phase and magnitude). Therefore we shall henceforth make the simplifying substitution of β for β^* in our computations.

Equation (7) also indicates a dependence of the variation upon the season. We see that the calculations shown in Fig. 20 are valid for both the summer and winter solstices. The corresponding curves for the spring and fall equinoxes are shown in Fig. 22. Evidently their significant properties are not affected by the season.

Simple theory calculations for other latitudes of incidence are plotted in Figs. 23–25.

The computations given above were all for a solar magnetic moment of 1.0×10^{34} gauss-cm^3. We can equally well apply the process of analysis for a moment of, say, 0.42×10^{34} gauss-cm^3. These results are shown in Figs. 26 and 27 for radiation incident at 56° and 65°, respectively. In the former case there is a very important change in the shape of the curves of waxing and waning, one which alters the diurnal variation of total intensity in a most marked manner (see Fig. 3). When the cut-off values of the magnetic rigidity for incidence at 51° and 45° are compared with the openings of the allowed cone (see Fig. 18), it becomes clear that the lesser solar moment produces virtually no diurnal variation at these two latitudes.

Finally, we use the times of waxing and waning to determine the range of intensities (or energies) which correspond to "forbidden" radiation. This radiation, indicated by the shaded regions of the graphs, is assumed to arrive at 90 percent of its full intensity, to a first approximation. We remember that this intensity results from the scattering of particles into solar "forbidden" orbits,[16] which otherwise would contain no particles whatever. The percentile intensity in these orbits is actually a function of the energy of the particles. But because of the doubt concerning the existence of any permanent solar magnetic moment, there is no point in our attempting higher degrees of approximation at this stage. Therefore we take the average loss of intensity, 10 percent, to apply to radiation of any energy.

Hence, in order to compute the drop in total intensity for each moment of the day, we need only take 10 percent of the range of "forbidden" intensities given by the curves of waxing and waning for that instant of local solar time. This total drop is next subtracted from the integral intensity corresponding to the cut-off momentum, which is taken to be 100 on the scale of relative intensity. The intensities obtained by the subtraction are then plotted as functions of local time, thus providing us with the final descriptions of the diurnal variation in total intensity (see Figs. 1–6).

IV. DISCUSSION

It is instructive to compare the shapes and characteristics of Figs. 20–27 with the corresponding curves of total diurnal variation (see Figs. 1–6). Particular interest attaches to the position of the maximum, and to the region of the sudden rise to it. We see that at low latitudes of incidence the time-centers are so spread out by the strong terrestrial magnetic field that they tend to level off the variation in total intensity. As we pass to higher latitudes, the earth's field becomes weaker, so that particles of different momenta are dispersed less. Therefore the time-centers do not spread out so greatly, and consequently the amplitude of the variation increases. In this region of latitude, the time-centers and times of waxing and waning vary with intensity in such a manner that at a certain time of day there is an extremely wide range of momenta which change intensity at practically the same instant. This produces the sudden increase in intensity seen in our final curves.

At still higher latitudes of incidence, the time-center curve straightens out so much that the curve for the time or waxing starts to round off, and this effect is reflected in the final results. As we continue to increase the latitude of observation, we see from Fig. 8 that the asymptotic velocity latitude will keep increasing for rigidities in the significant range $2.5<cp/e<6$ Bv, so that eventually, somewhere above 65° N latitude, the decreasing intersections with the solar allowed cone (see Fig. 17) will diminish the semidurations of full intensity. As a result, the amplitude of the total variation will start to decrease. The range of magnetic rigidities subject to changes in intensity becomes smaller and smaller, centering about 3.4 Bev. Finally, at the poles there is no variation in vertical intensity.

Thus we have a qualitative picture of the behavior of the diurnal variation in total intensity as a function of latitude of observation. By applying a process of interpretation to our fundamental curves giving the deflection due to the earth's magnetic field, we can make the description quantitative. By using better approximations for the individual variations and for the shape of the energy spectrum, we can derive more accurate descriptions whenever required. These descriptions provide us with a very powerful tool for testing the existence of a permanent solar magnetic moment and the nature of the spectrum, and therefore should prove to be quite valuable.

I wish to express my thanks to Mr. J. A. Wheeler, Ph.D., for his many invaluable suggestions, and to Messrs. W. G. Stroud and T. J. B. Shanley for helpful discussions.

The Cosmic-Ray Intensity Above the Atmosphere at the Geomagnetic Equator*

J. A. VAN ALLEN AND A. V. GANGNES
Applied Physics Laboratory, Johns Hopkins University, Silver Spring, Maryland
(Received December 15, 1949)

By means of G-M counter telescopes in an Aerobee sounding rocket fired from the USS Norton Sound, total charged particle cosmic-ray intensity above the atmosphere has been measured at the geomagnetic equator. An empirical zenith angle (θ) dependence of directional intensity, averaged over all azimuths, is found to be $j(\theta)=0.028(1+0.6\sin\theta)$, in which $j(\theta)$ is in absolute units (sec. cm² steradian)$^{-1}$. The deduced *vertical* intensity 0.028/sec./cm²/steradian is thought to be most nearly free of atmospheric albedo and, therefore, to be our best estimate of an upper limit for the primary intensity of charged particles of energy greater than 14 Bev (for protons). A comparison is made with previous results at geomagnetic latitude 41°N.

THREE Aerobee sounding rockets[1] have recently been fired from the USS Norton Sound in a joint expedition of this Laboratory and the U.S. Navy. The present note[2] briefly reports the total cosmic-ray intensity above the atmosphere as determined with a set of four threefold G-M telescopes carried to about 105 km altitude by Aerobee A-10. This firing was conducted on March 17, 1949, on the geomagnetic equator about six hundred miles off the coast of Peru.

One pair of crossed wide angle telescopes *AOB*, *XOY* was mounted so that the axes of the respective telescopes were inclined 45° to the rocket axis and at right angles to each other (Fig. 1a). As in previous work,[3] counts from *AOB*, *XOY*, *AOB* (*X* and/or *Y*), *XOY* (*A* and/or *B*) were telemetered. The second pair of telescopes *PQR*, *SQT*, with multiple event channel *PQR* (*S* and/or *T*), is shown in Fig. 1b.

The orientation of axes fixed in the rocket was determined by the combination of a magnetometer and a set of sixteen photoelectric cells, using the geomagnetic field and the sun's rays, respectively, as reference vectors.

A continuous telemetered record without breaks was obtained from −120 sec. to +317 sec. by combining the records of two independent receiving stations.[4]

TABLE I.[a] High altitude plateau data (60–210 sec.).

(1) *AOB* (total)	260 counts	(6) *PQR* (total)	161 counts
(2) *AOB* (*X* or *Y*)	48	(7) *SQT* (total)	189
(3) *XOY* (total)	271	(8) *PQR* (*S* or *T*)	23
(4) *XOY* (*A* or *B*)	43	(9) *PQRST*	19
(5) *XOYAB*	31		
Rate of telescope *AOB*, less all recorded multiple particle events 1.21±0.06 counts/sec.		Total rate of telescope *PQR* 1.07±0.06 counts/sec.	
Rate of telescope *XOY*, less all recorded multiple particle events 1.31±0.06 counts/sec.		Total rate of telescope *SQT* 1.26±0.06 counts/sec.	
Average net rate per telescope $N_{AOB,XOY}=1.26\pm0.04$ counts/sec.		Rate of telescope *PQR*, less all recorded multiple particle events $N_{PQR}=0.79\pm0.05$ counts/sec.	

[a] Errors given in this report are statistical probable errors.

Table I summarizes data in the flight period 60–210 sec. (all above the appreciable atmosphere), during which the axis of the rocket described a rather complicated motion but was tilted about 15° from the vertical in a southwesterly direction on the average and did not deviate more than 30° from the vertical at any time. The roll rate of the rocket about its longitudinal axis was accurately constant with a period of 3.53 sec.

The ratio of "multiple" to "single" events is similar to, but slightly less than, the ratio at $\lambda=41°$N,[3] with nearly identical equipment.

As discussed in reference 3, the guarding of the telescopes is believed to be quite efficient and there is very little material in the path of a particle whose trajectory lies within the solid angle of the telescopes. Therefore, the *net* rate of the telescopes has been taken to yield the true charged particle intensity.

The geometric factor for *AOB*, *XOY* telescopes for uniform intensity over their apertures is $N/e^3j=31.7$ cm²-steradian. Using this factor and making the minor corrections for intrinsic inefficiency, deadtime, and accidentals, we find the time-averaged directional intensity $j_{AOB,XOY}=0.0410\pm0.0014$/sec./cm²/steradian. Similarly, using the uniform intensity geometric factor,[5] $N/e^3j=22.7$ cm²-steradian for *PQR*, we find a time-averaged directional intensity $j_{PQR}=0.0355\pm0.0024$/sec./cm²/steradian. Unfortunately, events *SQT* (*P* or *R*) were not recorded. But, if there is made the reasonable supposition that the number of such events is equal to the number of *PQR* (*S* or *T*) events, then we have the provisional value $j_{SQT}=0.0440\pm0.0026$/sec./cm²/steradian.

The axis of telescope *PQR* was at an average zenith angle θ of about 15° during the data period considered. However, the above-calculated intensity j_{PQR} does not correspond to $\theta=15°$ because of the very wide acceptance angle in the plane of the G-M tube axes and because of apparent non-uniformity of intensity within this angle. When proper account is taken of the angular opening of *PQR*, an empirical zenith angle dependence

* Supported by the Navy Bureau of Ordnance under Contract NOrd 7386.

[1] Van Allen, Fraser, and Floyd, Science **108**, 746 (1948).

[2] A preliminary discussion was given at the Echo Lake Conference (June, 1949).

[3] Gangnes, Jenkins, and Van Allen, Phys. Rev. **75**, 57, 892 (1949).

[4] Operated by Mr. R. F. Ohlemacher and associates of the New Mexico College of Agriculture and Mechanic Arts and the U.S. Naval Unit, White Sands Proving Ground, New Mexico.

[5] H. E. Newell, Jr. and E. C. Pressly, Rev. Sci. Inst. **20**, 568 (1949).

of directional intensity, averaged over all azimuths, of

$$j(\theta)=0.028(1+0.6\sin\theta) \quad (1)$$

is found to yield good accord with all the experimental results. Equation (1) gives an approximate vertical intensity of charged particles above the atmosphere at $\lambda=0°$ of

$$j(0°)=0.028/\text{sec./cm}^2/\text{steradian.}$$

It is thought quite unlikely that this value differs from the true vertical intensity by as much as 15 percent.

It is of particular interest to compare these results with corresponding ones[3,6] at White Sands, New Mexico ($\lambda=41°$N). See Table II.

The fact that the "average" upper hemisphere intensities deduced from the single counter data are larger than those deduced from the telescope rates, is thought to be due to three principal reasons: (a) From a typical altitude of 90 km, the "top" of the atmosphere (55 km) lies at a dip angle of six degrees below the horizontal. Thus, the single counter is exposed to radiation over appreciably more than one hemisphere, even in the absence of atmospheric albedo. The "dip angle" radiation contributes to the counting rate of a telescope only in the special case in which the telescope includes such directions within its aperture.

(b) A more-or-less vertical single counter presents its greatest effective area horizontally—from which direction there is the maximum intensity.

(c) Any soft charged radiation present above the atmosphere need penetrate only the missile skin and one counter wall in order to register in a single G-M counter. In the telescopes which we have used, penetration of at least five counter walls is necessary in order to register a coincidence. A single counter is also much more susceptible to moderate energy γ-rays than is a telescope.

TABLE II. Comparison of intensities above the atmosphere at two geomagnetic latitudes.

Geomagnetic latitude \ Approximate zenith angle	0°	45°	"Average" intensity from single G-M counter data
0°	0.028	0.041	0.053
41°N	0.070	0.109	0.13
Ratio	0.40	0.38	0.41

In addition to Table II there may be noted the latitude ratio 0.36 of multiple particle events in the array *AOBXY*. No cosmic-ray phenomena have been reported in the literature to exhibit a more rapid experimental latitude dependence over this range of latitude than do our intensity data reported here.

We find a crude value of vertical intensity at the Pfotzer maximum of 0.13/sec./cm²/steradian at $\lambda=0°$.

Insofar as the vertical intensity above the atmosphere may be taken as proportional to the primary intensity, the two values 0.028 at $\lambda\doteq 0°$ and 0.070 at $\lambda=41°$ can be used to calculate the exponent of an assumed power law primary spectrum. The result for the differential number spectrum is $E^{-1.9}$, considerably flatter than otherwise deduced.

We are especially indebted to Captain T. A. Ahroon,

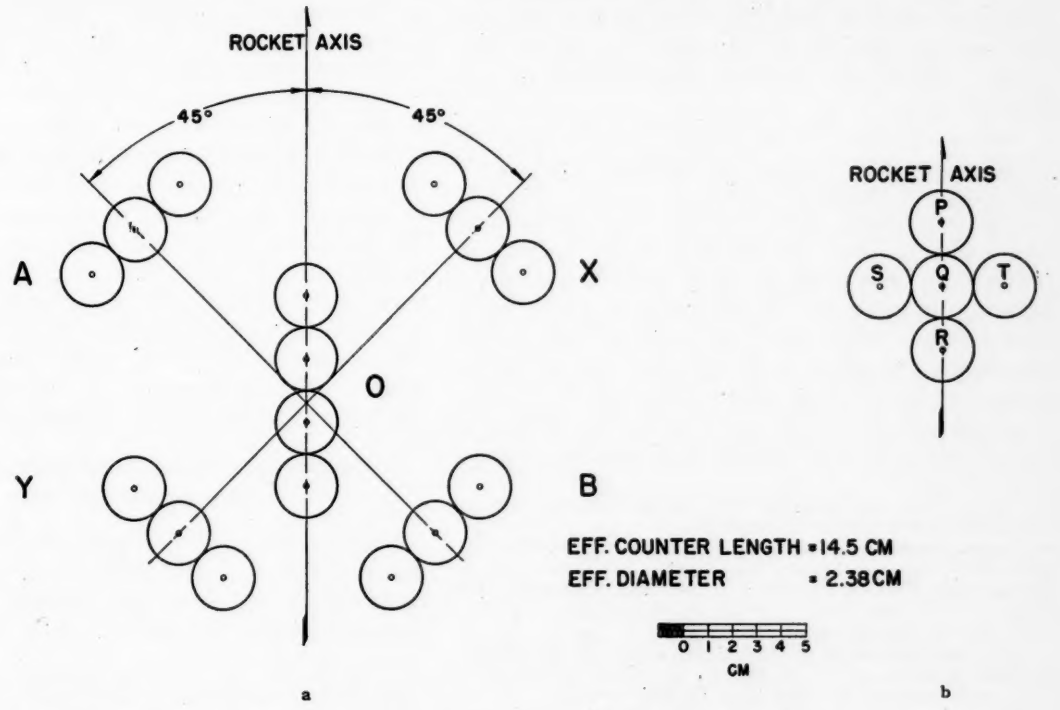

FIG. 1. Counter telescope arrangements.

[6] J. A. Van Allen, Echo Lake Conference (June, 1949). S. F. Singer, Echo Lake Conference (June, 1949).

USN, and the other officers and men of the USS Norton Sound for the conduct of the expedition and the rocket firing.

Added in proof: A check on the validity of the empirical Eq. (1) above is had by calculating the counting rate of a single G-M counter with axis vertical above the atmosphere. This rate is $\int_0^{90°} j(\theta) \cdot A(\theta) \cdot 2\pi \sin\theta d\theta$, in which $j(\theta)$ is given by Eq. (1), and $A(\theta)$ is the projected area of the cylindrical counter. The result for the counter used is 8.8 counts/second. The difference between this value and the observed counting rate 9.7±0.2 counts/sec. is reasonably attributable to reason (c) above and perhaps to lack of accuracy in (1).

PHYSICAL REVIEW VOLUME 77, NUMBER 7 APRIL 1, 1950

The Effect of Hydrostatic Pressure on the Curie Point of Barium Titanate Single Crystals*

W. J. MERZ
Laboratory for Insulation Research, Massachusetts Institute of Technology, Cambridge, Massachusetts

(Received December 30, 1949)

The influence of hydrostatic pressure on the Curie temperature of $BaTiO_3$ single crystals has been investigated. With increasing pressure a linear shift of the Curie point towards lower temperature is observed with a slope of -5.8×10^{-3} degree/atmos. This information allows us to calculate the change of the specific heat and of the compressibility at the Curie point according to Ehrenfest's relation. Thus it is possible to relate the pressure effect to the change of the lattice constant. The decrease of the Curie temperature with shrinking lattice constant is nearly the same as that observed when Sr ions are substituted for Ba in the titanate crystal. In addition, measurements have been made on the influence of pressure on the first order transition point near 0°C.

INTRODUCTION

THE research of this laboratory on the properties of barium titanate[1-6] has the long-range objective of arriving at an understanding of the mechanism of ferroelectricity. The relatively simple perovskite structure of $BaTiO_3$ and of the related columbates and tantalates[7] offers an easier access to this problem than the complex structure of the other two ferroelectric groups, rochelle salt and the alkali phosphates and arsenates.

Barium titanate is cubic above the Curie point (120°C). One question of prime importance is to learn how the Curie temperature, that is, the onset of spontaneous polarization, depends on the lattice parameters. The lattice constant can be reduced by hydrostatic pressure, and a shift of the Curie point would be expected. Arguments can be presented for predicting a shift in either direction. Under pressure, the lattice dimensions prevailing at the normal Curie point are realized at higher temperature, hence the Curie temperature may be raised. *Vice versa*, the successive replacement of barium ions by strontium ions reduces the lattice constant and moves the Curie point downwards, hence pressure may lower the Curie temperature. The results given in the present paper decide this question experimentally.

APPARATUS

The pressure apparatus* (Fig. 1) consists of a pressure generator and a crystal chamber interconnected by a steel capillary. Hydrostatic pressures up to 5000 atmos. were reached by inserting the generator in a standard hydraulic jack. The temperature in the crystal holder could be adjusted from that of liquid air through the Curie region up to *ca.* 150°C, made possible by using silicone oil as the hydrostatic pressure liquid. The behavior of the Curie point was determined by measuring the dielectric constant as a function of temperature and pressure at 10 kc. A thermocouple, inserted in a hole of the crystal holder casing about 2 mm from the crystal, served as the temperature control and allowed the measurement of relative temperature changes with a high degree of reproducibility (0.1°C).

Dependence of the Curie Temperature on Hydrostatic Pressure

In contrast to the behavior of rochelle salt, for which Bancroft[8] found a shift of the Curie point to higher temperatures with increasing pressure, we found the opposite behavior for $BaTiO_3$ single crystals. Up to

* Sponsored by the ONR, the Army Signal Corps, and the Air Force under ONR Contract N5ori-07801.

[1] A. von Hippel and co-workers, NDRC Contract OEMsr-191, Reps. VII (August, 1944) and XI (October, 1945); von Hippel, Breckenridge, Chesley, and Tisza, J. Ind. Eng. Chem. **38**, 1097 (1946).
[2] S. Roberts, Phys. Rev. **71**, 890 (1947).
[3] B. T. Matthias and A. von Hippel, Phys. Rev. **73**, 1378 (1948).
[4] R. D. Burbank and H. T. Evans, Jr., Acta Cryst. **1**, 330 (1948).
[5] P. W. Forsbergh, Jr., Phys. Rev. **76**, 1187 (1949).
[6] W. J. Merz, Phys. Rev. **75**, 687 (1949); **76**, 1221 (1949).
[7] B. T. Matthias, Phys. Rev. **75**, 1771 (1949).

* This unit was built by P. W. Forsbergh, Jr. on the basis of information received from Professor P. W. Bridgman's laboratory at Harvard University.
[8] D. Bancroft, Phys. Rev. **53**, 587 (1938).

about 2500 atmos. the Curie temperature θ falls linearly with increasing pressure with a slope dT/dp of -5.8×10^{-3} degree/atmos. (-5.74×10^{-9} degree cm²/dyne) (Fig. 2). At higher values of the pressure the results become more involved because of a dependence on the prehistory, that is, on the temperature at which the pressure is applied and on the value from which the pressure is increased or decreased. This seems to be due to the existence of the domains and their response to the external pressure. The best results (straight line) at these higher pressures are therefore obtained by starting the compression above the Curie temperature when no domains exist.

The characteristic of the dielectric constant *vs.* temperature retains its well-known shape[6] and only shifts to lower temperatures as the pressure is increased. However, there is a slight increase of the peak value of the dielectric constant at the Curie point at its position shifts downwards.

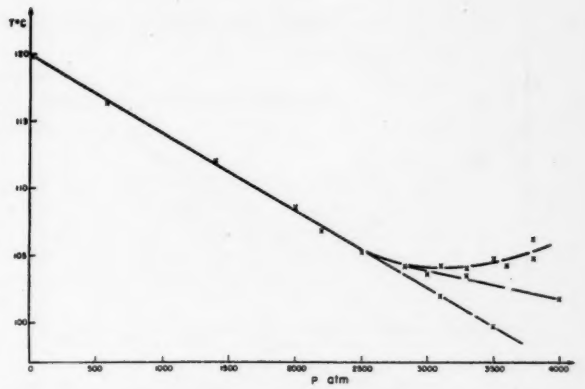

FIG. 2. Curie temperature *vs.* pressure. The divergence above 2500 atmos. because of prehistory is apparent.

DISCUSSION

The transition at the Curie point is of the second order, hence we can use Ehrenfest's relation[9] for the calculation of the change of the specific heat at the Curie point in contrast to the Clausius-Clapeyron equation which applies to a first order transition and gives the value of the latent heat. If Δc_p represents this change of the specific heat, ρ the density, θ the Curie temperature, and $\Delta\beta$ the change in the volume expansion coefficient at the Curie temperature, we have $dp/dT=\Delta c_p\cdot\rho/\theta\cdot\Delta\beta$. With $(dT/dp)_{p=0}=-5.74\times10^{-9}$ degree cm²/dyne as given above, $\rho=6.04$ g/cm³, $\theta=393°$K, and $\Delta\beta=3\Delta\alpha=-18\times10^{-6}$ degree^{-1} where $\Delta\alpha$ represents the change of the linear expansion coefficient obtained from the x-ray measurements of Megaw,[10] we get for the change of the specific heat at the Curie point $\Delta c_p=4.9\times10^{-3}$ cal./g degree. The value of Δc_p thus calculated is of the same order of magnitude as the measured values of Wul[11] (3×10^{-3}) and Harwood, Popper, and Rushman[12] (2.5×10^{-3}), but somewhat smaller than that of Blattner and Merz[13] (20×10^{-3}). The small value agrees with the interpretation of the transition as a displacive one[14] in contrast to the order-disorder transition for KH_2PO_4, where a much larger value of Δc_p is observed. For the rochelle salt transitions, also classified as displacive, one gets, using the measurements of Bancroft for Δc_p, the values of 14×10^{-3} and 4.1×10^{-3} for the two Curie points[5] in good agreement with the direct measurements of Wilson.[15]

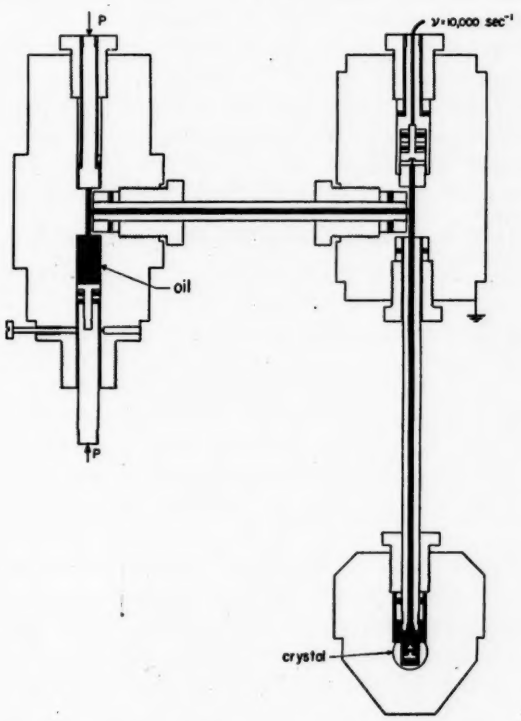

FIG. 1. Pressure apparatus.

Concerning dT/dp we have to expect for $BaTiO_3$ a negative value according to Ehrenfest's formula, since $\Delta c_p>0$ and $\Delta\beta<0$ as we traverse the Curie point from the ferroelectric tetragonal state to the cubic state. For rochelle salt we have dT/dp positive because both Δc_p and $\Delta\beta$ are positive at the upper Curie point and negative at the lower one.

Ehrenfest's formula for a transition of the second order can also be written as $dp/dT=\Delta\beta/\Delta k$ where $\Delta\beta$ is the change of the volume expansion coefficient at the Curie point as before and Δk is the change in the volume compressibility at the Curie point. With the known values of dp/dT and $\Delta\beta$ we obtain $+1.03\times10^{-13}$ cm²/dyne for Δk, that is, the volume compressibility

[9] P. Ehrenfest, Comm. Univ. Leiden, Suppl. **75b** (1933).

[10] H. D. Megaw, Proc. Roy. Soc. **A189**, 261 (1947).
[11] B. M. Wul, J. Phys. USSR **10**, 95 (1946).
[12] Harwood, Popper, and Rushman, Nature **160**, 58 (1947).
[13] H. Blattner and W. J. Merz, Helv. Phys. Acta **21**, 210 (1948).
[14] L. Tisza, "On the General Theory of Phase Transitions," N.R.C. Symposium, Cornell University, August, 1948.
[15] A. J. C. Wilson, Phys. Rev. **54**, 1103 (1938).

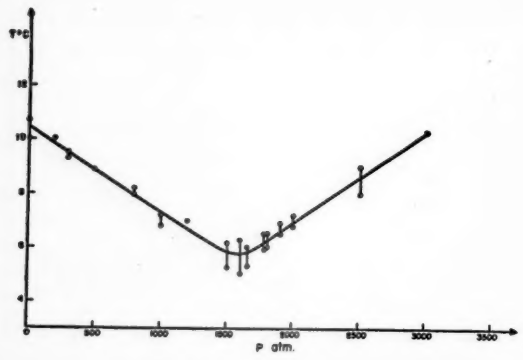

FIG. 3. λ-point *vs.* pressure.

is higher in the Curie region than above, quite analogous to rochelle salt at the upper Curie point.

The main interest of these measurements lies in the information they provide as to the dependence of the Curie point on the value of the lattice constant. The compressibility of $BaTiO_3$ can be calculated from Mason's values[16] of the elastic constants of ceramics and used in the first approximation for our single crystals. Mason found at room temperature a Young's modulus $Y_0=[\mu(3\lambda+2\mu)/(\lambda+\mu)]$ of 11.3×10^{11} dyne/cm² and $\lambda+2\mu=14.2\times10^{11}$ dyne/cm² where λ and μ are the Lamé elastic constants. Thus $\lambda=5.2\times10^{11}$ dyne/cm², $\mu=4.5\times10^{11}$ dyne/cm² and the volume compressibility $k=3/(3\lambda+2\mu)=12.2\times10^{-13}$ cm²/dyne. Hence the compressibility, as we traverse the Curie point with rising temperature, decreases as given above, by a value Δk corresponding to about 8.5 percent.

Now we can calculate the change of the lattice constant in the cubic region with applied pressure by assuming that the compressibility of the crystal is here $k-\Delta k$. Taking into account the thermal contraction of the crystal, we obtain finally for the ratio of the change of the Curie temperature to the change of the lattice constant the value $\Delta\theta/\Delta x=+3.3\times10^8$ degree/angstrom.

Rushman and Strivens[17] and other workers found a linear dependence of the Curie temperature and of the lattice constant on the amount of $SrTiO_3$ in $BaTiO_3$ crystals. For instance, a mixture of 64 percent $BaTiO_3$ and 36 percent $SrTiO_3$ gave a Curie temperature of 12°C with a lattice constant $a=b=c=3.9620$A. In comparing these values with those for $BaTiO_3$, with $\theta=120$°C and $a=b=c=4.0011$A, we derive $\Delta\theta/\Delta x=+2.8\times10^8$ degree/angstrom, a much better agreement with our value than one would expect since it can not be assumed that the change of the Curie temperature is due to the change of the lattice constant alone.

Effect of Hydrostatic Pressure on the First Order Transition Near 0°C

At this transition point we again find at first a decrease of the transition temperature with increasing pressure, but above *ca.* 1500 atmos. the situation is reversed (Fig. 3). Simultaneously a strong dependence on the prehistory is observed in this upper region. It may be that the change of the sign of dT/dp at 1500 atmos. is caused only by the domain pattern because at this transition point from the tetragonal to the orthorhombic state a considerable rearrangement of domains occurs.[5,6]

The transition point at about −80°C has not yet been investigated as it appeared that not much information would be gained, as in the case of the 0° transition, due to rearrangement of domains.

The writer wishes to thank Professor A. von Hippel for many helpful discussions during the course of this work, and to acknowledge the valuable work done by P. W. Forsbergh, Jr. in developing the pressure apparatus. The transfer of Dr. Forsbergh to Europe prevented him from carrying through this investigation.

[16] W. P. Mason, Phys. Rev. **74**, 1134 (1948).

[17] D. F. Rushman and M. A. Strivens, Trans. Far. Soc. **42A**, 231 (1946).

Lambda-Temperatures of Solutions of He^3 in He^4

OLIVE G. ENGEL AND O. K. RICE
Department of Chemistry, University of North Carolina, Chapel Hill, North Carolina
(Received December 30, 1949)

An expression for the effect of He^3 on the lambda-point of He^4 is developed from thermodynamic principles. Use is made of the idea that normal He^4 and superfluid He^4 are in equilibrium with each other and that the lambda-temperature is the temperature at which superfluid first appears. This expression contains the difference in enthalpy of normal fluid and superfluid. The lambda-points of mixtures containing large amounts of He^3 are discussed on the basis of various assumptions regarding this difference in enthalpy as a function of temperature.

AN equation

$$dT_\lambda/dx_3 = -T_\lambda[x_3(1-x_3)(1+6x_3) + (1-x_3)7.6/6R], \quad (1)$$

representing the shift in the lambda-temperature T_λ with the mole fraction x_3 of He^3 has been developed by J. W. Stout.[1] While based upon a thermodynamic development which is certainly correct, Stout's expression is restricted in its application by his assumption that the discontinuity of the specific heat at the lambda-point, ΔC_{p4}, remains constant and equal to its value in pure He^4 which Keesom gives as -7.6 cal. per mole per degree. This assumption means that Stout's equation will be accurate only in very dilute solutions of He^3. It represents accurately data obtained by Abraham, Weinstock, and Osborne.[2]

Another equation,

$$dT_\lambda/dx_3 = -RT_\lambda(r+1)/rS_\lambda, \quad (2)$$

involving different quantities, was developed by O. K. Rice.[3] In this equation S_λ is the molal entropy of liquid helium at the lambda-point, R is the gas constant, and r is a constant in the empirical equation for pure He^4

$$S = S_\lambda(T/T_\lambda)^r, \quad (3)$$

which gives the entropy below the lambda-point as a function of temperature.[4] Equation (2) also has a thermodynamic basis, but with the additional assumption that He^4 below the lambda-point can be considered to be a mixture of two fluids, normal He^4 and superfluid, and that these two are in equilibrium with each other. Equation (2) was derived only for very dilute solutions of He^3 in He^4, and in this concentration range it agrees well with the results obtained from Eq. (1) and with the experimental data.

It seems desirable to extend these considerations to concentrated solutions of He^3, and this will be the principal object of the present paper. We summarize herewith the assumptions and observations which we shall use as the basis of this further development:

(A) Superfluid helium may be considered either as a component or as a "phase" as was suggested by Tisza.[5] We assume that it has the character of a component in that the chemical potential of superfluid helium depends on the amount present. If it is treated as a phase, as was suggested by F. London,[4] it must not be regarded as a phase in the usual phase-rule sense. The lambda-transition is considered to be a second-order transition taking place without latent heat whether or not He^3 is present. According to the picture given by Rice[3] the lambda-transition initiates the formation of superfluid in a sort of fibroid form, and the superfluid continues to form over a range of temperatures below the lambda-point.

(B) The superfluid component (or "phase") is exceptional in that the partial molal entropy of superfluid is finite even under the condition that the concentration of superfluid approaches zero. This partial molal entropy of superfluid depends only on the mixing of superfluid with normal fluid[3] and with the isotope He^3.

(C) The lamba-point is the temperature at which the chemical potential of superfluid helium at zero concentration becomes equal to the chemical potential of the normal fluid. It was shown by Rice that essentially this statement follows from the assumption that the two forms of He^4 are in equilibrium with each other. It is probable that superfluid begins to appear slightly above the lamba-point, but it is in a different form (globules[3]) and may be neglected. We also neglect any effect which may result from the globules persisting below the lambda-point.

(D) The partial molal enthalpy of superfluid helium is independent of temperature and arbitrarily set equal to zero.*

We use notation as follows: μ_i equals chemical potential of component i ($i=3$, $4n$, or $4s$ for He^3, He^4 normal fluid, and He^4 superfluid, respectively); x_i equals mole fraction of component i; $\bar{S}_i$ equals partial molal entropy of component i; $\bar{H}_i$ equals partial molal enthalpy of component i; and subscript λ is used to indicate values at the lambda-point of the particular solution considered.

If we consider a closed system at constant pressure

[1] J. W. Stout, Phys. Rev. **76**, 864 (1949).
[2] Abraham, Weinstock, and Osborne, Phys. Rev. **76**, 864 (1949).
[3] O. K. Rice, Phys. Rev. **76**, 1701 (1949).
[4] F. London, Rev. Mod. Phys. **17**, 310 (1945).
[5] L. Tisza, Phys. Rev. **72**, 838 (1947).
* See W. Band and L. Meyer, Phys. Rev. **74**, 386 (1948).

containing a mole fraction x_3 of isotope He^3, a mole fraction x_{4n} of normal He^4, and a mole fraction x_{4s} of superfluid He^4, then, at the lambda-temperature where the mole fraction of superfluid is zero

$$d\mu_{4s,\lambda}=(\partial\mu_{4s}/\partial T_\lambda)dT_\lambda=-\bar{S}_{4s,\lambda}dT_\lambda,$$
$$d\mu_{4n,\lambda}=(\partial\mu_{4n}/\partial T_\lambda)dT_\lambda+(\partial\mu_{4n}/\partial x_3)_\lambda dx_3$$
$$=-\bar{S}_{4n,\lambda}dT_\lambda+(\partial\mu_{4n}/\partial x_3)_\lambda dx_3.$$

In a perfect solution

$$\mu_{4n}=f(T,P)+RT\ln x_{4n},$$
$$\partial\mu_{4n}/\partial x_3=(RT_\lambda/x_{4n})(\partial x_{4n}/\partial x_3)_\lambda=-RT_\lambda/x_{4n}$$

since along the lambda-curve where $x_{4s}=0$, $dx_{4n}/dx_3=-1$. Therefore,

$$d\mu_{4n,\lambda}=-\bar{S}_{4n,\lambda}dT_\lambda-(RT_\lambda/x_{4n})dx_3.$$

The chemical potential of the normal fluid is equal to the chemical potential of superfluid helium at the lambda-temperature (C). Consequently,

$$d\mu_{4s,\lambda}=d\mu_{4n,\lambda}$$

and

$$-\bar{S}_{4s,\lambda}dT_\lambda=-\bar{S}_{4n,\lambda}dT_\lambda-(RT_\lambda/x_{4n})dx_3. \quad (4)$$

Further, since the chemical potential is the partial molal free energy, it follows that

$$\mu_{4s,\lambda}=\bar{H}_{4s,\lambda}-T_\lambda\bar{S}_{4s,\lambda},\quad \mu_{4n,\lambda}=\bar{H}_{4n,\lambda}-T_\lambda\bar{S}_{4n,\lambda}.$$

Subtraction of the second expression from the first shows that

$$\bar{S}_{4s,\lambda}-\bar{S}_{4n,\lambda}=(\bar{H}_{4s,\lambda}-\bar{H}_{4n,\lambda})/T_\lambda=-\bar{H}_{4n,\lambda}/T_\lambda$$

since the partial molal enthalpy of superfluid is zero (D). With this substitution, Eq. (4) can be written

$$dT_\lambda/dx_3=-(RT_\lambda^2)/\bar{H}_{4n,\lambda}(1-x_3). \quad (5)$$

At the normal lambda-point Eq. (5) is identical with Eq. (2) above if one makes use of the value of $H_\lambda(=\bar{H}_{4n,\lambda})$ which follows from Eq. (3).

The equation is logical as was indicated by Rice[3] in that it indicates a lowering of the lambda-temperature with increase in the mole fraction of He^3. This would be expected because addition of He^3 lowers the escaping tendency (chemical potential) of the normal fluid and therefore shifts the equilibrium between superfluid He^4 and normal He^4.

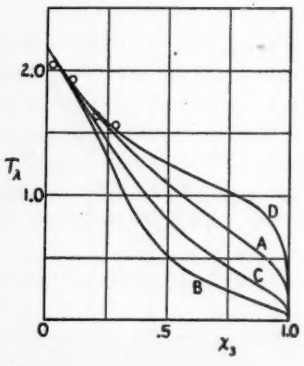

FIG. 1. Lambda-temperature *vs.* the mole fraction x_3. Experimental points circled.

If it is assumed that $\bar{H}_{4n,\lambda}$ is constant, and if the experimental value of 3.01 cal. per degree[3] for He^4 at the lambda-point is used (since at the lambda-point He^4 is practically all normal fluid) the solution of Eq. (5) is[6]

$$-1/T_\lambda=1.52\log(1-x_3)-0.457.$$

The locus is given as curve *A* in Fig. 1 where the points in circles are the recent experimental values of Abraham, Weinstock, and Osborne.[2]

However, $\bar{H}_{4n,\lambda}$ will not be strictly constant, and some adjustment should be made for the variation in it which must occur as the lambda-point shifts to lower temperatures. Specific heats just above the temperature where the lambda-point anomaly sets in may be considered to refer to the normal fluid, and we may attempt to extrapolate to temperatures below the lambda-point in order to gain some idea as to how the molal enthalpy of normal fluid will behave in this region.

Keesom[7] has recorded data on the specific heat of He^4 determined experimentally by Keesom and Clusius, by Dana and Kamerlingh Onnes, and by Keesom and Miss Keesom. The 1932 data of Keesom and Miss Keesom might indicate a region in which the heat capacity is constant at about 2.2 cal. per mole per degree just prior to the anomalous behavior of the specific heat as the lambda-point is approached. Unfortunately, the data are given for only a short range of temperature above the lambda-anomaly in the specific heat so that it cannot be said with assurance that there is not some slope in the specific heat curve. If the value of the heat capacity of normal fluid has become essentially constant at 2.2 cal. per mole per degree, the enthalpy should go to zero in less than one and a half degrees, and the entropy even sooner. To avoid this one might assume that the heat capacity remained constant over a short range of temperature and then followed a T^3-law to the absolute zero.

On the other hand, it would appear from the data of Keesom and Clusius, and from that of Dana and Kamerlingh Onnes that the specific heat of He^4 just above the lambda-anomaly might be a decreasing function of the temperature, and that as a first approximation the heat capacity might go to zero linearly as the temperature goes to zero.

Both cases seemed likely enough to deserve consideration. Each has been treated with respect to its effect on Eq. (5) and the results are represented by curves *B* and *C*, respectively, in Fig. 1. For purposes of comparison, the curve obtained by Stout[1] is also shown as curve *D* in Fig. 1. His curve is about the same as curve *A* until the mole fraction of He^3 becomes equal to 0.2.

[6] Just as we were finishing this paper we received a copy of a Letter to the Editor of the Physical Review by C. J. Gorter and J. de Boer, very kindly sent to us by Professor de Boer, in which a similar but not entirely equivalent expression for T_λ as a function of x_3 was given. See Phys. Rev. 77, 569 (1950).

[7] W. H. Keesom, *Helium* (Elsevier Publishing Company, Inc., New York, 1942), see p. 215.

In treating the first possible behavior of the specific heat curve discussed above, it was assumed that the heat capacity remained constant at 2.2 cal. per mole per degree down to 1.46°K. The temperature of 1.46°K resulted from the imposed condition that the entropy of the normal fluid (known to be 1.62 cal. per mole per degree at the lambda-point) should go to zero as T goes to zero. Below this temperature it was assumed that the heat capacity followed a T^3-law,

$$C_{p4n}=0.707T^3.$$

The constant 0.707 resulted from the condition that the heat capacity is 2.2 cal. per mole per degree at 1.46°K. Under the condition of constant heat capacity, Eq. (5) takes the form (with H_λ=constant=3.01 cal. mole^{-1})

$$dT_\lambda/dx_3=-RT_\lambda^2[H_\lambda-(2.19-T_\lambda)2.2]^{-1}(1-x_3)^{-1} \quad (6)$$

above 1.46°K, which can be integrated to give the part of curve B of Fig. 1 above 1.46°K. From the expression for the heat capacity used below 1.46°K,

$$\bar{H}_{4n}=0.177T^4+0.60.$$

The constant of integration is derived from the experimental fact that the total enthalpy of the normal fluid at the normal lambda-point is 3.01 cal. per mole. (With the heat capacity constant from the normal lambda-point to 1.46°K, the enthalpy at 1.46°K is found to be 1.404 cal. per mole.) Substitution of this expression for $\bar{H}_{4n,\lambda}$ in Eq. (5) gives

$$(0.177T_\lambda^2+0.60/T_\lambda^2)dT_\lambda=[-R/(1-x_3)]dx_3. \quad (7)$$

The solution of this differential equation is

$$0.059T_\lambda^3-0.60/T_\lambda=R\ln(1-x_3)+0.242. \quad (8)$$

The value of the constant of integration was found from the condition obtained from the integration of Eq. (6) that x_3 is 0.21 when T_λ is 1.46°K. Equation (8) gives curve B of Fig. 1 below 1.46°K.

In treating the second possible behavior of the specific heat curve we assume as noted that it is a straight-line function of zero intercept.

$$C_{p4n}=bT.$$

From the data of Keesom and Clusius and from those of Dana and Kamerlingh Onnes, the heat capacity is about 2.4 cal. per mole per degree when the temperature is 3°K from which b is found to be 0.8. This actually results in an entropy of the normal fluid which is slightly negative at 0°K, indicating that before 0°K is reached the value of C_{p4n} must drop below $0.8T$. However, the discrepancy is small, and no correction has been made for it.

From this expression for the heat capacity, the enthalpy becomes

$$\bar{H}_{4n}=0.4T^2+k.$$

And since the experimental value of H_λ is 3.01 cal. per degree at the normal lambda point (2.19°K), k is 1.09. Substitution of this expression for $\bar{H}_{4n,\lambda}$ in Eq. (5) gives

$$(0.4T_\lambda^2+1.09)dT_\lambda/T_\lambda^2=-Rdx_3/(1-x_3).$$

The solution of this differential equation is

$$0.4T_\lambda-1.09/T_\lambda=4.58\log(1-x_3)+0.378.$$

The constant is found to be 0.378 from the condition that T_λ is 2.19°K when x_3 is zero. This equation produced the values for curve C of Fig. 1.

The assumptions made have an interesting consequence. The constant in the expression for $\bar{H}_{4n}$ makes the enthalpy finite in each case at 0°K. It is, in fact, necessary that there should be an intercept in the enthalpy *vs.* temperature curve in order that the entropy of the normal fluid may not become negative. Since the enthalpy of superfluid is presumably constant and has been set equal to zero (D), this would indicate that superfluid helium has lower enthalpy at 0°K than normal fluid. It implies that if one could by-pass the lambda-transition and could cool He^4 to 0°K, the product would be supercooled normal fluid and not superfluid. In his recent article on the thermodynamics of liquid helium, Rice[3] has suggested that the superfluid condenses out in ordinary space as well as in momentum space. The superfluid is, nevertheless, in a highly dispersed state and, as we have noted in (A), has the character of a component rather than of a phase. Nevertheless, as Rice has pointed out, it would be necessary for the superfluid condensed in ordinary space to have an especially low energy in order to be stable. It need, therefore, occasion no surprise if the attempt to extrapolate the properties of normal fluid to 0°K indicates a residual enthalpy greater than that of the superfluid.

From the experimental results curve C would appear to be more probable than curve B. It seems likely that the true curve lies somewhere between curve A and curve B, and probably it is not far from curve C.

The equations and conclusions derived from this development depend, of course, upon the validity of the original assumptions. Further, in obtaining Eq. (5) the chemical potential of the normal fluid was found by using the thermodynamic expression for a perfect solution. In this regard, the most recent work of Weinstock, Osborne, and Abraham[8] seems to indicate that these solutions are not exactly ideal even above their lambda-temperatures in that their vapor pressures exceed those which would result from application of Raoult's law, so some modifications will be called for.

Note added in proof: J. G. Daunt and C. V. Heer [Bull. Am. Phys. Soc. 25 (No. 1), 38 (1950)] mention measurements of the lambda-point with solutions containing as much as 90 percent He^3. The two points they give fall close to curve C.

[8] Weinstock, Osborne, and Abraham, Phys. Rev. 77, 400 (1950).

Conservation of Flux by a Superconducting Torus

R. L. Dolecek and Jules de Launay
Naval Research Laboratory, Washington, D. C.
(Received December 16, 1949)

A superconducing torus was subjected to a magnetic field normal to the plane of the torus and the field distribution across the plane of the superconducting torus was determined experimentally. The magnetic field near the axis of the torus was found to have the same direction as the applied field, but near the inner surface of the torus the field reversed direction in such a manner that the total flux enclosed by the torus was zero. It is concluded that the magnetic field distribution about a superconducting torus in weak magnetic fields can be adequately described by classical electrodynamics and the assumption of perfect diamagnetism.

1. INTRODUCTION

USING the principle of superposition of magnetic fields and postulating the conservation of flux, one of the authors[1] has derived theoretical expressions for the magnetic field about a superconducting torus subjected to magnetic cycling. In order to subject to test the validity of the expressions obtained, an experimental determination of the field distribution about a torus was made.

The theoretical distribution of the magnetic field (H) for the case of an external uniform magnetic field (H_0) applied perpendicularly to the plane of a superconducting torus is shown in Fig. 1. This plot is for a torus whose mean radius R is 22.4 times the radius of the toroidal wire. Since the field is symmetrical about the axis of the torus, a two-dimensional plot of field intensity distribution along a diameter of the torus is given.

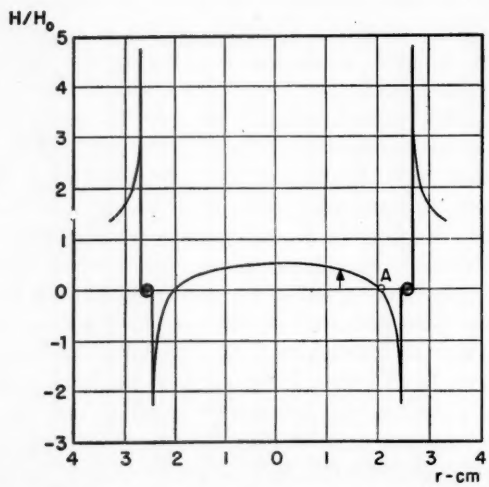

FIG. 1. Field distribution along a diameter of a superconducting torus for the case of an applied field H_0. The field direction and intensity are given by vectors drawn normal to the diameter and terminating on the curve. The position of the toroidal wire is indicated by the shaded circle. Example: at a distance $R/2$ from the center of the torus, the field is in the same direction as the applied field and equal to $0.405H_0$.

[1] Jules de Launay, "Electrodynamics of a superconducting torus," Naval Research Laboratory Report No. P-3441 (April, 1949).

The distribution in Fig. 1 is the one chosen for test. However, since precision measurement of field intensity and direction is beset with difficulties, it was decided to measure flux changes upon the application of H_0. Figure 2 gives the flux distribution to be expected.

The most significant characteristics of this flux distribution are:

(1) The location (r) of the maximum flux (point A), corresponding to the point A of Fig. 1.
(2) The slope of the curve between the point A and the inner surface of the torus.
(3) The slope of the curve external to the torus.

These will be most influenced by the transition from the state of normal conduction to superconductivity.

2. EXPERIMENTAL DESIGN

The theoretical treatment given by de Launay[1] is valid only so long as the torus is composed entirely of superconducting material and penetration depth is negligible. The experimental investigation, therefore, was restricted to the application of small fields (few gauss) to a torus cooled to the superconducting state under small (earth, uncompensated) applied magnetic field. By measuring the inductance of a very small coil wrapped directly upon the torus, transition of the

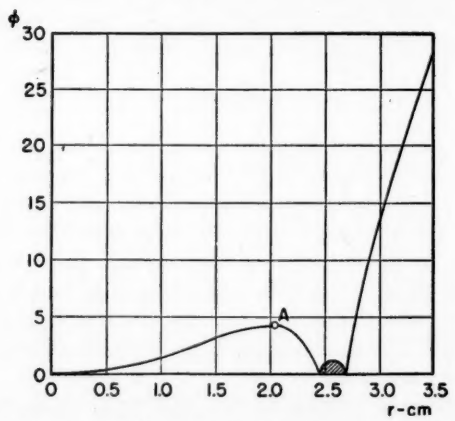

FIG. 2. Flux distribution obtained by integrating the distribution of Fig. 1 from the center of the torus outward (r). The position of the toroidal wire is indicated by the shaded semicircle. The flux ϕ (arbitrary units) is plotted as ordinate. The polar coordinate (r) is plotted as abscissa.

material into the superconducting state could be determined.

For the measurement of the flux distribution the torus was mounted in a solenoid and the e.m.f. generated in small concentric co-planar pick-up coils was measured when a 2000-cycle alternating current was passed through the solenoid. The mean diameters of the measuring coils were selected to yield information in the regions shown in Fig. 1. Construction data is given in Table I.

The field intensity in the solenoid was determined by comparison with a secondary standard. With the torus removed, the uniformity of the field was verified experimentally by measurement with the pick-up coils. For constant excitation current through the solenoid, the ratio of generated e.m.f. of coil area was determined. For this ratio the maximum deviation from the mean was 0.5 percent.

3. RESULTS

As the temperature of the lead torus was gradually lowered, the magnetic field about the torus passed gradually from an almost uniform distribution, corresponding to high resistivity of the lead, to a distribution indicating almost complete conservation of flux within the torus, corresponding to very high conductivity of the lead. At the transition temperature a very definite increase in slope of the flux distribution near the coil was observed. This was interpreted as the change to be expected by the transition to perfect conductivity and the change from a skin effect field penetration to the condition of superconductivity. A sudden decrease in the self-inductance of the small test coil wound on the torus verified that the abrupt change in slope and the onset of superconductivity occurred simultaneously. Below the transition temperature no change in flux distribution with further lowering of the temperature was noted. An absolute determination of the transition temperature was not attempted. However, by the use of a He gas thermometer the transition temperature was estimated to be about 7°K and the transition interval to be less than 0.1°K wide.

TABLE I. Geometry of lead torus and copper measuring coils used in experiment.

	Mean radius cm	Wire diameter cm	Number of turns
Torus	2.575	0.230	1
Coil 1	3.227	0.010	10
Coil 2	2.832	0.010	10
Coil 3	2.437	0.010	10
Coil 4	2.237	0.010	10
Coil 5	2.037	0.010	10
Coil 6	1.839	0.010	10
Coil 7	1.447	0.010	10
Coil 8	0.850	0.010	10

A comparison of the experimental results with the theoretical predictions is given in Fig. 3. The solid curve is a plot of the theoretical prediction and the circles indicate the experimental values determined with the measuring coils.

Instrumentation limited the absolute accuracy of the experimental results to approximately 2 percent. This accuracy was sufficient to verify the correctness of procedure and magnitude of effect but was inadequate for a precise test of the theoretical distribution. However, since the contour of the distribution is the important test, by conducting a complete test under constant conditions, the relative flux distribution can be obtained to a higher order of accuracy. This type of data is presented in Figs. 3 and 4, where the experimental point at A is made to coincide in magnitude with the theoretical curve.

In Fig. 3 the experimental data agree well with the theoretical prediction. Particularly noticeable is the region external to the torus where, because of the large slope, the theory is subjected to a good test. The scale of the plot of Fig. 3, however, is inadequate to show the goodness of fit in the internal region of the torus.

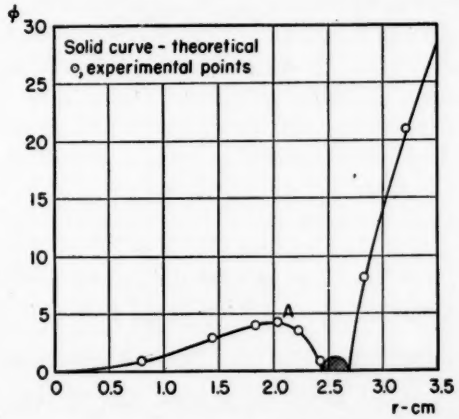

FIG. 3. Comparison of experimental results with theory. For inspection of contour, the experimental and theoretical magnitudes are forced to equality at the one point A.

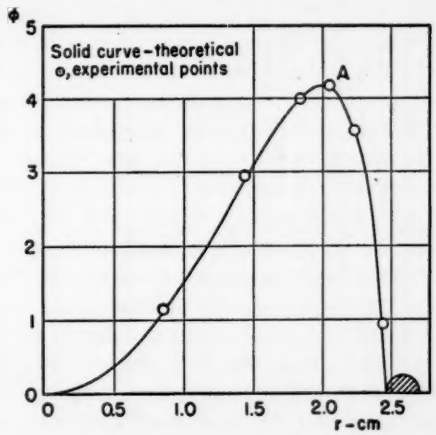

FIG. 4. Comparison of experimental results with theory for the inner region of the torus. This plot reproduces the inner portion of the curve of Fig. 3 on an expanded scale in order to show goodness of fit.

Figure 4 presents a plot of the internal region of the torus on an expanded scale. The high correlation of the experimental results to the theory is evident.

The experimental results of this investigation establish the validity of the assumptions of the principle of superposition of magnetic fields and the conservation of flux as used by de Launay[1] in describing the electromagnetic behavior of a superconducting torus under magnetic cycling. It is, therefore, felt that the results of his calculations can be applied with confidence to experimental investigations of the magnetic field distributions about superconducting tori.

PHYSICAL REVIEW VOLUME 78, NUMBER 1 APRIL 1, 1950

A New Method for Particle Injection into Accelerators

W. B. JONES, H. R. KRATZ, J. L. LAWSON, G. L. RAGAN, AND H. G. VOORHIES
General Electric Research Laboratory, Schenectady, New York
(Received December 29, 1949)

THE purpose of this note is to describe briefly a new method by which electrons have been injected into a betatron. This new method has made possible the production of a reasonable electron beam in the betatron phase of operation of the non-ferromagnetic synchrotron now in construction* at the General Electric Research Laboratory. This betatron is characterized chiefly by a small aperture (vertical aperture=0.05 orbit diameter, radial aperture=0.025 orbit diameter) and low rate of acceleration (about 10 to 15 volts per orbital turn). It is believed that the method can be applied with success to other accelerators, especially those employing small relative apertures and small energy increase per orbital turn.

Most betatrons seem to work and there have been many attempts to explain satisfactorily how the electrons were injected so that they did not subsequently hit the structure of the injector itself after a few revolutions. These explanations have included many possible effects, e.g., resonance conditions between orbital, vertical, and radial oscillation frequencies, effects caused by injected current flux linkage, space-charge considerations either in the "donut" or near the injector gun, etc.[1] In our first attempt to obtain a betatron beam in the non-ferromagnetic synchrotron we found that, while these phenomena may provide a successful means of injection in conventional betatrons, they did not appear to provide enough of an effect to give us an appreciable beam. We were, however, successful in developing a scheme that did provide efficient injection and which appears to have the very desirable properties of being readily understood and easily applied. This scheme involves two steps; the first is to provide a means of rapidly damping the radial or vertical oscillations for as large a number of revolutions as possible, and the second is to remove this damping agent before it causes subsequent undamping. We have found that the first of these conditions can be very easily met, as shown below, by proper control of the azimuthal variation of the index, n.[2] The second of these conditions is easily obtained by making the azimuthal pattern of n time-dependent in the proper way; in our case the azimuthal variation (producing beam damping) is reduced to zero some time late in the gun injection pulse.

The best method by which rapid beam damping can be produced depends upon the particular design of the betatron and, for definiteness, the following description is limited to a discussion of the conditions which pertain to our non-ferromagnetic betatron. The injector gun is displaced from the orbit in the Z (axial) direction (perpendicular to the radius and to the tangent of the orbit). The value of n is (at injection) nominally 0.25; this, however, has been made adjustable over wide limits. In this case one expects vertical (Z) oscillations of about one-half the orbital frequency so that after two orbital turns the injected electrons will find themselves back at the gun, and, if the gun has any finite physical size, will be intercepted. By experimentally tracing the beam we have found this to be true only when great care was exercised in providing an index, n, which was quite uniform in azimuth. When a particular azimuthal "bump" in n was provided, the Z oscillation amplitude was found to change markedly even after two orbital turns. A qualitative explanation for this phenomenon is shown in Fig. 1. This scheme is one which is similar to those considered by Langmuir and Davis.[3] One full Z oscillation cycle is shown for two different conditions of $n(\theta)$; first, when n is uniform and equal to 0.25 one gets the solid curve with no damping or undamping. The injector gun is shown in its proper position, and it will be noticed that, apart from small damping effects not considered here,[4] after two orbital

* The construction and development of this accelerator has been supported in part by ONR under Contract N7onr-332 Task I.

[1] See for example D. W. Kerst, Phys. Rev. 74, 503 (1948).

[2] In this definition the axial magnetic field is proportional to the minus nth power of the radius.

[3] R. V. Langmuir and L. Davis, Phys. Rev. 75, 1457 (1949). Also private communication.

[4] D. W. Kerst and R. Serber, Phys. Rev. 60, 47 (1941), showed the damping of oscillations caused by the increase of magnetic field (and hence restoring force) during a few orbital turns. How-

turns the electron is intercepted by the gun structure. However, if one provides, in the shaded region a value of n smaller than 0.25, denoted by n_1, and in the unshaded region a value of n larger than 0.25, called n_2, such that in each region one quarter-cycle of Z oscillation occurs, the Z oscillation amplitude will change monotonically (see dotted curve). This is caused by the requirement that the first quarter-cycle ray traced in the n_1 region must join in space and direction with the second quarter-cycle ray in the n_2 region; this requirement shows that the amplitude of each of these quarter-cycle oscillations is proportional to its wavelength, which in this case is inversely proportional to $(n)^{\frac{1}{2}}$. Thus the amplitude A_2 after two orbital turns in terms of the original amplitude A_0 will be

$$A_2/A_0=n_1/n_2,$$

and it is clear that one can very easily provide extremely rapid damping or undamping by the appropriate choice of n_1 and n_2. It is evident that the condition for damping requires that the first harmonic of $n(\theta)$ have a minimum in the half-orbital turn just following the gun and a corresponding maximum in the half-turn just preceding the gun. This condition is most readily produced by providing a "bump" in n at an azimuth of $\pm\pi/2$ from the gun; the sign of the bump is chosen to produce damping.

Damping by the above method is not a sufficient means of injecting electrons; satisfactory injection would require the practically impossible condition that the relative phase of the orbital and vertical oscillation remain fixed in time. Actually one can never quite adjust the values of n so that the damping shown in Fig. 1 continues indefinitely; after a while the particle instead of starting into a shaded region exactly at its extreme amplitude position will start into an unshaded region. In this case undamping will occur. In particular the Z oscillation amplitude will "beat" slowly at a rate which is the difference in frequency between the actual Z oscillation frequency and the synchronous Z oscillation frequency (one-half the orbital frequency). This feature makes two points evident; first, that large damping effects for a few turns can be experienced even though the average value of n is not very close to the synchronous value of $\frac{1}{4}$, and second (especially when n is not very near $\frac{1}{4}$), that if damping of this variety is used to clear the gun structure after two turns, undamping is sure to increase subsequently the Z oscillation amplitude to a value higher than its initial value. This essentially guarantees that if the beam goes more than two turns it will not last very many more without hitting the gun. This event can only be avoided by arranging the damping to be time-dependent; in particular, if the means of damping is suddenly removed before the Z oscillations can undamp beyond their initial amplitude, the injected beam will not be intercepted by the gun structure.

This is essentially the scheme we have tried successfully. We have used a coil system shown schematically in Fig. 2 to reduce the value of n over about an octant centered at an azimuth $+\pi/2$ after the gun. This particular scheme, one of many possible varieties, uses current in two coils, one above and one below the orbit, so arranged as to produce essentially a radial magnetic field proportional to Z (the coordinate perpendicular to the orbit radius and to the tangent and having its zero at the orbit).[5] Current in these coils produces strong damping; it is easy to turn off the damping current quickly because of the small inductance of the coil combination.

In practice, the damping current (in our case derived from a vacuum-tube cathode follower) is started by the same trigger which activates the pulse applied to the gun. At a controllable time later (during the time when the pulse on the gun has its proper value for injection), the current is switched off (actually decays with a time constant of 5×10^{-8} sec.). It is found experimentally that this switching-off time must be made just right or no beam is captured; if it comes too early the gun voltage is wrong, and if it comes too late the undamping effect described ruins the beam. In our case the switching-off time is critical to about one microsecond.

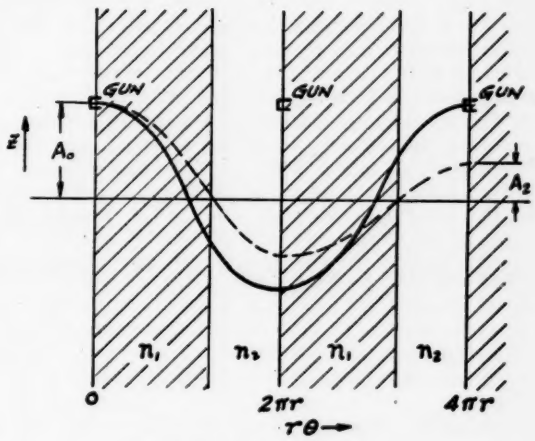

FIG. 1. Vertical (Z) oscillations.

ever, we are here concerned with a very slow rate of increase of field and will neglect this effect.

[5] There are many coil configurations which accomplish this; the one we have chosen has small inductance and is still efficient as a damper. We have also considered electrostatic means for altering the restoring forces on the electrons; this is clearly equivalent to the magnetic case and in many instances would be very practical. Electrostatic plates charged to potentials of the order of one hundred volts and arranged in the proper way can easily produce these effects. It is important to note that, since such small potentials can have such a marked effect on the beam, one needs to consider in detail the influence of the coating resistance on the walls of the "donut." With strong emission from the gun and resistance of the order 1000 ohms per square one can easily produce electrostatic fields of the magnitude we are here considering. Incidentally this effect may be responsible for assisting injection in many existing accelerators.

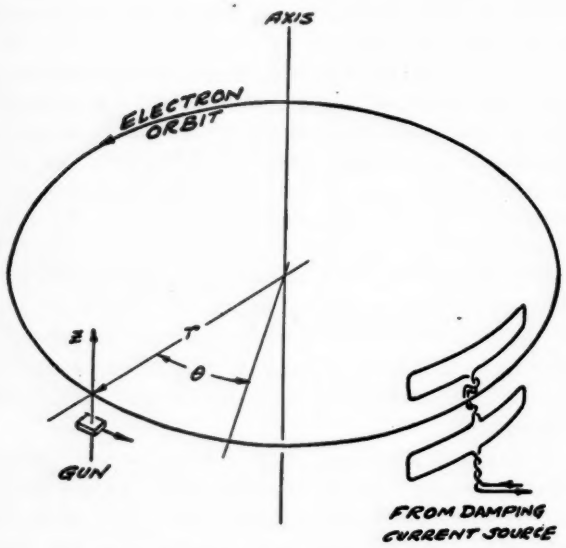

FIG. 2. Coil system to reduce value of n.

We find experimentally a number of necessary conditions for a strong betatron beam which substantiate the explanation given:

(1) The damping current must be switched off at the right time. As stated, virtually no beam is obtained unless the damping current is removed during the injection gun pulse.

(2) After the damping current is off, the azimuthal variation in n must be adjusted. After one has damped the beam it is necessary that no serious undamping occurs, and especially if one is near the $n=0.25$ resonance value it is imperative that the azimuthal variation in n be quite small.[6] In our case we have provided for local n controls in each octant; we find it necessary to adjust these controls to obtain a good beam.

(3) The best beam is obtained with a particular value of n. According to the principles outlined, the longest damping time (before undamping) occurs when the Z oscillation frequency is nearly synchronous with the orbital frequency. A little calculation shows that collection of electrons over our full "match" time of one microsecond requires the average value of n to be set within 0.01. We find experimentally that the best beam is obtained when the average n is set at about 0.25 (actually measured within ± 0.05) and that the beam is quite sensitive to a change in n of 0.01. Under the best condition we have traced the beam statically for eight to ten revolutions with no ambiguity. The beam was still damping satisfactorily and we have no reason to believe that damping would not occur for the whole match time of one microsecond.

(4) The condition for obtaining a beam is not sensitive to gun position; a good beam is obtained in our case for gun positions ranging from $1\frac{1}{2}$ in. from the orbit to $\frac{1}{2}$ in. (the minimum adjustment provided in the gun mount).

(5) A good beam is obtained even through small apertures. In one experiment an aperture ($\pm\frac{3}{4}$ in. in Z and $\pm\frac{1}{2}$ in. in radius) was inserted a half-turn around from the gun and the gun itself was moved to $\frac{1}{2}$ in. from the orbit (orbit radius=24 in.). No difficulty was experienced in getting a satisfactory beam through this combination.

Unfortunately we have not had time to measure the total beam current or even to compare it with others. We have, however, measured the beam current after a few revolutions directly on a small collector, and find it to be about 0.1 ma for a duration of about one microsecond. There seems to be no obvious reason why this charge is not caught into the final beam; a qualitative substantiation that a fairly large beam is actually caught is the observation that the beam pulse on a zinc-oxide photo-multiplier detector is considerably larger than the "main bang" (pulse produced by incidental collection of the initial electrons going only one half-turn) even when the injected electrons of 70 kev are accelerated to only 100 kev.

It is obvious that, while this above description applies to our injection scheme where the gun is displaced in the Z direction from the orbit, one uses the same arguments for radial injection. In the latter case one talks of radial oscillations instead of Z oscillations and adjusts $(1-n)$ instead of n to be nearly $\frac{1}{4}$. To produce damping one arranges $(1-n)$ to be somewhat smaller in the half-orbital turn after the gun than in the half-orbital turn just preceding the gun.

[6] See, for example, E. D. Courant, J. App. Phys. **20**, 611 (1949).

Letters to the Editor

PUBLICATION of brief reports of important discoveries in physics may be secured by addressing them to this department. The closing date for this department is five weeks prior to the date of issue. No proof will be sent to the authors. The Board of Editors does not hold itself responsible for the opinions expressed by the correspondents. Communications should not exceed 600 words in length.

Photo-Neutron Thresholds of Titanium[46] and Chromium[50]*

W. E. OGLE AND R. E. ENGLAND
Los Alamos Scientific Laboratory, Los Alamos, New Mexico
February 17, 1950

THE photo-neutron thresholds of Ti^{46} and Cr^{50} have been measured using the 20 Mev betatron at Los Alamos. The threshold values were determined by comparing the observed thresholds with the threshold of Cu^{63}, where the threshold for the $Cu^{63}(\gamma, n)Cu^{62}$ reaction was taken as 10.85 Mev. That value for the threshold of the copper reaction is the average of the value obtained by Baldwin and Koch,[1] by J. McElhinney *et al.*,[2] and by McElhinney and Ogle at Los Alamos.[3] The experimental arrangement was similar to that used by J. McElhinney *et al.*, at the University of Illinois.[2]

In both cases it was possible to irradiate the element under investigation and to observe the resultant activity. The total irradiation was in each case measured by means of an integrator circuit employing a photomultiplier phosphor combination and a standard current integrating circuit. The response of this integrator has been found to be proportional to that of a Victoreen R Thimble over the intensity ranges used in this experiment. The activity per integrator unit for a standard sample weight and for irradiating the counting geometry was determined as a function of the maximum energy of the bremsstrahlung spectrum from the betatron.

Both elements under consideration were in the form of the oxides. Extraneous activities due to the (n, γ) and (n, p) processes on various isotopes of the elements under consideration were observed in both cases. However, there was no difficulty in separating out the 42-minute positron period of Cr^{49} and the 3.08-hour period due to Ti^{45}. The data taken during this work indicate that the threshold for the $Ti^{46}(\gamma, n)Ti^{45}$ reaction is 13.3 $\pm$0.2 Mev, and that the threshold for the $Cr^{50}(\gamma, n)Cr^{49}$ reaction is 13.4$\pm$0.2 Mev.

* This document is based on work performed at the Los Alamos Scientific Laboratory of the University of California under Government contract W-7405-Eng. 36.
[1] George C. Baldwin and H. W. Koch, Phys. Rev. 67, 1 (1945).
[2] McElhinney, Hanson, Duffield, Becker, and Diven, Phys. Rev. 75, 542 (1949).
[3] J. McElhinney and W. E. Ogle, Phys. Rev., this issue.

The Cu^{63} Photo-Neutron Threshold*

J. MCELHINNEY AND W. E. OGLE
Los Alamos Scientific Laboratory, Los Alamos, New Mexico
February 17, 1950

THE threshold for the reaction $Cu^{63}(\gamma, n)Cu^{62}$ has been measured using the University of Illinois 20 Mev betatron by Baldwin and Koch[1] and by McElhinney *et al.*,[2] and found to be 10.9$\pm$0.2 Mev. The binding energy of a neutron in Cu^{63} has been measured through the $Cu^{63}(n, 2n)Cu^{62}$ reaction by Fowler and Slye.[3] Their value for that quantity, which is expected to be the same as the (γ, n) threshold, is 11.2$\pm$0.3 Mev.

Copper serves as a convenient energy calibration point for betatron work since it has a very sharp threshold. There was, however, some doubt in the minds of the authors as to the validity of the past determinations using a betatron. This doubt arose because of two possible uncertainties. (1) Neutrons from the betatron produce an activity that may be confused with the Cu^{62} activity and hence lead to an incorrect value of the threshold. (2) The apparent position of the threshold may possibly vary with the intensity of irradiation, that is, with the sensitivity of the detecting system. Hence, it was thought worth while to remeasure the (γ, n) threshold under varying conditions in order to check the above points.

Copper[62] decays by positron emission with a ten minute half-life. Copper,[66] which is formed upon bombardment by the betatron radiation by the reaction $Cu^{65}(n, \gamma)Cu^{66}$, decays by beta-emission with a five minute half-life. In the process of determining the threshold, the five minute period causes little difficulty until points are taken very close to the threshold, but there some error may be made in interpreting the data. In order to check this point the threshold was measured using both unshielded and cadmium shielded copper samples. The apparent threshold was also determined at two distances, one three times farther than the other from the target of the betatron, in order to check the effect of gamma-ray intensity on the apparent threshold. All measurements gave the same value of the (γ, n) threshold within one-half percent of each other. The value of the threshold determined in this work is 10.8$\pm$0.2 Mev, in good agreement with the values of Baldwin and Koch, and of McElhinney *et al.*

The energy scale of the betatron was calibrated by determining the (γ, n) thresholds of N^{14} and F^{19}. The thresholds of those reactions are assumed to be 10.54$\pm$0.1 Mev and 10.40$\pm$0.3 Mev, respectively.

* This document is based on work performed at the Los Alamos Scientific Laboratory of the University of California under Government contract W-7405-Eng 36.
[1] George C. Baldwin and H. W. Koch, Phys. Rev. 67, 1 (1945).
[2] McElhinney, Hanson, Duffield, Becker, and Diven, Phys. Rev. 75, 542 (1949).
[3] J. L. Fowler and J. M. Slye, Phys. Rev. 76, 169 (1949).

Thresholds for the Photo-Disintegration of Zr^{90}, Pr^{141}, As^{75}, I^{127}, and Ni^{58}*

W. E. OGLE, L. J. BROWN, AND A. N. CARSON**
Los Alamos Scientific Laboratory, Los Alamos, New Mexico
February 17, 1950

THE photo-neutron thresholds of several elements have been measured using the 20 Mev betatron at Los Alamos. The threshold values were determined by comparing the observed thresholds with the thresholds of N^{14} and F^{19}, where the threshold for the $N^{14}(\gamma, n)N^{13}$ reaction was taken to be 10.54 Mev and the threshold for the $F^{19}(\gamma, n)F^{18}$ reaction was taken to be 10.40 Mev.[1] The experimental arrangement was similar to that used by J. McElhinney *et al.*[2]

In all cases it was possible to irradiate the element under investigation and observe the resultant activity. The total irradiation was in each case measured with a Victoreen R Thimble. The activity per roentgen unit for a standard sample weight and counting geometry was then determined as a function of the maximum energy of the bremsstrahlung spectrum from the betatron. The maximum energy of the bremsstrahlung spectrum was varied by varying the amplitude of the magnet oscillation. Expansion of the electrons from the equilibrium orbit always took place at the peak of the magnetic flux wave, thus reducing any energy errors due to uncertainty in the time of expansion.

An automatic regulating circuit kept the magnet amplitude constant to 0.2 percent or better. The magnet amplitude, which is a measure of the maximum bremsstrahlung energy, was observed by measuring the voltage induced in two turns of wire around the legs of the betatron magnet with a model 19 Hickok voltmeter.

TABLE I. Thresholds for photo-nuclear reactions.

Parent isotope	Activity detected	Observed threshold (Mev)	Other work* (Mev)
I^{127}	13 d. β^-	9.45 ±0.20	
Pr^{141}	3.5 min. β^+	9.8 ±0.3	9.40 ±0.1
As^{75}	16 d. β^-, β^+	10.3 ±0.2	
Zr^{90}	4.5 m. ϵ^- 78 h. β^+	12.1 ±0.1 | Average 11.9 ±0.3 / 12.0 ±0.2	12.48 ±0.15
Ni^{58}	36 h. β^+	11.7 ±0.2	

* Hanson, Duffield, Knight, Diven, and Palevsky, Phys. Rev. 76, 578 (1949).

The results are shown in Table I. Zirconium^{90} decays either by 78-hour positron emission, or by 4.5-minute internal conversion or K-capture. The apparent threshold for the photo-disintegration of Zr^{90}, as determined by observation of the 78-hour period, was slightly less than that determined by observation of the 4.5-minute period. If the 4.5-minute period represents the decay by isomeric transition into the 78-hour isotope, one would expect the threshold observed by means of the 78-hour period to be somewhat less than that observed by the 4.5-minute period. However, since the errors quoted for the thresholds overlap, it is probably more logical to take 12.0±0.2 Mev as a mean value for the gamma-n threshold of Zr^{90}.

The authors would like to express their appreciation to Mr. Robert D. England for his very considerable help in keeping the betatron and the associated circuits running during the course of this work.

* This document is based on work performed at the Los Alamos Scientific Laboratory of the University of California under Government contract W-7405-Eng. 36.

** Now doing graduate work at George Washington University, Washington, D. C.

[1] J. Mattauch, *Nuclear Physics Tables* (Interscience Publishers, Inc., New York, 1946).

[2] McElhinney, Hanson, Becker, Duffield, and Diven, Phys. Rev. 75, 542 (1949).

True Magnitude of the Geomagnetic Secular Variation

C. J. SWIFT AND W. M. ELSASSER
Randal Morgan Laboratory of Physics, University of Pennsylvania, Philadelphia, Pennsylvania
February 14, 1950

IN order to analyze the geomagnetic secular variation in physical terms one extrapolates the surface field so as to obtain the field at the boundary of the earth's core[1] (this boundary, designated here by C, is almost halfway down to the earth's center). It follows from potential theory that the secular field at C is uniquely determined by the corresponding surface field under the highly plausible assumption that there are no sources of this field in the intervening layer. The extrapolation is usually carried out by means of a spherical harmonic analysis, but at C the series converges too slowly to be of much use. Vestine's[2] detailed maps of the secular variation show that the phenomena may be graphically described by a number of moderately rounded "hills", some positive, some negative, where the lines of constant rate of change of the field or potential are the contour lines of the hills. There are some 10 to 11 hills and dales on the whole earth at the present time.[3]

It is possible to achieve projection upon C of an individual "hill" having a circular boundary; for this purpose we employ solutions of the potential equation which vanish at the surface of a cone of half-angle ϑ_0. They are

$$\psi = r^{-n-1} P_n^m(\cos\vartheta) e^{im\varphi},$$

where n is non-integral, defined by $P_n^m(\cos\vartheta_0)=0$. The surface harmonics form an orthogonal set over the circular section of the sphere cut out by the cone. For not too large values of ϑ_0 (up to about 55°), P_n^m is well approximated by the Bessel function, $J_m[n^{\frac{1}{2}}(n+1)^{\frac{1}{2}}\vartheta]$. In practice the leading term of this series is by far the most useful, as for the higher terms n is so large that r^{-n-1} varies too rapidly to be significant, given the limited accuracy of the data. It follows from the orthogonality that the magnitude of the leading term furnishes, at any level below the surface, a lower limit for the r.m.s. value of the potential or field over the circular area. Numerical tests show that the observed hills, on averaging over the deviations from roundness, are well approximated by the lowest term in J_0.

For preliminary computations we have used Vestine's[2] maps of the variation of the vertical field component. These were replaced by an assembly of 10 to 11 circular regions whose aggregated area about equals that of the earth. The size of each region and the difference of the field at the center and at the circumference were chosen to correspond to the actual features of the maps. The radii of the regions range from 23° to 50°; the first term of each expansion gives an r.m.s. value at C, ranging between about 0.15 and 1.5 gauss/century, for individual regions. The grand total r.m.s. value is near 0.7 gauss/century (estimated error, 20 percent). Now the mean lifetime of these centers of secular variation is somewhat less than a century; hence on integrating over the mean lifetime it may be concluded that the secular variation corresponds to a fluctuating field at C whose vertical component has an r.m.s. magnitude of at least 0.5 gauss. The r.m.s. value of the vertical component of the main dipole field at C is 1 gauss; hence the variable part of the field is certainly not small compared to the constant part at C. These results seem to favor the explanation of both parts of the field by a common hydromagnetic mechanism proposed by one of us[1] as compared with the assumption of a separate "fundamental" origin of the dipole component parallel to the earth's axis.

[1] W. M. Elsasser, Rev. Mod. Phys. 22, 1 (1950).
[2] E. H. Vestine, Carnegie Institution of Washington Publications, Nos. 578 and 580 (1948).
[3] See some of Vestine's maps reproduced in reference 1.

A Determination of the Dipole Moment and Molecular Structure of Fluorosilane

A. HARRY SHARBAUGH, VIRGINIA G. THOMAS, AND BENJAMIN S. PRITCHARD
General Electric Research Laboratory, Schenectady, New York
February 14, 1950

WE have measured and identified the three rotational absorption lines arising from the $J=0\rightarrow1$ transitions of $Si^{28}H_3F$, $Si^{29}H_3F$, and $Si^{30}H_3F$. The spectrum consisted of a single absorption line for each molecular species and so is in harmony with present ideas that the Si^{28} and Si^{30} spins are zero and that Si^{29} spin is 1/2. It is possible that these spins might be incorrect if the nuclei had very small quadrupole coupling constants which resulted in an unresolvable hyperfine structure. The measured and derived constants are listed in Table I.

In principle one could determine unambiguously the three structural parameters of such a symmetric top molecule since moments of inertia have been measured for structures corre-

TABLE I. Molecular constants for SiH_3F (transition $J=0\rightarrow1$).

Species	ν_0(mc/sec.)	$I_B\times10^{40}$ (g-cm^2)	B_0 (mc/sec.)
$Si^{28}H_3F$	28,655.80 ±0.1	58.555	14327.9
$Si^{29}H_3F$	28,393.4 ±0.2	59.096	14196.7
$Si^{30}H_3F$	28,145.2 ±0.2	59.617	14072.6

sponding to the three different isotopic masses of Si. However, the uncertainties in the absolute values of the isotopic masses do not permit the evaluation of accurate values of the molecular configuration from these three nearly parallel equations relating the structural parameters with the moments of inertia. In order to avoid the parallelism it is necessary that one of the three moments of inertia be measured for a structure resulting from an isotope variation in another atom; in either the fluorine or the hydrogen atoms in this case.

Assuming an angle of $111°\pm1°$ for the HSiH angle, as is indicated from measurements on other monohalogen silanes, we compute $d_{SiF}=1.593\pm0.002$A and $d_{SiH}=1.503\pm0.036$A from the measurements on $Si^{28}H_3F$ and $Si^{30}H_3F$. These values were then checked with the measurements on $Si^{29}H_3F$ and found to be consistent. The d_{SiF} is thus about 0.04A longer than the corresponding distance (1.555A) found in $SiHF_3$.[1] This is consistent with the shortening (about 0.06A) of the CF bond in CHF_3 over that found in CH_3F.[2] Our value of 1.593A for d_{SiF} is considerably shorter than the sum of Pauling's covalent radii (1.81A). That this observed bond shortening is likely to be due to resonance with an ionic structure is born out by the sum corrected according to the Schomaker-Stevenson rule, *viz.*,

$$d_{SiF}=r_{Si}+r_F-0.09|X_{Si}-X_F|=1.61\text{A},$$

where the quantity in bars is the electronegativity difference of the silicon and fluorine.

From measurements of the Stark effect of the $Si^{28}H_3F$ line, we compute the dipole moment to be $1.268\pm0.013D$.

The authors gratefully acknowledge the assistance of Dr. Paul Zemany of this laboratory who checked the purity of the gas sample on the mass spectrometer.

[1] John Sheridan and Walter Gordy (private communication).
[2] Gilliam, Edwards, and Gordy, Phys. Rev. **75**, 1014 (1949).

Temperature Variation of Decay Times of Scintillation Phosphors

S. H. Liebson and J. O. Elliot
Electricity Division, Naval Research Laboratory, Washington, D. C.
February 16, 1950

A DECREASE in the decay times of gamma-scintillations with decrease in temperature of organic phosphors has been found by Kelley and Goodrich[1] of Oak Ridge and also by this Laboratory. Measurements made at this Laboratory of the variation of organic phosphor times with temperature using a shorted line technique give the following results: anthracene at 290°K—3.2×10^{-8} sec.; anthracene at 80°K—1.4×10^{-8} sec.; anthracene at 4°K—6×10^{-9} sec., which was within the resolving time of the photo-multiplier. That this behavior is probably characteristic of the molecules rather than the lattice is shown by the fact that mixtures of anthracene in naphthalene yielded approximately the same variation with temperature. These preliminary measurements are believed to have an over-all accuracy of better than 20 percent and are based on pulse shapes having the form $e^{-t/\tau}$. More accurate determinations of temperature variation are now in progress.

[1] G. G. Kelley and M. Goodrich, Phys. Rev. **77**, 138 (1950).

Interpretation of Underground Cosmic-Ray Data

Kenneth Greisen
Cornell University, Ithaca, New York
February 20, 1950

IN a recent note of the same title,[1] the author misrepresented the conclusions of Barnothy and Forro, and implied that the results of Miesowicz *et al.*[2] opposed the existence of the penetrating, non-ionizing component hypothesized by Barnothy and Forro. Actually, the soft, isotropic, non-ionizing radiation studied by Miesowicz *et al.* had been detected and investigated many years ago by Barnothy and Forro,[3] who originally suggested that it was largely composed of gamma-rays of radioactive origin, in agreement with the recent conclusions of Miesowicz. The *penetrating* non-ionizing radiation, suggested by Barnothy and Forro as necessary to interpret their absorption curves, is supposed to be of a quite different character, and on the question of the reality of this radiation the work of Miesowicz *et al.* apparently presents no information.

[1] K. Greisen, Phys. Rev. **76**, 1718 (1949).
[2] Miesowicz, Jurkiewicz, and Massalski, Phys. Rev. **77**, 380 (1950).
[3] J. Barnothy and M. Forro, Phys. Rev. **55**, 870 (1939).

N_2O Bands in the Solar Spectrum*

Robert R. McMath, A. Keith Pierce, Orren C. Mohler, Leo Goldberg, and Russell A. Donovan
McMath-Hulbert Observatory, University of Michigan, Pontiac, Michigan
February 14, 1950

NITROUS oxide in the earth's atmosphere was first detected spectroscopically by Adel[1] through observation of the ν_1 fundamental at 7.8μ. Subsequent confirming observations of other N_2O bands at 3.9μ, 4.1μ, 4.5μ, and 8.6μ were made by Migeotte[2] at Ohio State University and by Shaw, Sutherland, and Wormell[3] at Cambridge University.

The laboratory observations of Plyler and Barker[4] suggest that additional weaker bands of N_2O may appear in the solar spectrum in the spectral region below 3.6μ accessible to the high dispersion spectrometers and Cashman PbS cells[5] of the McMath-Hulbert Observatory at Lake Angelus and at the Mount Wilson Observatory. The expected bands, $2\nu_2+\nu_3$ at 2.97μ, $2\nu_3$ at 2.26μ, and $2\nu_1+\nu_3$ at 2.13μ, have all been found in the solar spectrum. The 2.97μ and 2.26μ bands are badly blended, the former with a band of H_2O and the latter with lines of CH_4 and H_2O. The bands at 2.13μ and 2.26μ are absent on tracings made with the noonday sun but appear quite plainly at solar altitudes less than about 10°. Comparison of telluric and laboratory intensities suggests an atmospheric abundance for N_2O equivalent to that in a layer 4 mm thick at NTP.

Study of the solar tracing of the 2.13μ-band has revealed that each line is asymmetrically widened on the long wave-length side, indicating the presence of a weaker overlapping band of the same spacing. The asymmetry of the lines has been confirmed by a laboratory tracing made with a carbon arc as a source and an absorption cell containing 25 cm of N_2O at atmospheric pressure. The laboratory tracing shows two additional very weak bands of N_2O, not recorded by Plyler and Barker, at 2.16μ and at 2.28μ. The latter band is overlapped by the negative branch of the 2.26μ-band. The band at 2.16μ is very probably caused by the transition from the ground state to $\nu_1+2\nu_2+\nu_3$, for which the calculated position is 4633.9 cm^{-1}. It has not yet been determined whether the faint bands overlapping those at 2.13μ and 2.26μ are isotopic or perhaps originate from an excited vibrational state.

The 2.16μ-band has been found in the solar spectrum on a sunset tracing made by Mr. Dale Vrabec at the Mount Wilson Observatory on September 25, 1949. The path length involved was of the order of 50 air masses.

We wish to thank Dr. I. S. Bowen for making available the Snow Solar Telescope under a guest investigator arrangement between the Mount Wilson and Palomar Observatories and the McMath-Hulbert Observatory. We also acknowledge with gratitude the continued assistance by McGregor Fund of Detroit.

* Supported in part by Contract N6onr-232-V with the ONR.
[1] A. Adel, Astrophys. J. **90**, 627 (1939).
[2] M. Migeotte, *The Atmospheres of the Earth and Planets* (University of Chicago Press, Chicago, 1949), p. 284.
[3] Shaw, Sutherland, and Wormell, Phys. Rev. **74**, 978 (1948).
[4] E. K. Plyler and E. F. Barker, Phys. Rev. **38**, 1827 (1931).
[5] Robert R. McMath and Orren C. Mohler, J. Opt. Soc. Am. **39**, 903 (1949).

On the Origin of the Sodium *D*-Lines during Twilight

R. PENNDORF
Geophysical Research Directorate, AF Cambridge Research Laboratories, Cambridge, Massachusetts
February 6, 1950

THE experimental evidence concerning the sodium flash during twilight reveals the following facts: (1) The end of the flash is connected with sunset at a certain altitude in the atmosphere. (2) The flash is produced between about 90 and 105 km (emission region), the thickness of which varies from day to day. (3) The flash ends before the emission region enters the earth shadow, corresponding to a shadow region at about 45 km above the earth; this is presumably the ozone shadow. (4) The maximum intensity of the *D*-lines during twilight is about 2×10^9 photons/cm² column and sec. (5) Calculations show the solar radiation producing the flash must be either around 2950 or 2100A, if the shadow is caused by atmospheric ozone.

The existing hypotheses on the origin of the flash are unable to explain these experimental facts. Therefore a chemiluminescent process is proposed, which has been studied in the laboratory by Bawn and Evans.[1] The mechanism is as follows: the primary reaction is

$$Na+N_2O\rightarrow NaO+N_2+1.32\text{ ev}. \quad (1)$$

The secondary reactions are

$$NaO+Na_2\rightarrow Na_2O^*+Na'(^2P)+0.84\text{ ev}, \quad (2)$$
$$Na'(^2P)\rightarrow Na(^2S)+\lambda5890\text{A}. \quad (3)$$

However, in the atmosphere a complete cycle must exist to produce the *D*-lines steadily. Therefore Na_2O, produced by reaction (2), must be dissociated photochemically. The process is

$$Na_2O+h\nu(\lambda\leq2031\text{A})\rightarrow Na_2+O. \quad (4)$$

The existence of N_2O in the upper atmosphere is beyond doubt and the emission region 90–105 km is bound to its vertical distribution, but not to that of sodium.

In order to check this hypothesis, the intensity-time curves measured by Vegard and Kvifte[2] are calculated theoretically, using the oxygen and ozone absorption coefficients for λ2031A and the vertical ozone distribution. It was found, that the intensity-time curves are very sensitive to the vertical distribution of ozone. Thus the ozone content has been obtained between 35 and 70 km and found in accordance with the theory of the origin of atmospheric ozone. Moreover the ozone content agrees with the values found experimentally by the "Umkehr" effect.[3]

A detailed report has been completed and will be published elsewhere.

[1] C. E. H. Bawn and A. G. Evans, Trans. Faraday Soc. **32**, 1570 (1937).
[2] L. Vegard and G. Kvifte, Geofys. Publ. **16**, Nr. 7 (1945).
[3] F. W. P. Goetz, Ergebn. kosm. Phys. **3**, 263 (1938).

Nuclear Magnetic Moments of the Gallium Isotopes

G. J. BÉNÉ, P. M. DENIS, AND R. C. EXTERMANN
Institut de Physique, Université de Genève, Geneva, Switzerland
February 9, 1950

IN their survey of nuclear magnetic moments, H. Taub and P. Kusch[1] noticed a discrepancy between the moments of the isotopes of gallium as determined from spectroscopic data and from magnetic resonance experiments. As was pointed out by Kusch and Foley (unpublished data), this discrepancy is real and is well beyond the limits of the experimental errors.

For the two isotopes, the spectroscopic values[2] $M(Ga^{69})=2.001$ and $M(Ga^{71})=2.543$ are 0.65 percent smaller than the corresponding resonance values[3] $M(Ga^{69})=2.0145$ and $M(Ga^{71})=2.559$.

By applying to the spectroscopic values the Rosenthal-Breit[4] and Kopfermann[5] corrections, assuming a spreading of the charge and magnetic moment over the whole nuclear volume, we are led to a corrective factor which for light nuclei is of the order of $(2ZR_0)/a_0$, where Z is the nuclear charge, $R_0=1.5\cdot10^{-13}A^{\frac{1}{3}}$ is the radius of the nucleus, $a_0=h^2/(4\pi^2me^2)$ is the radius of the first Bohr orbit for the hydrogen atom. We find a correction of 0.72 percent, in good agreement with the experimental discrepancy.

As Crawford and Schawlow[6] pointed out, the magnetic part of the correction, which for light nuclei is of the same order of magnitude as the charge correction, becomes relatively smaller for heavy nuclei.

Hence in our calculation this second correction is slightly overestimated. Thus we see that the spreading of the magnetic moment and of the charge in the nuclei account completely for the discrepancy between the spectroscopic and resonance data.

[1] H. Taub and P. Kusch, Phys. Rev. **75**, 1481 (1949).
[2] G. Becker and P. Kusch, Phys. Rev. **73**, 584 (1948).
[3] R. V. Pound, Phys. Rev. **73**, 1112 (1948).
[4] J. Rosenthal and G. Breit, Phys. Rev. **41**, 459 (1932).
[5] H. Kopfermann, *Kernmomente* (Leipzig, 1940), p. 17.
[6] M. Crawford and A. Schawlow, Phys. Rev. **76**, 1310 (1949).

Beta-Gamma Angular Correlation

THEODORE B. NOVEY
Argonne National Laboratory, Chicago, Illinois
February 20, 1950

MEASUREMENTS on angular correlation in beta-gamma-ray cascades have been made using anthracene scintillation counters in connection with liquid nitrogen cooled 1P21 photomultiplier tubes. The gamma-sensitive crystal consists of a fairly clear cylindrical piece of anthracene $\frac{7}{8}$ in. thick and 1 in. in diameter. A layer of crystals about 30 mg/cm² thick and 0.9 in. in diameter, formed by rapid cooling of a boiling saturated benzene solution of anthracene, provided a counter with a 100 percent counting efficiency for beta-particles.

The sources were mounted on rubber hydrochloride films (*ca.* 0.6 mg/cm²) and were located in the center of a plastic vacuum chamber 6 in. in diameter. This minimizes back and air scattering of the beta-particles and wall scattering of the gamma-rays. A mica window (3 mg/cm²) was located at the beta-crystal counter position. The crystal counters subtended a solid angle of about 0.04 steradian at the source. Measurements were taken at 0° and 90°.

A coincidence circuit utilizing blocking-oscillator pulse shaping and pentode mixing was used with a resolving time of 0.08 microsecond.

Tm^{170} was chosen for investigation because of its high *ft* value (6.3×10^8).[1] Preliminary measurements indicated a high correlation with a value of $\epsilon=0.4\pm0.1$ assuming the correlation function $(1+\epsilon\cos^2\theta)$.[2] Coincidence studies were made on the nuclide to ascertain which radiations showed the correlation. Results were found in general agreement with those of Fraser.[3] They indicated a branching of about 20 percent with about 90 percent conversion of the resulting 84 kev gamma-ray. The *K* x-rays of Yb^{170} were found to contribute to the gamma-counting rate to the extent of 43 percent at zero gamma-absorber. The existence of only a few percent of gamma-radiation per decay accounted for the low coincidence rates obtainable (*ca.* 1 count/min.) when the true and chance coincidence rates became comparable.

The angular correlation measurements were repeated with and without a 1 g/cm² Cu absorber over the gamma-counter. This absorbs 95 percent of the x-rays but only 40 percent of the gamma-rays. Beta-absorption was sufficient to prevent counting of conversion electrons. In order to obtain a higher coincidence rate the vacuum chamber was removed and the counters moved to posi-

tions subtending solid angles of 0.16 steradian at the source (source to counter distance *ca.* 2 inches). The results are shown in Table I. The correlation doubles as expected when the x-rays are

TABLE I. Coefficient ϵ in the correlation function $1+\epsilon\cos^2\theta$.

Nuclide	Coincident radiations	ϵ (this work)	ϵ (others)
Tm^{170}	$\beta-\gamma$	-0.104 ± 0.037	
	$\beta-\gamma$	-0.259 ± 0.053 (1 g/cm² Cu)	
Rb^{86}	$\beta-\gamma$	$+0.035\pm0.020$	
Co^{60}	$\beta-\gamma$	$+0.003\pm0.015$	-0.003 ± 0.01[6]
Sc^{46}	$\beta-\gamma$	$+0.006\pm0.026$	
	$\gamma-\gamma$	$+0.130\pm0.040$	$+0.20\ \pm0.035$[7]

absorbed. This is consistent with the expected isotropic distribution of K x-rays. These particular results are still somewhat uncertain on an absolute basis as no vacuum chamber was used and scattering in air reduces the correlation. A forbidden-shaped beta-spectrum is thus indicated in the gamma-branch. Spectrographic coincidence measurements are in progress to investigate this point and to obtain the angular correlation as a function of the beta-energy.

The correlation in Rb^{86}, $\epsilon=-0.094\pm0.015$, reported by Frankel,[4] was examined. Cs^{134} impurity was removed by an ion exchange column separation. Coincidences were measured at 0° and 90° and no negative correlation found. A possible small positive correlation as given in Table I is in agreement with preliminary unpublished results of other independent workers.[5]

As a check on the apparatus, measurements were made on the $\beta-\gamma$-coincidences from Co^{60} and the $\beta-\gamma$- and $\gamma-\gamma$-coincidences from Sc^{46}. For the $\gamma-\gamma$-measurements a thick crystal replaced the thin beta-crystal. The results shown in Table I are in agreement with other workers.[6,7]

I am grateful to D. W. Engelkemeir for the use of the scintillation coincidence counting equipment, and to R. Garwin for many helpful discussions and the suggestion of the possibility of finding angular correlation in Tm^{170}.

[1] J. Richards and D. Saxon, ANL-4237 (December, 1948); Phys. Rev. **76**, 186 (1949).
[2] D. L. Falkoff and G. E. Uhlenbeck, Phys. Rev. **73**, 649 (1948); C. N. Yang, Phys. Rev. **74**, 772 (1949).
[3] J. S. Fraser, Phys. Rev. **76**, 1540 (1949).
[4] S. Frankel, Phys. Rev. **77**, 747(A) (1950).
[5] Garwin, Shaknov, and Deutsch (private communications).
[6] R. L. Garwin, Phys. Rev. **76**, 1876 (1949).
[7] E. L. Brady and M. Deutsch, Phys. Rev. **72**, 870 (1947).

New Beta-Emitting Isotopes in Region of Tungsten*

M. LINDNER AND J. S. COLEMAN
State College of Washington, Pullman, Washington
February 20, 1950

SAMPLES of tungsten, rhenium, and osmium which had received considerable neutron exposures in a nuclear reactor were examined for products of consecutive neutron-capture by the heaviest stable isotope of each element. Thus, W^{188}, Os^{194}, and Re^{189} resulting from successive neutron captures in W^{186}, Os^{192}, and Re^{187}, respectively, were sought. A long-lived activity was found in the rhenium after decay of 50-day Re^{184}. Further work is being done to ascertain whether this is due to impurity, to a nuclide attributable to mass 189, or to the recently described[1] Re^{183} of 240-day half-life. Association with the latter is hardly likely in view of the activation with slow neutrons. Neither W^{188} nor Os^{194} could be observed directly owing to masking by comparatively large amounts of long-lived known isotopes of these elements formed by first-order neutron capture, but the presence of Re^{188} and Ir^{194} daughters in tungsten and osmium, respectively, demonstrate conclusively the presence of the two parent activities. All half-lives appear to be of the order of months, but further work is being done to determine these values accurately, and the data will be reported at a later date.

* This work has been performed under contract with the AEC.
[1] G. Wilkinson and H. G. Hicks, Phys. Rev. **77**, 314 (1950).

Erratum: A Cloud-Chamber Study of Cosmic-Ray Nuclear Interactions at 3260 Meters Elevation

[Phys. Rev. **77**, 342 (1950)]
W. W. BROWN AND A. S. MCKAY
Cornell University, Ithaca, New York

THE portion of text from line 6, column 1, page 343, commencing with "The median angle . . ." to line 6, column 2, page 343, ending with ". . . showers were recorded" was meant to be printed as a continuation of the abstract.

Are Mesons Elementary Particles?

H. M. MOSELEY AND NATHAN ROSEN
University of North Carolina, Chapel Hill, North Carolina
February 10, 1950

IN a recent paper with the above title, Fermi and Yang[1] investigated the possibility of considering the π-meson as a composite particle formed by a nucleon and an antinucleon. This idea is related to one on which we have been working for some time.[2] However our results differ from those of Fermi and Yang. We find that the $^1S_0$ state has to be excluded because its energy tends to zero rather than to 2 Mc^2 as the interaction goes to zero. On the other hand the $^3P_0$ state appears to give an acceptable solution. These results apply to the case of the vector interaction adopted by Fermi and Yang.

If one takes the tensor type of interaction he finds that $^1S_0$ solutions exist for one sign of the interaction parameter and $^3P_0$ solutions for the other. Since it would follow that not only a proton and an antineutron but also a proton and a neutron would form composite particles, it appears that this type of interaction must be discarded.

Details of the calculations will be published shortly.

[1] E. Fermi and C. N. Yang, Phys. Rev. **76**, 1739 (1949).
[2] N. Rosen, Phys. Rev. **74**, 128 (A) (1948); H. M. Moseley, Phys. Rev. **76**, 197 (A) (1949).

Commutator Equations for Fields Derived from a Variation Principle

CHRISTOPHER GREGORY
University of Hawaii, Honolulu, Hawaii
January 26, 1950

IN view of the recent developments of "commutator"[1] or "quantal"[2] equations for fields, it may be of interest to see whether such equations can be developed directly from a variation principle. We shall take as an example the electromagnetic field in vacuum in this report, the work for other types of fields in current use in quantum mechanics being quite similar.

For the electromagnetic field in vacuum, the integrand in the variation principle which leads to the classical equations is

$$L=-\tfrac{1}{4}F^{\mu\nu}F_{\mu\nu}, \qquad (1)$$

where $F^{\mu\nu}$ and $F_{\mu\nu}$ are the contravariant and covariant components respectively of the field strengths defined in terms of the vector potentials A_μ in the usual fashion. Four of Maxwell's equations in vacuum follow from

$$\delta \int L\, d^4x = 0. \tag{2}$$

To obtain the quantal equations directly it is necessary to replace (1) and (2) by

$$G = -\tfrac{1}{4}(F^{\mu\nu})_{mn}(F_{\mu\nu})_{nm} \tag{3}$$

and

$$\delta G = 0, \tag{4}$$

respectively. In (3), $(F^{\mu\nu})_{mn}$ and $(F_{\mu\nu})_{nm}$ are the matrix elements of $F^{\mu\nu}$ and $F_{\mu\nu}$, respectively. Thus, *G is essentially the trace of the classical Lagrangian.* Also in (3)

$$F_{\mu\nu} \equiv i[p_\mu, A_\nu] - i[p_\nu, A_\mu], \tag{5}$$

where the p's are the momentum operators.[1,3] In (4), the variation is taken with respect to the matrix elements of the vector potentials A_ν.

To show that the "quantal" equations follow from the above prescription, we must calculate δG. From (3) and (5)

$$\begin{aligned}
\delta G &= -\tfrac{1}{2}(F^{\mu\nu})_{mn}\delta(F_{\mu\nu})_{nm} \\
&= -(i/2)(F^{\mu\nu})_{mn}\delta([p_\mu, A_\nu] - [p_\nu, A_\mu])_{nm} \\
&= -(i/2)(F^{\mu\nu})_{mn}\delta([p_\mu, A_\nu])_{nm} \\
&= -i(F^{\mu\nu})_{mn}\delta(p_\mu A_\nu - A_\nu p_\mu)_{nm} \\
&= -i(F^{\mu\nu})_{mn}\delta\{(p_\mu)_{nk}(A_\nu)_{km} - (A_\nu)_{nk}(p_\mu)_{km}\} \\
&= -i(F^{\mu\nu})_{mn}\{(p_\mu)_{nk}\delta(A_\nu)_{km} - (p_\mu)_{km}\delta(A_\nu)_{nk}\} \\
&= -i\{(F^{\mu\nu}p_\mu)_{mk}\delta(A_\nu)_{km} - (p_\mu F^{\mu\nu})_{kn}(A_\nu)_{nk}\} \\
&= +i([p_\mu, F^{\mu\nu}])_{mk}\delta(A_\nu)_{km}.
\end{aligned} \tag{6}$$

If δG is to vanish for arbitrary variations of the matrix elements of the A_ν we must have

$$i([p_\mu, F^{\mu\nu}])_{mk} = 0,$$

or equivalently

$$i[p_\mu, F^{\mu\nu}] = 0, \tag{7}$$

in operator notation. Equation (7) together with the relation

$$i[p_\mu, F_{\nu\sigma}] + i[p_\nu, F_{\sigma\mu}] + i[p_\sigma, F_{\mu\nu}] = 0, \tag{8}$$

which is a consequence of the definition (5), are the "quantal" equations for the Maxwell field in vacuum.

I wish to thank the California Institute of Technology for the facilities offered me during my sabbatical leave.

[1] H. S. Snyder, Phys. Rev. **72**, 68 (1947); H. Yukawa, Prog. Theor. Phys. **2**, 209 (1947).
[2] R. J. Finkelstein, Phys. Rev. **75**, 1079 (1949).
[3] The units are chosen here so that $\hbar = 1$.

Angular Correlation in the Reaction $B^{10}(n, \alpha)Li^{7*}(\gamma)Li^7$

B. Rose and A. R. W. Wilson
Atomic Energy Research Establishment, Harwell, Berkshire, England
February 15, 1950

THE angular correlation between the α-particle and the γ-ray emitted in the slow neutron reaction $B^{10}(n, \alpha)Li^{7*}(\gamma)Li^7$ will yield information on the spin of the excited state of Li^7 involved,[1,2] provided the Li^{7*} does not lose its orientation during the recoil. This is unlikely owing to the relative magnitudes of the mean life of the state[3] (10^{-13} sec.), and of the period associated with the h.f.s. splitting[4] of Li^7 (10^{-9} sec.). In particular, a non-zero correlation will exclude the possibility that the excited state has spin $\frac{1}{2}$. The correlation has been measured as follows.

A uniform 1.4-cm square B^{10} foil of thickness ~0.3 mg/cm² was irradiated with neutrons from the Harwell pile, the α-particles emitted at right angles to the neutron beam entering a proportional counter through a 1.4-cm square grid, distant 3.2 cm from the foil. The γ-rays emitted at right angles to the neutron beam were detected in the 37-mm diameter crystal of a scintillation counter which could be rotated about the neutron beam, the distance of the mid-plane of the crystal from the boron film being about 6 cm.

The α-γ-coincidence rate per α-particle, ρ, corrected for random coincidences, was measured at twenty different values of the angle θ between the axes of the counters, and varied by a few percent only (which was also the order of the statistical error of each count), over the angular range $-110°$ to $+110°$. Owing to the extremely high γ-ray background, the genuine coincidence rate was approximately 50 percent of the random rate, and a circuit was therefore devised to monitor continuously the product of the coincidence resolving time and the γ-counting rate, so that the value of the random coincidence rate per α-particle could be determined free from drifts in the resolving time.

Systematic errors due to γ-scattering by the source holder, proportional counter, and adjacent shielding material were measured by replacing the boron film by a thin irradiated gold source of similar dimensions, and measuring the consequent γ-distribution. Corrections of the order of 2 percent were found necessary over a limited range of angles.

The corrected value of ρ was fitted to a curve of the form $a_0 + a_1\cos\theta + a_2\cos^2\theta$, the coefficients a_0 and a_2 being determined as functions of a_1 by the least squares method. The parameter a_1 was determined from the eccentricity (~0.010 in.) in the mounting of the boron film and the mean velocity of the Li^7 nuclei at the instant of radiation, which was calculated from the measurements of Elliott and Bell[3] on the mean life of this γ-ray. No correction was applied for the Döppler effect, as the energy dependence of the γ-counter efficiency was small. The resultant value of a_2/a_0, corrected for effects due to counter apertures and the extent of the source, was then the degree of correlation, C, for ideal geometry.

The mean of five determinations of C was -0.9 ± 1.2 percent, the error being the standard error. It should be noted that the range of values of C obtained by allowing V to vary from zero to the full recoil velocity is $+2.6$ to -1.3 percent.

This result rules out all correlations listed by Feld[1] and by Devons[2] with the exception of the spherically symmetrical, and those resulting from mixed transitions over very limited ranges of the mixtures. There is therefore no evidence from this experiment that the spin of the Li^{7*} state involved is not $\frac{1}{2}$.

Further details and discussion will be published elsewhere.

[1] B. T. Feld, Phys. Rev. **75**, 1618 (1949).
[2] S. Devons, Proc. Phys. Soc. **62A**, 580 (1949).
[3] L. G. Elliott and R. E. Bell, Phys. Rev. **74**, 1869 (1949).
[4] Kusch, Millman, and Rabi, Phys. Rev. **57**, 765 (1940).

Erratum: Evidence for Multiple Meson and γ-Ray Production in Cosmic-Ray Stars

[Phys. Rev. **76**, 1735 (1949)]

M. F. Kaplon, H. Bradt, and B. Peters
University of Rochester, Rochester, New York

THE following misprints occurred in this letter: Line 6, third paragraph should read: ". . . that is 21 more tracks." In the equation, the member $\frac{1}{8}$ should be altered to $1/\bar{\gamma}$.

Production of π-Mesons by High Energy Electrons*

E. Strick and D. ter Haar†
Department of Physics, Purdue University, Lafayette, Indiana
February 16, 1950

IN connection with the synchrotron project under way at Purdue University, it was felt useful to make an estimate of the cross section for meson production by high energy electrons. Since it was found in the case of the production of mesons by

nucleon bombardment that different methods of calculation might easily lead to different answers, if proper care is not taken to take all important terms into account,[1] we have calculated the cross section for meson production by electrons of extremely high energies by two different methods.

First we used the straightforward third-order perturbation treatment. We used a charged scalar meson field in all our calculations. The calculations are straightforward though tedious, and for the case where the bombarding electron has a very large energy they lead to the following expression for the cross section σ:

$$\sigma_1 = k(g^2/\hbar c)(e^2/\hbar c)^2(\hbar/\mu c)^2(M/\mu)\log(E_0/Mc^2), \qquad (1)$$

where E_0 is the energy of the bombarding electron, μ the mass of the meson, M the mass of the bombarded nucleon, and k a numerical constant of the order of magnitude unity.

The same result was obtained independently by using the impact parameter method, i.e., the so-called Weizsäcker-Williams method.[2,3]

It can be shown that recoil effects can be neglected in the computations leading to Eq. (1). Equation (1) gives only the most important term of a complicated expression and is, therefore, only correct for large values of E_0, i.e., just in the region where the Weizsäcker-Williams method should give reliable results.

For energies just above the threshold, the cross section turns out to be given by

$$\sigma_2 = k(g^2/\hbar c)(e^2/\hbar c)^2(\hbar/\mu c)^2\epsilon^{\frac{1}{2}}, \qquad (2)$$

where ϵ is $(E_0-E_t)/E_t$, if E_t is the threshold energy. Equation (2), which was obtained by the third-order perturbation method, is the first term in a series in ascending powers of ϵ.

For $E_0=300$ Mev, the cross section is about 10^{-31} cm^2 per nucleon.

We can compare the results of Eqs. (1) and (2) with the predictions made by dimensional considerations.[4] For energies just above the threshold energy, dimensional considerations give exactly the same[4] as Eq. (2). For high energies, the matrix element apparently depends on the energy, and the energy dependence of the cross section is different from an inverse square as one should expect at first.[5] The same effect was found to occur in case the bombarding particles were nucleons.[1]

Sneddon and Touschek[6] have calculated the cross section for meson production by electrons, using pseudoscalar fields. The remarkable fact is that they obtain the same cross sections as we do for scalar mesons.[7]

* Partial assistance by ONR is acknowledged.
† Present address: Plastics Institute, Julianalaan 134, Delft, Netherlands.
[1] E. Strick and D. ter Haar, Phys. Rev. 76, 304 (1949).
[2] C. F. von Weizsäcker, Zeits. f. Physik 88, 612 (1934).
[3] E. J. Williams, Phys. Rev. 45, 729 (1934).
[4] The difference between the exponent of Eq. (2) and that found in Eq. (3B) of reference 5 is due to the fact that in our calculations leading to Eq. (2) we have not taken into account the momentum of the nucleon in the Fermi gas inside a nucleus. If a single proton is bombarded, the cross section is given by Eq. (2), but if nuclei are bombarded, the calculations are more complicated because of the zero-point energy of the nucleons inside the nucleus. The same difference occurs in the case of the photomesic effect and was discussed in reference 5.
[5] D. ter Haar, Science 108, 57 (1948).
[6] I. N. Sneddon and B. F. Touschek, Proc. Roy. Soc. 199A, 352 (1949).
[7] The occurrence of an extra factor $\log_e$ in their expression for σ_2 is, as far as we can see, only apparent.

On the Ratio of Positive and Negative Photo-Mesons

OTTO HALPERN
University of Southern California, Los Angeles, California
February 14, 1950

A REPORT[1] was made recently of calculations which had been carried out to arrive at a theoretical explanation of the ratio of positive and negative photo-mesons observed. Our own unpublished calculations, although not quite as general as those reported in reference 1, have led to similar results with a characteristic difference which can perhaps be best illustrated by referring to the case of scalar coupling between π-mesons and nucleons, these last being treated as heavy Dirac particles. Here the formula of Brueckner and Goldberger[1] does not seem to take into account the processes in which the spin of the proton changes while the incident quantum is absorbed. The matrix element associated with these electromagnetic processes retains a finite value at the threshold; it occurs symmetrically (neglecting relativistic terms for nucleons) in the formulas for the cross sections of the production of mesons of both signs. On the other hand, the matrix element associated with absorption of a quantum by the proton without change of its spin differs from zero only in the production of the *negative mesons where it gives rise to the asymmetry discussed by Brueckner and Goldberger*, and there goes to zero at the threshold energy.

It is true that the matrix element referring to spin change is considerably smaller than the other, for higher energies; its observation near the threshold may become more difficult due to the capture of slow negative mesons by nuclei.

Furthermore, we encounter here a characteristic limitation of the presently accepted theory of elementary particles which has its origin in the anomalous moment of the proton (and neutron). Theory at present allows us to make quantitative predictions if the proton is treated as a Dirac particle and to make reasonable guesses if one attempts to account for the anomalous moments. Experiments near the threshold can be expected to furnish important information concerning the behavior of the anomalous moment in relativistic processes. Here the theoretical results become dependent upon the type of mesonic interaction chosen.

Summing up the results of our calculations, it can be stated that the threshold value of the cross section for the creation of photo-mesons is finite *as far as the electromagnetic matrix elements are concerned* and (if neutrons are treated as Dirac particles) is independent of the sign of the mesons created. The energy dependence of the ratio of positive to negative mesons created should give information about the anomalous moments and the type of meson interaction.

[1] K. A. Brueckner and M. L. Goldberger, Phys. Rev. 76, 1725 (1949).

Determination of the Maximum Energy of the β-Rays from 16-Hour Am^{242}

JEAN M. GRUNLUND,* B. G. HARVEY, N. MOSS, AND L. YAFFE
Chemistry Branch, Atomic Energy Project, National Research Council of Canada, Chalk River, Ontario, Canada
February 14, 1950

A SAMPLE of carefully purified Am^{241}, mounted on Al foil, was irradiated in the NRX pile. The active material was dissolved off the foil using 8 M HNO_3 and the solution diluted to a standard volume. An aliquot of the sample was placed on a thin Formvar film ($\sim$50 μg/cm^2) and evaporated so that essentially a weightless point source was formed. Its activity was then measured using a Geiger-Müller counter with an end window (1.9 mg/cm^2).

An absorption curve of the radiation from the irradiated sample of Am^{241} was taken. The technique employed was similar to that used by Yaffe and Justus[1] to determine the maximum energy of S^{35}. The initial sample used was large enough to give a count of about 10,000 counts per minute in our geometry. Various aluminum absorbers were placed in position and the counts recorded until the transmitted intensity was reduced by a factor of 10. An additional sample of americium was then added to the original one so that the count was about 10,000 per minute with the last absorber used in position, and additional absorbers were then added. This procedure was repeated, never counting less than 1000 counts per minute. The samples were then related to

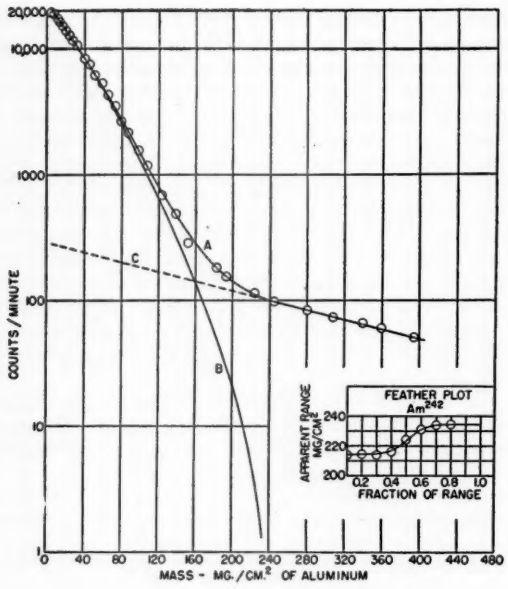

FIG. 1.

the original one by ratios to give a continuous absorption curve, which has a very well-defined end point. The sample itself was used as a reference to check the stability of the counter, no corrections for the decay during the experiment then being necessary.

The absorption curve, shown in Fig. 1, has two components. The soft component, β-radiation, was shown to come from 16-hour Am^{242} produced by this neutron irradiation, and to decay with the correct half-life. The hard component C, which is unrelated to Am^{242}, is probably due to x-radiation from Am^{241}. This was subtracted from A to give B, the absorption curve of the 16-hour component alone.

A Feather[2] type of analysis was made using UX_2 as a standard. Depending on which range-energy relationship is used, a slightly different energy value will be obtained, as is shown in Table I. The maximum energy, E, is in Mev, and the range, R, is in g/cm^{-2} Al.

The first three values agree well, with the Feather result differing considerably from them. This is caused by the low value (compared with the others) used by Feather for the range of the β-rays from RaE, which displaces his curve.

We propose a value of 0.63±0.01 Mev (obtained by equally weighting the first three results and averaging) as the maximum energy of the β-rays emitted by Am^{242}. This differs from a previous value obtained by Seaborg *et al.*[6] of a range of 280 mg/cm^{-2} Al with a resulting energy of 0.8 Mev.

TABLE I. Maximum energy of β-rays.

	Relation	Range from UX_2 used by worker	Range from Am^{242}	Maximum energy
Flammersfeld[a]	$E=1.92(R^2+0.22R)^{\frac{1}{2}}$	1.105	0.234±2	0.62±0.01
Glendenin[b]	experimental curve	1.105	0.234±2	0.65±0.01
Sargent[c]	$E=\frac{R+0.094}{0.526}$	1.126	0.238±2	0.63±0.01
Feather[a]	$E=\frac{R+0.160}{0.543}$	1.105	0.234±2	0.72±0.01

* See reference 2.
[a] A. Flammersfeld, Zeits. f. Naturforsch. **2a**, 370 (1947).
[b] L. E. Glendenin, Nucleonics 2, 12 (1948).
[c] B. W. Sargent, Can. J. Research **A17**, 82 (1939).

* Present address: Department of Chemistry, University of Southern California, Los Angeles, California.
[1] L. Yaffe and Katharine M. Justus, Can. J. Research **B26**, 734 (1948).
[2] N. Feather, Proc. Camb. Phil. Soc. **35**, 599 (1938).
[3] G. T. Seaborg, R. A. James, and L. O. Morgan, Nuclear Science Abstracts 1, 322 (1948), A1066.

The Effect of Cold Working on the Electrical Resistivity of Copper and Aluminum

J. W. RUTTER
Metallurgy Department, University of Toronto, Ontario, Canada
AND
JAMES REEKIE
Physics Department, Royal Military College of Canada, Kingston, Ontario, Canada
February 14, 1950

AS is well known, the electrical resistivity of a nearly pure metal can be regarded as made up of two parts, the first being temperature independent and the second depending only on the impurity content and degree of internal strain in the metal. We can express this as

$$\rho=\rho_T+\rho_0,$$

ρ_T being the "thermal" resistance and ρ_0 the "residual" or "dislocation" resistance.

Using polycrystalline copper and aluminum of the highest purity available (Johnson, Matthey Ltd., "H-S" brand, purity better than 99.999 percent) we have carried out experiments over a range of temperatures to measure the effect of cold working on the resistivity. The metals were in the form of rods, cold working from the annealed state being carried out by drawing at uniform speed through diamond dies.[1]

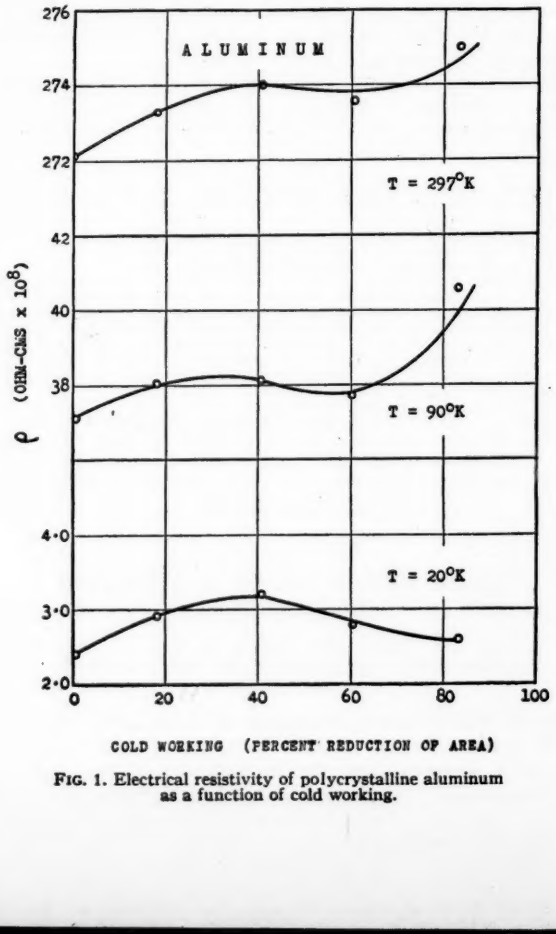

FIG. 1. Electrical resistivity of polycrystalline aluminum as a function of cold working.

It would be expected that the plastic strain of a metal should increase the term ρ_0 without appreciably affecting the temperature-dependent resistance. Our results appear to indicate, however, that cold working has a considerable effect on ρ_T as well as on ρ_0. Thus if $\Delta\rho$ is the change in resistivity due to cold working we can write

$$\Delta\rho=\Delta\rho_T+\Delta\rho_0.$$

Hence, *if* $\Delta\rho_T$ *is zero*, we should have merely, $\Delta\rho=\Delta\rho_0$. Now according to very general theoretical considerations ρ_0 is independent of temperature, so that $\Delta\rho$ (which is the *absolute* value of the increase in resistivity caused by cold working) should also be independent of temperature. Experimental results show that this is not the case. In Fig. 1, ρ is shown as a function of cold working for three different temperatures in the case of aluminum. It can be deduced immediately that $\Delta\rho$, for all degrees of cold working, *does* depend on the temperature; e.g., at 40 percent reduction of area $\Delta\rho$ is found to be 1.9×10^{-8}, 1.0×10^{-8} and 0.8×10^{-8} ohm-cm at temperatures of 297°K, 90°K and 20°K, respectively. Similar results are found for copper. Hence we conclude that, since $\Delta\rho$ is not independent of temperature, $\Delta\rho_T$ cannot be zero.

The same conclusion follows from another consideration. It will be clear that even with metals of the present degree of purity the observed values of ρ at 20°K will be comprised largely of the "residual" resistance term ρ_0. Hence an approximate value of ρ_T can be obtained by taking the difference between ρ at 297°K and ρ at 20°K. (A better value for ρ_0 would, of course, have been obtained by measuring ρ at still lower temperatures, but we were not able to make observations below 20°K at the time.) In Fig. 2,

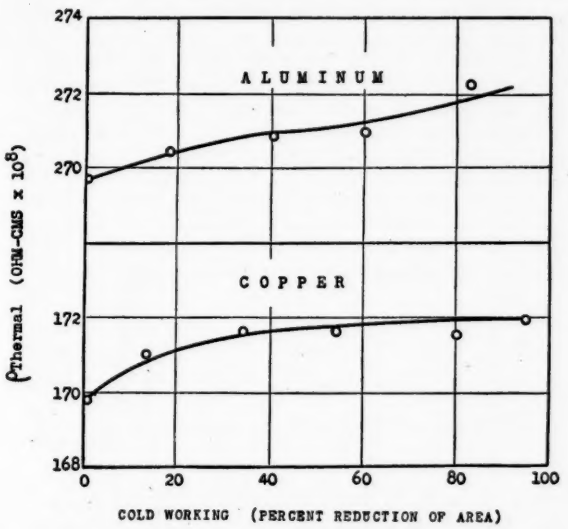

FIG. 2. Variation of thermal component of resistivity with cold working.

ρ_T obtained in this way is shown as a function of cold working for both aluminum and copper. It is immediately obvious that $\Delta\rho_T$ is not zero, and in fact, at high degrees of cold working, amounts to somewhat over 1 percent of the room temperature value of ρ, for both metals. From consideration of Figs. 1 and 2 it can further be deduced that for aluminum at, for example, 50 percent reduction of area, $\Delta\rho_T$ amounts to 0.5 percent and $\Delta\rho_0$ amounts to 0.2 percent of the room temperature value of ρ. For copper the corresponding figures are $\Delta\rho_T=0.9$ percent and $\Delta\rho_0=0.4$ percent.

These results therefore suggest that the change in resistivity which occurs on cold working is due not only to an increase in the "dislocation" resistance ρ_0, but also to an increase which takes place in the temperature dependent resistance ρ_T. In addition, the above figures indicate that $\Delta\rho_T$ is about twice as large as $\Delta\rho_0$ in the present experiments.

According to recent theoretical estimates of Mackenzie and Sondheimer[2] an increase in dislocation resistance of 0.4 percent would correspond, in polycrystalline cold-worked copper, to the formation of approximately 2×10^{11} dislocation pairs per cm². This estimate agrees much more closely with the figure obtained from measurements[3] of the energy stored during work hardening, *viz.* 2.9×10^{11}, than do previous estimates based on results which did not recognize a change in the thermal component of resistance with cold working.

[1] We are greatly indebted to the Canadian Wire and Cable Company of Toronto who provided facilities for cold working the metals used.
[2] J. K. Mackenzie and E. H. Sondheimer, Phys. Rev. **77**, 264 (1950).
[3] J. S. Koehler, Phys. Rev. **60**, 398 (1941).

Fine Structure of HDO near 3.7μ in the Solar Spectrum*

R. M. CHAPMAN AND J. H. SHAW
Mendenhall Laboratory of Physics, Ohio State University, Columbus, Ohio
February 15, 1950

IN the region between the 3.2μ water vapor band and the nitrous oxide band at 3.9μ, the solar spectrum shows many strong absorption lines, most of which are dependent on the amount of water vapor in the atmosphere. Many of these lines have now been identified with lines in the HDO spectrum obtained in the laboratory.

Atmospheric HDO was first observed by Adel[1] in the 7.2μ region of the solar spectrum. Recently, the 3.68μ band of HDO in the atmosphere has been observed by Gebbie, Harding, Hilsum, and Roberts[2] using a LiF prism spectrometer and a path length of about 1¼ miles at sea level.

In the present work, both the laboratory and solar spectra were obtained on a prism-grating spectrometer, utilizing a 7200-line/in. echelette, replica grating and a Perkin-Elmer thermocouple with their 13-cycle/sec. amplifier.

For the laboratory spectra, a 10-cm absorption cell with silver chloride windows was used, which could be heated to about 40°C. At this temperature, the vapor pressure is about 50 mm of Hg, which gives absorption lines strong enough for favorable comparison with solar spectra taken on days of low atmospheric water vapor content.

Spectra were recorded with the absorption cell, (a) evacuated, (b) saturated with the vapor from pure D_2O, and (c) saturated with the vapor from a 50-50 mixture of H_2O and D_2O. At equilibrium the latter mixture contains about 50 percent HDO and equal parts of H_2O and D_2O.

In the region 3.4 to 3.8μ in the laboratory spectra no lines due to H_2O were present, but the two strong bands of D_2O gave rise to many unwanted lines, in addition to those due to HDO. Comparison with the pure D_2O spectrum, however, permitted elimination of many of the interfering D_2O lines and positive identification of about 50 lines of HDO in the laboratory spectrum. These lines have been compared with lines in the solar spectrum of the same region and were found to match in position and relative intensity.

A tracing of the solar spectrum in this region is reproduced in Fig. 1 on which absorption lines identified with HDO are marked with dots. All frequencies are corrected to vacuum and the maximum absorption is about 35 percent.

Undoubtedly other lines not marked are also due to HDO, but their identification was made uncertain by the interference of intense D_2O absorption lines on the laboratory comparison spectra. These intense lines were also checked against the solar spectrum but no trace of them could be found, indicating, as would be expected, that the amount of D_2O in the atmosphere is negligible as compared with the amount of HDO.

Day to day fluctuation in the intensities of some of the unidentified lines relative to those of HDO indicate that other gases contribute to the absorption in this region.

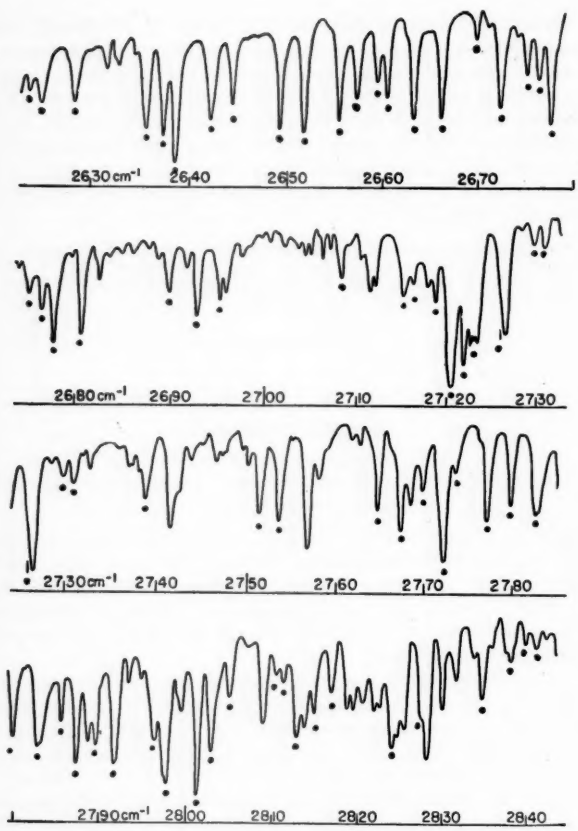

FIG. 1. Some lines of HDO in the solar spectrum near 3.7μ.

For a more thorough investigation of the HDO laboratory spectrum, it is planned to use an absorption cell of the multiple-reflection type with a path length of at least four meters. By using such a long path length, the ratio of D_2O to HDO can be reduced considerably without lessening the intensity of the HDO absorption.

* This work was supported in part by Contract No. AF19(122)65 between the U. S. Air Force and The Ohio State University Research Foundation, through sponsorship of the Geophysical Research Directorate, Air Materiel Command.

[1] A. Adel, Astrophys. J. **90**, 627 (1939).

[2] Gebbie, Harding, Hilsum, and Roberts, Phys. Rev. **76**, 1534 (1949).

Neutrons from the Bombardment of Li^6 by Deuterons*

WARD WHALING† AND J. W. BUTLER
The Rice Institute, Houston, Texas
February 14, 1950

WHEN lithium enriched in the mass six isotope became available through the AEC, it was felt worth while to examine the neutrons from the following reactions:

$$Li^6+H^2 \rightarrow Be^7+n^1+3.30 \text{ Mev} \quad (1)$$

$$Li^6+H^2 \rightarrow He^4+He^3+n^1+1.68 \text{ Mev}. \quad (2)$$

The yield curve for neutrons from these reactions has already been reported.[1]

In the present experiments the neutron energy spectrum has been analyzed from cloud-chamber photographs of recoil protons in the direction of the deuteron beam. A target of $Li_2{}^6SO_4$, 375 μg per cm^2 (about 150 kev at the bombarding energy used) was irradiated with 595-kev deuterons from the Rice Institute Van de Graaff generator. The low bombarding energy was chosen to minimize the neutrons from deuteron bombardment of carbon contamination on the target and on the tube wall in the analyzing magnet.

The neutron energy was determined from the range of the recoil protons in a Wilson cloud chamber filled with CH_4 and C_2H_5OH at 2 atmos. pressure. The cloud chamber was 17 cm from the target in the direction of the deuteron beam, the sensitive volume subtending a maximum angle of 16° at the target. Only tracks within 10° of the direction of the incident neutrons were accepted. Tracks shorter than 8 mm (corresponding to a 1-Mev recoil) were not counted because of the difficulty of determining their direction.

From some 6000 photographs, 1100 acceptable tracks were found. The number of tracks lying within 250-kev intervals are plotted in the histogram of Fig. 1. The curve in Fig. 1 gives the relative neutron spectrum and was obtained from the histogram by dividing by the neutron-proton scattering cross section.[2]

To extend the energy measurements to lower values, the chamber was filled with H_2 and C_2H_5OH at 2 atmos. These tracks were not so sharp as before, and only tracks longer than 1.3 cm (500 kev) were counted. With the same geometry as before, 160 tracks were measured for neutron energies below 1500 kev. The energy distribution, corrected for cross section and fitted to the higher energy spectrum, is shown by the open circles in Fig. 1.

In order to determine whether or not the 435-kev state of Be^7 reported by Brown, Chao, Fowler, and Lauritsen[3] appears in this reaction, the tracks corresponding to neutrons in the 3- to 4-Mev energy range have been analyzed in smaller energy intervals. The number of tracks in 100-kev intervals is shown in Fig. 2. The asymmetric shape of the spectrum and the one high point at 3.35 Mev (400 kev below the energy of neutrons from the formation of Be^7 in the ground state) may be interpreted as an indication that this 435-kev state in Be^7 is formed in this reaction. Although it is not definite from Fig. 2 that this excited state does appear in this reaction, one might conclude that if it is formed, only about 30 percent or less of the disintegrations result in the excited state.

Using the peak of the curve at 3.75 Mev in Fig. 2, as the energy of the neutrons from the formation of Be^7 in the ground state, the Q-value calculated for the reaction is 3.27 Mev.

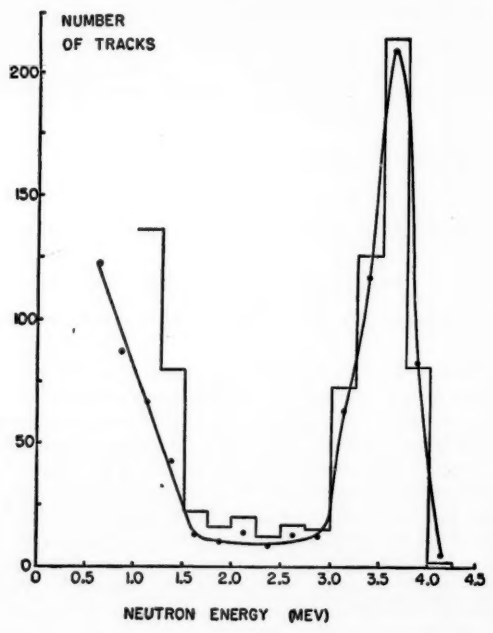

FIG. 1. Number of recoil tracks in 250-kev intervals. Smooth curve has been corrected for $n-p$ scattering cross section. Solid circles refer to data in CH_4 and open circles to data in H_2. Point at 1.12 Mev is common to both sets of data.

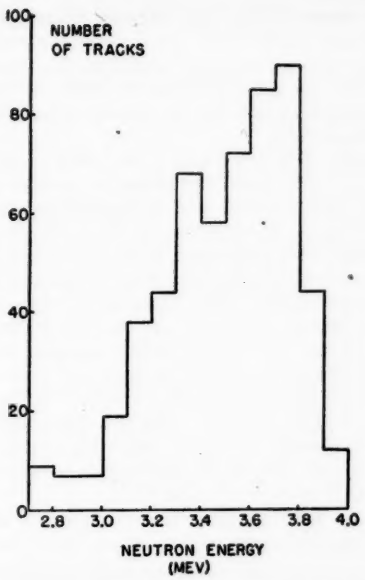

FIG. 2. Number of recoils in 100-kev intervals.

The neutrons below 1.5 Mev show a continuous distribution in energy and so may be attributed to reaction (2). Although the shape of the curve was not determined below 0.5 Mev, it appears that somewhat fewer than one-half of the neutrons come from reaction (1), if the angular distributions of the competing reactions are the same.

Mandeville, Swann, and Snowdon[4] have determined the neutron energy spectrum for these two reactions by measuring the recoil proton tracks in photographic emulsions. They used a bombarding energy of 900 kev and measured the neutrons emitted at an angle of 90° to the deuteron beam. Their data indicate that about two-thirds of the neutrons come from reaction (1), if the angular distributions of both reactions are assumed to be the same. These two experiments together indicate that either the angular distributions of the neutrons from the two reactions are not the same or that the relative yields of the reactions change with the bombarding energy.

* This work was supported by the Research Corporation and by the Joint Program of the ONR and AEC.
† AEC fellow.
[1] Whaling, Evans, and Bonner, Phys. Rev. **75**, 688 (1949).
[2] Bailey, Bennett, Bergstralh, Nuckolls, Richards, and Williams, Phys. Rev. **70**, 583 (1946).
[3] Brown, Chao, Fowler, and Lauritsen, Phys. Rev. **78**, 88 (1950).
[4] Mandeville, Swann, and Snowdon, Phys. Rev. **76**, 980 (1949).

Neutron Groups from the Reaction $Li^7(p, n)Be^7$

BERNARD HAMERMESH AND VIRGINIA HUMMEL
Argonne National Laboratory, Chicago, Illinois
February 7, 1950

RECENT reports[1-4] indicate the existence of at least one excited state in Be^7 within 1 Mev of the ground state. Therefore, the reaction $Li^7(p, n)Be^7$ should give rise to at least two groups of neutrons of different energies depending upon whether the reaction leads to Be^7 in the ground state or in an excited state.

Photographic plates (Ilford C2 emulsions 50μ thick) have been exposed to neutrons produced in this reaction by protons with energies of 2.705 and 3.120 Mev from the Argonne electrostatic accelerator. By studying the recoil protons in the emulsions the energies of the neutrons can be found. The photographic plates were mounted at 0° to the proton beam and 10 cm from the 10-kev thick metallic lithium target.

After processing the plates, the tracks were measured in a microscope with an oil immersion objective. Tracks were considered to be acceptable for measurement if they showed no detectable dip into the emulsion and if they deviated from the incident neutron direction by an angle less than arctan $\frac{1}{3}$. This procedure leads to a larger acceptable range of solid angles for the short tracks than for the long tracks. This will accentuate the intensity of a group of neutrons arising from an excited state relative to the group arising from transitions leading to the ground state of Be^7.

The energies of the recoil protons were determined from their ranges by using the Ilford range-energy curves.[5] The neutron energy is found from the recoil proton energy E_p by the use of the relation $E_n = E_p/\cos^2\theta$ where θ is the angle between the incident neutron direction and the recoil proton.

Figure 1 shows a histogram of the number of neutrons in a 25-kev range for each of the incident proton energies. The letter A locates the center of gravity of the main group of neutrons and B the center of gravity of a clearly resolved group arising from an excited state in Be^7. The centers of gravity were found by first subtracting a constant background of two tracks from each block in the histogram and then locating the center of gravity in the usual fashion. For the 2.705-Mev data A is found to be at 937 kev and B at 472 kev. For the 3.120-Mev data, A is at 1364 kev and B is at 896 kev. In the forward direction the neutrons in the main groups should have energies of 1.000 and 1.423 Mev, respectively. In each case the center of gravity of the group A is found 63 kev below its calculated position in terms of the accelerator calibration, but the energy difference between the two values of A is 427 kev which is a remarkable coincidence and indicates that the Ilford range-energy curve used is quite good. Since the value of B from the 3.120-Mev data is relatively close to that of A from the 2.705-Mev data, one would expect to find a reliable value for the separation of the B state from the ground state if the 3.120-Mev data is used. The energy difference from A to B in the 3.120-Mev data yields a value of 428±20 kev for the level separation. The 2.705-Mev data cannot be expected to yield a very reliable result since the B group now corresponds to proton recoils of approximately 5μ in length. In this region the slope of the range-energy curve is changing rapidly so relatively large errors may be expected. The A to B difference in this case yields a value of 408±35 kev for the height of the corresponding excited state of Be^7 above the ground state. The points labeled C indicate the expected location of the 205-kev group reported by Grosskreutz and Mather[1] and the point D indicates their 745-kev group. The latter group cannot be excited at 2.705 Mev bombarding proton energy.

To compare the relative intensities in the various groups, one must correct for the following: (1) different accepted solid angles for different track lengths; (2) different probability of leaving the

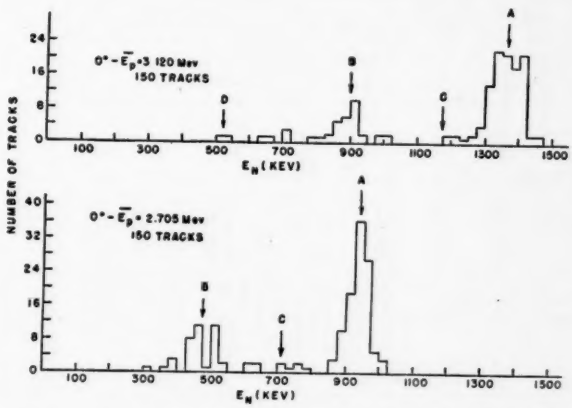

FIG. 1. Neutron groups from the reaction $Li^7(p, n)Be^7$. Note that the relative intensities of the neutron groups have not been corrected.

emulsion for different track lengths; (3) variation of (n, p) scattering cross section with energy.

Table I shows the total correction factor that must be applied to each of the groups before determining their relative intensities.

TABLE I. Correction factors for neutron groups.

Proton energy \ Neutron group	Main group ground state *A*	205 kev *C*	428 kev *B*	745 kev *D*
2.705 Mev	1	0.55	0.25	—
3.120 Mev	1	0.67	0.38	0.16

Using the correction factors of Table I the intensity of the 428-kev group relative to the main group is 0.08 ± 0.02 for both sets of data. If there is a group at *D* there are only two tracks in the data which could correspond to this group. The relative intensity is found to be less than one percent. It is difficult to decide whether there is a group corresponding to the points marked *C*. The number of tracks that can be assigned reasonably to such a group in each case is no more than could be considered to be background. In each set of data there are about six tracks that may be considered to be in such a group. The relative intensity would be five percent of the main group if all of these did arise from a level at 205 kev in each set of data.

[1] J. C. Grosskreutz and K. B. Mather, Phys. Rev. **77**, 580 (1950).
[2] Brown, Chao, Fowler, and Lauritsen, Phys. Rev. **78**, 88 (1950).
[3] T. Lauritsen and R. G. Thomas, Phys. Rev. **78**, 88 (1950).
[4] Johnson, Laubenstein, and Richards, Phys. Rev. **77**, 413 (1950).
[5] Lattes, Fowler, and Cuer, Proc. Phys. Soc. **59**, 883 (1947).

The $3\nu_3$-Band of Telluric CO_2 in the Solar Spectrum*

LEO GOLDBERG, ORREN C. MOHLER, A. KEITH PIERCE, AND ROBERT R. MCMATH
McMath-Hulbert Observatory, University of Michigan, Pontiac, Michigan
February 14, 1950

OBSERVATION of the lines of the $3\nu_3$-band of telluric CO_2 that appear in the solar spectrum is possible only when the earth's atmosphere is very dry. Numerous strong lines of the 0 2 1, 1 0 1, 1 2 0, and 2 0 0 bands of H_2O occupy the same wavelength region. One of the results of guest investigator arrangement between the Mount Wilson and Palomar Observatories and the McMath-Hulbert Observatory, for the direct-intensity recording of the solar spectrum, is a spectrophotometric tracing made on an exceptionally dry day (December 20, 1949), at Mount Wilson, California. The weakened H_2O absorption unmasks many lines of the $3\nu_3$-band of CO_2.

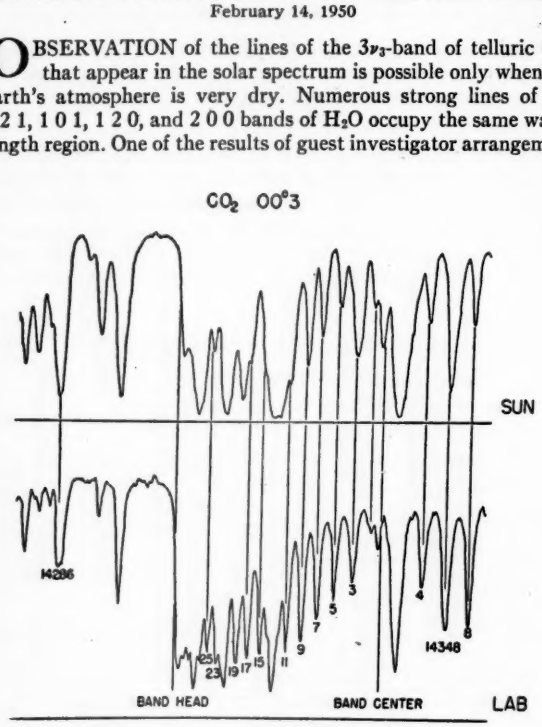

FIG. 1. The $3\nu_3$-band of CO_2 in the solar spectrum, with laboratory comparisons.

The top half of Fig. 1 is a part of this record; the bottom half is a laboratory comparison. The intensity increases upward from the straight line below each tracing. Broken lines connect corresponding features of the two tracings and indicate the positions of the band head and band center. The numbers 14,286 and 14,348 are the wave-lengths in angstroms of the absorption lines immediately above them. Beneath the CO_2 lines in the laboratory tracing are the upper quantum numbers for the lines in the short wave-length branch, and the lower quantum numbers for the lines in the long wave-length branch of the band.

14,308A(H_2O) and 14,313A(H_2O) complicate the strong CO_2 band head at 14,305A in the solar spectrum, and the line at 14,338A(H_2O) obscures the band center. On all tracings obtained up to December 20, 1949, H_2O lines completely mask the analogous isotopic ($C^{13}O_2^{16}$) band head at 14,700A.

We wish to acknowledge continued financial aid from the McGregor Fund of Detroit.

* Report on work supported in part by Contract N6onr-232-V with the ONR.

A Precise Determination of the Energy of the Cs^{137} Gamma-Radiation*

LAWRENCE M. LANGER AND R. DOUGLAS MOFFAT
Indiana University, Bloomington, Indiana
February 16, 1950

FOR the absolute calibration of nuclear spectrometers, it has become common practice to make use of the photo-electrons ejected from a radiator or the internal conversion electrons resulting from a gamma-ray of known energy. Since the shape of photo-lines depends somewhat on the position of the source relative to the radiator and also on the thickness of the radiator, the use of an internal conversion line appears to be preferable. Although the energy of the Au^{198} gamma-ray has been measured with great precision,[1] the relatively short half-life provides a calibration source of only temporary utility. It is felt that the conversion electrons from the 0.66-Mev gamma-ray which follows the disintegration of Cs^{137} provide a much more suitable calibration standard. The 33-year half-life makes possible the preparation of an essentially permanent laboratory source of monoenergetic electrons. There is also the advantage that the conversion line lies at a higher energy and is completely separated from the main nuclear beta-spectrum. In an attempt to establish Cs^{137} as a calibration standard, the energy of the internal conversion electrons has been carefully determined by direct comparison with that of the 0.4112-Mev gamma-ray of Au^{198}.

The measurements were made with the 40-cm radius of curvature, 180 degree focusing, shaped magnetic field spectrometer.[2] A composite source of Au^{198} and Cs^{137} was prepared on a 0.00025-in. Al backing. The source was 0.25 cm wide and 2.5 cm high and was spread with the aid of insulin. An electrically grounded source of mechanical permanence was thus obtained. The scattering from the aluminum backing causes only a slight broadening of the lines and does not affect the energy determinations which are made in terms of the extrapolation of the high energy edges. The source thickness was estimated to be 0.03 mg/cm² of Au^{198} and 0.1 mg/cm² of Cs^{137}.

Figure 1 shows a typical momentum distribution curve of the electrons which are internally converted in the *K* shells of Hg^{198} and Ba^{137}. For these measurements, the detecting slit was 0.40 cm wide and the distance between the center of the source and the center of the slit was $2\rho = 80.58$ cm. In determining the energy

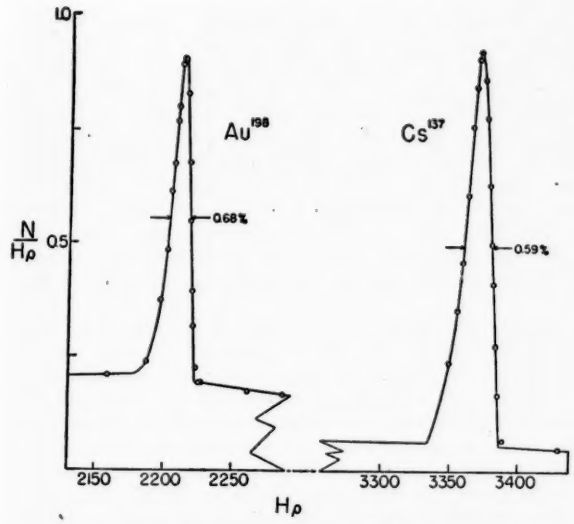

FIG. 1. Internal conversion electrons from Au^{198} and Cs^{137}.

from the extrapolated high energy edge, a small correction was made for the finite resolution by using for ρ, one-half the minimum distance between source and detector slit. In all cases the magnetic field was measured immediately below and above each line by means of a flip coil and ballistic galvanometer as well as by balancing the voltage picked up by a continuously rotating search coil against that picked up in a standard Helmholtz field. The interpolation of points actually on the lines was made in terms of the energizing current of the magnet which was stabilized electronically to about 0.01 percent and measured by means of a type K potentiometer and standard resistance. In any one run, the magnet current was varied only in one direction. On the basis that the electrons from the Au^{198} gamma-ray correspond to an extrapolated high energy edge of $H\rho=2219.6$ gauss-cm, the electrons following the Cs^{137} disintegration are observed at $H\rho=3381$ gauss-cm. The corresponding kinetic energy of the electrons is 0.6239 Mev and the energy of the gamma-radiation is 0.6614 ±0.0007 Mev.

Additional runs were made on the Cs^{137} conversion lines with the same source but with the detector slit reduced from 0.40 cm to 0.20 cm. The profiles of the lines are shown in Fig. 2. Even with

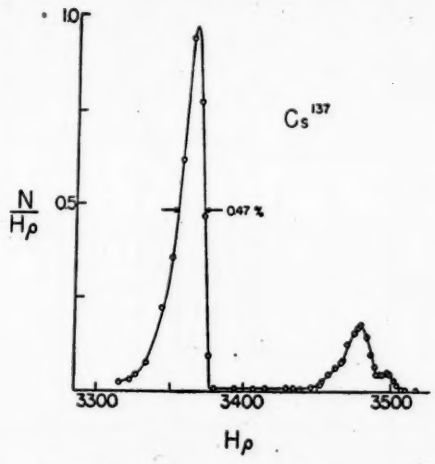

FIG. 2. Internal conversion electrons from Cs^{137}.

the extremely high resolution employed, the broadening of the lines because of backing and source thickness is such that the individual L and M lines are not sufficiently separated to be useful for additional calibration purposes. The calibration in terms of the K line is summarized in Table I.

TABLE I. Gamma-ray energies.

	H gauss-cm	Electron energy Mev	K binding Mev	Gamma-energy Mev
Au^{198}	2219.6	0.3280	0.0832	0.4112
Cs^{137}	3381	0.6239	0.0375	0.6614 ±0.0007

* This work was assisted by a grant from the Frederick Gardner Cottrell fund of the Research Corporation and by the Joint Program of ONR and AEC.

[1] DuMond, Lind, and Watson, Phys. Rev. 73, 1392 (1948).
[2] L. M. Langer and C. S. Cook, Rev. Sci. Inst. 19, 257 (1948).

On the $\gamma-\gamma$-Angular Correlation in Pd^{106}

J. A. SPIERS
Clarendon Laboratory, Oxford, England
February 15, 1950

WE denote the successive γ-emissions and nuclear spins in Pd^{106} by

$$J_1 \xrightarrow{\gamma_2} J_2 \xrightarrow{\gamma_1} 0$$

the ground state of Pd^{106}, (even-even), being taken to have zero spin. The measured angular correlation[1] of γ_1 and γ_2 is given by

$$W(\theta)=1-1.66\cos^2\theta+2.16\cos^4\theta.$$

As Ling and Falkoff[2] have shown, this cannot be explained theoretically on the assumption that γ_2 is pure quadrupole ($J_2=2$) and γ_1 pure quadrupole ($J_1=0$) or mixed dipole-quadrupole ($J_1=1, 2, 3$). Also γ_2 cannot be dipole ($J_2=1$) or there would be no $\cos^4\theta$-term in $W(\theta)$.

The author[3] has calculated the correlation to be expected on the assumption that γ_2 is pure octupole ($J_2=3$) and γ_1 pure octupole ($J_1=0$), pure quadrupole ($J_1=1$) and mixed dipole-quadrupole ($J_1=2, 3$). Using the obvious notation WJ_1J_20 we obtain:[4]

$$W_{030}=1+111\cos^2\theta-305\cos^4\theta+225\cos^6\theta,$$
$$W_{130}=1+(47/54)\cos^2\theta-(15/27)\cos^4\theta,$$
$$W_{230}=2|\alpha|^2(23-9\cos^2\theta)+5|\beta|^2(8-3\cos^2\theta+5\cos^4\theta)+6(30)^{\frac{1}{2}}R(1-3\cos^2\theta),$$
$$W_{330}=16|\alpha|^2(13+9\cos^2\theta)+(48/9)|\beta|^2(51+3\cos^2\theta-20\cos^4\theta)+96R(1-3\cos^2\theta).$$

None of these functions fits the facts; for instance, none of them has a $\cos^4\theta$-term whose coefficient is or can be made positive and of order of twice the constant term.

Higher values of J_1 ($J_1=4, 5, 6$, with $J_2=2, 3$) were also tried, with the same result.

It is possible however to account for $W(\theta)$ in a very simple manner if we are willing to suppose that one of the excited levels of Pd^{106} consists in fact of two levels with different spins but sufficiently close together in energy not to have been resolved. $W(\theta)$ is then a superposition of two correlation functions sharing a common value of J_1 (or J_2).

One at least of these two functions must have a $\cos^4\theta$-term whose coefficient is positive and twice the constant term. Of all the functions with $J_2=2, 3$, and $J_1=0$ to 4, only W_{020} satisfies this condition. The second function cannot then have $J_1=0$ also, since this would forbid completely the observed crossover transition γ_2; we are left with functions of the form WJ_120, the upper excited level being the one that is in fact two levels, with spins $J_1=0$ and $J_1'=1, 2, 3$, respectively (see Fig. 1).

Assuming for a start that γ_1' is a pure dipole, and taking $J_1'=1$, we have

$$W(\theta)=AW_{020}+BW_{120}$$
$$=A5/4(1-3\cos^2\theta+4\cos^4\theta)+B3/8(3-\cos^2\theta),$$

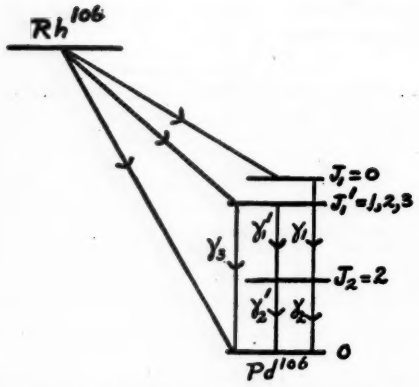

FIG. 1. Proposed level scheme of Pd^{106}.

where B/A = intensity of γ_1'/intensity of γ_1, and the constants 5/4, 3/8 are for normalization of the respective correlation functions.

If we choose B/A to give correctly the observed coefficient of $\cos^2\theta$, we obtain $B/A=1.12$, and $W(\theta)=1-1.66\cos^2\theta+2.0\cos^4\theta$. Similarly $J_1'=2$ yields, for $B/A=0.91$, $W(\theta)=1-1.66+2.4\cos^4\theta$, while $J_1'=3$ yields, for $B/A=1.04$, $W(\theta)=1-1.66\cos^2\theta+2.15\cos^4\theta$.

Thus all three assumptions $J_1'=1, 2, 3$ enable the observed $W(\theta)$ to be accounted for, with γ_1' a pure dipole. *A fortiori*, the same holds if γ_1' is a dipole-quadrupole mixture; i.e., if we are free to adjust the parameters $|\alpha|^2$, etc., as well as B/A.

Higher values of J_1' may also be consistent with the observed $W(\theta)$, though these are less likely for other reasons.[5]

Parities of the levels.—If, as Peacock's considerations of β-decay[5] suggest, the upper excited levels have the same parity as the ground state, then the measured correlation between direction of emission and polarization of γ_1 and γ_2[6] requires that the intermediate level have the same parity as the others. On Hamilton's theory[7] the proposed scheme of Fig. 1 then gives the same theoretical curve as that calculated in reference 6 for two successive electric quadrupoles; opposite parity would give the reciprocal of this curve.

The scheme of Fig. 1 is, of course, purely tentative unless the doubling of the upper excited level can be confirmed by further experiments.

[1] E. L. Brady and M. Deutsch, Phys. Rev. **72**, 870 (1947); **74**, 1541 (1948).
[2] D. S. Ling and D. L. Falkoff, Phys. Rev. **76**, 431 (1949); **76**, 1639 (1949).
[3] J. A. Spiers (to be published).
[4] For the meaning of $|\alpha|^2$, $|\beta|^2$ and R see reference 2.
[5] W. C. Peacock, Phys. Rev. **72**, 1049 (1947).
[6] M. Deutsch and F. Metzger, Phys. Rev. **74**, 1542 (1948).
[7] D. R. Hamilton, Phys. Rev. **74**, 782 (1948).

Neutron Production in Various Substances by 50-Mev X-Rays

G. C. BALDWIN AND F. R. ELDER
Research Laboratory, General Electric Company, Schenectady, New York
January 30, 1950

MEASUREMENTS of rates of production of neutrons by 22-Mev x-rays in various materials have been reported by Price and Kerst.[1] The present measurements were made by an essentially identical technique. Fast photo-neutrons emitted at 90° were detected after moderation by the 44-sec. Rh^{103} activity. The moderator, a 6-in. cube of paraffin, was surrounded on all sides by a cadmium-lined paraffin shield 8 in. thick; a 3-in. cadmium-lined hole in the shield allowed neutrons from a sample placed in the x-ray beam from a 50-Mev biased betatron[2] to enter the detector. An aperture in a lead shielding wall defined a beam 8.3 cm in diameter at the sample position, 3 m from the target. As the detector was 1 m from the beam axis no photo-neutrons were generated in the detector or shield and it was found unnecessary to enclose the entire betatron in a neutron shield. Whenever possible samples were shaped so as to utilize the entire beam. Liquid samples were held in a 350-cm^3 aluminum container. Samples were exposed for 3 min. and counted from 44 to 220 sec after irradiation. An R Thimble in a 1/8-in. lead intensifier on the beam axis at 4.69 m was used in conjunction with a monitoring rhodium foil placed close to the betatron to determine the exposure, transmission and absorption of radiation by the sample. All readings were corrected for background measured without sample.

Absolute neutron yields were computed from these data after a calibration exposure with a 200-mC Ra-α-Be source at the sample position. Computation of k, the neutron yield per mole per unit beam intensity ($1r$ measured in 1/8-in. of lead) included allowance for attenuation of the radiation in the thick samples. Neutron yields are given in Fig. 1. For 50-Mev x-rays they can be fitted closely by the relation $k=1860Z^2$ neutrons per mole r.

Several points shown in Fig. 1 taken at 22 Mev to check the relation $k=50Z^3$ found by Price and Kerst,[1] can be fitted by $k=(25\pm5)Z^3$. The coefficient in the Illinois data is reduced from 50 to 28 when corrected for the ratio, 1.75, on intensification by lead and Bakelite.[3] The agreement is good.

Relative yields of (γ, n) reactions at 50 Mev, determined by Perlman and Friedlander,[4] show the same trend as the present data although individual yields vary more widely from the Z^3 relation.

It is noteworthy that for lead the yields at 50 and at 22 Mev are equal; it is to be presumed from this that the neutron-generating processes in lead are induced mainly by quanta below 22 Mev. Values of k for copper were determined at a series of x-ray energies.

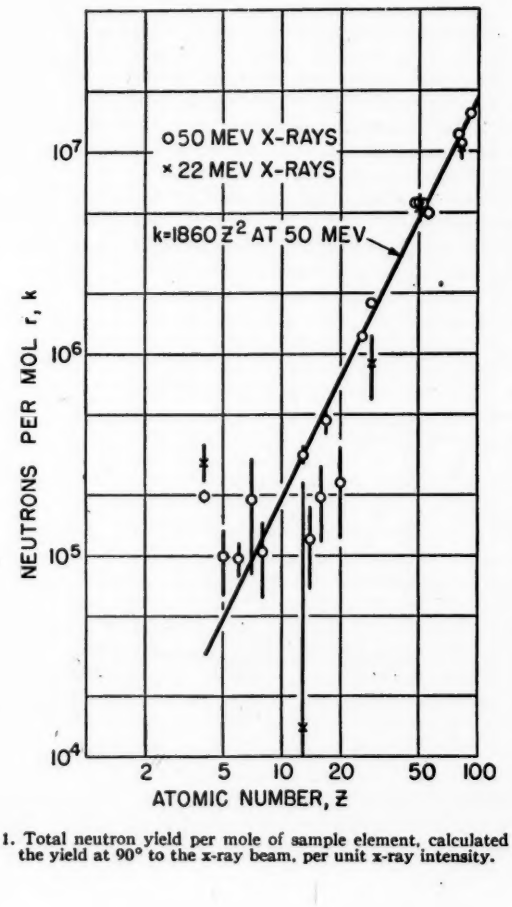

FIG. 1. Total neutron yield per mole of sample element, calculated from the yield at 90° to the x-ray beam, per unit x-ray intensity.

The resulting yield curve resembles the $Cu^{63}(\gamma, n)$ yield curve[5] up to the latter's maximum at 25 Mev, beyond which the former continues to rise to a maximum at 40 Mev. Above 40 Mev, k slowly decreases in the same manner as the (γ, n) yield, indicating that relatively few neutrons are generated by quanta above this energy.

The k-values in Fig. 1 are related to cross sections for photoneutron production, σ_n, by the formula

$$k = N \int_0^{50} \sigma_n(E)\phi(E)dE$$

where N is Avogadro's number and ϕ is the flux of quanta per r. This has been calculated[5] for 50-Mev x-rays to be $3.5\times10^7/E$. The carbon data give $\int \sigma_n dE = 1.4\pm0.3\times10^{-25}$ cm² Mev. As this is the value obtained by Lawson and Perlman for the (γ, n) cross section,[6] either no neutron-producing multiple disintegrations occur in carbon or this value of $\phi(E)$ is low.[7]

Measurements of the total cross section of graphite for neutrons detected by the rhodium-moderator combination employed indicate that the average energy of neutrons from carbon is nearly that of Ra-α-Be neutrons, and is appreciably higher than that of neutrons from lead.

[1] G. A. Price and D. W. Kerst, Phys. Rev. **76**, 182A (1949).
[2] W. F. Westendorp, Phys. Rev. **71**, 271 (1947).
[3] Quastler *et al.*, Am. J. Roentgenology Rad. Therapy **61**, 591 (1949).
[4] M. L. Perlman and G. Friedlander, Phys. Rev. **74**, 442 (1948).
[5] G. C. Baldwin and G. S. Klaiber, Phys. Rev. **73**, 1156 (1948).
[6] J. L. Lawson and M. L. Perlman, Phys. Rev. **74**, 1190 (1948).
[7] Recent measurements in this laboratory indicate that this value of ϕ may be low by a factor of three. (E. R. Gaerttner and M. L. Yeater, private communication.)

Neutron Binding Energies in Pb^{207}, Pb^{208} and in Bi^{210}

B. B. Kinsey, G. A. Bartholomew, and W. H. Walker
Division of Atomic Energy, National Research Council of Canada, Chalk River, Ontario, Canada
February 20, 1950

THE energies of the gamma-rays arising from neutron capture in Pb^{206}, Pb^{207} and Bi^{209} have been measured with the aid of a coincidence pair spectrometer. The technique of energy measurement has been described briefly in an earlier letter.[1] The coincidence spectra obtained by using lead oxide in an aluminum container and pure metallic lead are shown in Fig. 1. The capturing isotope is indicated for each radiation. The energy of the radiation is obtained by adding about 25 kev to the energy found by extrapolating the high energy slope to zero. With metallic bismuth a single weak but unusually broad coincidence peak was found. The energies are: (a) from lead, 6.68 ± 0.04 Mev and 7.37 ± 0.02 Mev; (b) from bismuth, 4.170 ± 0.015 Mev.

Since the energy set free in the capture of a neutron by a nucleus with even charge and even mass number is always less than that produced by an adjacent even-odd type, the binding energy released by capture in Pb^{206} will be less than that released by capture in Pb^{207}. This suggests that the 6.68 Mev γ-ray arises from capture in Pb^{206}. Further, its energy is in good agreement with the threshold energy of the (γ, n) reaction,[2] *viz.*, 6.85 ± 0.20 Mev. The 7.37 Mev radiation therefore must originate in capture in Pb^{207}. Since the first excited state of Pb^{208} lies at the unusually high level of 2.62 Mev, the 7.37 Mev radiation must be due to the direct transition to the ground state and its energy is equal to the binding energy.

As pointed out by K. Way,[3] the binding energy of a neutron in Pb^{209} is probably much lower than in the other isotopes of lead. A radiation with this energy could not be detected by the present method because of the low neutron capture cross section of Pb^{208} and because of the reduced sensitivity of the spectrometer at low energies. The neutron binding energy of Pb^{209} may be deduced from the present results, the energy of the decay of Pb^{209}, and the energy set free in the disintegrations by which RaD (Pb^{210}) passes to Pb^{206}. We obtain 4.81 ± 0.08 Mev for the binding energy of the neutron in Pb^{210} and 4.35 ± 0.12 Mev for that in Pb^{209}. The latter figure and the present results are in agreement with those obtained recently in a study of the (d, p) reactions in lead and bismuth.[4]

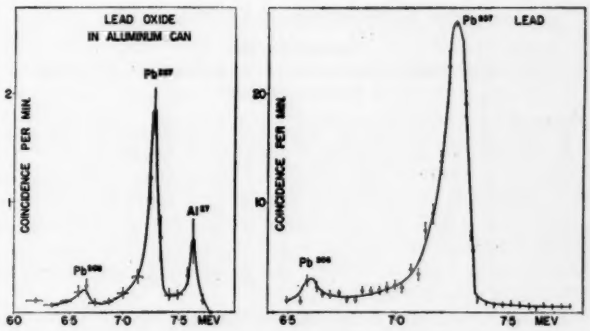

FIG. 1. Pair spectrogram of the neutron capture γ-rays produced by lead oxide and lead.

It is very surprising that no radiations of lower energy were observed in the spectrum of lead. The simplicity of the spectrum obtained is similar to that observed from the lightest elements; for example, from beryllium and carbon. No radiation was found at 4.75 Mev, which is the energy of the radiation to be expected from a transition to the 2.62 Mev level in Pb^{208}. Possibly such a radiation would be too weak to be detected unless the direct transition to the ground state was forbidden by selection rules. In the case of Pb^{208}, and possibly also of Pb^{207}, we conclude that the direct radiative transition to the ground state is allowed and that the level density in these isotopes is much less than at corresponding excitations in other heavy elements which we have studied, such as Au^{198}.

The ratio of the thermal neutron capture cross section of Pb^{207} to that of Pb^{206} can be estimated if it is assumed that only transitions to the ground state occur in significant amount. After correcting for the energy sensitivity of the pair spectrometer, we find this ratio to be about 7.

The unusual width of the bismuth peak may be due to the transitions to the low energy levels which are known to exist in Bi^{210} (RaE).

[1] Kinsey, Bartholomew, and Walker, Phys. Rev. **77**, 723 (1950).
[2] Hanson, Duffield, Knight, Diven, and Palevsky, Phys. Rev. **76**, 578 (1949).
[3] K. Way, Phys. Rev. **75**, 1448 (1949).
[4] J. A. Harvey, Bull. Am. Phys. Soc. **25**, No. 1, 41 (1950).

The Possible Existence of a Constant Third-Order Difference among the Nuclear Magic Numbers

Frank A. Valente
Physics Department, Georgetown University, Washington 7, D.C.
February 17, 1950

THERE seems to be some indication that a constant third-order difference may possibly exist among the nuclear magic numbers. If, according to the explanation afforded by the linear oscillator of the nuclear model,[1] these numbers are taken to be 14, 28, 50, 82, and 126, then the first-order differences among them are 14, 22, 32, 44; the second-order differences, 8, 10, 12; and the third-order difference is constant at a value of 2.

On the assumption that this constant value of the third-order difference is a fundamental fact, the magic number, M, is computable from the readily derivable expression $M=(N^3+5N)/3$ in which N assumes the integer values 1, 2, 3, 4, 5, 6, 7, 8, etc. Then, according to this rule, the magic numbers should be 2, 6, 14, 28, 50, 82, 126, 184, etc.; 8 and 20 are notably absent. The terminal point of the series occurs, of course, at the magic number beyond which all others are proven or known to be physically impossible.

[1] Haxel, Jensen, and Suess, Phys. Rev. **75**, 1766 (1949).

The Interaction of Pi-Mesons*

ORESTE PICCIONI
Brookhaven National Laboratory, Upton, Long Island, New York
February 20, 1950

THE identification of pi-mesons as at least a principal component of the secondary particles of a hard shower[1] encouraged a tentative experiment[2] on the nuclear interaction of those particles. The results showed, in my interpretation, a very small cross section for the nuclear absorption of pi-mesons in flight. This absorption process was thought to be of the same type as a pi-minus star with a larger energy involved, where particles other than mesons would be emitted.

Greisen,[3] discussing in general the present evidence on nuclear interactions of pi-mesons, suggests for the experiments of reference 2 a different interpretation from that which I gave. Greisen's points are: (1) pi-mesons may have interactions not leading to the disappearance of the meson, but involving a loss of only a part of the meson energy; (2) such "nuclear losses" may increase the probability of recording a delayed coincidence, with respect to the case in which only ionization losses are present; (3) Experiment III of reference 2 shows that a large fraction of the delayed coincidences is due to mesons produced very near to the point where they stop inside the iron.

My experiment would indeed not give any evidence for a process in which the meson does not disappear.

In reference 2, I already wrote that scattering could not practically affect my results. The only process which could have had a significant effect on these results is the complete nuclear absorption of pi-mesons *before* the end of their range.

On the other hand, even if we assume that nuclear losses, accompanied or not by a measurable scattering, are important, my interpretation of Experiment IV of reference 2 would still be correct. Nuclear losses would just increase *both* the number of *HS* delayed coincidences and of the stopped mesons. The conclusion that every *positive* meson stopped generates a decay electron would not be changed.

The meson production inside the iron deserves some further remarks. Experiment III, on which Greisen bases his computation, gave only eleven counts. In addition, these have to be corrected because of the inefficiency of the anticoincidence tray D and for the casuals. This gives 10 ± 6 percent instead of 18 ± 5 percent for mesons which might be produced in the lower layer of the absorber. Further, the average number of four ionizing particles quoted by Greisen does not apply to the counter assembly used in this experiment. The correct number is definitely smaller.

If a large fraction of mesons were produced inside the iron by nucleons, the flux of ionizing particles A_2BC should be much larger than is observed and should be mainly composed of protons, which is against the evidence of Experiment I.

Indeed, Berkeley experiments[4] show that the cross section σ_π for meson production by nucleons bombarding an element like iron is less than 10^{-27} cm^2 for a nucleonic energy of around 350 Mev. Above that energy the cross section is supposed to increase, although not very rapidly.[5] If we assume that at an energy of 1 Bev σ_π is still less than the geometrical cross section, we see that for each meson produced in the iron we are bound to have several neutrons of more than 1 Bev entering the iron. At such an energy, the evidence from photographic plates shows that the protons are about as frequent as neutrons.[6] Now the spectrum of protons at the level of tray C, some 16 inches of lead from the top of the apparatus, cannot be made up of only high energy protons. Indeed, there is no reason to think that such a spectrum is richer on the high energy side than the spectrum of protons in the atmosphere, such as can be deduced from the experiments of Anderson.[7] In this way one concludes that for each pi-meson created inside the iron by the nucleonic cascade, much more than ten protons should cross the tray C. Actually the tray C is crossed only by less than five ionizing particles for each meson stopped in the iron, and certainly not all of them are protons.

The situation is different if we assume that even at energies of a few hundred Mev mesons may easily multiply. One meson producing another meson inside the iron, so that two mesons would appear, either emerging from or being stopped in the iron, would balance for one nuclear absorption.

If actually the meson multiplication has a large cross section even at low energies, one is surprised that it has not been noticed in the cloud-chamber experiments of Fretter and others.[8-10] On the contrary, it has been found that in the large majority the interactions have the same appearance of the nucleon-produced stars of low energy. For such events of low energy, the most frequent "stars," no transition effect was observed in photographic emulsion.[11] Finding 200 g/cm^2 as the absorption length in ice, Harding, Lattimore, and Perkins[12] interpret the result as an indication that stars *are not* produced by unstable particles.

As a conclusion we think that further experiments are certainly needed before considering as "established" any statement on the nuclear interaction of pi-mesons. At the present time we do not see that the nucleonic cascade can furnish the explanation of our results under the assumption of a large cross section for nuclear absorption of pi-mesons. If a cascade is going to reconcile our results with, say, a geometrical cross section for nuclear absorption, it seems, on the basis of the present experimental information, that the cascade has to be made up of pi-mesons almost exclusively. Such a process is bound to be observed experimentally, for instance, for the lack of neutral particles participating to the development of the cascade.

Experiments in this line are already on the point of being performed by Dr. R. L. Cool and the writer.

* Work done at Brookhaven National Laboratory under the auspices of the AEC.
[1] O. Piccioni, Phys. Rev. **77**, 1 (1950).
[2] O. Piccioni, Phys. Rev. **77**, 6 (1950).
[3] K. Greisen, Phys. Rev. **77**, 713 (1950). I am indebted to Dr. Greisen for sending me his manuscript.
[4] Kindly communicated by H. Bradner.
[5] H. Bethe and B. Rossi, Echo Lake Conference (June, 1949).
[6] Brown, Camerini, Fowler, Heitler, King, and Powell, Phil. Mag. **40**, 862 (1949).
[7] Adams, Anderson, Lloyd, Rau, and Saxena, Rev. Mod. Phys. **20**, 334 (1948).
[8] W. B. Fretter, Phys. Rev. **76**, 511 (1949).
[9] Lovati, Mura, Salvini, and Tagliaferri, Phys. Rev. **77**, 284 (1950).
[10] W. W. Brown and A. S. McKay, Phys. Rev. **77**, 342 (1950). The authors give an erroneous condition for the nuclear absorption to be detected by my apparatus.
[11] Harding and Perkins, Nature **164**, 285 (1949).
[12] Harding, Lattimore, and Perkins, Nature **163**, 319 (1949).

Photo-Alpha-Reactions in Oxygen and Nitrogen

C. H. MILLAR AND A. G. W. CAMERON
Atomic Energy Project, National Research Council of Canada, Chalk River, Ontario, Canada
February 23, 1950

IN an experiment searching for new photo-nuclear reactions involving the emission of heavy particles ($Z\geq2$), an Ilford E1 emulsion, 100 microns thick, was exposed to 200 roentgens of γ-radiation from the 24-Mev betatron at the University of Saskatchewan. The plate was enclosed in cadmium at the middle of a cubic foot of paraffin to eliminate reactions caused by photoneutrons. The γ-ray beam was filtered through 20 cm of aluminum to reduce low energy radiation. A modified Van der Grinten "grain-gradation" development[1] of the plate minimized γ-ray fogging, suppressed proton tracks, and made α-particle tracks distinguishable from those of heavier particles.

The principal types of events found in 2 cm^2 of this plate included about 200 measurable three-pronged α-particle stars from the photo-disintegration of C^{12} via the 3 Mev excited level[2] of Be^8, 25 measurable four-pronged α-particle stars from the break up[3] of O^{16}, and 1010 single α-particle tracks attributed to photo-alpha-reactions in the Ag and Br of the emulsion.

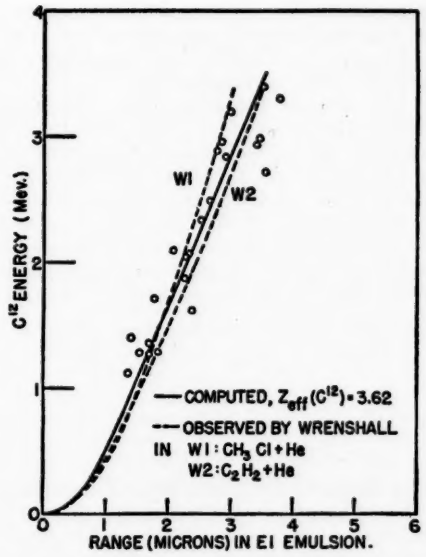

FIG. 1. Range-energy relationship for C^{12} ions in E1 emulsion. Experimental points show $E_r(\alpha)$ *vs.* range. Solid curve shows $E_r(R)$ *vs.* range for $Z_{eff}(C^{12})=3.62$.

A few α-particle tracks having a short, heavy stub at the origin were attributed to photo-alpha-reactions in light nuclei, in which the recoil fragment had small charge and sufficient energy to leave a measurable track. The only elements of this kind present in the emulsion are carbon, nitrogen, and oxygen; since carbon normally disintegrates into a three-pronged α-particle star, it was suspected that these events might be due to the reactions $N^{14}(\gamma, \alpha)B^{10}$ and $O^{16}(\gamma, \alpha)C^{12}$. These assignments were confirmed by the following analysis.

The energy of each recoil fragment, $E_r(\alpha)$, was calculated from the momenta and energies of its associated α-particle and γ-ray on the assumptions that it was either (1) B^{10} or (2) C^{12}. On these same assumptions it was also possible to calculate two values for the energy of the recoil nucleus, $E_r(R)$, from the functional form of the general range-energy relationship: $E/M=f(Z_{eff}^2R/M)$, by making use of the known range-energy relationship for α-particles for which a value $Z_{eff}=2$ was used. For the recoil fragment, Z_{eff}, the ionic charge, is less than the nuclear charge since at low energies not all the atomic electrons are stripped from their orbits;[4] and it will vary from point to point along the track. However, by applying this method of analysis to the experimental range-energy points for light nuclei used in Knipp and Teller's paper,[4] we are convinced that over the limited range of energy in our experiment a constant value of Z_{eff} for the recoil nuclei is a satisfactory approximation in each case. A preliminary study of our data indicated that a value of $Z_{eff}=0.6Z$ was sufficiently accurate to identify the reactions.

For each event the recoil energies as calculated by the above two methods were compared and in most cases it was found that $|E_r(\alpha)-E_r(R)|$ was less than 0.5 Mev on one assumption as to the identity of the recoil nucleus which served to identify the reaction, and was considerably greater for the alternative assumption. In this manner, of the 32 events studied, 23 were identified as the $O^{16}(\gamma, \alpha)C^{12}$ reaction and 8 as the $N^{14}(\gamma, \alpha)B^{10}$ reaction. One event, which disagreed with both of the above assumed reactions, agreed with the assumption that it was the photo-disintegration of C^{12} via the ground state of Be^8.

Figure 1 shows the range-energy relationship for C^{12} ions in E1 emulsion thus obtained. From the individual points a mean $Z_{eff}(C^{12})=3.62$ was calculated, and the solid line is the curve obtained from the functional equation using this value. Wrenshall[5] studied recoiling C^{12} ions in two gas mixtures and reduced the range-energy relationships thus found to standard air. By applying to these de Carvalho's stopping power formula,[6] reduced in range by 3 percent to convert from C2 to E1 emulsions, the curves $W1$ and $W2$ were obtained. The agreement with our data is satisfactory.

Figure 2 shows the range-energy relationship for B^{10} ions obtained in the same way with $Z_{eff}(B^{10})=2.94$ giving the best fit.

We should like to thank Dr. R. N. H. Haslam and his coworkers at the University of Saskatchewan for making the betatron irradiations, Dr. B. W. Sargent for his interest and advice on the experiment, and Mr. R. G. Hayman for his assistance in searching the plates.

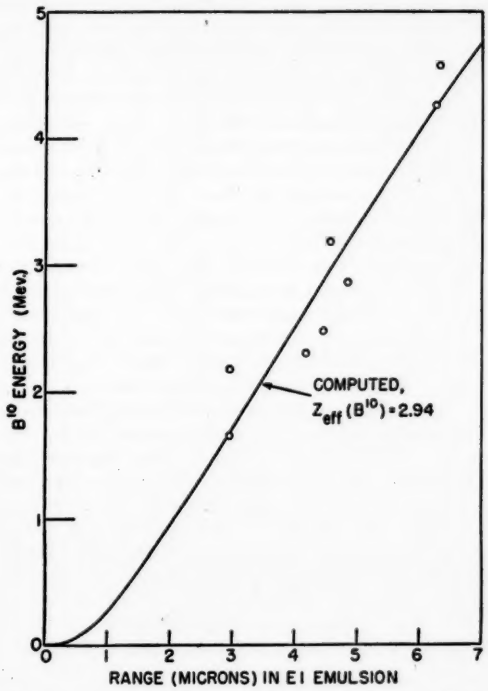

FIG. 2. Range-energy relationship for B^{10} ions in E1 emulsion. Experimental points show $E_r(\alpha)$ *vs.* range. Solid curve shows $E_r(R)$ *vs.* range for $Z_{eff}(B^{10})=2.94$.

[1] H. Yagoda, *Radioactive Measurements with Nuclear Emulsions* (John Wiley and Sons, Inc., New York, 1949), p. 62.
[2] Hänni, Telegdi, and Zünti, Helv. Phys. Acta **21**, 203 (1948).
[3] Goward, Titterton, and Wilkins, Proc. Phys. Soc. (London) **A62**, 460 (1949).
[4] J. K. Knipp and E. Teller, Phys. Rev. **59**, 659 (1941).
[5] G. A. Wrenshall, Phys. Rev. **57**, 1095 (1940).
[6] H. G. de Carvalho, Phys. Rev. **76**, 1729 (1949).

The Raman Spectrum of Bromine

H. STAMMREICH
Department of Physics, University of São Paulo, São Paulo, Brazil
January 23, 1950

IN collaboration with Oswaldo Sala we have developed recently an experimental technique for obtaining Raman spectra excited by He 5875.6A. Details concerning the construction of intense He-lamps and a luminous Raman arrangement will be given elsewhere.

With this arrangement we have attempted to measure the Raman spectrum of gaseous bromine using a 50-cm long Raman tube; the first 10 cm were illuminated by the exciting radiation. The tube contained pure Br_2; the pressure was about 900 mm at

85°C. We employed a Lane-Wells three-prism Raman spectrograph with a reciprocal dispersion of 63A/mm in the region of the exciting line.

Most unexpectedly we obtained by an exposure of 15 hours not only the fundamental Raman frequency, but also the shifts corresponding to the first and second overtones with comparable intensity. The reproduction shown in Fig. 1 is an enlargement of the original spectrum.

The frequencies and relative intensities of the Raman shifts are given in Table I.

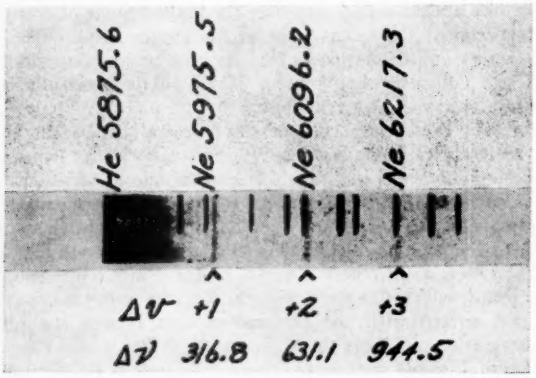

FIG. 1. Raman spectrum of bromine.

From observations on band spectra[1] we have $w_e=323.86$ cm^{-1} and $w_ex_e=1.15$ cm^{-1}. From these data we should expect in first approximation a fundamental Raman frequency of 320.4 cm^{-1} as compared with the observed value of 316.8 cm^{-1}. This difference is 3 or 4 times larger than our measuring error. On the other hand, the small anharmonicity of the three observed frequencies agrees very satisfactorily with the above value of w_ex_e and confirms our value.

From 316.8 cm^{-1} we calculate for the molecule Br^{79}-Br^{81} the uncorrected force constant

$$f=2.35\times10^5 \text{ dynes/cm.}$$

The appearance of the intense overtones is the more surprising when one considers that of all Raman-investigated diatomic molecules the Br_2 molecule approximates best to the simple model of the harmonic oscillator. It seems that even first overtones have never been observed in the Raman spectra of diatomic molecules; in polyatomic molecules they appear in rare cases very weakly. Their intensities compare with the intensities of the fundamental frequencies roughly as the square of the ratio of nuclear distance to displacement. Applying this general rule we should expect in the case of bromine an intensity ratio of nearly $10^6:10^3:1$ between the fundamental frequency and the first and second overtones.

The relative intensities given above were measured by comparing the density of the lines with intensity marks. They do not represent the true intensity ratio. Reabsorption of the scattered radiation in the bromine gas weakens the fundamental frequency; on the other hand, the spectral sensitivity of the photographic plate employed is somewhat lower in the region of the second overtone. In any case, the true intensities are not very far from those indicated.

TABLE I. Raman lines of bromine.

$\Delta\nu$	$\Delta\nu$(cm^{-1})	Rel. int.
+1	316.8	1
+2	631.1	0.85
+3	944.5	0.47

There is no doubt that we have here true overtones corresponding to transitions $\nu=+2$, $+3$, and not a case of multiple scattering. This results obviously from the relative intensities and also from the observed anharmonicity.

We hope to investigate with a spectrograph of greater dispersion and resolving power the finer vibrational details of the observed frequencies. Besides the isotope effect, we have to expect a structure coming from the participation of the different initial vibrational states. For our temperature conditions the statistical weights of the fundamental and of the first and second excited vibrational states correspond approximately to the ratio 100:45:13. Unfortunately, the absorption of shorter wave-lengths in the bromine gas prohibits the observation of anti-Stokes shifts.

[1] H. Sponer, *Molekülspektren I* (Tabellen, Berlin, 1935).

Decay Time of Stilbene Scintillations as a Function of Temperature

R. F. POST AND N. S. SHIREN
Stanford University, Stanford University, California
February 23, 1950

USING 931-A photo-multipliers and a pulsed-counter technique described in the accompanying letter we have photographed scintillation pulses from trans-stilbene and have used these to obtain decay time data at isolated temperatures down to that of liquid nitrogen. The observed pulse rise times were about 10^{-9} second. Since this time is considerably shorter than the measured decay times, the data were analyzed simply by comparison of the photographed pulses (smoothed by tracing) with plotted exponentials. The trans-stilbene was used in crystalline form, and was of high purity. In an attempt to obtain a rough comparison with the work of Kelley and Goodrich[1] we have also analyzed a few counts from a crystal of anthracene of unknown purity, at the same temperatures at which the stilbene data were taken. Our value for the decay constant of anthracene at liquid nitrogen temperature agrees with theirs and also with the value obtained by Collins.[2] However, at the higher temperatures our values are noticeably lower than those found by Kelley and Goodrich. The explanation of the discrepancy is not known, but it should be noted that the anthracene pulses consistently showed a very ragged structure at room temperature, making the drawing of the exponentials a matter of individual judgment. The stilbene data, on the other hand, were satisfactorily smooth at all of the temperatures. Our results for stilbene and anthracene are given in Table I, together with their r.m.s. deviations from the mean.

In the experimental set-up, the last 2 dynodes of the photomultiplier were bypassed with 0.0005 microfarad condensers to prevent dynode voltage variations. Further voltage stabilization during the pulses was achieved by using 100-ohm resistors in the dynode divider network, connected by fairly short leads to the tube socket. Two different tubes were used in obtaining the stilbene data, and no appreciable differences were noted in the data obtained from either at the same temperature. No saturation effects were noted in the performance of the photo-multipliers at even the highest scintillation pulse amplitudes. Because of the rapid rise time of the count pulse, delivered from a low impedance source (a terminated 100-ohm coaxial lead) directly to the plates of the oscilloscope tube, it was necessary to use a 100-ohm damping resistor in series with the connection from the coax center con-

TABLE I. Decay time (to $1/e$) in microseconds.

Temp.	−196°C	−78°	27°
Trans-Stilbene	0.0044 ±0.0005	0.0049 ±0.0006	0.006 ±0.001
Anthracene	0.010 ±0.002	0.018 ±0.002	0.023 ±0.005

ductor to the deflecting plate. This damped the shock-excited oscillations of the series resonant circuit comprised of the inductance of internal leads to the deflection plates plus the deflection plate capacity. The RC time constant of this network was then approximately 6×10^{-10} second.

[1] C. G. Kelley and M. Goodrich, Phys. Rev. 77, 138 (1950).
[2] G. B. Collins, Phys. Rev. 74, 1543 (1948).

Performance of Pulsed Photo-Multiplier Scintillation Counters*

R. F. Post and N. S. Shiren
Stanford University, Stanford University, California
February 23, 1950

In an attempt to develop higher speed counting equipment for use with the Stanford linear accelerators, we have applied pulse methods to the operation of scintillation counters with the following results. We have pulsed several 931-A photo-multipliers to voltages as high as 5 kv, without voltage breakdown. Pulse lengths up to 2.5 microseconds have been used, the upper limit being set by the pulser. Using an Ag_{110} gamma-source, we have observed stilbene scintillation counts with a rise time of about 10^{-9} second, and with a maximum height of about 80 volts. The pulses were delivered from the photo-multiplier into 100-ohm RG7U coaxial cable, terminated at its output end. They were displayed by a 5RP11A high voltage cathode-ray tube with no intermediate amplification. The observed rise-times are probably made appreciably longer by transit time and lead inductance effects within the oscilloscope tube.

Not all of the tubes tried withstood the highest pulse voltages, but those that did gave infrequent and small noise counts. There did not seem to be any consistent correlation between excellence of performance at low d.c. voltages and that under high voltage pulse operation. The single 1P21 tube which was tried, though satisfactory at the usual d.c. voltages, happened to be inferior to any of the several 931A tubes tried, from the standpoint of voltage breakdown and noise. However, this tube may not have been representative. A tendency for noise count rates to increase near the end of the longer pulses was noted for all tubes. This suggests that pulsed operation greatly reduces the incidence of that part of the noise due to accumulative ionization effects in the multiplier. It was also found that the use of an external shield, pulsed to the cathode potential strikingly reduced the noise counts.

From an analysis of photographs of individual counts, and by the use of very short delay line clippers, we have established that the rise time of a typical scintillation pulse is 10^{-9} second or less, and that the total duration of single-electron noise pulses is about 5×10^{-10} second, in rough agreement with the value calculated by Sard.[1] At the high voltages employed, effects due to transit time variations should be reduced by more than a factor of two. In addition to the effects of the oscilloscope characteristics on the measured value of pulse lengths, it is probable that the noise pulses are somewhat lengthened by the effect of lead inductances in the photo-multiplier tube itself, since, from Sard's calculation one would expect to find noise pulse durations of about 2×10^{-10} sec. at these voltages. High voltage operation improves the focusing properties of the photo-multiplier,[2] and increases the current output at which space charge effects become important. This latter fact is borne out by the experimental results. At 5 kv, no saturation effects have been observed, even for output currents approaching one ampere. From the height of the single-electron noise pulses observed, we estimate that the current gain of an average tube is about 10^9 with no saturation up to the highest scintillation pulses observed.

Our pulsing circuit was designed to deliver square pulses of extremely uniform amplitude. However, at the highest pulse voltages used, pulse regulation is less important, since these voltages per stage are near those corresponding to the maximum of the secondary emission multiplication curve. Although we have not tried pulsing at extreme repetition rates, the evidence to date suggests that this would be entirely feasible, especially if d.c. clearing fields were applied to the tube during the time between the pulses.

The pulsed scintillation counter could be used in the investigation of extremely short-lived isomeric states. We are preparing to carry out experiments of this kind, as a test of the method, by photographing the parent and delayed events as presented on a fast oscilloscope sweep. Beta- and gamma-events will be distinguished by the use of two counters, each connected to a single deflection plate. By placing selective absorbers in front of one of the counters, the gamma-events can be identified from their sense on the oscilloscope trace.

We have also applied the method to the measurement of phosphor decay times, with the results quoted in the accompanying letter. A paper describing the method in more detail, as applied to fast counting and coincidence work, is in preparation.

* The accelerator program is supported by ONR Contract N6onr-25116.
[1] R. D. Sard, J. App. Phys. 17, 768 (1946).
[2] G. A. Morton, RCA Rev. 10, 525 (1949).

Terphenyl and Dibenzyl Scintillation Counters

R. Hofstadter
Palmer Physical Laboratory, Princeton University, Princeton, New Jersey
and
S. H. Liebson and J. O. Elliot
Naval Research Laboratory, Washington, D. C.
February 23, 1950

Terphenyl (*p*-diphenylbenzene) and dibenzyl[1] (diphenylethane) crystals appear to be two useful additions to the class of aromatic materials used in scintillation counters. Some of the properties of these materials have been determined and are given in Table I, where anthracene and stilbene are listed for comparison. Each of the new materials forms excellent crystals from the melt. Dibenzyl crystals are remarkably clear although they sometimes crack when taken from the mold. On the other hand terphenyl crystals are rugged and appear to be among the most durable of presently known organic scintillators. We have not yet succeeded in growing colorless terphenyl crystals, the present ones being slightly yellow but clear. It is probable that removal of the impurity producing the yellow coloration will increase the pulse height. The speed, good handling characteristics, and pulse height of terphenyl recommends its use in certain applications of scintillation counters. Dibenzyl has been obtained from the Matheson Company and (yellow) terphenyl from the Eastman Kodak Company.

Table I. Properties of scintillation counters.

	Decay constant (±10 percent)	Relative efficiency	Spectrum	Melting point °C
Anthracene	3.4×10^{-8} sec.	1.00	4450A	217
Stilbene	1.2×10^{-8} sec.	0.60±0.10	4080 4200	124
Terphenyl—Sample A	1.0×10^{-8} sec.	0.65±0.10	3900	213
Sample B	1.2×10^{-8} sec.		4050 4300	
Dibenzyl—Sample A	1.5×10^{-8} sec.	0.60±0.10	3520	52.5
Sample B	1.7×10^{-8} sec.		3710 3950 weak	

This work was partially supported by the U. S. Army Signal Corps and ONR.

[1] Previously investigated by W. S. Koski and C. C. Thomas (Phys. Rev. 76, 308 (1949)), who found that this material gave pulses only slightly over background and much poorer than stilbene.

Proceedings of the American Physical Society

MINUTES OF THE MEETING AT STANFORD UNIVERSITY, CALIFORNIA, DECEMBER 29 AND 30, 1949

THE 296th meeting of the American Physical Society was held at Stanford University on December 29 and 30, 1949. About 200 members of the Society registered. Two post-deadline papers were accepted. The first one was a striking 16-mm picture prepared by A. T. Oliver of the Radiation Laboratory of the University of California, Berkeley. The picture, which runs for about 15 minutes, shows tracks in photographic emulsion as seen through the microscope. The emulsion was exposed in connection with experiments using the 335-Mev synchrotron at Berkeley. The second paper was a report on "Meson Induced Fission in Uranium" by S. G. Al-Salam, also from the Radiation Laboratory at Berkeley. The invited paper A1 was not given because the speaker was unable to make the trip to the meeting. Paper C14 was read by title.

The presiding officers at the various sessions were: Dr. W. N. Arnquist of the Office of Naval Research, Professors R. T. Birge, J. Kaplan, F. Bloch, D. L. Webster, Paul Kirkpatric, and L. I. Schiff.

J. KAPLAN, *Local Secretary for the Pacific Coast*
University of California
Los Angeles, California

Invited Papers on the General Programme

Progress in Upper Air Research at N. O. T. S. C. T. ELVEY, *U. S. Naval Ordnance Test Station, Inyokern.*

The Near-Infra-Red Spectrum of the Night Sky and Aurora. A. B. MEINEL, *Lick Observatory.*

The Study of High Polymer Molecules by Light Scattering. BRUNO H. ZIMM, *University of California, Berkeley.*

The Stanford University Microwave Laboratory. MARVIN CHODOROW, *Stanford University.*

The Fine Structure of Singly Ionized Helium. MIRIAM SKINNER, *Columbia University.*

Application of Magneto-Hydrodynamics to Cosmic-Ray Physics and Geomagnetism. EDWARD TELLER, *University of Chicago.*

Contributed Papers

A4. Infra-Red Spectra of the Night Sky, Aurora and Afterglows.* JOSEPH KAPLAN, *University of California, Los Angeles.*—Meinel's recent spectroscopic studies of night sky and aurora in the infra-red made with a grating spectrograph and hypersensitized Eastman I-N plates are discussed in the light of infra-red studies of nitrogen and oxygen afterglows by Kaplan. The most significant result of this comparison is the suggestion that the atmospheric system of O_2, first observed in emission in the night sky by Meinel, and in a laboratory afterglow by Kaplan, originates below 100 km at a level where recombination of normal oxygen atoms can proceed rapidly enough to account for these bands. This is based on the high intensity of the atmospheric bands which originate on $v=0$, in both night sky and afterglow and the proposal that the remarkable enhancement of $v=0$ in the laboratory is a criterion for excitation by atomic recombination. It is also suggested that diffuse bands due to NO_2, also observed in the laboratory afterglow, will account for other unidentified radiations in the night sky between λ4000 and λ9000.

* Work done under contract with ONR.

B2. The Differential Equations of Nuclear Induction.[1] F. BLOCH AND R. K. WANGSNESS,* *Stanford University.*—The phenomenon of nuclear induction has been originally[2] described by a system of differential equations, intended to give the qualitative features of the observed signals in terms of two characteristic relaxation times. A rigorous quantum-statistical method has been devised to investigate the limits of validity of these equations. Based upon the generally valid Boltzmann equation for the density matrix, it is shown that the simpler original equations for the components of the nuclear polarization are likewise generally valid for nuclei with spin ½ and valid for higher spin if the coupling of the nucleus with the surroundings at temperature T is due to its magnetic dipole and if $H\mu \ll hT$. Other cases of the validity of these equations, as well as cases, where they are not applicable, are discussed.

[1] Work assisted by the Joint Program of the ONR and AEC.
* AEC Predoctoral Fellow.
[2] F. Bloch, Phys. Rev. 70, 460 (1946).

B3. Coincidence Studies on the Decay of Hf^{181}.* W. C. BARBER, *Stanford University.*—In spite of a considerable amount of work on the decay scheme of (Hf^{181}),[1-4] there is no general agreement as to the assignment of the excited states of the product nucleus, Ta^{181}. In the present work coincidence measurements, employing anthracene and stilbene scintillation counters, have been made on the Hf^{181} radiations in the hope of making a fairly complete description of the Ta^{181} levels. The results of these measurements to date include the following: (1) Energetic electrons ($E_0>0.25$ Mev), having the absorption properties of nuclear β-rays, are found in coincidence with hard γ-rays ($E\sim0.4$ Mev). Experiments employing delayed coincidences show these radiations to be time coincident to within 10^{-8} second, thus ruling out the decay scheme proposed by Wiedenbeck and Chu,[2] where the β-decay of Hf^{181} leads directly to the 22 μsec. metastable state first detected by DeBenedetti and McGowan.[1] (2) γ-rays of energy

approximately 0.4 Mev are found in coincidence with softer γ-rays, which by absorption appear to consist of 140-Kev γ-rays and K x-rays of Ta. The time delay between these transitions is also about 10^{-8} sec. or less.

* Assisted by the Joint Program of ONR and AEC.
[1] S. DeBenedetti and F. K. McGowan, Phys. Rev. **74**, 728 (1948).
[2] K. Y. Chu and M. L. Wiedenbeck, Phys. Rev. **75**, 226 (1949).
[3] J. Benes *et al.*, Nature **162**, 261 (1948).
[4] E. N. Jensen, Phys. Rev. **76**, 958 (1949).

B4. The Magnetic Moment of the Proton in Units of the Nuclear Magneton. C. D. JEFFRIES, *Stanford University.*—An experiment in progress to measure directly the ratio of the proton magnetic moment μ_P to the nuclear magneton μ_N is described. The method has been suggested by Alvarez and Bloch[1] and consists essentially in performing two experiments in the same homogeneous magnetic field: (1) An experiment in which the Larmor precession frequency ω_L of a spinning proton is observed; (2) an experiment in which the "cyclotron" frequency ω_C of a revolving proton is observed. Then $\mu_P/\mu_N = \omega_L/\omega_C$. The Larmor frequency is measured by the method of nuclear induction.[2] The apparatus for measuring the cyclotron frequency will be described and preliminary results will be reported.

[1] L. W. Alvarez and F. Bloch, Phys. Rev. **57**, 111 (1940).
[2] F. Bloch, Phys. Rev. **70**, 460 (1946).

B5. Chemical Analysis by Proton Scattering. S. RUBIN, *Stanford Research Institute,* AND V. K. RASMUSSEN, *California Institute of Technology.*—The dependence of the velocity of initially monoenergetic scattered protons on the mass of the scattering nucleus has been applied to the analysis of minute samples of unknown substances. The velocity spectrum of the elastically scattered protons is measured with a high resolution magnetic spectrograph, giving the identification and relative proportions of the elements in the target. Under suitable conditions, this technique can be used to detect and identify elements in surface concentrations as low as 10^{-10} g/cm^2. Much higher resolution is required to identify heavy elements than light ones. It has been calculated that the resolution of all elements should be possible, if the accelerator voltage can be regulated to one part in 12,000 for proton bombardment, or one part in 3000 for alpha-particle bombardment, with corresponding spectrograph resolution. With the available apparatus, elements up to $Z\sim30$ have been resolved. Analyses have been made of samples obtained by depositing thin layers of airborne particulate matter on beryllium and aluminum backings by means of a jet impactor, for air pollution studies. The principal advantage of such an analytical method is that it makes it possible to use spot-sampling devices even for very dilute contaminants.

B6. A Nuclear Induction Radiofrequency Spectrometer.* W. G. PROCTOR AND F. C. YU, *Stanford University.*—A nuclear induction[1] apparatus has been made into a recording spectrometer similar in principle to one developed by Pound.[2] The steady magnetic field is modulated by a small sweep while the common frequency of the receiver and transmitter is slowly changed by a clock drive. When the frequency is correct for resonance, the Fourier component of the signal at the sweep frequency is proportional to the derivative of the resonance mode being observed; if the receiver output is detected by a lock-in amplifier, this derivative is plotted by a recording d.c. milliameter. The spectrometer has been in use at Stanford for about a year and has been used to determine the magnetic moments, signs and spins of a number of isotopes. New experimental results will be given.

* Assisted by the Joint Program of the AEC and the ONR.
[1] F. Bloch, Phys. Rev. **70**, 460 (1946).
[2] R. V. Pound, Phys. Rev. **72**, 637 (1947).

B7. Design and Construction of an X-Ray Microscope. ALBERT V. BAEZ AND PAUL KIRKPATRICK, *Stanford University.*—A reflection type x-ray microscope has been constructed for use with the soft x-rays from a General Electric diffraction tube with chromium target. Glass mirrors, both uncoated and metal coated, are used. Uncoated mirrors have the better polish but smaller critical angles. Elliptical mirrors have been built up by selective metallic condensation on glass. The figure of such mirrors is good but the surface finish is inferior. The optical system consists of two mirrors set close together with their faces at right angles in a manner hitherto described. A single-stage magnification, adjustable from 50 to 100 diameters, is obtained. Air absorption is avoided by filling the microscope with helium at one atmosphere. Objects and films may be changed without important loss of time or gas. Focusing is accomplished by varying the angles of incidence while watching the images on a fluorescent screen. Performance tests are in progress.

B8. High Energy Deuteron Break-Up. L. I. SCHIFF, *Stanford University.*—It is shown that the leading term in the asymptotic expansion of the matrix element of a multipole operator between ground-state deuteron wave function ($l=0$) and plane wave for high plane wave energy depends only on a particular term in the expansion of the deuteron potential energy about the origin. If this potential has the form $MV(r)\hbar^2 = A_{-1}/r + A_0 + A_1 r + A_2 r^2 + \cdots$, and the ground-state deuteron wave function $R(r)$ is normalized to unity at the origin, then

$$\int R(r) r^l P_l(\cos\theta) e^{ikr\cos\theta} d\tau_k \to \infty \frac{4\pi i^{l+s+3}}{2^{l+1} k^{l+s+5}} \times \frac{\Gamma(s+2l+5)\Gamma(\frac{1}{2}s+2)}{(s+2)(s+3)\Gamma(\frac{1}{2}s+l+3)} A_s,$$

where s is the smallest *odd* number for which $A_s \neq 0$. This result is of interest in connection with the high energy photoeffect of the deuteron and deuteron breakup by π^--meson capture. For explicit calculations at all energies it is convenient to use a potential for which the ground-state wave function has a simple analytic form. A wide variety of such potential shapes is found by assuming a sufficiently flexible form for $R(r)$ and inverting the wave equation. These potentials can be chosen to be monotonic, with various behaviors near the origin; they fall off exponentially for large r.

B9. Nuclear Induction Apparatus for Observing Signals in Gases. M. E. PACKARD, *Stanford University.*—In order to measure nuclear relaxation times in gases, it is advantageous to observe the line structure in detail. To aid in these measurements, a nuclear induction apparatus has been developed with a signal-to-noise ratio which is adequate for observing signals from protons in gases at moderate pressures, directly on a cathode-ray oscillograph. The apparatus uses an electromagnet which has been especially shimmed to give a field which is homogeneous to within 0.02 gauss out of 10,000 gauss over the sample area. The signal is preamplified by a grounded-cathode grounded-grid type of r-f amplifier which gives a good noise figure. For quantitative measurements, the noise band width is reduced without sacrificing detail by photographically averaging the signal over many sweep cycles. The apparatus has been built with r-f circuits which can be simultaneously tuned to two frequencies so that the gyromagnetic ratios of two gases in a mixed sample can be measured in exactly the same magnetic field.

B10. Semiconductors as Low Temperature Thermometers. I. ESTERMANN, *Carnegie Institute of Technology.**—The large temperature coefficient of the resistivity of semiconductors suggests their usefulness as secondary thermometers. Above room temperature, elements containing semi-conducting oxide mixtures (thermistor thermometers)[1] are satisfactory, but

their resistance at low temperatures is too high for practical applications. Very pure elementary semiconductors, such as germanium and silicon, show a non-linear current voltage relationship at low temperatures and internal rectification.[2] A study of the resistivity of 13 germanium and 4 silicon samples with varying amounts of additions between 1.8°K and 20°K indicates that germanium samples with a resistivity of the order of 0.05 ohm-cm at room temperature are free from these undesirable properties. Below 4°K their resistivity can be expressed by an equation of the form $\rho = A \exp(\theta/T)$. Typical values of the temperature coefficient of resistance are: 0.8 percent at 70°K, 1.7 percent at 20°K, 2.5 percent at 4°K, and 16.5 percent at 2°K. Temperature measurements to 0.001°K can easily be carried out. Reproducibility after warming up to room temperature was 0.01°K, but it is expected that this figure can be reduced considerably.

* This work was carried out at the National Bureau of Standards with assistance by an O.N.R. contract.
[1] Becker, Green, and Pearson, Trans. A.I.E.E. **65**, 711 (1946).
[2] Estermann, Foner, and Zimmerman, Phys. Rev. **75**, 1631 (1949); Gerritsen, Physica **XV**, 427 (1949).

B11. The Polarization of Starlight. LEVERETT DAVIS, JR., *California Institute of Technology*.—The observed[1,2] polarization of starlight, which is associated with the reddening produced by interstellar dust, could be explained by the fact that the small dust grains, which are probably not spherical, preferentially weaken that part of the light for which the electric vector is parallel to the long axis of the grain. However, one must find some mechanism that will partially align the rapidly spinning grains. The only suitable field seems to be a galactic magnetic field, **B**. The grains should contain a few percent iron atoms and hence their a.c. susceptibility might have a significant imaginary part. Because of energy dissipation, their short axes would then tend to become parallel to **B**. The disorienting effect of the collisions of ions of mass m with the grains of mass M is assumed to have a relaxation time $\tau M/m$, where τ is the mean time between collisions. With these assumptions, a uniform field of 3×10^{-5} gauss might produce the observed polarization. Since the planes of polarization are nearly parallel for stars separated by 300 light years, **B** must be approximately homogeneous over very large regions.

[1] J. S. Hall, Science **109**, 166 (1949).
[2] W. A. Hiltner, Astrophys. J. **109**, 471 (1949).

C1. Production of Mesons by X-Rays, Part I: Experimental Method. R. STEPHEN WHITE, EDWIN M. MCMILLAN, AND JACK M. PETERSON, *University of California, Berkeley*.—A preliminary study has been made of the π^-/π^+ ratio, the energy distribution of π-mesons, and the cross section for production of π-mesons observed at angles near 90° to the beam direction. Mesons were produced by the collimated x-ray beam which traversed a 1 by 3-inch cylindrical carbon target. The mesons were detected in stacks of Ilford C-2 nuclear plates of 100 micron emulsion thickness placed azimuthally about the target behind appropriate lead absorbers. The x-ray beam was monitored by means of an ionization chamber. The maximum densities of mesons obtained were about 100 mesons per square centimeter. The exposures were limited by the single grain background. The distribution of mesons with depth in the emulsion was uniform except for 10 microns nearest each surface. The angular distribution of π-mesons was compatible with isotropic emission from a finite line source. The distribution of μ^+-mesons in angle with the beam direction was found to be isotropic. From separate plots of ρ- and σ-mesons *versus* angle to the beam direction a ratio for π^-/σ was obtained which is compatible with the value of Adelman and Jones.[1] This work was performed under the auspices of the AEC.

[1] F. L. Adelman and S. B. Jones, Phys. Rev. **A75**, 1468 (1949).

C2. Production of Mesons by X-Rays, Part II: Experimental Results. JACK. M. PETERSON, EDWIN M. MCMILLAN, AND R. STEPHEN WHITE, *University of California, Berkeley*.—The ratio of the number of negative to that of positive π-mesons produced in carbon by the x-rays from the 335-Mev electron synchrotron is not observed to have any statistically significant variation with energy in the range 30 to 150 Mev; the average value is 1.7 ± 0.2. This value is considerably different from our first published value of 10.[1] A part of this difference may be real, since the original value was found under different conditions; however, a considerable part of the difference probably comes from the less reliable technique employed earlier. An energy spectrum of mesons emitted near 90° to the x-ray beam has been measured from 20 to 150 Mev, the lower limit being set by the thickness of the carbon target. The spectrum has a maximum near 35 Mev. The integral of the spectrum leads to a total cross section of 5×10^{-28} cm² per carbon nucleus per "quantum" plus or minus a factor of two. Mesons have been observed also with the synchrotron operated at 200 Mev; the meson energy distribution extends only to about 35 Mev and the yield is considerably less than at 335 Mev. This work was sponsored by the AEC.

[1] E. M. McMillan and J. M. Peterson, Science **A109**, 438 (1949).

C3. Production of Mesons by X-Rays, Part III: Theory. KEITH A. BRUECKNER, *University of California, Berkeley*.—Calculations have been made by Feshbach[1] and Foldy[2] on the production of scalar, pseudoscalar, and vector mesons by photons. Perturbation theory in the weak coupling approximation was used and the nucleons were treated non-relativistically. The calculations have been redone including all relativistic effects and extended to the case of pseudovector mesons. The results obtained vary critically with the type of meson theory used. Comparison with the experimental results of McMillan, Peterson, and White indicates that the pseudoscalar theory gives the most acceptable predictions of angular and energy distributions and of the magnitude of the cross section. The mesons of spin one are excluded because of their strong coupling to the high energy components of the photon spectrum. The scalar meson theory gives a strongly anisotropic angular distribution in contrast with that observed. It is further found that the excess of negative over positive mesons observed is predicted by all of the theories and is due to the current carried by the nucleons. This work was sponsored by the AEC.

[1] Herman Feshbach and Melvin Lax, Phys. Rev. **76**, 134 (1949).
[2] Leslie L. Foldy, Phys. Rev. **76**, 372 (1949).

C4. Transition Curves in Lead of X-Rays, Causing Nuclear Reactions. I. Experimental. K. STRAUCH, *University of California, Berkeley*.—Polystyrene and copper foils stacked between lead absorbers were bombarded with the synchrotron x-ray beam using maximum energies of 200 and 335 Mev. The foil activities produced by the reactions $C^{12}(\gamma, n)C^{11}$ and $Cu^{63}(\gamma, n)Cu^{62}$ were measured and plotted against depth in lead. The resulting transition curves of those photons responsible for these reactions show (1) an initial drop due to photon absorption; (2) a maximum due to multiplication by the cascade process; (3) an exponential decrease. The area under these curves or "track length," determines a mean energy of photons causing these reactions. Preliminary calculations give energy values of 20 and 30 Mev for the copper and carbon reactions respectively; this is in agreement with the excitation curves measured by Baldwin and Klaiber.[1] This method is being used to measure the mean photon energies causing several reactions: $Zn^{64}(\gamma, n)Zn^{63}$, $Zn^{64}(\gamma, 2n)Zn^{62}$, $Zn^{64}(\gamma, pn)Cu^{62}$, $Al^{27}(\gamma, 2pn)Na^{24}$, $Ta^{181}(\gamma, ?)70$ minutes. Results will be presented. This work was supported by the AEC.

[1] G. C. Baldwin and G. S. Klaiber, Phys. Rev. **73**, 1156 (1948).

C5. Transition Curves in Lead of X-Rays Causing Nuclear Reactions. II. Theoretical. L. EYGES, *University of California, Berkeley.*—The transition curves obtained by Strauch can be explained quantitatively by the cascade theory of showers. This theory can be made to give a fairly accurate expression for the total area under the transition curves, i.e., the "track length" corresponding to the mean energy of the photons responsible for the reactions observed. The behavior of the transition curve at its beginning (up to about 1 radiation length) can also be calculated fairly accurately, and this behavior gives a check on the mean photon energy as determined by the track length. This work was sponsored by the AEC.

C6. Design of the Bevatron Quarter Scale Operating Model. D. C. SEWELL, W. M. BROBECK, E. O. LAWRENCE, AND E. J. LOFGREN, *University of California, Berkeley.*—The model Bevatron magnet is constructed of ½-inch thick laminations with a 13½×41-inch aperture which is centered on an 11½-foot radius. It is pulsed 20 times per minute by a 540 kw d.c. flywheel generator. The field rises to a peak of 1000 gauss in 200 milliseconds; this allows a proton energy of 6½ Mev. The magnet is divided into four quadrants which are spaced 5 feet from one another at the ends. A 0.7-Mev proton beam from a 20-inch cyclotron is deflected electrostatically into the machine at one of these straight sections. The 23-inch long r-f accelerating electrode is placed in the straight section diametrically opposite the injection point. Movable horizontal and vertical defining vanes are in the remaining two straight sections. Probes for monitoring the beam can be moved radially into the beam from the inner radius at the quadrant ends. The vacuum tube has a 9½×39½-inch aperture and is built of 0.031-inch thick stainless steel. It is constructed in 5 degree sections that are insulated from one another to minimize eddy current effects. This development was sponsored by the AEC.

C7. Bevatron Model Radiofrequency System. Q. A. KERNS, W. R. BAKER, G. M. FARLY, AND J. RIEDEL, *University of California, Berkeley.*—A saturable-reactor tuned oscillator at the magnet shunt drives a self-tracking power amplifier at the accelerating electrode. The ferroxcube reactor is temperature controlled to ±0.1°C, and the main saturating winding is a single loop of manganin threading the cores and soldered directly across the 0.001 ohm shunt. Oscillator frequency is linear to 1 percent with magnet current over a 3:1 frequency range. The frequency slope varies with the $L-C$ ratio and with the fractional magnet current through an additional loop of 10±1 times the main loop resistance. Frequency level adjustment and corrections of up to ±5 percent are obtained by controlling the current in an auxiliary 35 turn saturating winding as a suitable function of shunt voltage. The amplifier output tube load is a larger ferroxcube reactor resonating with the 400 $\mu\mu$f accelerating electrode capacity. Phase discriminator control of the saturating current to this reactor gives automatic tuning from 0.38 to 1.4 mc. Plate voltage modulation permits r-f voltages up to 1900 peak, and 50–2000 μsec. rises of adjustable curvature. This work was sponsored by the AEC.

C8. Bevatron Model Operating Results. E. J. LOFGREN, W. M. BROBECK, E. O. LAWRENCE, D. C. SEWELL, *University of California, Berkeley.*—The model bevatron (proton synchrotron) has accelerated protons from 0.7 Mev to 6½ Mev. About 10^{-8} coulombs are injected from a cyclotron in a 1 μsec. pulse every 4 seconds. With the tank diaphragmed to aperture of 6×18 inches ½ percent of the ions attain the final energy. If the tank aperture is increased to 9×26 inches, the beam is increased by a factor 7. If it is decreased to 4½×16 inches the beam is reduced by a factor 9. Normal tank pressure is 2.10^{-6} mm. The beam decreases exponentially with tank pressure and is reduced to $1/e$ by a pressure change of $1.7\cdot10^{-6}$ mm. The final energy of the protons may be varied by changing the duration of the r-f pulse. The resulting beam *vs.* final energy curve is nearly flat after 4 Mev. The minimum required accelerating voltage is 600 and the beam increases nearly linearly with r-f volts to 1400 after which it is constant to 1900, the highest available. Sponsored by the AEC.

C9. Theoretical Discussion of the Performance of the Model Bevatron. LLOYD SMITH, A. A. GARREN, AND L. R. HENRICH, *University of California, Berkeley.*—Measurements obtained from the bevatron model provide a basis for comparing the operation of an actual machine with the general theory of the proton synchrotron. The sensitivity of the accelerated beam to variation in magnetic field at injection, starting frequency, dee voltage and other parameters can be interpreted consistently in terms of the size, shape and location of the phase stable region. Some conclusions may also be drawn about frequency tracking, loss of ions due to scattering and the effect of straight sections on the orbits of the ions—problems which are peculiar to the bevatron. Here also the effects are in reasonable agreement with the theoretical estimates. This work was done under the auspices of the AEC.

C10. An Experiment for Measuring Heavy Meson Production by High Energy Particles. H. A. WILCOX AND C. RICHMAN, *University of California, Berkeley.*—An experimental method has been devised for measuring the heavy-meson production cross section of nuclei bombarded by charged particles from the Berkeley synchro-cyclotron. A target composed of the material to be studied is inserted in the external beam of the cyclotron. The beam is integrated after it has traversed the target. Positive and negative π-mesons leave the target with various energies E_π and at various angles θ to the direction of the beam. Blocks of Al and Cu are arranged so that the mesons leaving at any given angle θ are stopped in these blocks at positions determined by the kinetic energies with which they started. Nuclear emulsions are embedded in the blocks to sample the population of stopped mesons. The observed mesons are identified as positive if they give rise to a μ-decay, and as negative if they produce a nuclear star. From the numbers of π^+- and π^--mesons observed in the various regions of these emulsions, the differential production cross sections σ_+ and σ_- (in cm² Mev^{-1} steradian^{-1} per target nucleus) are inferred as functions of the angle θ and meson energy E_π. This work was sponsored by the AEC.

C11. Measurement of the Production of Positive and Negative π-Mesons by 345-Mev Protons on Carbon. C. RICHMAN AND H. WILCOX. *University of California, Berkeley.*—The method for measuring the production of mesons that we described[1] has been applied to the production in carbon. Thin graphite targets were bombarded by the 345-Mev external proton beam produced by the Berkeley 184-inch synchrocyclotron. The mesons coming off at 90° to the beam were observed at the ends of their ranges by means of C-3 nuclear emulsions embedded in suitable aluminum and copper blocks. The beam was integrated. The energy spectrum of mesons from carbon at this angle has a broad maximum at around 40 Mev. It drops off on both sides of this maximum, and on the high energy side extends up to about 140 Mev. The cross section for the combined production of positive and negative π-mesons at the maximum is $(3.4\pm0.4)\cdot10^{-30}$ cm² Mev^{-1} steradian^{-1} per carbon nucleus. The cross section integrated over meson energy is $(2.4\pm0.3)\cdot10^{-28}$ cm² steradian^{-1} per nucleus. These cross sections are uncorrected for nuclear absorption in the blocks. The ratio of positive to negative π-mesons from carbon, obtained by integrating the positive

and negative spectra separately over meson energy, has a value of 5.0 ± 1.4 This work was sponsored by the AEC.

[1] H. A. Wilcox and C. Richman, previous paper.

C12. Measurement of Production of Positive and Negative π-Mesons in Lead by 345-Mev Protons. MITCHEL WEISSBLUTH, *University of California, Berkeley.*—The experimental arrangement described by Wilcox and Richman[1] was used to obtain the spectrum of positive and negative π-mesons emitted by lead when bombarded by 345-Mev protons. Mesons were observed in C-3 nuclear emulsions at 90° to the beam direction. The combined spectrum of positive and negative mesons extends to about 120 Mev with a peak at about 30 Mev. The cross section at the peak is $(2.1\pm.4)\times10^{-29}$ cm^2 Mev^{-1} steradian^{-1} per lead nucleus. The cross section integrated over meson energy at 90° is $(8.9\pm2.4)\times10^{-28}$ cm^2 steradian^{-1} per nucleus. These cross sections are uncorrected for nuclear absorption in the blocks. Comparison of the peak cross section for lead with that for carbon[2] shows that they are consistent with the assumption that these cross sections are approximately proportional to the geometrical cross sections of the two nuclei. The ratio of positive to negative mesons from lead, obtained by integrating each spectrum separately over meson energy, is 1.5 ± 1. This work was sponsored by the AEC.

[1] H. A. Wilcox and C. Richman, paper presented at this meeting.
[2] C. Richman and H. A. Wilcox, paper presented at this meeting.

C13. Energy and Angular Distribution of π-Mesons Produced by 350-Mev Protons. T. B. TAYLOR* AND G. F. CHEW, *University of California, Berkeley.*—The energy and angular distributions of π-mesons produced by 350-Mev protons have been calculated on the assumption that the matrix element for the process is a constant. The cases of target nucleons which are free or which are bound in nuclei are considered. A heavy nucleus is considered to be a degenerate Fermi gas of neutrons and protons. A model which takes into account the finite size and mass of the nucleus is used for light nuclei. Interference effects, Coulomb effects, and the possibility that mesons will be scattered by nucleons on their way out of the nucleus have been neglected. The shapes of the calculated energy distributions agree with experimental distributions from carbon[1] and from lead[2] for meson energies for which Coulomb effects are unimportant. The orders of magnitude of the matrix elements calculated near threshold from various present meson theories are the same,[3] and these give cross sections of the same order of magnitude as those measured. This work was sponsored by the AEC.

* Now at Los Alamos Scientific Laboratory.
[1] C. Richman and H. A. Wilcox (accompanying abstract).
[2] M. Weissbluth (accompanying abstract).
[3] K. A. Brueckner (private communication).

C14. Nuclear Disintegration under Different Absorbers. H. SUN AND HARRIET H. FORSTER, *University of Southern California.*—Kodak and Ilford nuclear emulsion plates have been used to measure the attenuation of the star producing radiation under lead and paraffin. The photographic plates, completely surrounded by the adsorber, were exposed to the cosmic radiation at an altitude of 30,000 ft. Data will be presented showing the rate of occurrence of stars under the various absorbing materials and under varying thicknesses of lead. The results show an exponential absorption of the star producing radiation for large thicknesses of lead, with a corresponding absorption depth of about 250 g/cm^2; a transition effect of the star producing radiation has been found to occur within the first two centimeters of lead.

D1. The Positive-Negative Ratio for π-Mesons Produced in Complex Nuclei. GEOFFREY F. CHEW AND JACK L. STEINBERGER, *University of California, Berkeley.*—Energies available from existing accelerators are not sufficiently high to warrant the treatment of meson production, in the bombardment of complex nuclei by neutrons and protons, as a two-nucleon process only. A theoretical investigation of the effect of the other nucleons present has been undertaken, particularly as regards the positive-negative π-meson ratio. It will be shown that the exclusion principle leads to a favoring of positives over negatives when the incident particle is a proton and vice versa when it is a neutron. The effect should increase with meson energy at a fixed incident nucleon energy and decrease with incident nucleon energy at a fixed meson energy. Calculations for the special case of the deuteron will be reported, to show the probable order of magnitude of the effect.

D2. Meson Mass Measurements. F. M. SMITH, WALTER H. BARKAS,* A. S. BISHOP, HUGH BRADNER, AND EUGENE GARDNER, *University of California, Berkeley.*—This is the third progress report on a program for measuring meson masses at the 184-inch Berkeley cyclotron, the first two reports having been given at meetings of the American Physical Society at Berkeley[1] and Seattle.[2] Mass values announced at the Berkeley meeting were based on range-energy data of Lattes, Fowler, and Cuer.[3] Recent range-energy measurements of Bradner *et al.*[4] are more pertinent to the present problem, and the previous mass values have been corrected. Also, other small corrections have been made. Present best values are: $m_\pi=276\pm6$, $m_\mu=210\pm4$ electron masses. A program is in progress to measure meson masses by comparison with the proton mass. It is thought that this method will give more accurate values than the method used previously. No results from this study are available yet. This work was sponsored by the AEC.

* ONR, San Francisco, California.
[1] E. Gardner, Phys. Rev. **75**, 1468 (1949); A. S. Bishop, Phys. Rev. **75**, 1468 (1949); C. M. G. Lattes, Phys. Rev. **75**, 1468 (1949).
[2] Bishop, Bradner, and Smith, Phys. Rev. **76**, 588 (1949).
[3] Lattes, Fowler, and Cuer, Proc. Phys. Soc. (London) **59**, 883 (1947).
[4] Bradner, Barkas, Smith, and Bishop, Phys. Rev. (to be published).

D3. Observations on Tracks in Electron Sensitive Emulsions. FRANK L. ADELMAN, *University of California, Berkeley.*—Low ionization tracks from π^--meson stars have been studied with Ilford G-5 emulsions. Only about 5 percent of the star prongs were found to be heavy particles of lower ionization than 30-Mev protons, in contradiction to hypotheses of Marshak[1] and Fujimoto, Hayakawa, and Yamaguchi.[2] The energy was estimated by grain counting, with the assumption that the grain density of a 10–100-Mev proton is inversely proportional[3] to its velocity. Some electrons were found to be associated with meson endings. However, the heavy random grain and low energy electron background tends to mask high energy electron tracks and to make the definite assignment of a low energy electron to a star or star prong generally uncertain. The numbers of prongs per star agreed within the statistical errors with the work of Adelman and Jones.[4] The investigation reported here is being continued. This work was sponsored by the AEC.

[1] R. Marshak, Abstract for Echo Lake Cosmic-Ray Symposium (1949).
[2] Fujimoto, Hayakawa, and Yamaguchi, Prog. Theor. Phys. (in press).
[3] M. Blau, Phys. Rev. **75**, 279 (1949).
[4] F. L. Adelman and S. B. Jones, Phys. Rev. **75**, 1468(A) (1949).

D4. Nuclear Cross Sections for X-Rays from the Berkeley Synchrotron. A. C. HELMHOLZ AND K. STRAUCH, *University of California, Berkeley.*—The x-rays from the 335-Mev electrons accelerated in the Berkeley synchrotron have been used to produce radioactive elements by (γ, n), $(\gamma, 2n)$, and (γ, pn) reactions. The use of thin foils and β-ray standards has provided the number of radioactive atoms per unit beam irradiation. The relative cross sections for the total x-ray beam, assuming that for $C^{12}(\gamma, n)C^{11}$ is 1.0 are: $Cu^{63}(\gamma, n)14$; $Cu^{65}(\gamma, n)17$; $Zn^{64}(\gamma, n)12$; $Zn^{64}(\gamma, 2n)1.1$; $Zn^{64}(\gamma, pn)3$. The ratio $(\gamma, n)/(\gamma, 2n)$ is in qualitative agreement with that from the measurements of Perlman and Friedlander.[1] The large

value of (γ, pn) is surprising and is being further investigated. Using a $1/E$ spectrum for the x-rays, measurements of the energy flux by Blocker and Kenney,[2] and 20 Mev for the effective x-ray energy, we find a preliminary value for the $Cu^{63}(\gamma, n)$ cross section of 10^{-24} cm² Mev, in agreement with that of Lawson and Perlman.[3] Portions of this work have been sponsored by the AEC.

[1] M. L. Perlman and G. Friedlander, Phys. Rev. 74, 442 (1948).
[2] W. Blocker and Robert W. Kenney, Abstract No. D8.
[3] J. L. Lawson and M. L. Perlman, Phys. Rev. 74, 1190 (1948).

D5. Observations on Grain Counting and the Photographic Emulsion. J. KENT BOWKER, *University of California, Berkeley.*—Following the grain-counting technique of other experimenters[1-3] a study was conducted to find the mass of the negative π-meson. The thirty-six mesons and seven protons counted were registered in Ilford C-2, 100 μ-emulsions exposed in such a manner that the particles enter the edge of the emulsion and are stopped within 4 mm. The mass of the meson was found to be $264\binom{+26}{-22}m_e$. The large spread in masses led to an examination of the emulsion, which revealed a sensitivity variation in the region where the particles were found. Subsequently many other plates were exposed to particles or light, and the number of developed grains was counted or measured photometrically. A study showed that the sensitivity is greatest at an edge and decreases to uniformity only after 4 mm from that edge. Mean grain-counts of mesons at the edge and in the center of a plate were found to differ by as much as 5 percent. This paper is based on work performed with the support of the AEC.

[1] Lattes, Occhialini, Powell, Proc. Phys. Soc. 61, 173 (1948).
[2] Barkas, Gardner, and Lattes, Phys. Rev. 74, 1558(A) (1948).
[3] L. Van Rossum, Comptes Rendus 228, 676 (1949).

D6. Production of C^{11} by High Energy Particles. LEE AAMODT, VINCENT PETERSON, AND ROBERT PHILLIPS, *University of California, Berkeley.*—The absolute cross section as a function of proton energy for the reaction $C^{12}(p, pn)C^{11}$ has been measured from threshold to 350 Mev using protons from the Berkeley 32-Mev linear accelerator and from the deflected beam of the 184-inch cyclotron. Polystyrene foils were counted in beta-counters calibrated against Na^{24} and Au^{198} coincidence standards, and against RaE standards. The proton current was integrated by means of suitable Faraday cups and low leakage condensers. The cross section has a broad peak of about 80 mb at 60 Mev and falls to one-half this value by 350 Mev. The usual "stacked-foil" technique cannot be used with 350-Mev protons because of high absorption in copper ($\sigma_a \sim 0.8$b) used to degrade the proton energy. Measurements of the absorption of protons in carbon are also being made to correct the published relative excitation curves for the reactions $C^{12}(d, dn)C^{11}$ and $C^{12}(\alpha, \alpha n)C^{11}$,[1] and $C^{12}(p, pn)C^{11}$ in the intermediate energy region[2] which were determined using stacked carbon disks. Absolute values of the (d, dn) and $(\alpha, \alpha n)$ cross sections for 190-Mev deuterons and 380-Mev alphas will be given. This work was sponsored by the AEC.

[1] R. L. Thornton and R. W. Senseman, Phys. Rev. 72, 872 (1947).
[2] W. W. Chupp and E. M. McMillan, Phys. Rev. 72, 873 (1947).

D7. The Beta-Spectra of Zn^{62} and Cu^{62}. RAYMOND W. HAYWARD, *University of California, Berkeley.*—The beta-spectra of Zn^{62} and Cu^{62} have been investigated in a magnetic lens type spectrograph. The Zn^{62} formed by a $Cu^{63}(d, 3n)Zn^{62}$ reaction in the 184-inch cyclotron decays with a half-life of 9.2 hours, thus offering a convenient method of investigating its 10.1 minute half-life daughter Cu^{62} which decays in equilibrium with the Zn^{62}. Analysis according to the Fermi theory yields a straight line Fermi plot for the Cu^{62} spectrum with an upper energy limit of 2.91 ± 0.01 Mev and upon subtraction of the Cu^{62} contribution a straight line plot is also obtained for the Zn^{62} spectrum with an upper energy limit of 0.665 ± 0.010 Mev. The relative number of disintegrations of the Zn^{62} and Cu^{62} indicates that the Zn^{62} decays 10 percent of the time by positron emission and the remainder by K-capture. In addition, two conversion peaks are found corresponding to the K and L conversion peaks of a 41.8 ± 0.4-kev gamma-ray following the Zn^{62} decay. From the ratio of the number of K and L conversion electrons it is found that the transition is of either an electric or magnetic dipole type. This work was assisted by the AEC.

D8. Showers Initiated by 335-Mev Bremsstrahlung. WADE BLOCKER AND ROBERT W. KENNEY, *University of California, Berkeley.*—The variation of cascade shower intensity with depth has been determined for showers produced in lead, copper, aluminum, and carbon by the 335-Mev bremsstrahlung from the Berkeley synchrotron. The collimated beam from the synchrotron passed through a monitor ionization chamber and fell normally upon closely stacked plates of the element under study. The shower particles from various thicknesses of this element were then observed by a detector ionization chamber situated behind the plates. An essentially infinite amount of the element under study was placed behind the detector chamber to provide backscattered radiation. This contribution to the total intensity was very considerable in the case of lead. Shower intensities in the initial half-radiation length allow the thin-layer pair production and Compton contributions to the shower to be derived. The ordinates and abscissae of the maxima of the shower curves are compared with theory. The exponential tails of the shower curves give the gamma-ray absorption coefficients at the energy of minimum absorption cross section. These values are compared with theory. A thin sheet of lead observed by an ionization chamber gave ionization values which are used to derive the total energy of the x-ray beam. This work was sponsored by the AEC.

D9. A Fast Neutron Spectrometer Employing Li^6 Impregnated Emulsions. G. R. KEEPIN, JR.* AND J. H. ROBERTS, *Northwestern University.*—Observation of $Li^6(n, \alpha)H^3$ within an impregnated emulsion provides an accurate measure of both energy and direction of the incident neutrons. Preliminary studies using thermal neutrons have been reported.[1] Calibration with monoenergetic neutrons indicates resolution of at least ± 75 kev for $0 < E_n < 2$ Mev. Given E_n and θ, the laboratory angle between alpha and triton tracks, two triton energies are possible from the conservation laws. Similarly there are two values of $R_\alpha + R_t$, the sum of alpha and triton ranges. We identify the larger value as the case favoring the triton, f_t, the smaller as the f_α case. E_n, regarded as a function of θ and $R_\alpha + R_t$, is least sensitive for f_t disintegrations with $\theta \simeq 180°$. Thus, for maximum energy resolution we select only f_t disintegrations with $175° \leq \theta \leq 180°$. Continuous spectra must be corrected for the energy dependence of: (1) probability that $175° \leq \theta \leq 180°$, (2) Li^6 cross section, and (3) geometrical selection criteria. The Li^6 technique is uniquely suited to measurements inside a material medium where perturbations introduced by the detector must be minimized and where collimation is impossible.

* Now AEC Postdoctoral Fellow at Radiation Laboratory, University of California, Berkeley.
[1] G. R. Keepin, Jr., and J. H. Roberts, Phys. Rev. 76, 154 (1949).

D10. Measurement of Protons Produced in the Synchrotron Beam. A. SILVERMAN AND C. LEVINTHAL, *University of California, Berkeley.*—A proportional counter telescope with two counters each with an active region of one and one-half inches diameter and one and one half-inches deep is used in

coincidence. By adjusting separate pulse height discriminators in each counter, the system may be used to count protons entering the first counter with energies between 1.5 and approximately 5 Mev. The resolving time of the system is approximately 0.5 μsec. With the synchrotron beam spread out over two milliseconds, the time resolution and pulse height discrimination combined with adequate shielding reduces the electron γ-ray background to a small fraction of the proton counting rate. The energy distribution arising from several different elements will be discussed. This work was sponsored by the AEC.

D11. Excited States of the Mirror Nuclei Be^7 and Li^7. A. B. BROWN, C. Y. CHAO, W. A. FOWLER, AND C. C. LAURITSEN, *California Institute of Technology.**—A low energy group of α-particles has been found to result from the reaction $B^{10}(p, \alpha)Be^{7*}$, indicating the existence of an excited state of Be^7. Observation of this group, which has not previously been found, and separation of the group from protons elastically scattered by the thin B^{10} targets was made possible through high resolution magnetic analysis supplemented by absorption techniques. A broad resonance is indicated near 1.5-Mev proton energy. The Q-values of the reactions leading to the ground state and to the excited state were found to be 1.148 ±0.006 Mev and 0.714±0.008 Mev, respectively. The excited state thus is 0.434±0.005 Mev above the ground state. On the basis of approximately equal neutron-neutron and proton-proton forces, plausible arguments[1] can be advanced which indicate that this state corresponds to the excited state in Li^7 at 0.478 Mev.

* This work was assisted by the Joint Program of the ONR and the AEC.
[1] Fowler, Delsasso, and Lauritsen, Phys. Rev. 49, 561 (1936).

D12. Gamma-Radiation from an Excited State of Be^7.* T. LAURITSEN AND R. G. THOMAS,† *California Institute of Technology.*—In earlier work at this laboratory[1] a γ-ray line at 420 kev was reported to appear in the bombardment of B^{10} with protons and was attributed to excitation by inelastic scattering of a state of B^{10} at that energy. After the discovery, by Brown *et al.*[2] of a group of α-particles corresponding to the formation of Be^7 in an excited state in the reaction $B^{10}(p\ \alpha)Be^{7*}$, the γ-radiation was re-examined in the magnetic lens spectrometer and compared more carefully with the 414-kev line[3] in $Be^9(d\ n)B^{10*}$ with the result that the two γ-ray energies were found to differ by 15 kev, yielding 429±5 kev for the Be^{7*} line.[4] The excitation function and absolute cross section for this radiation agree well with those found for the α-particle group. In a search for the corresponding radiation from $Li^6(d\ n)Be^{7*}$, a target of Li^6SO_4 was bombarded with 1450-kev deuterons. The line at 429 kev appeared, together with the well-known line at 478 kev from $Li^6(d\ p)Li^{7*}$, with an intensity very nearly equal to the latter.

* This work was assisted by the Joint Program of the ONR and the AEC.
† AEC Fellow.
[1] Lauritsen, Fowler, Lauritsen, and Rasmussen, Phys. Rev. 73, 636 (1948).
[2] A. B. Brown, *et al.* (preceding abstract).
[3] Rasmussen, Hornyak, and Lauritsen, Phys. Rev. 76, 581 (1949).
[4] We are indebted to the AEC for the loan of the B^{10} metal and the enriched Li^6SO_4 used in these experiments.

D13. Gamma-Radiation from $C^{13}+d$.* R. G. THOMAS† AND T. LAURITSEN, *California Institute of Technology.*—When C^{13} is bombarded with deuterons the reactions $C^{13}(d\ \alpha)B^{11}$, $C^{13}(d\ n)N^{14}$, and $C^{13}(d\ p)C^{14}$ occur. A neutron group[1] indicating a level in N^{14} at 5.1±0.3 Mev and a proton group[2] corresponding to a level in C^{14} at 5.2±0.3 Mev have been reported. Gamma-radiation of 5.5 Mev accompanying these reactions has been observed.[1,3] In an attempt to obtain more precise information on the γ-radiation we have bombarded a carbon target, enriched to 50 percent C^{13}, with 1.42-Mev deuterons and observed the secondary electrons with a magnetic lens spectrometer of 2 percent resolution and 2½ percent solid angle. Photoelectrons from a thorium converter indicate γ-rays of 3.4, 2.3, 1.6, and 0.73 Mev in addition to the known lines from $C^{12}+d$ at 3.1 and 0.51 Mev. Secondary Compton electrons from a beryllium converter indicate γ-rays of 3.4, 5.1, 5.7, and 6.1 Mev. There is some indication of a weak γ-ray of 3.9 Mev.

* This work was assisted by the Joint Program of the ONR and the AEC.
† AEC Fellow.
[1] W. E. Bennett, *et al.*, Phys. Rev. 59, 781 (1941).
[2] R. F. Humphreys and W. W. Watson, Phys. Rev. 60, 542 (1941).
[3] T. W. Bonner, *et al.*, Phys. Rev. 59, 214A (1941).

D14. The Low Energy α-Particles from $F^{19}(p\alpha)O^{16}$.* C. Y. CHAO, A. V. TOLLESTRUP, W. A. FOWLER, AND C. C. LAURITSEN, *California Institute of Technology.*—We have recently determined the energies and intensities of four low energy α-groups from the reaction $F^{19}(p\ \alpha)O^{16*}$ at the resonances between $E_p=300$ kev and 1400 kev. The proton beam was produced by an electrostatic generator, the target was a thin layer of ZnF_2 deposited on a copper strip and the α-particles emerging at 138° were analyzed by a double-focusing magnetic spectrograph. The Q-values of the four groups are found to be $Q_x=2.061\pm0.010$, $Q_1=1.977\pm0.008$, $Q_2=1.204\pm0.008$ and $Q_3=1.002\pm0.008$ Mev, corresponding respectively to the pair level and the three γ-ray levels. These Q-values when added to the corresponding pair energy or γ-ray energy recently obtained by Rasmussen, Hornyak, Lauritsen, and Lauritsen[1] give an average value of $Q=8.113\pm0.030$ for the reaction $F^{19}(p\ \alpha)O^{16}$. The relative intensities of the three α-groups preceding γ-ray emission are found to vary considerably from resonance to resonance. We have measured the γ-ray intensity simultaneously with the measurement of α-particles. By assuming isotropic angular distributions, the ratio of the total number of α-particles to that of γ-rays is found to be very close to unity at all the γ-ray resonances investigated.

* Assisted by the joint program of the ONR and the AEC.
[1] To appear in the Phys. Rev.

E1. Production and Annihilation of Antiprotons. C. W. HELSTROM, *California Institute of Technology.*—The cross section for the reaction: negative meson+proton→antiproton +neutron+proton, has been calculated by the usual perturbation theory. The threshold energy is 4μ, where μ=rest energy of the proton. The cross section reaches a maximum of $\sim 0.03(g^2/\hbar c)r^2$ at an incident meson energy of 27μ, and then drops off. g=meson coupling constant; $r=g^2/\mu$. The cross section for production of neutron-antiproton pairs in nucleon-nucleon collisions has been calculated by the Weizsäcker-Williams method. The cross section is $\sim 0.01(g^2/\hbar c)^2r^2$ in the region of 30-Bev incident nucleon energy. The antiproton may be annihilated by collision with a proton to form a pair of charged mesons; the cross section is $\frac{1}{4}\pi r^2 c/v$ non-relativistically, where v=velocity of the incident antiproton. Annihilation into a pair of neutral mesons vanishes as v/c. The cross section for the process: neutron+antiproton→negative meson+neutral meson is $\frac{1}{4}\pi r^2 c/v$ at low energies. Bound in the Coulomb field of a proton, the lifetime against annihilation into charged mesons is $\sim 10^{-17}$ sec. in the singlet ground state or $\sim 10^{-10}$ sec. in the triplet state. The pseudoscalar interaction has been used in all these calculations. This work is being carried on under a fellowship of the E. I. du Pont de Nemours Company.

E2. Further Remarks on Neutron Optics. OTTO HALPERN AND CHARLES B. SHAW, JR.,* *University of Southern California.*—The previously[1] given theory of neutron refraction and double-refraction has been extended to cover those cases in which capture and *incoherent* scattering processes are also present. These processes can be formally accounted for by the

introduction of a complex index of refraction. In close analogy to the electromagnetic case total reflexion at the critical angle becomes imperfect in the presence of an index of absorption. This effect is of some importance in the production of polarized neutron beams by total reflexion, an experiment suggested a year ago[2] and recently carried[3] out by using Co[4] as reflector. The extended theory may also be useful for the interpretation of total reflexion experiments carried out with strong absorbers like Cd, the scattering cross section of which is difficult to determine. In some modifications of H the large incoherent cross section will influence the results of experiments dealing with refraction and reflexion phenomena.

* Now at the University of Chicago.
[1] Halpern, Hamermesh, and Johnson, Phys. Rev. 59, 981 (1941).
[2] O. Halpern, Phys. Rev. 75, 343 (1949).
[3] J. Hughes and M. T. Burgy, Phys. Rev. 76, 463 (1949).
[4] M. Hamermesh, Phys. Rev. 75, 1766 (1949).

E3. A Proposed Decay Scheme for $_{72}Hf^{181}$ (46 day, 5.7 hour). S. B. BURSON AND K. W. BLAIR, *Argonne National Laboratory.*—A determination of the radiations of $_{72}Hf^{181}$ (46 day) has been made by absorption and coincidence methods. Upon delaying one couter 8.5 microseconds ($\tau = 7.25$ μsec.) aluminum absorptions indicate a delayed beta of 0.40 Mev coinciding with several conversion electron groups. This, together with the absence of delayed gamma-coincidences, indicates that the beta leads directly to the 22-microsecond isomeric state of $_{73}Ta^{181}$. Absorptions of the conversion electrons coinciding with the delayed beta indicate energies corresponding to the 0.47, 0.34, and 0.13-Mev gamma-rays previously reported by others from spectrographic data. A 5.5-hour beta-activity in hafnium (C. O. Muehlhause, ANL-4097) was also examined and tentatively assigned to an isomeric state of Hf^{181}, approximately 0.087 Mev below the 46-day state. Absorption in lead of the photon radiations of this period is indistinguishable from that of the 46-day period. No delayed coincidences accompanied this activity. Absorptions in aluminum of the prompt $\beta - e^-$-coincidences indicate that a beta of about 0.45 Mev coincides with electron groups similar to those observed in the 46-day period. A decay scheme is proposed.

E4. Proton-Proton Scattering at 12.4 Mev.* BYRON T. WRIGHT AND F. E. FARIS,† *University of California, Los Angeles.*—A scattering camera having complete cylindrical symmetry about the proton beam direction has been constructed. An annular-shaped film on whose surface are latent circular reference lines is placed in the camera with its plane perpendicular to the beam direction. For a particular point on the film the angular range within which scattered protons can be received is defined by the edges of an annular slit which lies between the film and the hydrogen filled scattering volume. Background due to protons is limited to those which are successively scattered by three slit edges. A Faraday cup in a separate chamber is used to integrate the beam and to measure its integral range in Al curve. To date the differential cross section at 90 degrees (c.m.) at 12.4 Mev has been observed. These results are being analyzed and will be presented.

* This work was supported in part by the Joint Program of the ONR and the AEC.
† Now with North American Aviation, Inc.

E5. High Energy Scattering—Theoretical. RICHARD S. CHRISTIAN, *University of California, Berkeley.*—The 280-Mev $n-p$ scattering[1] experiments are in agreement with the predictions of the potential models[2] proposed on the basis of scattering below 90 Mev, showing that large velocity dependent forces are not present. The 350-Mev $p-p$ results,[3] however, show an anomalously high and flat cross section. The flatness of the cross section cannot be interpreted in terms of a primarily S-way interaction, since the magnitude is some 10 times larger than expected and twice $4\pi\lambda^2$. Since central forces tend to concentrate the scattering in a forward cone ($\sim$15–20°), the only possible interpretation is by means of a very short range tensor force, e.g., calculations show that an $\exp(-r/R)/r^2$ tensor radial dependence ($R \sim 2\times10^{-13}$ cm) gives agreement at 350 Mev without altering the low energy agreement. The essential feature of this model appears to be a strong tensor interaction at distances less than 0.5×10^{-13} cm. This work was sponsored by the AEC.

[1] Kelly, Leith and Wiegand, Phys. Rev. 76, 589(A) (1949), and private communication.
[2] R. Christian and E. W. Hart, in press.
[3] O. Chamberlain and C. Wiegand, private communication.

E6. A Multiple Scattering Deflector for the 184-Inch Cyclotron. C. E. LEITH, *University of California, Berkeley.*—The electromagnetic deflector[1] for the 184-inch cyclotron provides a deflected 350-Mev proton pulse of 0.1 μsec. duration with a repetition rate of 60 cycles. The short duration of this pulse makes it difficult to use counters of existing types in doing many types of particle experiments. A deflector system will be described which lengthens the proton pulse duration to 50 μsec. maintaining the same repetition rate. A 0.1-cm thick Th scatterer is placed at the position usually occupied by the electric deflector. Some of the protons multiply scattered in passing through the Th experience the correct deflection to allow them to enter the magnetic channel and thus be brought out of the cyclotron. The time average proton current obtained in this way outside of the main shielding is 10^{-12} ampere in a 2.5-cm diameter beam. This current is 10^{-2} times that obtained with the electric deflector. It will be shown that this deflector system is applicable at any energy. This development was sponsored by the AEC.

[1] W. M. Powell *et al.*, Rev. Sci. Inst. 19, 506 (1948).

E7. Absorption of π^--Mesons in Hydrogenous Materials. W. K. H. PANOFSKY AND H. F. YORK, *University of California, Berkeley.*—A π^--meson captured in hydrogen cannot convert the proton into a neutron without emission of an additional particle, presumed to be a 130 Mev γ-ray. This γ-ray was looked for using the pair spectrometer of Bjorklund, Crandall, Moyer, and York.[1] π^--produced in the target of the 184-inch cyclotron were captured in CH_2 and LiH converters. Using the absolute cross section for meson production as determined by Richman and Wilcox[2] the expected γ-ray yields were calculated. The results indicate that, if the γ-ray process occurs, less than 1 part in 1000 of the π^- captured in CH_2 are converted on H and less than 1 part in 200 of the π^- captured in LiH are converted on H. Studies using high pressure hydrogen are in progress. This work was sponsored by AEC.

[1] Bjorklund *et al.*, Phys. Rev. (to be published).
[2] Private communication.

E8. High Energy Photons from Proton Nucleon Collision. W. E. CRANDALL, B. J. MOYER, AND H. F. YORK, *University of California, Berkeley.*—The yield and energy spectrum for high energy photons from a target bombarded by protons of energy over 175 Mev in the 184-in. cyclotron are presented here. For 345-Mev protons, the energy spectra for various angles of observation, when transformed to a system with $\beta = 0.32$ in the direction of the incident proton beam, become identical. A calculation of the absolute yield, based on spherical symmetry in this unique system, gives a cross section of 1×10^{-27} cm^2 per carbon nucleus. The peak of the energy spectrum curve in this system comes at approximately 75 Mev. Possible sources of this radiation have been considered. Nucleon isobars appear to be ruled out since nucleons with energy of 250 Mev would be required in the nucleus. Bremsstrahlung neither fits the shape of the energy spectrum nor the magnitude of the yield for protons above 200 Mev. Excited π-mesons appear unlikely due to energy balance considerations. Neutral

mesons, with a rest mass of 300 ± 25 electron masses and a lifetime of less than 10^{-11} sec., decaying into two photons seem to fit all data observed. This development was sponsored by AEC.

E9. Non-Equilibrium Cyclotron Orbits. WALTER H. BARKAS,* *University of California, Berkeley.*—Trajectories are described in cylindrical coordinates (r, ϕ, z). Equilibrium orbits exist in the median plane $(z=0)$ only with momenta $p=mr\dot{\phi}=(e/c)rH_z(r,0)$. The vector potential contains one component $A_\phi(r,z)\equiv A$, and ϕ is an ignorable coordinate. The general motion in the (r, z) plane is derivable from a scalar potential,

$$U=\frac{1}{2m}\left(\frac{Q}{r}-\frac{e}{c}A\right)^2,$$

leading to a "boundary of libration," $[\pm p+(e/c)A]r=mr_1^2\dot{\phi}_1+(e/c)r_1A_1=Q$, where the subscript 1 refers to any point on the orbit. In the median plane

$$p=e\int_{r_1}^{r_2} rH_z dr/c(r_1\cos\lambda_1-r_2\cos\lambda_2),$$

where the subscripts refer to two points on the trajectory, and $\tan\lambda=1/r(dr/d\phi)$. The orbit in the median plane is:

$$\phi=\arcsin\left[\frac{(R_2-R_1)\sin\tau}{2r}\right]+a_0\tau+\sum_{n=1}^{\infty}a_n\sin n\tau,$$

with

$$\cos\tau=\frac{R_2^2+R_1^2-2r^2}{R_2^2-R_1^2},$$

R_1 and R_2 being the limits of libration. The a_n and the libration limits are evaluated from $A_\phi(r,0)$, together with the observed values of r_1, r_2, λ_2, and $\phi_2-\phi_1$. λ_1 is then determined from the orbit equation. Accurate calculation of particle momenta for the determination of meson masses is the immediate purpose of this work. This work was sponsored by AEC.

* ONR, San Francisco, California.

E10. Ratio of Positive to Negative π-Meson Yields from Various Targets Bombarded by 345 Mev Protons. H. BRADNER AND S. B. JONES, *University of California, Berkeley.*—Nuclear plate techniques have been used to investigate the yields of high energy mesons produced in various targets by 345 Mev protons. Fifty Mev π^+- and π^--mesons which leave the target at 90° to the incident beam direction are bent in opposite directions by the cyclotron magnetic field, and pass through channels in a copper block. The mesons are then slowed down in an absorber, and finally recorded in nuclear emulsion plates. Neglecting possible differences in nuclear absorption of π^+- and π^--mesons, the ratio of yields can be obtained by counting the relative numbers of π^+- and π^--mesons in equal volumes of emulsions in the two plates. Preliminary results give π^+/π^--ratios of 2.7 ± 2 for Be, 4.8 ± 0.5 for C, 5.4 ± 1 for Al and 4.3 ± 2 for Cu. The errors quoted are statistical probable errors. This work was sponsored by AEC.

E11. Phenomenological Interpretation of $p-p$ Scattering at 32 Mev. H. P. NOYES, *University of California, Berkeley.*—Analysis of linear accelerator data on 32 Mev $p-p$ scattering in terms of static potentials indicates qualitative differences between $n-p$ and $p-p$ nuclear forces. The angular distribution is compatible with pure ^1S scattering of phase shift approximately 50°, but customary static potentials predict additional ^1D scattering incompatible with the data. Central scattering in odd (triplet) states cannot resolve this discrepancy but tensor force scattering in odd states is peaked at 90°. Hence the D wave can be masked by a tensor force with the same magnitude of angular variation although this raises the total cross section. A tensor potential of about half the magnitude of the singlet potential, when added to the exponential well given by Blatt and Jackson[1] as the best fit at low energies, gives the correct angular dependence without destroying the agreement at lower energies. This model gives an absolute magnitude about 5 percent too high which could be lowered by using a well slightly shallower than the exponential, or by using different radial dependence in singlet and triplet states. This work was sponsored by AEC.

[1] J. M. Blatt and J. D. Jackson, Phys. Rev. (to be published).

E12. Auger Effect in the Decay of At^{211}. LAWRENCE S. GERMAIN,* *University of California, Berkeley.*—At^{211} decays by both K capture and alpha-particle emission. The K capture decay leads to Po^{211} which emits an alpha-particle with a half-life of 5×10^{-3} second. It has been possible to record the At^{211} activity in photographic emulsions by soaking the plates in a water solution containing the At activity. Both the 5.92 Mev At^{211} alpha-particles and the 7.34 Mev Po^{211} alpha-particles were visible in the plates and easily distinguished by their characteristic ranges. Some of the Po^{211} alpha-tracks were found to have a short electron track at one end. These electrons had the proper energy to be Auger electrons from the K capture decay at At^{211}. The number of Po^{211} alpha-tracks associated with short electrons divided by the total number of Po^{211} alpha-tracks gives the fraction at At^{211} K capture decays which give rise to Auger electrons. This ratio, which is the percent internal conversion of the K x-rays, was found to be $(9.25\pm0.50$ percent). Some evidence was found to indicate that Bi^{207}, the result of the alpha-decay of At^{211}, decays by K capture. This work was sponsored by AEC.

* Now at Reed College, Portland, Oregon.

E13. An Iteration Procedure in the Rayleigh-Ritz Principle. E. GERJUOY, *University of Southern California,* AND HAROLD GRUEN, *University of California, Los Angeles.**—Let H be an operator whose ground state energy is E_1, and φ a trial function such that the integrals $(\varphi, H^r\varphi)=(H\varphi, H^{r-1}\varphi)=\cdots(H^r\varphi,\varphi)$ exist and are equal for any positive integer r. Define $\Gamma_A\equiv H-A$ and $\beta_n(A)\equiv(\varphi,\Gamma_A{}^n\varphi)$, where A is a parameter. Then $E_1\leqslant A+\beta_3/\beta_2=F_3(A)$. Moreover, $F_3(A)$ has a single minimum. If this minimum occurs at A', then $F_3(A')\leqslant(\varphi,H\varphi)/(\varphi,\varphi)$. The equality holds only if φ is an eigenfunction. Since $F_3(A)=(\Gamma_A\varphi, H\Gamma_A\varphi)/(\Gamma_A\varphi,\Gamma_A\varphi)$, the function $(H-A')\varphi=\varphi^1$ may be regarded as a new trial function, superior to φ, and in fact the best function of the class $\Gamma_A\varphi$. Repeating the process of minimizing F_3 using the new trial function φ^1, a decreasing sequence of upper bounds to E_1 is obtained, which presumably converges to E_1 if $(\varphi,\psi_1)\neq0$, where ψ_1 is the ground state wave function of H. Since φ can often be chosen so that the integrals $(\varphi, H^r\varphi)$ are readily evaluated, this procedure may prove useful. Possible applications will be discussed. If $F_n(A)\equiv A+\beta_n/\beta_{n-1}$, n odd, and if its (only) minimum occurs at A_0, then it follows that $E_1\leqslant F_n(A_0)\leqslant(\varphi,H\varphi)/(\varphi,\varphi)$. Thus the functions F_n can also be used to generate improved estimates of the ground state.

* Junior Fellow of the National Bureau of Standards, Institute for Numerical Analysis, University of California, Los Angeles, California.

F1. Mass Spectrometric Studies of Oxide Cathode Sublimation Phenomena. R. H. PLUMLEE, *Radio Corporation of America.*—Mass spectrometric techniques have been utilized to study sublimation characteristics of materials used in electron tubes. General processes induced thermally and by electron bombardment have been studied as well as specific phenomena charactertiics of individual materials. Preliminary results noted include (1) the inefficiency of electron bombardment for producing material transport, (2) the complex thermal evaporation of oxide cathode constituents, (3) the absence of

positive ion evaporation from oxide cathodes, (4) confirmation of mechanisms for negative ion formation in vacuum systems, and (5) the liberation of molecular oxygen from oxide cathodes as a function of electron emission.

F2. New Bands in the $3p^1\Pi - ls^1\Sigma$ System of the Hydrogen Molecule. C. R. JEPPESEN AND PAUL E. PFLUEGER, *Montana State University.*—The absorption spectrum of hydrogen has has been re-examined with a view to observation of new bands associated with the normal electronic state. At very low pressures, only the $3p^1\Pi - ls^1\Sigma$ progression having v' greater than 2 is observed. This progression, discovered by Hopfield,[1] occurs in great strength because of pre-dissociation in vibrational states having v' greater than 2. At higher pressures this absorption becomes continuous, making observation of other systems impossible. The 0−0, 1−0, and 2−0 bands of this system were observed for the first time, however, and their rotational analysis confirms the previous study[2] of ten emission bands of this system.

[1] J. J. Hopfield, Nature 125, 923 (1930).
[2] C. R. Jeppesen, Phys. Rev. 54, 68 (1938).

F3. The Sensitivity of a Positive Ion Space Charge Detector.* R. R. EGGLESTON AND G. L. WEISSLER, *The University of Southern California.*—In order to measure photoionization in N_2 and other gases as a function of wavelength in the vacuum ultraviolet, it was thought that the "Kingdon Cage" positive ion space charge detector[1] would be most apt; particularly since this instrument is only sensitive to positive ions and will not be affected by stray electrons. A preliminary study was made to investigate its sensitivity by generating a known number of positive ions in the gas within the detector diode (N_2 at 8.8×10^{-3} mm Hg) and plotting this number against the deflection of a bridge galvanometer. With 8 volts across the diode we were able to detect of the order of 50 positive ions present at any instant. This last figure was arrived at by using estimates of positive ion life times following a procedure suggested by Kingdon.[1] Since the present rough data were obtained with very simple equipment, it seems indicated to follow up Kindgon's work on ion life times with modern oscillographic techniques, and to enhance the sensitivity of the detector by use of resonant—and/or pulse-amplifiers in the bridge circuit.

* This work is being carried on under an ONR contract.
[1] K. H. Kingdon, Phys. Rev. 21, 408 (1923).

F4. The Influence of the Piezo-Electric Effect on Tribo-Electrification.* JOHN W. PETERSON, *University of California, Berkeley* (introduced by Leonard B. Loeb).—The piezo-electric effect has been suggested as a possible explanation for tribo-electric charging in cases where at least one piezo-electric crystalline material is involved.[1] To investigate this suggestion, measurements have been made of the charge acquired by amorphous quartz particles in sliding over a crystalline quartz plate, which can be compressed to give the desired piezo-electric surface charge. The quartz particles average 400 microns in diameter, receiving an average negative charge of 4×10^4 electrons per particle with zero surface charge on the plate. The same amount of charge is transferred from either positive or negative surface charges, and this amount does not exceed twelve percent of the total surface charge of the plate. With maximum surface charge, the piezo-electric contribution to the charge of the particles is less than twenty percent of their total charge.

* These studies supported by ONR Funds.
[1] L. B. Loeb, Science, 102, 573 (1945).

F5. The Electrical Charges on Dust Particles.* W. B. KUNKEL, *University of California, Berkeley* (introduced by Leonard B. Loeb).—A method for the determination of the charge and size of falling droplets developed by Hopper and Laby was used to measure the charges on the individual particles of large samples of dispersed powders. The behaviour of various materials as well as the effect of different methods of dispersion were investigated. Practically all particles proved to be charged, both positive and negative signs occurring simultaneously. When any contact between dissimilar substances was avoided, the charges balanced, leaving the cloud neutral. In these cases the average charge per particle was roughly proportional to the surface area of the particles independent of the method of dispersion. No difference in polarity between large and small particles was noted. No effect of humidity could be discovered, mainly because of the remarkable invariance of the moisture content of such fine non-hygroscopic powders. When different powders were mixed, the charge distribution showed marked asymmetry. When the dusts were blown against different surfaces mainly the larger particles displayed a predominance of one sign. Magnitude and sign of the excess charge depended on the substances and processes involved. In addition to this study the equilibrium charge distribution in coarse aerosols was investigated.

* These studies supported by ONR Funds.

F6. Choice of Gap Forms for Corona Breakdown Studies and the Electrostatic Field in a Point-to-Plane Gap.* L. B. LOEB, J. H. PARKER, E. E. DODD, AND W. N. ENGLISH, *University of California, Berkeley.*—Various electrode geometries are discussed with reference to their suitability for quantitative laboratory investigations of corona discharge phenomena so that the use of a convenient geometry to standardize data can be recommended. The recommended geometry is the "point-to-plane" gap consisting of a hemispherically capped circular cylinder of 0.025 or 0.050 cm radius at a gap length 160 times its radius from a perpendicular plane. In order to evaluate the Townsend integral involved in the threshold theories for the various phenomena, the axial electrostatic field intensity for the point-to-plane gap is needed so that the first Townsend coefficient can be determined. An approximation method is employed which yields the desired field to ±1 percent as a table of values at various points in the gap. The resulting Townsend integrals at experimentally determined pre-onset burst pulse threshold for the point-to-plane gap and for the confocal paraboloid gap are compared and found to be in relatively good agreement.

* These studies supported by ONR Funds.

F7. Point-to-Plane Corona Studies in Dried Air.* H. W. BANDEL, *University of California, Berkeley* (introduced by Leonard B. Loeb).—A current, visual, and oscilloscopic study of point-to-plane corona in dried air has been made to obtain a comprehensive set of consistent data, and to compare with the work of Miller[1] using co-axial cylinders. Polished, hemispherically capped platinum points of 0.25, 0.5, and 1.0 mm diameter have been used, with gap length to point radius ratio of 160, for a series of seven pressures from atmospheric to 10 mm Hg, and from low voltages up to breakdown. A thorianite ore source of gamma-rays was used for triggering, and with negative points comparison work has been done using ultraviolet light. In dried air with positive points it was found that pre-onset streamers occur only with higher pressures and larger points in agreement with the Loeb-Meek streamer theory and the known high absorption of ultraviolet by water vapor. Under some conditions, with larger negative points at high voltage the discharge undergoes a transition from the characteristic Trichel pulse corona to a Townsend type discharge with no pulses and no Faraday dark space.

* These studies supported by ONR Funds.
[1] Charles G. Miller, PhD. Thesis, University of California, 1949.

F8. Mass Measurements of Cosmic-Ray Particles.* T. C. MERKLE, JR., E. L. GOLDWASSER, AND R. B. BRODE, *University of California, Berkeley.*—The analysis of mass measurements of the particles in the cosmic radiation at sea level indicates that under a 6-inch wooden roof about as many protons as mesons are found in the energy region below 300 Mev. The presence of some heavy particles with ranges and curvatures that indicated masses of about 1000 Me were also observed. However, the relative number of these particles copared with protons has been found to depend on the quality of no field control tracks observed. The distortions observed are not statistical in the sense that most of the no field controls show curvatures of less than 1/60 M^{-1}. However, among these tracks appears an occasional control track with a positive curvature of 1/10 M^{-1}. Because of the non-statistical character of the observed curvature distortions, it is possible to be misled as to the quality of the tracks by taking too few control observations. The combination of a few of the 1/10 M^{-1} distortions with the proton tracks appears to account for the particles of apparent mass of about 1000. It has been found possible, by control of such factors as temperature gradients, rubber diaphragm tension, vapor saturation and speed of expansion, to operate the chamber for periods of many days with no control track showing curvatures over 1/30 M^{-1}. In these periods, no particles of apparent mass of 1000 have been observed.

* Assisted by the Joint Program of the ONR and the AEC.

F9. The Ratio of Positive to Negative Particles in the Cosmic Radiation at 3650 Meters Elevation.* R. B. BRODE, *University of California, Berkeley.*—The ratio of positive to negative particles in the cosmic radiation has been measured at an elevation of 3650 meters on White Mountain, California. This ratio has been measured for particles that have a range in iron of over 60 cm and a momentum of from 1.0 to 2.5 Bev/C. The values observed for this ratio for the vertically incident radiation are 1.32 ± 0.02 at 100 meters elevation; 1.30 ± 0.03 at 3650 meters; and 1.32 ± 0.03 at 3650 meters, under an absorbing layer of 45 cm of lead. This amount of lead is equivalent to the atmosphere between 100 meters and 3650 meters. A series of observations at 34° and 56° from the vertical in the east and west directions is partially completed and results on these measurements will be reported.

* Assisted by the Joint Program of the ONR and the AEC.

F10. Production of Penetrating Showers in Carbon.* JOHN R. GREEN AND W. B. FRETTER, *University of California, Berkeley.*—During the summer of 1949, pictures were obtained of penetrating showers produced in carbon at 3650 meters on White Mountain, California. The cloud chamber had an illuminated region of 18″×22″×5″, contained ten 1″ graphite plates with four ½″ lead plates underneath them for identification of penetrating particles, and was filled with argon and sufficient pure alcohol for saturation. The actuating system required that at least one particle enter at the top of the chamber, and that at least three (or, if desired, two) particles emerge from 2″ of lead underneath the chamber. Analysis of but a small number of the penetrating showers observed indicates a high probability that one or more of the particles produced will initiate a secondary event, such as a second penetrating shower, a burst or star, or an abnormal scattering. There is also indication that the production of penetrating particles might at times be accompanied by direct production of electrons or of other particles that introduce electrons into the shower very near the initial event. Most of the penetrating showers included gamma-rays which produced electron pairs or showers farther down in the carbon and lead plates.

* Assisted by the Joint Program of the ONR and the AEC.

F11. Extensive Showers under Water.* W. B. FRETTER AND JOHN ISE, JR., *University of California, Berkeley.*—Although there is considerable evidence that multiple electronic cores separated by appreciable angles occur in penetrating showers, attempts to find multiple cores in air showers have failed. It has been proposed that the cores, if they exist, are concentrated in a region of a meter or two in diameter where the high density of particles makes the analysis by counters or ionization chambers difficult. As an air shower passes into water, however, the lower energy particles are absorbed and after a *density* (not z-dependent) transition effect the entire shower might be concentrated in a very small area. Thus multiple cores separated by small distances might be detected under water. A preliminary experiment to investigate air showers under water has been done in a lake at an elevation of 7500 feet. Counting rates were taken under 9 feet of water as a function of distance between counter trays. Fourfold coincidences, requiring two particles in each tray and twofold coincidences requiring one particle in each tray were taken. No striking effect was found, but counting rates were high and the experiment seems promising if greater depths of water are used.

* Assisted by the Joint Program of the ONR and the AEC.

F12. Photographic Evidence for the Existence of a Meson of More than 450 Electron Masses. HARRIET H. FORSTER, *University of Southern California.*—Photographs will be presented of a cosmic-ray event in which a charged particle comes to rest in the emulsion of a photographic plate and produces a nuclear disintegration with the emission of at least eleven charged particles. On the basis of grain density and scattering one of the emitted particles can be identified as a meson, presumably a π-meson. A calculation of the excitation energy of the disintegrating nucleus based on the energies of the particles stopping in the emulsion gives a lower limit of 450 or 525 electron masses for the rest mass of the incident particle depending whether the emitted meson was a μ- or π-meson. The range together with the range energy relations for charged particles in the photographic emulsion permits placing a lower limit of 10^{-12} sec. for the lifetime of the incident meson. The even which was found in an Ilford C_2 plate exposed for several hours at 30,000 ft. will be discussed in detail. Special reference will be made to heavy mesons reported by other investigators.[1]

[1] C. R. LePrince-Ringuet, Rev. Mod. Phys. 21, 42 (1949).

F13. Preliminary Results—Operation of a High Power Electron Linear Accelerator.* R. F. POST, *Stanford University.*—Electrons have been accelerated with a new 12 foot "Prototype" electron linear accelerator. This accelerator is designed to reach an ultimate energy of 60–70 Mev with large peak beam currents. The accelerator is intended as a prototype section of the 1-Bev electron accelerator under construction at Stanford.

* This project is supported by ONR, Contract N6-onr-25116.

F14. Theory of the No Load Characteristics of Saturable Reactors with Hysteresis, I. ALFREDO BAÑOS, JR. AND WILLIAM B. MCLEAN, *University of California, Los Angeles, and U. S. Naval Ordnance Test Station, Inyokern.*—Renewed interest in the characteristics of saturable reactors, particularly in their application to magnetic amplifiers, stems from the remarkable magnetization properties exhibited by recently developed materials known commercially as Mumetal, Orthonol, Deltamax, etc. These materials have in common a very narrow hysteresis loop rising almost vertically to a sudden and very flat saturation curve. Heretofore, all attempts to predict theoretically the performance of such a saturable reactor with a spirally wound core of any of these materials (a) have assumed no hysteresis, and (b) have endeavored to

approximate the d.c. magnetization curve by means of empirical formulas or by means of straight line segments. In either case, assuming an alternating e.m.f. applied to the primary winding, one wishes to obtain the Fourier coefficients of the currents flowing in the primary and secondary windings as well as in the rather important d.c. bias winding. Without neglecting hysteresis and approximating the $B-H$ curve and hysteresis loop of these materials by means of straight line segments we have been able to compute the Fourier coefficients mentioned above in terms of a minimum number of parameters; namely, the residual magnetization B_r, the coercive force H_c, and the slopes μ_1 and μ_2 of the saturation and rising portions of the idealized magnetization curve respectively. The results presented here consider separately the cases of maximum induction above and below the "knee" of the magnetization curve as well as the effect of d.c. bias. In a later paper we propose to present a comparison between the theory and measurements now in progress at the Naval Ordnance Test Station.

SUPPLEMENTARY PROGRAMME

SP1. Heat of Dissociation of Nitrogen.*† JOSEPH KAPLAN, *University of California, Los Angeles.*—A new method is presented for selecting between the Herzberg value of 7.384 ev for the heat of dissociation (D) of nitrogen molecules ($N_2 \times {}^1\Sigma$) into normal nitrogen atoms (^4S), and Gaydon's value of 9.764 ev. This is based on an experimental proof that the $A^3\Sigma$ level of N_2 dissociates into one normal and one excited atom. It would have to dissociate into normal atoms if D were 9.76 ev. This experimental proof is the result of observations which show that those Vegard-Kaplan bands which originate on $v'=0$ are observed in auroral afterglows only when atomic recombination is taking place, and when metastable atoms in *either* the ^2P or ^2D levels are involved. If the products of dissociation of the $A^3\Sigma$ level are ^2P and ^4S, and $D=7.38$ ev, the Birge-Sponer extrapolation for this level is then too small by 0.08 ev. If the products of dissociation are ^2D and ^4S, the extrapolation is too great by 1.10 ev. This is a reasonable excess. On the basis of these interpretations of auroral afterglow spectra, the Herzberg value of 7.384 ev appears to be the correct one.

* Work done under contract with ONR.
† To be given after Session A if time permits.

SP2. A Constant-Mass Electron in Uniform Fields.* F. W. WARBURTON, *University of Redlands.*—The reciprocal force of relative electrodynamics expressed in a power series of $1/c$,[1] describes apparent increase in mass in deflection experiments in uniform fields. In the uniform electric field E_x between condenser plates, the force reduces to

$$F_x = Ee[1+(\dot{x}^2+\dot{y}^2+\dot{z}^2)/2c^2-2b\dot{z}^2/c^2 + (4b-1)(d/2-z)\ddot{z}/c^2+\cdots].$$

The coefficient $b=\frac{1}{2}$ provides the decreased force replacing increased mass, and gives increased force as the electron decelerates at the target. A similar expansion in a uniform magnetic field **B** involves the $1/c^4$ terms including the acceleration factor $\mathbf{f}/c^2$ as well as those containing the relative factor v^2/c^2. In balanced fields with **v** transverse to **E** and to **B** the acceleration terms are zero. In the magnetic field alone the centripetal acceleration terms combine with the v^2/c^2 terms. Comparison with experiment then determines another coefficient in the series.

* To be given after Session G if time permits.
[1] F. W. Warburton, Phys. Rev. 69, 40 (1946).

Author Index to Papers Presented at the Stanford Meeting

Aamodt, Lee, Vincent Peterson, and Robert Phillips—No. D6
Adelman, Frank L.—No. D3
Baez, Albert V. and Paul Kirkpatrick—No. B7
Bandel, H. W.—No. F7
Baños, Alfredo, Jr. and William B. McLean—No. F14
Barber, W. C.—No. B3
Barkas, Walter H.—No. E9
Beinel, A. B.—No. A3
Bloch, F. and R. K. Wangsness—No. B2
Blocker, Wade and Robert W. Kenney—No. D8
Bowker, J. Kent—No. D5
Bradner, H. and S. B. Jones—No. E10
Brade, R. B.—No. F9
Brown, A. B., C. Y. Chao, W. A. Fowler, and C. C. Lauritsen—No. D11
Brueckner, Keith A.—No. C3
Burson, S. B. and K. W. Blair—No. E3
Chao, C. Y., A. V. Tollestrup, W. A. Fowler, and C. C. Lauritsen—No. D14
Chew, Geoffrey F. and Jack L. Steinberger—No. D1
Christian, Richard S.—No. E5
Crandall, W. E., B. J. Moyer, and H. F. York—No. E8
Davis, Leverett, Jr.—No. B11
Eggleston, R. R. and G. L. Weissler—No. F3
Estermann, I.—No. B10
Eyges, L.—No. C5
Forster, Harriet H.—No. F12
Fretter, W. B. and John Ise, Jr.—No. F11
Gerjuoy, E. and Harold Gruen—No. E13
Germain, Lawrence S.—No. E12
Green, John R. and W. B. Fretter—No. F10
Hayward, Raymond W.—No. D7
Halpern, Otto and Charles B. Shaw, Jr.—No. E2
Helmholz, A. C. and K. Strauch—No. D4
Helstrom, C. W.—No. E1
Jeffries, C. D.—No. B4
Jeppesen, C. R. and Paul E. Pflueger—No. F2
Kaplan, Joseph—Nos. A4, SP1
Keepin, G. R., Jr. and J. H. Roberts—No. D9
Kerns, Q. A., W. R. Baker, G. M. Farly, and J. Riedel—No. C7
Kunkel, W. B.—No. F5
Lauritsen, T. and R. G. Thomas—No. D12
Leith, C. E.—No. E6
Loeb, L. B., J. H. Parker, E. E. Dodd, and W. N. English—No. F6
Lofgren, E. J., W. M. Brobeck, E. O. Lawrence, D. C. Sewell—No. C8

Merkle, T. C., Jr., E. L. Goldwasser, and R. B. Brode—No. F8
Noyes, H. P.—No. E11
Packard, M. E.—No. B9
Panofsky, W. K. H. and H. F. York—No. E7
Peterson, Jack M., Edwin M. McMillan, and R. Stephen White—No. C2
Peterson, John W.—No. F4
Plumlee, R. H.—No. F1
Post, R. F.—No. F13
Proctor, W. G. and F. C. Yu—No. B6
Richman, C. and H. Wilcox—No. C11
Rubin, S. and V. K. Rasmussen—No. B5
Schiff, L. I.—No. B8
Sewell, D. C., W. M. Brobeck, E. O. Lawrence, and E. J. Lofgren—No. C6
Silverman, A. and C. Levinthal—No. D10
Smith, F. M., Walter H. Barkas, A. S. Bishop, Hugh Bradner, and Eugene Gardner—No. D2
Smith, Lloyd, A. A. Garren, and L. R. Henrich—No. C9
Strauch, K.—No. C4
Sun, H. and Harriet H. Forster.—No. C14
Taylor, T. B. and G. F. Chew—No. C13
Thomas, R. G. and T. Lauritsen—No. D13
Warburton, F. W.—No. SP2
Weissbluth, Mitchel—No. C12
White, R. Stephen, Edwin M. McMillan, and Jack M. Peterson—No. C1
Wilcox, H. A. and C. Richman—No. C10
Wright, Byron T. and F. E. Faris—No. E4